UNIVERSITY OF Southampton

University of Southampton Research Repository
ePrints Soton

Copyright © and Moral Rights for this thesis are retained by the author and/or other copyright owners. A copy can be downloaded for personal non-commercial research or study, without prior permission or charge. This thesis cannot be reproduced or quoted extensively from without first obtaining permission in writing from the copyright holder/s. The content must not be changed in any way or sold commercially in any format or medium without the formal permission of the copyright holders.

When referring to this work, full bibliographic details including the author, title, awarding institution and date of the thesis must be given e.g.

AUTHOR (year of submission) "Full thesis title", University of Southampton, name of the University School or Department, PhD Thesis, pagination

http://eprints.soton.ac.uk

UNIVERSITY OF
Southampton
School of Chemistry

UNIVERSITY OF SOUTHAMPTON

FACULTY OF ENGINEERING SCIENCE AND MATHEMATICS

School of Chemistry

An Investigation into the Transcription of DNA in DOPE-based Systems

By Josephine Charlotte Corsi

Thesis submitted for the degree of Doctor of Philosophy

November 2010

UNIVERSITY OF SOUTHAMPTON

ABSTRACT

FACULTY OF ENGINEERING SCIENCE AND MATHEMATICS
SCHOOL OF CHEMISTRY

Doctor of Philosophy

AN INVESTIGATION INTO THE TRANSCRIPTION OF DNA IN DOPE-BASED SYSTEMS

by Josephine Charlotte Corsi

The work outlined in this thesis is concerned with the transcription of DNA that is associated with the ordered nanoarchitecture of the inverse hexagonal phase of the phospholipid dioleoyl phosphatidylethanolamine (DOPE). The observation of transcription from these lipoplex systems was novel and unexpected[1] and the work presented here forms part of a body of experiments aimed to increase the understanding how production of mRNA occurs under these experimental conditions.

A transcription system was developed from a commercially available kit and optimised to produce high yields of full-length mRNA from a linear dsDNA template. The effect of different buffer components on transcription from a liquid crystal system, and how that liquid crystal system differs from transcription from an isotropic solution *in vitro* were explored.

As the DNA forms an integral part of the H_{II} phase, experiments were undertaken to assess the effect of including DNA on the lipid phase architecture. In addition to the behaviour of DOPE/DNA mixtures, the effect of the cationic lipid dioleoyl trimethylammonium propane (DOTAP) on the phase behaviour and phase structural parameters of these mixtures was assessed. Polarising light microscopy and x-ray scattering experiments were used to generate an experimental phase diagram of lipid/DNA mixtures. The formation of the inverse hexagonal phase in DOPE/DNA and DOPE/DOTAP/DNA mixtures was observed using coarse-grained molecular dynamics techniques in order to assess their efficacy as a tool for predicting the phase behaviour of lipoplex systems[2].

In order to assess the ability of these lipoplex systems to transfect cells, a dispersion of the inverse hexagonal phase of DOPE/DNA and DOPE/DOTAP/DNA mixtures (achieved by addition of 10% (w/w) pluronic F-127 coblock polymer to the lipid and subsequent sonication) was used to introduce the gene coding for the fluorescent coral protein AmCyan into HeLa cells.

DECLARATION OF AUTHORSHIP

I, Josephine Corsi

declare that the thesis entitled

AN INVESTGATION INTO THE TRANSCRIPTION OF DNA IN DOPE-BASED SYSTEMS

and the work presented in the thesis are both my own, and have been generated by me as the result of my own original research. I confirm that:

- this work was done wholly or mainly while in candidature for a research degree at this University;
- where any part of this thesis has previously been submitted for a degree or any other qualification at this University or any other institution, this has been clearly stated;
- where I have consulted the published work of others, this is always clearly attributed;
- where I have quoted from the work of others, the source is always given. With the exception of such quotations, this thesis is entirely my own work;
- I have acknowledged all main sources of help;
- where the thesis is based on work done by myself jointly with others, I have made clear exactly what was done by others and what I have contributed myself;
- parts of this work have been published as:

1. Corsi, J.; Dymond, M. K.; Ces, O.; Muck, J.; Zink, D.; Attard, G. S., DNA that is dispersed in the liquid crystalline phases of phospholipids is actively transcribed. *Chemical communications* **2008,** (20), 2307-9.

2. Corsi, J.; Hawtin, R. W.; Ces, O.; Attard, G. S.; Khalid, S., DNA lipoplexes: formation of the inverse hexagonal phase observed by coarse-grained molecular dynamics simulation. *Langmuir* **2010,** *26* (14), 12119-25.

Signed: ……..

Date:……..

Acknowledgements

I would like to acknowledge the following people, without whom the production of this thesis and the research carried out towards it would not have been possible.

Firstly I would like to thank my supervisor, Prof. George Attard, who inspired my research career and who has always provided ample supervision and encouragement towards my endeavours both in and out of the laboratory. Without his willingness to believe in my ability, his sensitive approach to supervision and fostering of independence this thesis would not be as diverse as it currently is. I would also like to thank all other members of the Attard group with whom I have overlapped for their support, with special mention to Dr. Marcus Dymond, without whom my research would undoubtedly have suffered untold setbacks.

The simulations carried out towards this thesis would not have been possible without the guidance of Dr. Syma Khalid, who generously took me under her wing and supervised that portion of my research. It is a privilege to have been involved with the early years of the Khalid research group. I would also have had considerable difficulty if it weren't for Dr. Robert Hawtin, from whom I took over the simulated system. I would also like to thank Prof. Jonathan Essex for being there as my advisor over the last three years; his perspective has been invaluable, especially with regards to the simulation studies. My former housemates Michael Bodnarchuk and Andrew Guy were also very generous with their time and in giving me a crash course in the theory behind simulation.

The x-ray diffraction experiments would not have been possible without the support of the Membrane Biophysics Group at Imperial College London. I would like to acknowledge Dr. Oscar Ces, who has been incredibly generous with both his own time and that of his instruments, and Dr. Gemma Shearman for always being willing to help with my experiments. I would also like to extend thanks to all members of the Membrane Biophysics Group, who have all been welcoming and helpful during my many visits to their laboratory.

The confocal microscopy and mammalian cell experiments would not have worked without the guidance of Dr. David Johnston of the Biomedical Imaging Unit at Southampton General Hospital. It is through his insight and experience that I was able

to design my experimental system; it was he who helped me to get it to work, and gave me much encouragement.

I would like to extend my gratitude to my family, who have always been there at the other end of the phone to listen through the good days and the bad. Without their love and unwavering support, completion of this thesis would have been so difficult. I would also like to mention my boyfriend, Ali, and his family who have offered so much encouragement and enthusiasm throughout the last three years. I have made many good friends in Southampton over the last six years, and I am thankful to all of them for being there.

Finally, I wish to acknowledge the Neonuclei EC project from whence came the funding for the early part of my research and the opportunity to meet with several of our international collaborators, and the University of Southampton Life Science Interface, which has supported my Ph.D. and the remainder of my research. Our collaborators on the Neonuclei project provided a welcoming and supportive platform from which to present and discuss my early research findings, and for this I am extremely grateful.

Abbreviations used in this thesis

Lipids

CAC	**Critical aggregation concentration**
C_0	**Curvature**
H_{II}	**Inverse hexagonal**
H_{II}^C	**Inverse hexagonal complexed with DNA (Safinya nomenclature)**
LPA	**Lysophosphatidic acid**
DMRIE	**Dimyristyloxypropyl-3-dimethyl-hydroxy ethyl ammonium**
DMPE	**Dimyristylphosphatidyl ethanolamine**
DOPC	**Dioleoylphosphatidyl choline**
DOPE	**Dioleoylphosphatidyl ethanolamine**
DOSPA	**2,3-dioleyloxy-N-[2(spermine-carboxamido)ethyl]-N,N-dimethyl-1-propanaminiumtrifluoroacetate**
Type 0	**Lipid with zero natural curvature**
Type I	**Conical lipid with positive curvature**
Type II	**Inverse conical lipid with negative curvature**
Φ_{DOPC}	**Weight fraction DOPC (Safinya group experiments)**
Φ_{DOPE}	**Weight fraction DOPE (Safinya group experiments)**
κ	**Bending modulus**

Nucleic Acids

ATP	**Adenine triphosphate**
bp	**Base pair**
CTP	**Cytosine triphosphate**
DNA	**Deoxy-ribose nucleic acid**
dsDNA	**Double stranded deoxy-ribose nucleic acid**
GTP	**Guanine triphosphate**

mRNA	**Messenger ribose nucleic acid**
RNA	**Ribose nucleic acid**
TTP	**Thymine triphosphate**
UTP	**Uracil triphosphate**
rATP	**Ribose adenine triphosphate**
rCTP	**Ribose cytosine triphosphate**
rGTP	**Ribose guanine triphosphate**
rUTP	**Ribose uracil triphosphate**

Transcription Experiments

A_{260}	**Absorbance of light of wavelength 260 nm**
DTT	**Dithiothreitol**
K_{eq}	**Equilibrium constant**
K_p	**Partition coefficient**
LC	**Liquid crystal phase**
RNase	**Ribonuclease enzyme**
SN	**Supernatant phase**
T7	**Bacteriophage T7**
T7 RNAP	**Bacteriophage T7 RNA polymerase**
UV-vis	**Quatification involving absorbance of light in the UV and visble ranges**
ΔG	**Gibbs free energy**

Structural Studies

CCD	**Charge-coupled device (detector)**
d	**Plane separation**
$\underline{k}_i$	**Wavevector of incident beam**

$\underline{k_s}$	**Wavevector of scattered beam**
Q	**Scattering vector**
SAXS	**Small angle x-ray scattering**
TIFF	**Tagged Image File Format (data image file)**
XRD	**x-ray diffraction**
λ	**Wavelength**
θ	**Angle**

Simulation

CG	**Coarse-grained**
GROMACS	**Groningen Machine for Chemical Simulation**
E	**Energy**
MARTINI	**MARrink Toolkit INItiative (forcefield)**
N	**Number of molecules**
MC	**Monte-carlo**
MD	**Molecular dynamics**
MM	**Molecular mechanics**
MPI	**Message passing initiative**
P	**Pressure**
RDF	**Radial distribution function**
QM	**Quantum mechanical**
T	**Temperature**
V	**Volume**
μ	**Chemical potential**

Transfection

AmCyan	**Cyan fluorescent protein from coral reef**

DMEM	**Dulbecco's modified Eagle's medium**
DLS	**Dynamic light scattering**
DIC	**Differential interference contrast (microscopy)**
FCS	**Fetal calf serum**
HeLa	**Human cervical cancer cell line**
LCSM	**Laser scanning confocal microscopy**
LCN	**Liquid crystal nanoparticles**
Opti-MEM	**Reduced serum DMEM**
PBS	**Phosphate buffered saline**
PCR	**Polymerase chain reaction**
TE	**Transfection efficiency**

DNA templates

BamHI	**Restriction enzyme BamHI**
GFP	**Green fluorescent protein**
Lin-T7-GFP	**Linearised plasmid containing gene for GFP under T7 control**
Lin-T7-luc	**Linearised plasmid with luciferase gene under T7 control**
NotI	**Restriction enzyme NotI**
pAmCyan	**Commercial plasmid carrying AmCyan gene**
pAmT7Pol	**pAmCyan with T7 RNAP gene in place of AmCyan**
PT7luc	**Commercial plasmid with luciferase gene under T7 control**
XmnI	**Restriction enzyme XmnI**

Generic symbols

Å	**Angstroms**
cm^2	**Squared centimetres**
°C	**Degrees celsius**

h	**Hours**
K	**Degrees Kelvin**
k_B	**Boltzmann's constant**
µg	**Micrograms**
μm^2	**Squared micrometres**
min	**Minutes**
mM	**Millimolar**
Mol %	**Mole percentage**
nm	**Nanometres**
ns	**Nanoseconds**
T	**Temperature**
pH	**$-\log_{10}[H^+]$**
Wt %	**Weight percentage**

Table of Contents

Chapter 1. Introduction

1.1 An introduction to phospholipids

Phospholipids are one example of the large number of amphiphilic molecules that includes soaps, detergents and other molecules of biological relevance. The lipophilic component of an amphipile is a long hydrocarbon chain, while hydrophilic "head" group possibilities include charged species such as carboxylates, sulfates, sulfonates, phosphates and amines, or uncharged polar groups such as alcohols and ethyleneglycols. Some amphiphilic molecules have multiple hydrophilic and hydrophobic moieties; examples of such a species include block copolymers and proteins. Many amphiphiles are molecules of biological significance; cholesterol, glycolipids, fatty acids, bile acids and saponins are all amphiphilic species. Phospholipids are the major component of biological membranes, and along with glycolipids and cholesterol form the fluid lamellar bilayer structure that acts as a selectively-permeable barrier between intracellular and extracellular environments, and between separate intracellular compartments.

1.2 Lipids as Lyotropic Liquid Crystals

The amphipathic molecules studied in the experiments outlined in this thesis (the phospholipids DOPE and DOTAP) form aggregates driven by the hydrophobic effect[3], with specific architectures dictated by geometric packing constraints on the system. The molecules in these architectures are arranged such that the polar and non-polar components segregate, separating lipophilic and aqueous environments. Once the concentration of the amphiphile, such as a phospholipid, is raised above the critical aggregation concentration (CAC, also termed critical micellar concentration for systems where micelles are formed), spontaneous aggregation of the lipid is observed[4]. Typical CAC values for DOPE is estimated to be in the region of 10^{-12} mol dm^{-3} (based on the behaviour of phosphocholine)[5], while single chain amphiphiles tend to have larger CAC values (such as 10^{-7} – 10^{-6} mol dm^{-3} and 10^{-4} – 10^{-1} mol dm^{-3} for lyosophospholipids and surfactants, respectively). It is worth highlighting that values for the CAC of lipid species are difficult to determine and may be altered by the chemical reactivity for the lipid; this likely results in a CAC for DOPE that is significantly smaller that 10^{-12} mol dm^{-3}. The formation of aggregates arises from the hydrophobic effect and minimizes contact between the hydrocarbon chains and water.

In addition to the well-described cell membrane other, non-bilayer structures are formed by amphiphiles; the most common non-bilayer phase observed in biological systems is the inverse hexagonal phase[6]. The ability of phospholipids to form both membrane and non-bilayer architectures is known as polymorphism, and the precise structure formed depends on a number of factors, including lipid type, hydration, temperature and salt concentration[4]. Lipids are an example of a lyotropic liquid crystal; they are therefore materials that have properties that are associated with both solids and liquids. Liquid crystals are defined as having long-range orientational order, but only short-range positional order[4, 7, 8], such that the molecules are arranged into a particular crystal shape, but individual molecules are free to diffuse within that architecture. The term lyotropic means that the phases formed by a specific mixture of lipids is determined by the water content of the mixture, as well as the overall 'shape' of the lipid, a parameter that is linked to the preference of the lipid for structures with varying degrees of interfacial curvature[6].

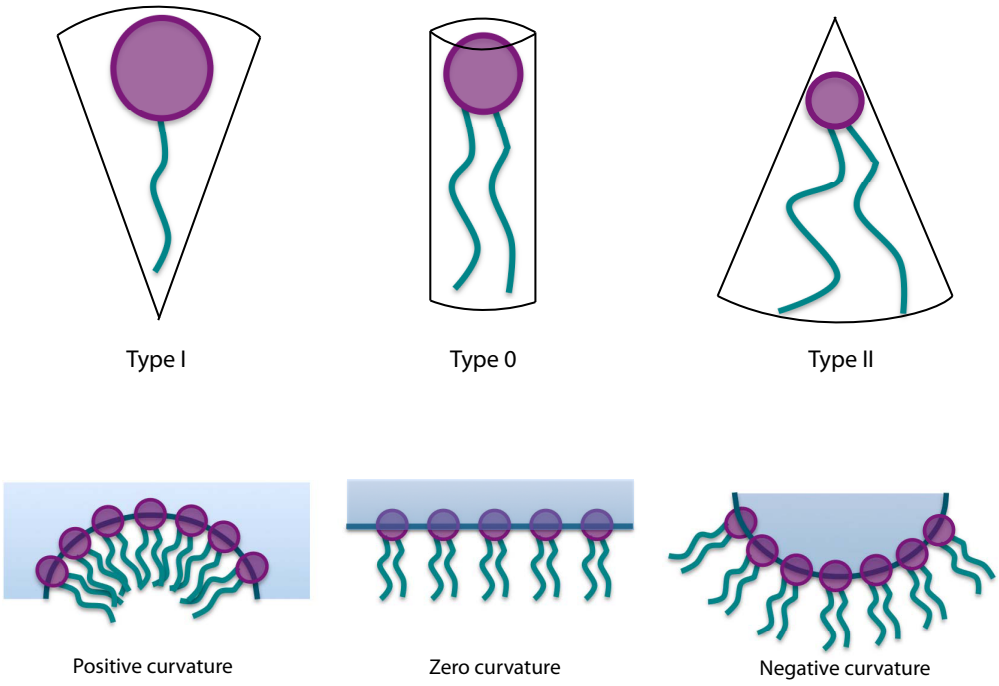

Figure 1: Diagrams depicting the 'shapes' of type 0, I and II lipids, and schematics representing different types of curvature at the oil-water interface of lyotropic lipid mesophases.

Amphiphiles are grouped into three classes that are associated with the curvature preferences of the molecule; these are type 0, type I and type II. Type I lipids are depicted as cone-shaped molecules with a large head group and a long thin tail, while

type 0 lipids are considered to be cylindrical[9]. Type II lipids have a shape described as 'inverse conical'[10] where the polar head group occupies much less space than the hydrocarbon chains. This classification of lipid types is displayed in figure 1.
At high water contents type I amphiphiles, such as detergents, form micelles; these are globular structures formed as the lipid tail groups are enclosed in a capsule formed by the polar head groups. The shape of these structures may be spherical but they can also be rod-like, toroidal or oblate.[11] At lower hydration levels these micelles may become arranged in a cubic lattice to give the micellar cubic phase. As the water levels in the system decrease further these micellar structures fuse to become long cylindrical micelles, which form a hexagonal lattice.[3, 4, 11]

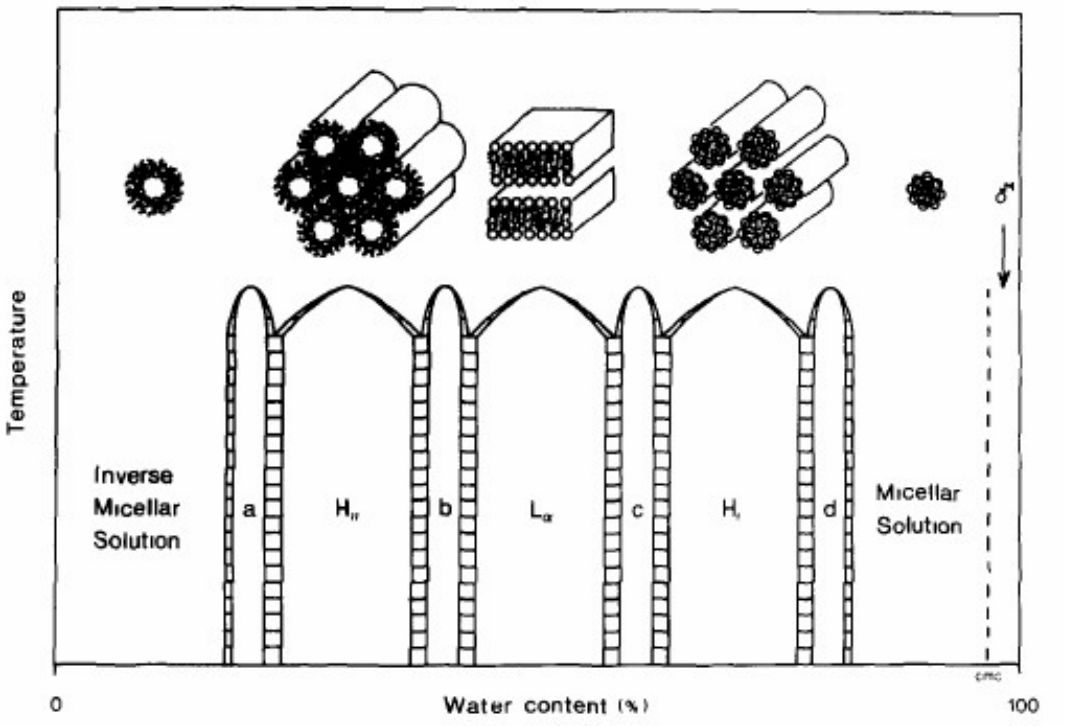

Figure 2: Hypothetical lyotropic binary phase diagram for the case where the phase transitions are induced by varying the water content. Reproduced with permission from reference 5.

Type 0 lipids, i.e. those with zero curvature, form lamellar phases. The lamellar phase is probably the best-known mesophase, owing to the fact that it forms the basis of the structure of the cell membrane. Lamellar liquid crystal structures often consist of infinite planar sheets stacked in a one-dimensional lattice, ribbons of finite width and infinite length that are organised in a two-dimensional lattice (see figure 3) or discs of finite size organised in a three-dimensional lattice.[3, 7]

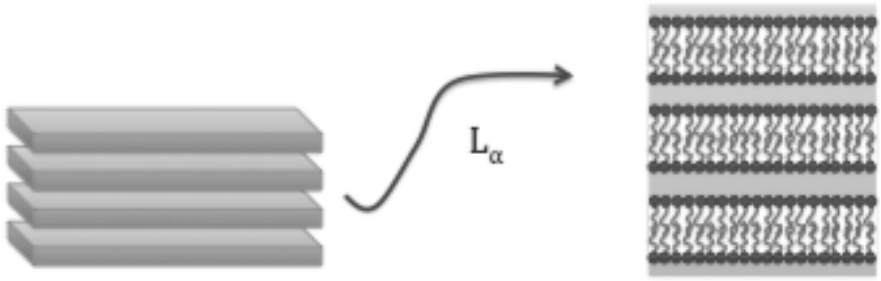

Figure 3: two-dimensional array of stacked bilayers

Type II lipids have a tendency to form inverse phases, as a result of their preference to form interfaces that have negative curvature, such as in the inverse hexagonal phase, where long aqueous channels having a circular cross-section, form in a hexagonal arrangement.[6] While it is true that inverse phases have a very low water content, they do not necessarily occur only at low hydration. As a result of the low CAC, the inverse hexagonal phase of DOPE is kinetically stable will form and in excess water with a limiting hydration.

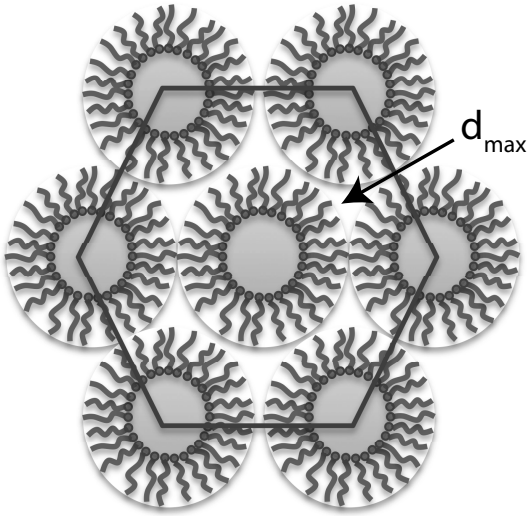

Figure 4: Schematic of inverse hexagonal phase, highlighting position d_{max}

The limiting hydration for the H_{II} phase of DOPE is 11 water molecules per lipid[12], and at water contents greater than this excess water is expelled from the lipid phase. Increasing the water of the bulk H_{II} phase above the limiting hydration causes an increase in the radius of the aqueous channels, which results in the position labeled d_{max} (see figure 4) becoming further from the water/oil interface. At hydration greater

than the limiting hydration of the system, the distance between d_{max} and the interface would exceed the length of the lipid tail; this is entropically unfavourable and would not occur[4].

The lipids used in the work detailed in this thesis were dioleoyl phosphatidyl ethanolamine (DOPE, a naturally occurring type II lipid), and dioleoyl trimethylammonium propane (DOTAP, a synthetic type 0 lipid).

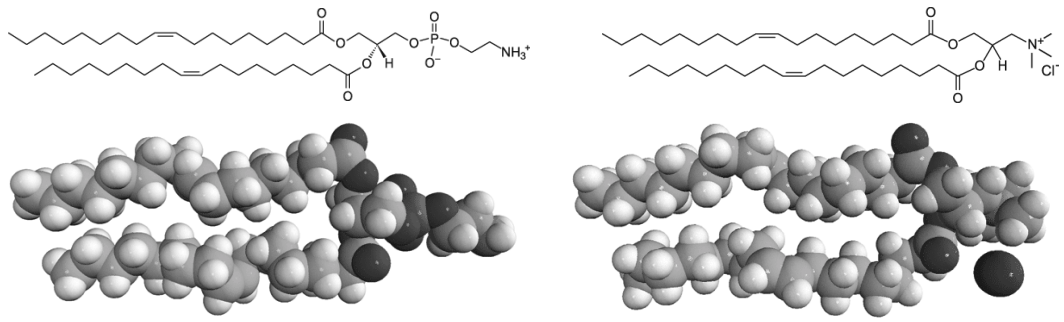

Figure 5: Chemdraw and spacefill structures of DOPE (L) and DOTAP (R)

1.3 Lipoplexes - Lipid and DNA Complexes

Two main structures for lipoplex systems have been resolved using synchrotron small angle x-ray scattering (SAXS) and these structures have been linked to their ability to transfect cells.[13]

The first structure, termed the lamellar-sandwich complex (L_{α}^{C}) and based on periodically repeating opposing bilayers with DNA sandwiched between (see figure 6),[14] has been characterized for mixtures of dioleoyl phosphatidylcholine (DOPC) and DOTAP. Mixtures of DOPC, DOTAP and DNA were studied using synchrotron SAXS for weight fractions of DOPC (Φ_{DOPC}, see equation 1.1) between 0 and 0.75.

$$\Phi_{DOPC} = \frac{DOPC(wt)}{DOPC(wt) + DOTAP(wt)} \qquad \textbf{(1.1)}$$

It was observed that the strong long-range repulsion between opposing bilayers of a 1:1 mixture of DOPC and DOTAP ($\Phi_{DOPC} = 0.5$) were screened by the addition of DNA.[15] This was characterized by a reduction in the lattice parameter of the complex from 39 Å in the absence of DNA to 26 Å in the presence of DNA (the distance equivalent to the DNA duplex surrounded by one hydration shell).

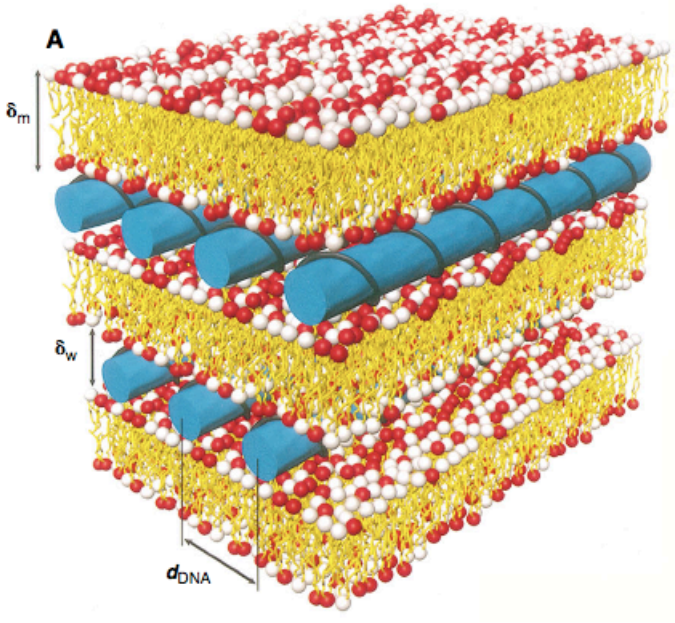

Figure 6: Lamellar sandwich complex (L_α^C) reproduced with permission[14]

The second structure, termed the honeycomb structure (H_{II}^C)[16] consists of the inverse hexagonal phase detailed in figure 7 with DNA occupying the aqueous channels. The structural parameters of this phase were studied for mixtures with Φ_{DOPE} between 0.26 and 0.85. The H_{II}^C structure with a unit cell spacing of 67.4 Å was observed for mixtures with $\Phi_{DOPE} > 0.7$, with an aqueous channel diameter of 28 Å. The unit cell of the H_{II}^C complex was observed to increase to 74.4 Å for $\Phi_{DOPE} > 0.85$.

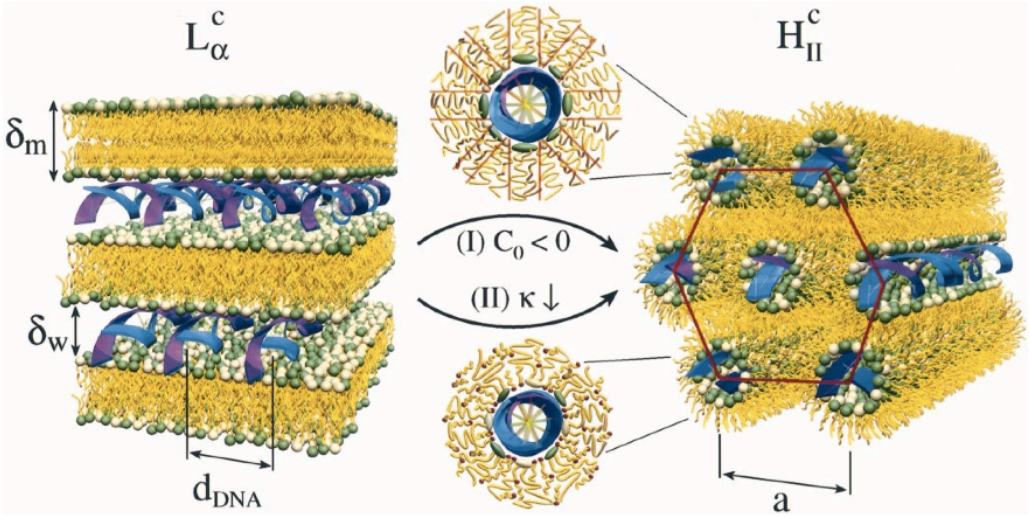

Figure 7: Transition between L_α^C and H_{II}^C complexes; reproduced with permission[16]

At lipid/DNA mixtures with Φ_{DOPE} = 0.65 the lamellar and inverse hexagonal structures were observed to coexist, while at Φ_{DOPE} = 0.26 a lamellar complex was observed with a lattice parameter of 63.5 Å. As detailed in figure 1 there are two pathways for the transition from L_α^C to H_{II}^C complexes. The first (pathway I) involves decreasing the natural curvature of the interface (C_0) until it is negative, by replacing DOPC with DOPE. The second route to the H_{II}^C phase involves addition of hexanol to the L_α^C mixture, reducing membrane rigidity (κ).[13]

1.4 Lipoplexes for Gene Delivery

Lipoplexes have been used as alternatives to viral methods for gene delivery for around two decases, and are the subject of several review articles.[13, 17-20] The main advantage of using non-viral delivery methods for gene therapy lies in their ease of production and comparative lack of an immune response.[19] The mechanism of transfection (that is, transfer of a piece of DNA into a cell and subsequent gene expression) is, however, poorly understood, resulting in low transfection efficiencies when compared with their viral counterparts.

Cationic-lipid mediated gene therapy employs lipid mixtures with an overall positive charge to form complexes with the negatively charged DNA molecules. Different 'helper lipids' are added to the cationic lipid to alter the phase of the complex, thus affecting transfection efficiency. Type II lipids, such as DOPE, are added to increase the negative curvature preferences of the system, and drive the mixture towards an inverse hexagonal phase, while type 0 lipids like DOPC are commonly added to form lamellar 'liposomal' complexes.

There are differences in the transfection efficiency observed when considering gene delivery using the L_α and H_{II} complexes. It would appear that complexes that have an inverse hexagonal geometry are more efficient at cellular entry; this is likely a result of the high degree of fusogenicity associated with DOPE.[21] Lipoplexes are believed to enter the cell through endocytic pathways, and the type II character of DOPE may help stabilize the non-bilayer intermediates that are believed to occur locally in the cell membrane during the internalization process. Once inside the cell it is necessary for the DNA to dissociate from the lipoplex.[22] It is observed that L_α systems, involving a type 0 helper lipid offer more efficient DNA-dissociation than their H_{II} counterparts. Any increase in efficiency that this may cause is, however, cancelled out by their lower efficiency during cellular uptake.[16, 20, 21, 23]

1.5 An alternative approach?

It is apparent that inverse hexagonal lipoplex systems offer much promise as potential gene delivery agents. Of particular relevance is the process of creating a dispersion of lipoplex particles by the addition of a coblock polymer (such as pluronic F-127, see figure 8) and sonication; several excellent review articles are available on this subject.[24, 25] Pluronic F-127 contains multiple hydrophilic and hydrophobic moieties, providing an excellent material for covering the vertices of the hexosomes.

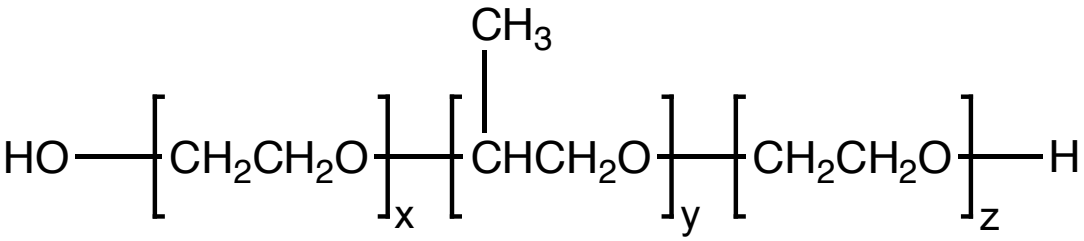

Figure 8: Structure of Pluronic F-127; y = 65.2, x = z = 200.4

While previous work has focused on the use of cationic lipids to drive transfection, it is apparent that cellular entry of lipoplex systems is significantly enabled by the use of DOPE as the helper lipid.[26, 27] It may, therefore, be postulated that the lipid termed the 'helper' may in fact be providing a significant driving force towards the main aim of transfection procedures i.e. uptake of DNA into cells and subsequent expression of a desired gene product.

The main barrier to transfection in this method is likely to be release of the DNA from the H_{II} complex,[22] which may be improved by reducing the cationic lipid, and thus the electrostatic attraction between the DNA and the lipid phase. One of the most commonly used cationic lipids for this purpose is DOTAP, which is listed as being cytotoxic at concentrations greater than 150 μg ml^{-1},[28] (roughly 0.5 ng per cell in the experiments carried out in this study), which provides another reason for reducing the cationic lipid component of the system. It is observed from the literature that transfection using a lipid system containing only DOPE has not been explored. Complexes of DOPE and DNA are known to occur in systems that contain divalent metal species,[29] as these ions screen the charges from the phosphate headgroups of the lipid molecules, creating an overall positive charge at the oil/water interface. Electrostatic interaction between these positively charged ions and the negative phosphate backbone of DNA, combined with the entropic increase provided by release of counterions coordinated to DNA solution,[30] provides a driving force for incorporation of DNA duplexes into the inverse hexagonal phase of DOPE. It is therefore not

necessary to include DOTAP in the lipid mixture for lipoplex formation. If lipoplexes of DOPE and DNA are able to successfully transfect cells, the level of toxicity observed is likely to be lower than that of DOTAP-containing systems, as DOPE is a phospholipid that occurs naturally.[24] The absence of an overall positive charge in the lipid portion of the lipoplex may also result in DNA that is more easily dissociated from the lipoplex, yielding higher transfection efficiencies.

1.6 Experiments described in this thesis

In this thesis the reproducible production of mRNA from DNA that is incorporated into a DOPE lipoplex system with a H_{II}^C structure is explored. The effect of DOTAP on this mixture was monitored using experimental techniques, with particular interest on the amounts of the cationic lipid DOTAP that could be incorporated before disruption of the inverse hexagonal phase was observed. Dispersions of this H_{II}^C complex, and mixtures containing DOTAP at concentrations lower than 20 mol % in DOPE were then used to introduce DNA to HeLa cells in order to assess the effect of DOTAP on the qualitative yield of transcription/translation.

The diagram presented as figure 9 shows an overview of the experiments discussed in this thesis, and their locations within the text.

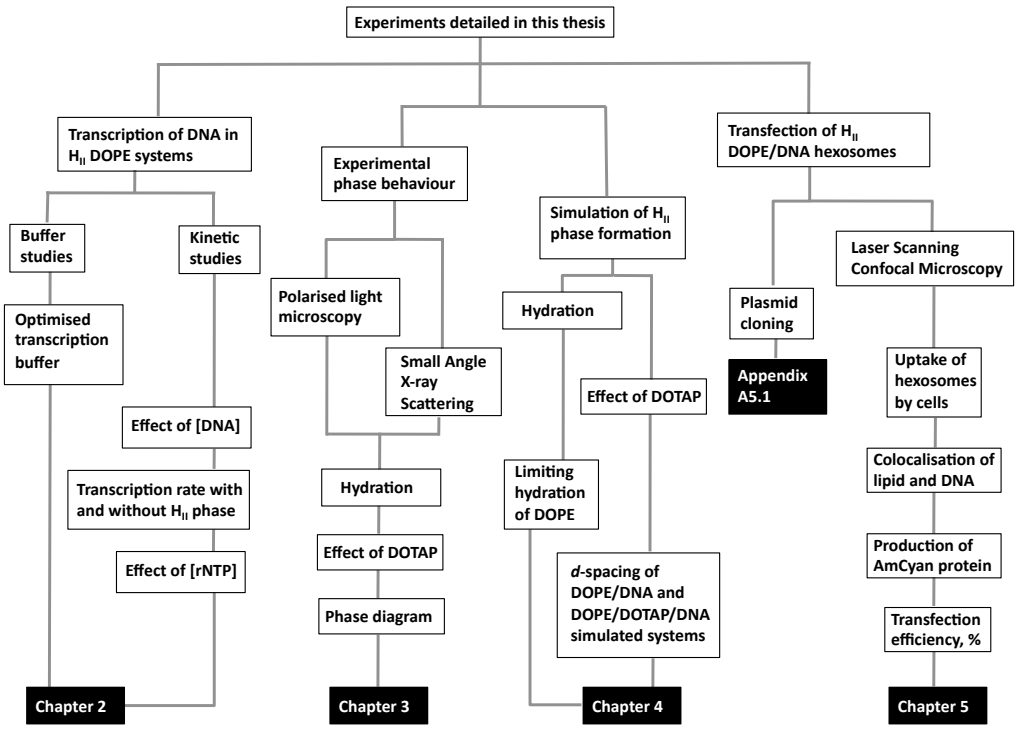

Figure 9: Chart showing the experiments described in this thesis, and how they are arranged within the text.

Chapter 2

A study into the transcriptional availability of DNA that is colocalised with the inverse hexagonal phase of DOPE

The observation of transcription from a DNA template that is associated with the inverse hexagonal phase of the phospholipid DOPE was recently reported. The experiments that gave this observation were based on transcription using a commercial kit supplied by Ambion. The objective of the experiments carried out in this chapter was to develop a transcription system that is independent of commercially available kits and contains only essential components. It was important that the purpose and necessity of all components was assessed and understood in terms of their effects on transcriptional yield (defined as total concentration of messenger RNA produced that is of the expected length and undegraded) in the presence and absence of the inverse hexagonal phase of DOPE. An understanding of the roles of buffer components in transcription in the presence and absence of an inverse hexagonal phase allows the effects on transcriptional activity to be rationalised in terms of those resulting from the presence of the lipid, and those that are caused by the inclusion or exclusion of buffer ingredients.

2.1 An introduction to transcription and cellular protein production

The process of transcription involves the polymerase-driven copying of the genetic code held within a piece of DNA to produce a complementary piece of messenger RNA (mRNA). The mRNA produced is a relatively short-lived copy of the genetic information that behaves as a sort of 'working copy' and is used instead of the DNA, which can be viewed as the 'master copy'. Once produced the mRNA is expelled from the nucleus, into the cytoplasm, ready for the process of translation. This mechanism of protein production occurs continuously within cells.

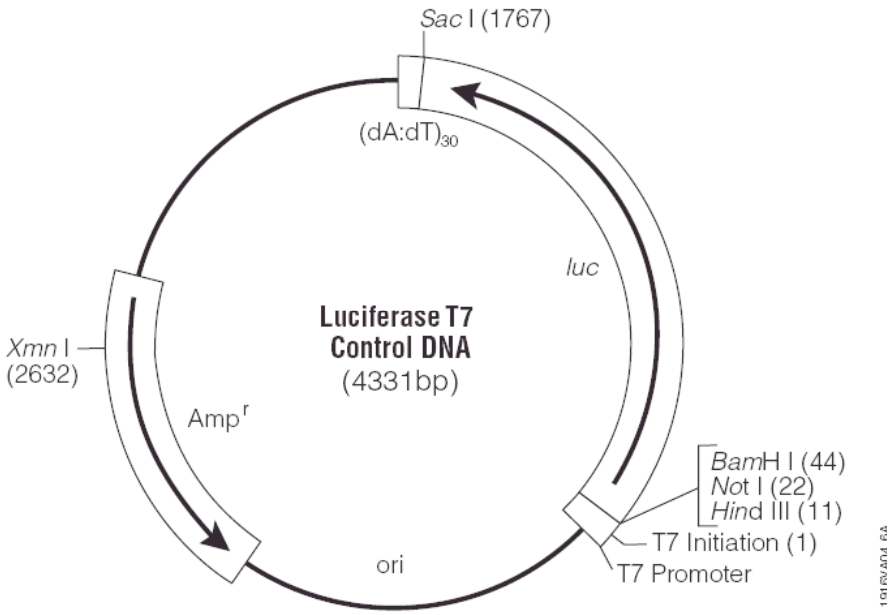

Figure 10: plasmid map of template DNA. Plasmid is restricted at XmnI site (left), 2632 base pairs from the T7 promoter site (bottom right).

2.2 The transcription system used in this study

The system used for this transcription study involves a DNA template 4331 base pairs in length, containing a T7 promoter region (class II), a gene encoding for luciferase (the luminescent protein found in fireflies), and an ampicillin resistance gene. A system based on T7 RNA polymerase (T7 RNAP) was chosen, as T7 RNAP is a well-studied bacteriophage polymerase for which the crystal structures that arise at various key stages in the transcription mechanism are known. The T7 luciferase control plasmid is grown as a plasmid in *E. coli,* purified and cut using the restriction enzyme XmnI (see figure 10). The template is restricted such that when T7 RNA polymerase transcribes

the resulting messenger RNA is 2632 nucleotides in length, and therefore easily distinguishable from the template DNA by gel electrophoresis.

2.2.1 An introduction to Transcription by T7 RNA polymerase

T7 RNA polymerase is a 98 kDa single subunit enzyme homologous to the DNA polymerase I class of enzymes, which provides a useful system for studying transcription *in vitro*[31]. The transcription cycle has been well-studied and consists of an initiation complex, which is responsible for synthesis and release of short, abortive transcripts, of between 7 and 10 base pairs in length, before isomerisation to form a stable elongation complex[31, 32]. The isomerisation process involves major structural rearrangements that are important for stability and processivity of the transcription complex, including the formation of a cavity, which accommodates 8-9 base pairs of a DNA-RNA hybrid and pores for entry of the template DNA and exit of the messenger RNA from the active site[33-35]. The initiation of transcription occurs via promoter recognition in which a 17 base pair promoter (sequence: TAATACGACTCACTATAGGGAGA) is bound by a β-hairpin specificity loop to the major groove of B-DNA, through specific interactions between DNA base pairs and the side chains of the loop. There are also interactions between the specificity loop and the minor groove of DNA. The binding site consists of 300 amino acid residues at the N-terminus and is unique to T7 RNA polymerase[35]. Studies have shown that two types of binding exist for T7 RNAP and DNA; promoter and non-promoter binding. Promoter binding has been shown to be relatively insensitive to ionic strength but sensitive to the helical structure of the DNA, suggesting that it is dependent on specific base interactions. Non-promoter binding was found to be insensitive to the superhelicity of the DNA template, but rather sensitive to ionic strength, such that a concentration of 40 mM sodium chloride is sufficient to prevent binding[36]. This difference in the nature of binding types is suggestive that only specific binding results in initiation of transcription.

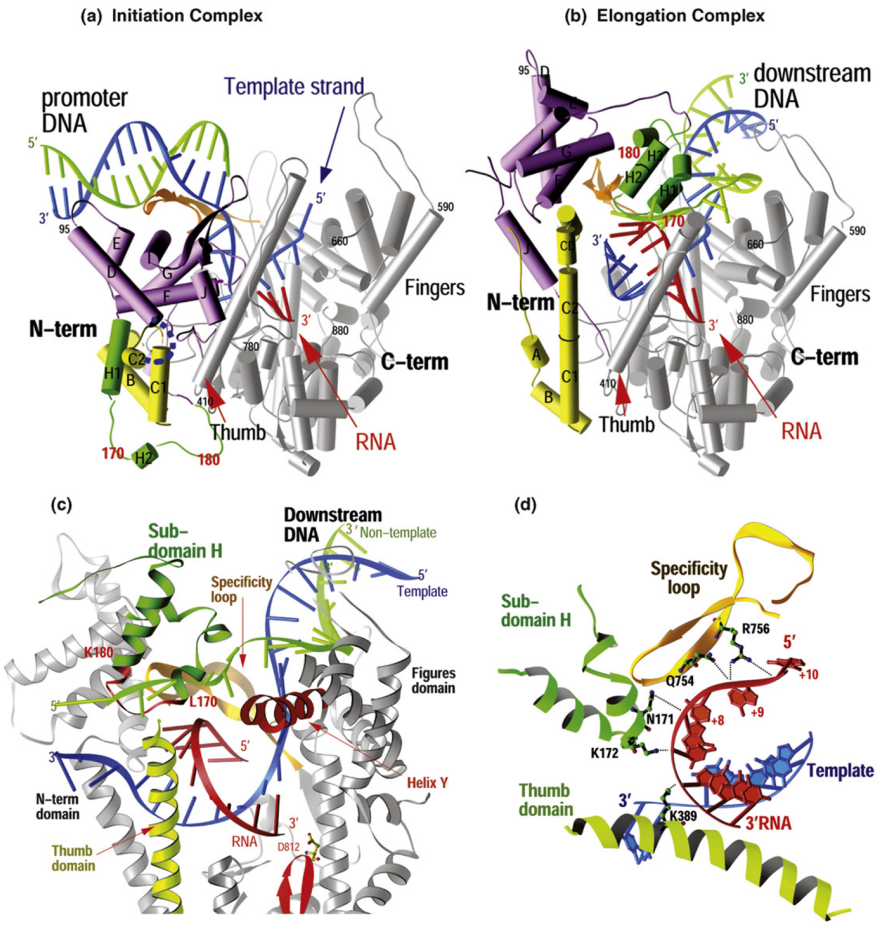

Figure 11: Comparison of the structures of the T7 RNAP initiation and elongation complexes (A) and (B) and views of the transcription bubble (C) and (D). The initiation complex (A) and elongation complex (B) have been orientated equivalently by superimposing their palm domains. Helices are represented by cylinders and beta strands by arrows. The corresponding residues in the NH_2-terminal domains of the two complexes that undergo major refolding are colored in yellow, green, and purple, and the COOH-terminal domain (residues 300–883) is colored in gray. The template DNA (blue), nontemplate DNA (green), and RNA (red) are represented with ribbon backbones. The proteolysis-susceptible region (residues 170–180) is a part of subdomain H (green) in the elongation complex and has moved more than 70 A° from its location in the initiation complex. The specificity loop (brown) recognizes the promoter during initiation and contacts the 50 end of RNA during elongation, whereas the intercalating hairpin (purple) opens the upstream end of the bubble in the initiation phase and is not involved in elongation. The large conformational change in the NH_2-terminal region of T7 RNAP facilitates promoter clearance. This figure was made with the program Ribbons. (C) Interactions of the transcription bubble and heteroduplex in the elongation complex with domain H (green and red) and specificity loop (brown). Proteolytic cuts within the red loop in subdomain H reduce elongation synthesis. Thumb alpha-helix (yellow) and alpha-helix Y (orange) are analogously involved in strand separation. (D) Side chains from subdomain H (green), the specificity loop (brown), and the thumb that interact with the single-stranded 5' end of the RNA transcript and facilitate its separation from the template. The DNA substrate in the initiation complex consisted of duplex promoter DNA from 1 to 17 and a 5' nucleotide overhang of the template strand (nucleotides 1–5) at the 5' end. The DNA used in the elongation complex contained 10 bp of downstream duplex DNA, a 10 nucleotide noncomplementary DNA 'bubble' and a 10 bp upstream duplex DNA that is disordered in the structure.
Reproduced, with permission, from Steitz, T.A., Curr Opin Struct Biol (2009), doi:10.1016/j.sbi.2009.09.001

The structural rearrangements from the initiation to the elongation complex are largely centred on the amino terminal of the RNA polymerase, which may be thought of as

consisting of three subdomains. An assembly of six alpha-helices is rotated by 220° and through 30 Å to make room for the DNA-RNA hybrid[37], while a loop of protein moves from one side of the amino terminus to the other side of the helical subdomain and refolds to form part of the RNA exit pore. It appears that the elongation complex is stabilised by interactions of the protein with downstream DNA, the DNA-RNA hybrid and the emerging transcript[38], and only occurs during a situation that provides all of these components[34, 35]. While the conformations of the initiation and elongation complexes are well documented, the pathway through which these rearrangements are made, as well as the timescale over which they happen are still unclear[37]. There are two proposed mechanisms; the first (the scrunching model) suggests that the DNA-RNA hybrid remains fixed at a length of roughly 3 nucleotides, and the extension of the transcript to 8-9 nt in length occurs as a result of local conformation changes in the polymerase and scrunching of the DNA template, which is the followed by a major conformational rearrangement[35, 39]. The second model, known as the inchworm model, involves gradual rearrangement and refolding of the polymerase to accommodate the growing RNA-DNA hybrid as it extends from 3 base pairs to the 8-9 base pairs observed in the elongation complex[34, 35, 40]. There is evidence to support the second proposed mechanism in the form of fluorescence assays showing the 5' end of the growing RNA chain remaining in the heteroduplex up to a length of 10 base pairs[41], suggesting an incremental increase in the length of the RNA-DNA hybrid.

The completion of the transcription cycle is marked by termination, which involves release of the transcript and dissociation of the polymerase from the template. After the change in conformation to the elongation complex, the transcript RNA threaded through the exit channel may not be released until transcription is finished. In order for the cycle to resume, the enzyme must undergo a conformational change from the elongation complex back to the initiation conformation before transcription may recommence[37]. Analysis of termination at class II promoters shows enhancement of termination signals by T7 lysozyme (the inhibitor of T7 RNA polymerase); as this is known to impede transition from a initiation complex to an elongation complex, it has been hypothesised that termination at class II signals may occur via a reversal of the transition from initiation to elongation complex[42-44]. The experiments detailed in this report are from theT7 luciferase control plasmid shown in figure 10; in this case, termination of transcription occurs when the polymerase reaches the end of the template DNA and therefore is not regulated by termination signals, although the

conformational changes discussed must occur before the next transcription cycle can begin.

2.2 Development of a transcription system

Examination of literature showed that there are two main systems for studying transcription using T7 RNA polymerase; high and low ionic strength conditions. Low ionic strength conditions involve using tris as a buffer at a concentration of 10 mM, while the high ionic strength conditions use a tris concentration of 40 mM. Other buffer components deemed necessary are magnesium chloride, which provides Mg^{2+} ions that are essential for transcription; spermidine, a naturally occurring and ubiquitous polyamine that has been shown to enhance transcription; a surfactant such as triton X-100 or tween-20; 1,4-dithio-dl-threitol (DTT), which preserves disulfide bonds in proteins; and, of course, ribonucleotides. Other ingredients that are routinely added include inorganic pyrophosphatase (for removal of pyrophosphate produced as a by-product of transcript elongation that has been shown to initiate denaturation of RNA in *E. coli*), as well as ribonuclease inhibitors (such as RNasin, Promega). The concentrations of these ingredients vary from source to source but after reviewing the information available it was decided that the assay conditions of transcription would be as follows:

Buffer component	Assay concentration
Trizma	40 mM
$MgCl_2$	25 mM
Spermidine	2.5 mM
Triton X-100	0.16mM
DTT	10 mM
RNasin	**50nM**

Table 1: Transcription buffer components and working concentrations in 20µl transcription assay

This buffer (or variations based on it) was used throughout this study to obtain messenger RNA from the linearised T7 plasmid used previously, in the absence of a liquid crystal phase. A typical transcription experiment follows the protocol described by Ambion[45] and involves adding the aforementioned buffer ingredients (as a 10x stock solution) to the appropriate amount of nuclease-free water, then adding to this mixture 20 mM mixed ribonucleotides (5 mM of each) and 1 µg linear template DNA. A solution of 40 units of T7 RNA polymerase (6.8×10^{-8} mol dm^{-3}, 0.8 µl), to produce a 20µl total

reaction volume, was used to start the reaction. This transcription reaction is run at 37 °C as a homogeneous lipid-free sample. For transcription from systems consisting of DNA associated with inverse hexagonal DOPE, a lipid button containing DOPE and DNA was assembled according to the method described in appendix A1, and to this was added a 20µl transcription mixture containing transcription buffer, mixed ribonucleotides and T7 RNA polymerase, assembled in the order indicated above. In all cases reaction mixtures were assembled on ice. Where possible, larger volumes of the other reaction components were assembled (water, transcription buffer, ribonucleotides, and where appropriate, DNA) before being divided into 19.2µl aliquots ready for enzyme addition, thus reducing the errors abundant in pipetting small volumes. Care was taken when adding the enzyme to ensure no extra enzyme was present on the outside of the pipette tip, as this would have had large effect on the transcriptional yield. For reactions involving transcription buffers deficient in one of the aforementioned components a specific 10x stock solution was assembled that was deficient in this ingredient as detailed in appendix A2.1.

Once it was established that this buffer supported transcription, it was important to establish a nucleotide concentration that reliably produced transcript RNA. The Megascript kit used a total nucleotide concentration of 30 mM although this proved to be too high for the system described in table 1 and gel electrophoresis showed that RNA bands from samples containing this quantity of nucleotides were less strong; it is likely that the transcription buffer from the Megascript kit was enhanced with pyrophosphatase enzymes and engineered to produce high yields of RNA. From quantification presented elsewhere in this report (see figures 39 and 40) it was apparent that the nucleotide concentration that produced messenger RNA most reliably was 20 mM (5 mM each of ATP, GTP, CTP and UTP).

The purification of RNA from all samples was carried out using a protocol was adapted from the commercially availably RNeasy lipid tissue mini kit (Qiagen)[46]. This kit couples an organic extraction of the lipid (using Qiazol lysis reagent, 500µl, and chloroform, 100µl), separating RNA and lipids into the aqueous and organic phases respectively, with column purification of the RNA. Qiazol lysis reagent is a mixture of phenol and guanidine isothiocyanate which, when mixed with chloroform, causes a phase separation. RNA is extracted from the upper aqueous phase, DNA from the interphase and proteins from the organic phase. Guanidine isothiocyanate is a chaotropic denaturing agent, which disrupts the three-dimensional structure of

macromolecules, without guanidine isothicyanate the DNA appears in the aqueous phase and is not separated from the RNA. The RNA was then bound to the silica spin columns from equal proportions of the extracted aqueous phase and 70% ethanol before being washed with buffers as directed in the kit. The column was dried by centrifugation for 5 minutes to prevent solvent carry-over into the sample before RNA was eluted in 100µl RNase-free water. This method was used even when lipid was not included in the experiment to allow greater comparison of the data.

Analysis of the transcript RNA was performed by gel electrophoresis, showing that the RNA produced was of the length expected (2632 base pairs) and not degraded by RNases. The quantification of results was carried out using the Nanodrop ND-1000 UV-visible spectrometer, to obtain the concentration of RNA from the absorbance of light with wavelength of 260nm, using a sample volume of 2µl. This concentration was then converted to an overall yield (in µg) based on a total sample volume of 100 µl. The Nanodrop is a commercially available instrument supplied with information detailing the following errors and ranges: for samples in the concentration range of 2 – 100 ng μl^{-1}, the accuracy of the nanodrop reading is ± 1.5 ng μl^{-1}, for samples with concentration greater than 100 ng μl^{-1} the accuracy is given as ± 2%, the upper limit for RNA samples is 3000 ng μl^{-1}. This instrument has been tested for its consistency and reproducibility using samples of known concentrations of both DNA and RNA, which have been diluted and tested, and also tested over periods of several weeks to a few months, and values given were found to be in good agreement with the manufacturers' tolerances. It should be noted, however, that while RNA concentration does not fall over time, if stored at -20 °C, the RNA itself may become degraded so it is always sensible to use the Nanodrop in conjunction with gel electrophoresis, and as soon as possible after the RNA production. Samples that are known to have been in contact with ribonucleases often exhibit no concentration depletion from the nanodrop readings (that is that the observed concentration does not decrease on storage) but produce smeared results by gel electrophoresis, similar to those observed in figure 19.

It should be noted that all data presented in this report include error bars that represent the standard deviation. Where data are described as 'normalised' this allows for the correction of yield relative to positive control samples, allowing for decreased activity of T7 RNA polymerase over a relatively short timescale (of the order of weeks). A full description of this is given in chapter 7 entitled Protocols.

2.3 Assessing the roles of spermidine and triton X-100

Spermidine is known to precipitate DNA in solution; this is shown by the protection of DNA from shearing, and also from X-ray diffraction studies. DNA condensation by spermidine occurs suddenly when 90% of the negative charges of the sugar-phosphate backbone have been neutralised[47, 48], the most likely cause for this is a counter-ion effect (as proposed by Manning[49]) as this is also observed by trivalent inorganic cations, such as $Co^{3+}(NH_3)_6$,[50, 51] which are structurally unrelated to the polyamines. It has been shown that rather than bridging two separate DNA molecules, polyamines interact with individual duplexes[52]; linear dichroism and light scattering experiments have shown that dilute solutions of DNA treated with spermidine or spermine undergo cooperative condensation to produce rods, spheres, toroids and complex aggregates, which can be examined using electron microscopy[47, 50, 53, 54]. Increased conversion of DNA from its B form to the Z form in the presence of low concentrations of polyamines has been observed, although similar effects have been shown by divalent cations (at higher concentrations) and $Co^{3+}(NH_3)_6$[55]; it is worth mentioning, however, that DNA condensed by spermidine was still transcriptionally active, while DNA condensed with $Co^{3+}(NH_3)_6$ was not transcriptionally active[56, 57]. Inhibition of T7 RNA polymerase by $Co^{3+}(NH_3)_6$ was ruled out as increasing the ionic strength reversed the compaction and transcription levels returned to that of naked DNA. While the precise role of spermidine in transcription is unknown, it is clear that it shows significant interactions with nucleic acids and is important in many cellular processes.

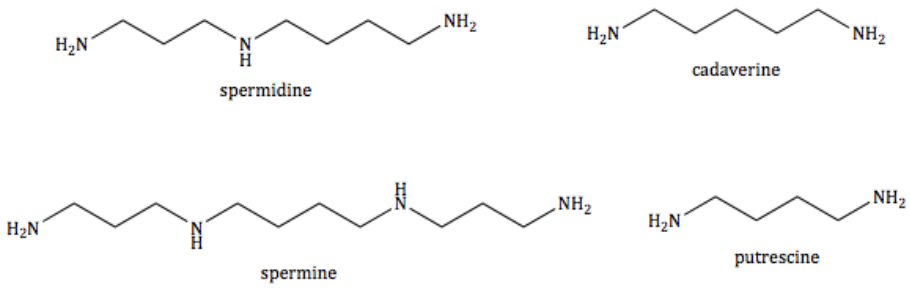

Figure 12: Structure of polyamine species common in cells

Triton X-100 is a non-ionic surfactant comprised of a hydrophilic oligothylene oxide group, containing 9.5 ethylene oxide units on average, coupled to a hydrophobic hydrocarbon group. Triton is one of a number of surfactants (along with tween-20)

used to replace carrier proteins, such as BSA that were used in transcription reactions in the early 1990s[58, 59]; for this reason it can be argued that its role in transcription is relatively unimportant and that the presence of triton in the transcription mixture is for historical reasons.

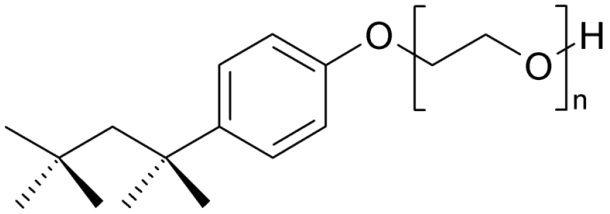

Figure 13: Structure of triton X-100

In the interest of developing a system as simple as possible, spermidine and triton were removed from the transcription buffer, both separately and then together. The yield of mRNA after 2.5 hours of transcription, in keeping with the Megascript protocol used for the original studies, was measured using the nanodrop ND-1000.

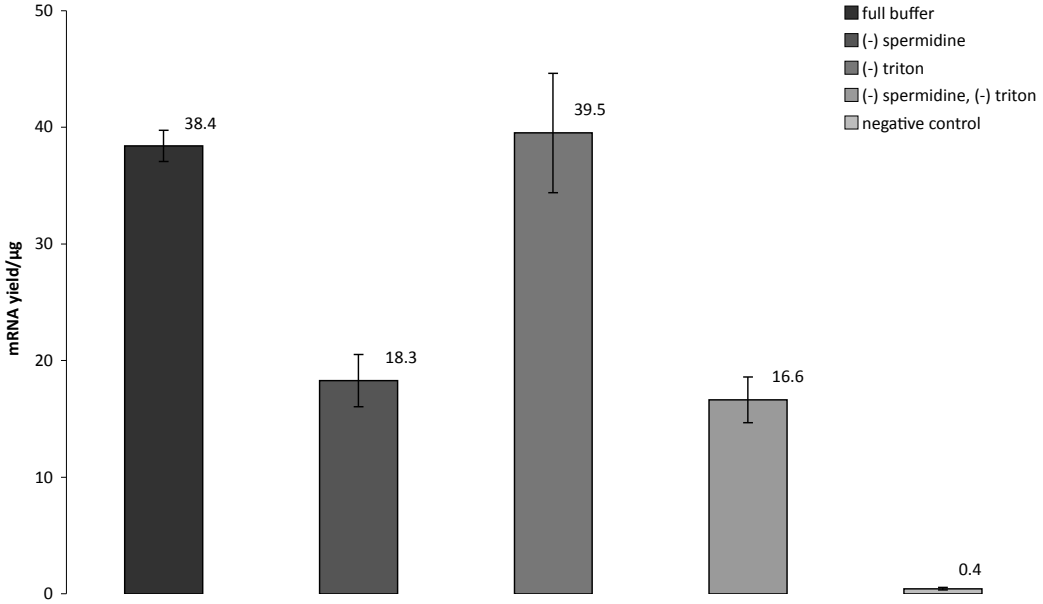

Figure 14: Graph showing the effect of removing spermidine and triton on transcript RNA production. L-R: full buffer, buffer without spermidine, buffer without triton, buffer without spermidine or triton, negative control. Data collated and normalised – see appendix B, table 5.

2.3.1 Transcription without spermidine

When spermidine is removed from the transcription buffer, a decrease in the production of transcript RNA by as much as one half is observed (when compared with

transcription from buffers containing spermidine). This is in good agreement with literature observations for T7 RNA polymerase under the same conditions (the enhancement of transcription upon addition of spermidine is much greater at lower ionic conditions, e.g. 10 mM Tris). Transcription from this buffer produces a yield of mRNA of 47.7% relative to the full buffer.

2.3.2 Transcription without triton X-100

Removal of triton X-100 from the transcription buffer does not affect transcriptional yield. This is apparent as the concentration of RNA measured is the same as that of the positive control, within the accuracy of the experiment, and gel electrophoresis shows strong bands of RNA for samples that contain the full buffer or are lacking in triton only. Transcription from this buffer produces a yield of mRNA of 102.9% relative to the full buffer.

2.3.3 Transcription without spermidine or triton X-100

Transcription without spermidine or triton X-100 shows a significant decrease in transcription comparable with that observed when only spermidine is removed. This suggests that the loss of activity is caused by spermidine removal, rather than removal of triton. Together, these results show that spermidine is not essential for transcription although enhances it greatly, while triton does not appear to be necessary for successful transcription. Transcription from this buffer produces a yield of mRNA of 43.2% relative to the full buffer.

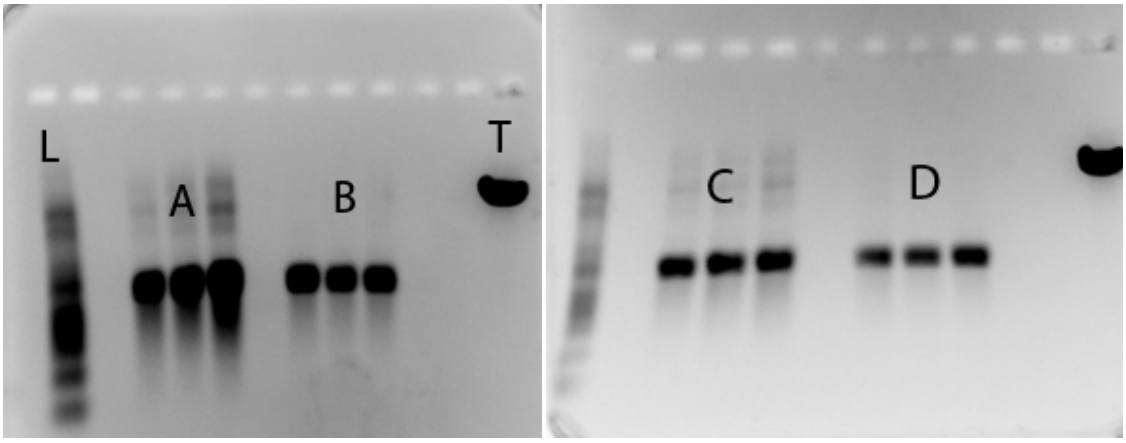

Figure 15: Gel electrophoresis images from transcription of lin-T7-luc DNA under different buffer conditions. L: ladder; T: template DNA; A: full buffer; B: buffer deficient in spermidine; C: buffer deficient in triton X-100; D: buffer deficient in both spermidine and triton X-100.

Figure 15 shows that in all buffers tested, transcript RNA length is constant. RNA produced in buffers A and C, both of which contain spermidine, are of higher

concentrations. This is apparent from the banding observed on the gel, caused by RNA secondary structure, indicating that surplus RNA was not denatured by incubation in the loading buffer. This pattern is in good agreement with the quantification data.

2.4 Assessing the roles of spermidine and triton X-100 in H_{II} DOPE

The effects of spermidine and triton X-100 (both separately and together) on the transcriptional yield of mRNA were established from the experiments detailed in figure 14. Samples containing DNA associated with the inverse hexagonal phase of DOPE (H_{II} DOPE) were made as described (Appendix A1) and prepared for transcription by rehydration with isotonic saline (0.15M, 2.5ul) before incubation on the block heater (40°C, 1 hour). Earlier work in the group focussed on small angle x-ray diffraction (SAXS) of lipid/DNA samples, including the DOPE mixtures used in this study. It was found that addition of DNA to H_{II} DOPE did not disrupt the inverse hexagonal phase although it caused an increase in the lattice parameter from 5.2 nm to 5.6 nm. This is in good agreement with the extensive literature on the nanostructure of DNA-lipid mixtures.[1, 13, 16, 18-20, 23, 60-74] It has also been observed that after transcription (or indeed, during incubation with the transcription mixture) the lipid liquid crystalline phase remains intact and retains hexagonal phase characteristics when viewed through a polarising light microscope (birefringence, feathery texture, high viscosity)[1]. These observations are consistent with the observation that lipid buttons used in the transcription experiments retain their shape and appearance throughout the reaction. The phase behaviour of the samples used in transcription studies, using polarised light microscopy and small angle x-ray diffraction is explored in chapter 3 of this thesis.

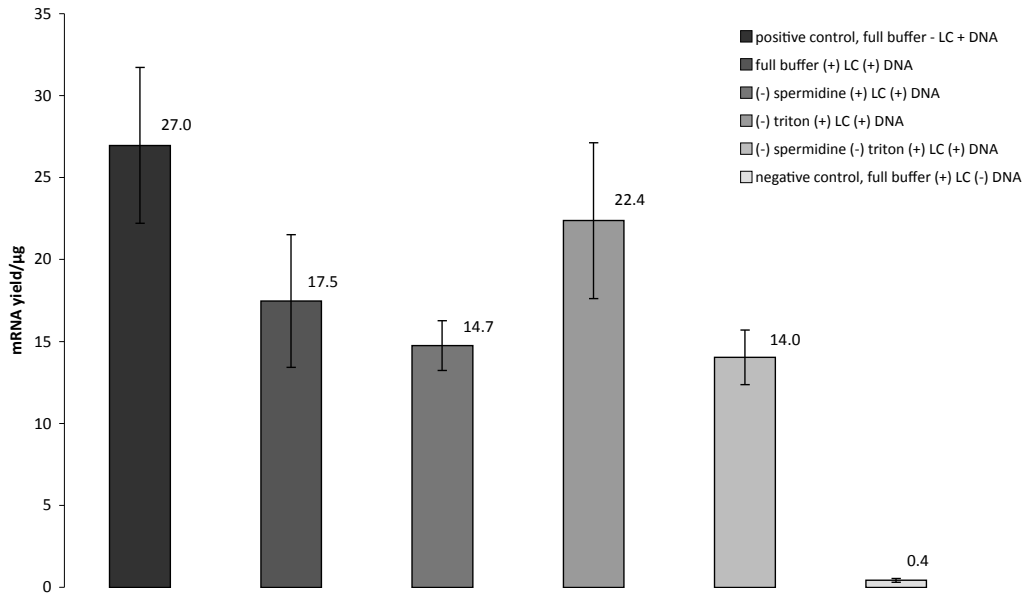

Figure 16: Graph showing production of transcript RNA from buffers deficient in spermidine and triton X-100, template DNA incorporated into the inverse hexagonal phase of DOPE. L-R: positive control, no lipid; full buffer, DOPE/DNA; buffer deficient in spermidine, DOPE/DNA; buffer deficient in triton X-100, DOPE/DNA; buffer deficient in spermidine and triton X-100, DOPE/DNA; negative control, DOPE only, no template DNA. For data see appendix B, table 7.

Figure 16 shows that transcriptional activity from the DNA associated with H_{II} DOPE is decreased by roughly one third, when compared with a positive control sample containing no lipids; this decrease is more pronounced in the presence of triton X-100. It is also apparent that a decrease in transcript RNA production is seen when spermidine is removed from the transcription buffer, although this decrease is less than had been observed previously, in the absence of DOPE. Figure 14 shows that in the absence of a liquid crystal phase removing spermidine from the transcription buffer causes the transcriptional yield to fall to half the value of the positive control. Transcript RNA poduction without spermidine in the presence of H_{II} DOPE is roughly half that of the positive control (which does not contain lipids) within error. This shows that decreases in transcript RNA yield caused by spermidine removal are not significantly different in the presence or absence of an inverse hexagonal phase. An explanation for this could be a result of the ability of triton to partition on to the surface of the lquid crystal phase; the concentration of triton X-100 in the transcription buffer (0.16mM) is below the critical micellar concentration (0.2 mM), meaning that ordinarily triton molecules will not form aggregate structures, but in the presence of a liquid crystal phase aggregation will occur. It is therefore possible that the triton on the surface of the H_{II} phase is able to interfere with the interaction between DNA and polymerase, causing a decrease in mRNA yield. This theory is reinforced by the fact that

when triton X-100 is removed from the transcription reaction, in the presence of H_{II} DOPE, the yield of mRNA appears to increase.

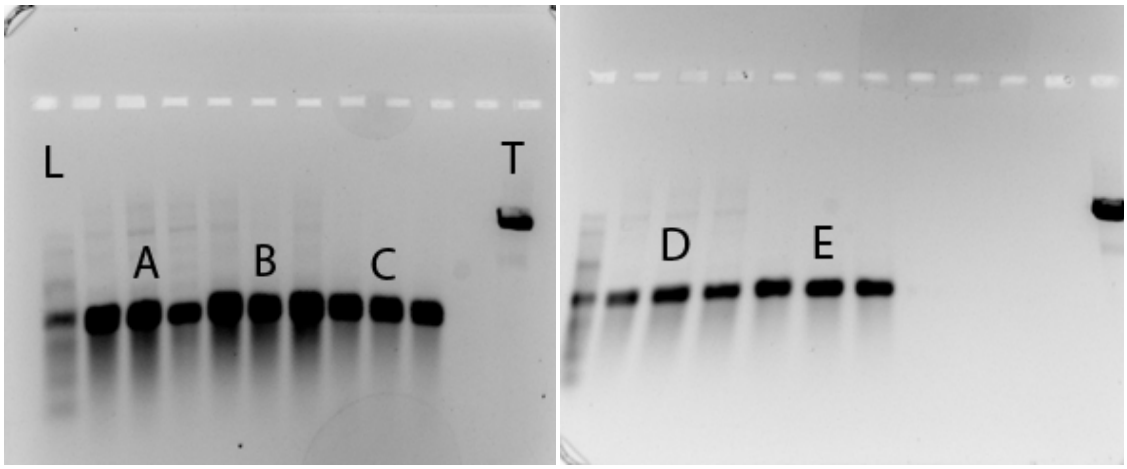

Figure 17: Gel electrophoresis images from transcription of DNA located within H_{II}DOPE, under different buffer conditions. L: ladder; T: template DNA; A: full buffer (no lipid); B: full buffer (+) DOPE; C: buffer deficient in spermiding (+) DOPE; D: buffer deficient in triton X-100 (+) DOPE; E: buffer deficient in both spermidine and triton X-100 (+) DOPE.

2.5 Transcription without a ribonuclease inhibitor

Ribonuclease inhibitors, such as RNasin (Promega), are included in transcription reactions to reduce the impact of ribonuclease enzymes (RNases) on transcript RNA. RNases are ubiquitous, and excluding them from experiments can be very difficult. Experiments were conducted in the absence of RNasin to ascertain whether it was necessary for transcription. Such experiments were carried out in the presence and absence of inverse hexagonal DOPE to see whether the liquid crystal phase offers any protection from RNAses when compared to solution-only experiments.

While it can be seen in the graph (figure 18) that removing RNasin from the transcription reactions causes an apparent increase in transcript RNA, as calculated from the A_{260} value of the eluted RNA, it is clear from the gel electrophoresis image (figures 19 and 20) that RNasin is required in the transcription mixture to prevent degradation of the RNA. Figure 18 shows that removing RNasin from the transcription mixture is not an option as any discrepancies in the length of the RNA as a result of incomplete transcription, for example, would not be detectable from degradation by RNase action. It is therefore necessary to ensure a system that produces RNA of the correct and complete length detectable by gel electrophoresis. Any increase in the Nanodrop readings could not automatically be assigned as being an increase in transcription activity.

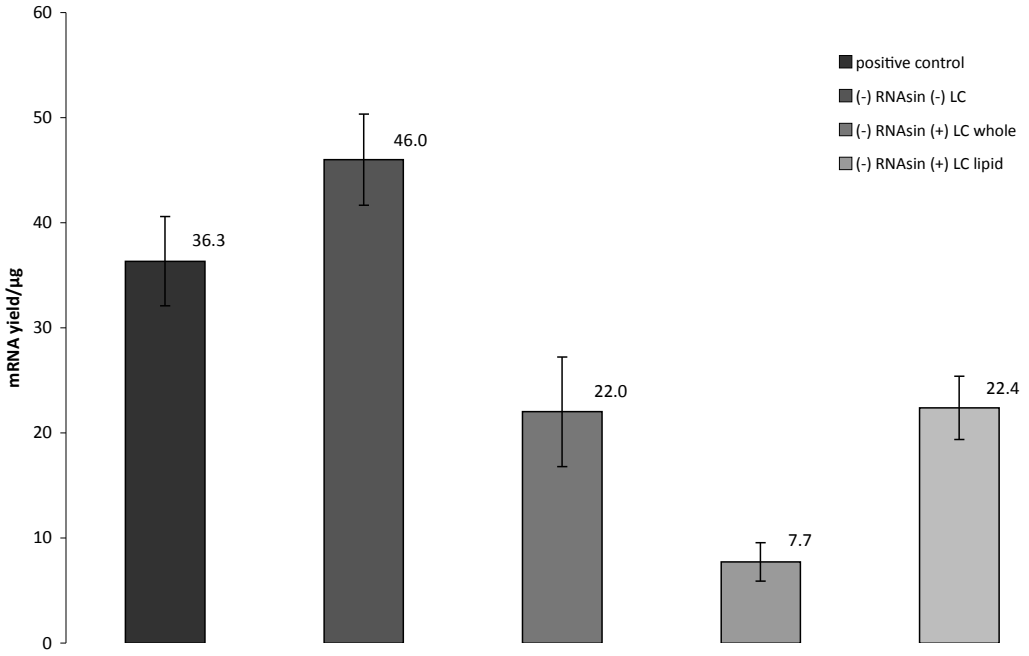

Figure 18: Normalised data from transcription in buffers deficient in RNasin; L-R, positive control (full buffer, -LC), without H_{II} DOPE, and with H_{II} DOPE, whole sample, liquid crystal and supernatant. Note how removing RNasin causes an apparent increase in transcript RNA when compared with the positive control. See appendix B, table 26.

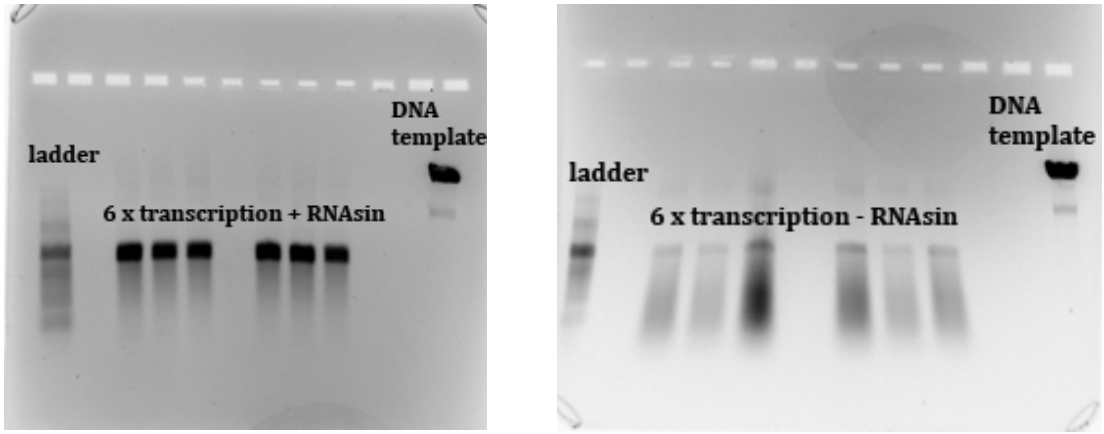

Figure 19: Gel electrophoresis showing the effect of RNasin on transcript RNA. Left: Transcript RNA in the presence of RNasin, visible as neat bands comparable to the 3000 bp band of the ladder (NEB) and shorter than the DNA template. Right: Transcript RNA produced in the absence of RNasin, visible as weak bands comparable to the 3000 bp marker with degraded smears at lower molecular weight.

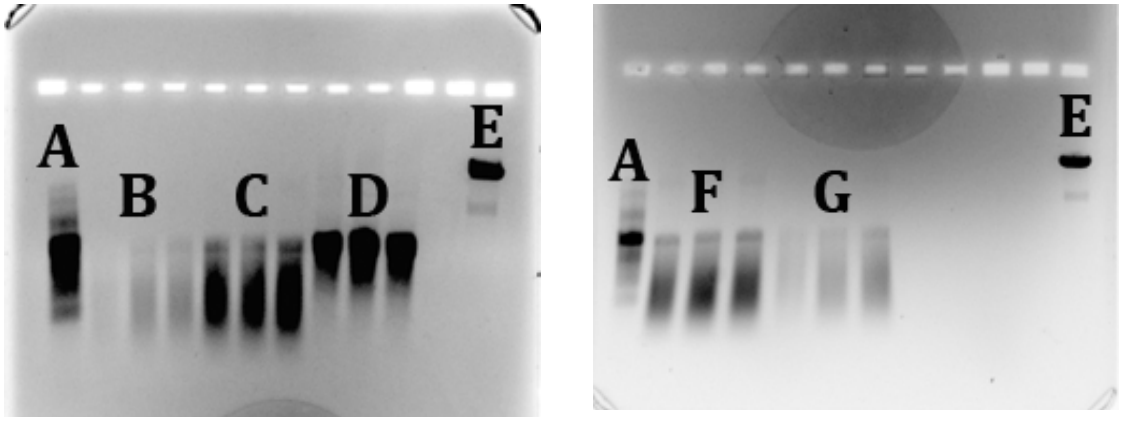

Figure 20: gel electrophoresis images of transcription from buffers without RNasin. A: ladder, brightest band corresponds to 3000bp RNA; B: transcript RNA from LC phase, note streaking of sample; C: RNA from supernatant, note streaking of sample; D: positive control (+ RNasin), with slight overloading of sample; E: template DNA; F: RNA from buffer without RNasin, no liquid crystal phase; G: RNA from buffer without RNasin, DOPE/DNA liquid crystal phase, whole sample extract.

2.6 Comparison of buffer components in the presence and absence of H_{II} DOPE/DNA

The effects of removing individual buffer components from transcription reactions were compared by expressing the messenger RNA yield for different solutions as a fraction over that of the positive control. This is shown in figure 21.

A

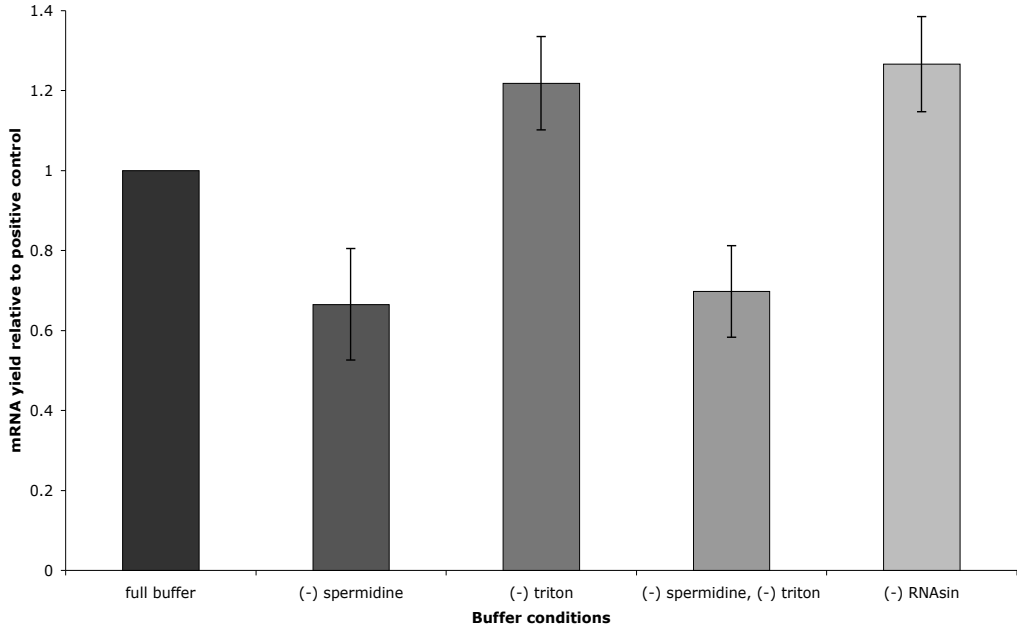

B

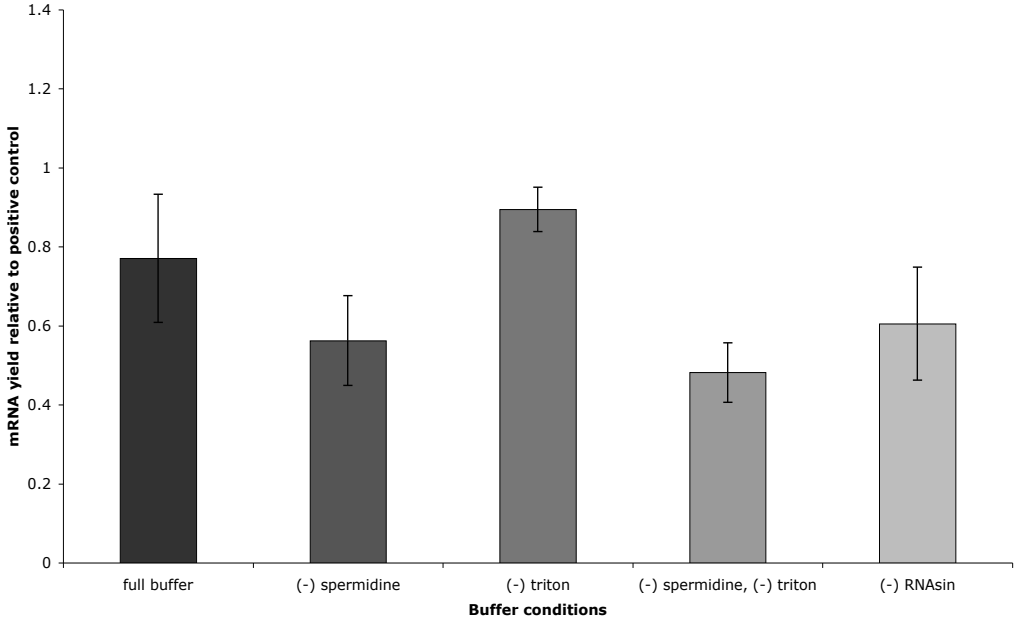

C

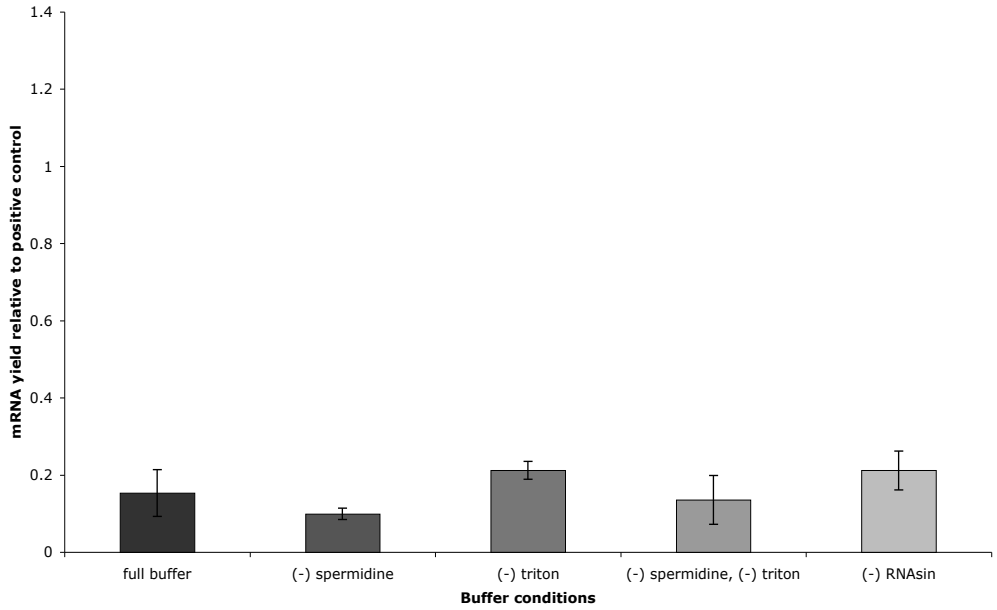

D

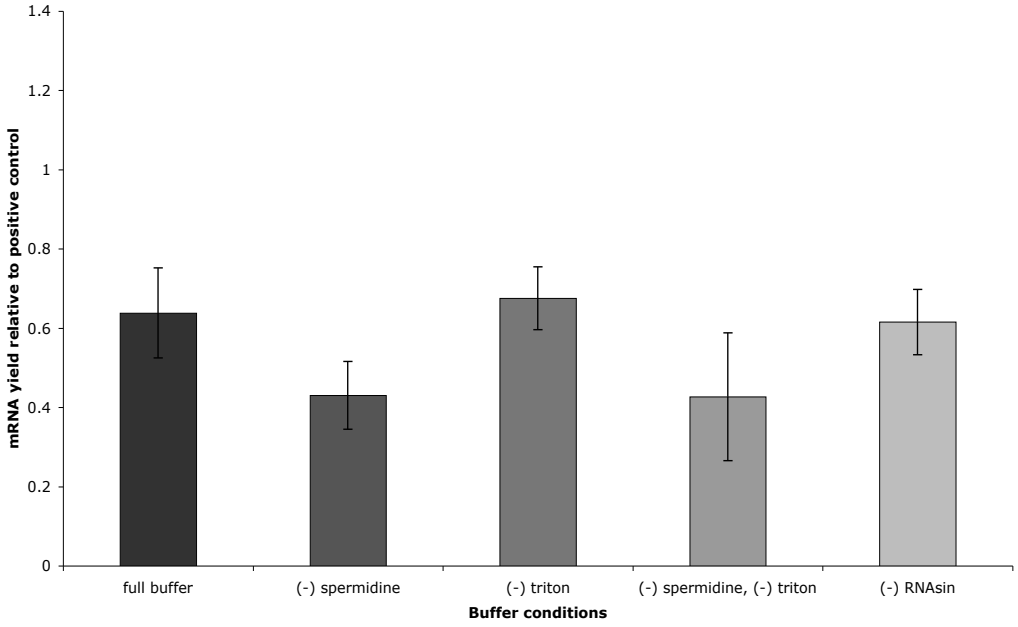

Figure 21: mRNA yield for each buffer experiment carried out relative to the mean mRNA yield for a standard positive control transcription reaction (i.e. full buffer, no lipid, 1µg lin-T7-luc DNA, 20 mM rNTPs, 2 hours incubation at 37 °C). A: Transcription buffer variations relative to full buffer (no lipid); B: DOPE/DNA transcription (whole sample)/full positive control (no lipid); C: DOPE/DNA transcription (liquid crystal phase)/full positive control (no lipid); D: DOPE/DNA transcription (supernatant phase)/full positive control (no lipid). L-R (in each data set): full buffer; buffer deficient in spermidine; buffer deficient in triton X-100; buffer deficient in both spermidine and triton X-100; buffer deficient in RNasin ribonuclease inhibitor. All experiments contributing to this figure contained 1µg lin-T7-luc DNA, 20 mM rNTPs, with 2 hours incubation at 37 °C. See appendix B, table 20.

The graphs presented in figure 21 indicate how the different buffer compositions affect the mRNA yield of transcription from four different sample types. The sample types include transcription with no lipid (figure 21 A), transcription from DNA in H_{II} DOPE, whole sample (liquid crystal and supernatant, figure 21 B), transcription from DNA in H_{II} DOPE, liquid crystal phase only (figure 21 C) and transcription from DNA in H_{II} DOPE, supernatant only (figure 21D). It is clear that the general trend in mRNA yield is conserved across the four different sample types. Figure 21 shows that removing triton x-100 from the transcription buffer causes an increase in the yield of mRNA. Transcription in the absence of triton appears to be higher in all situations, and does not cause degradation of RNA. Removing RNasin from the buffer causes degradation of RNA; RNasin cannot, therefore, be removed from the buffer, despite an apparent increase in mRNA yield in its absence. In all cases it is also seen that removal of spermidine reduces the transcriptional yield by as much as one half, in accordance with previous studies.

2.7 Partition coefficients of RNA transcribed in the H_{II} phase of DOPE

The mRNA produced was isolated from the liquid crystal and supernatant phases of the transcription sample and the mRNA yield from each phase was obtained and compared. Initially it was thought that analysing and comparing the location of transcribed messenger RNA would provide insights into the detailed mechanism of transcription, including the location of transcription, but recent work carried out has shown that the partition coefficient of DNA and RNA differ greatly. Results show that double stranded DNA is largely associated with the liquid crystal phase, while RNA is largely located in the supernatant phase, and these observations are supported by the literature. The partition coefficient experiments were also carried out under different buffer conditions to ascertain whether the reaction conditions had any effect on the partition coefficient of RNA. Samples were split into lipid and supernatant components by removing 15 µl of supernatant (from an estimated 16 µl remaining after incubation at 37 °C for two hours) from the finished transcript and recovering it to a new tube. Samples were then processed as normal, with the RNeasy kit.

2.7.1 Calculation of the partition coefficient of mRNA

The following equations demonstrate how the UV-visible sprectral data can be used to work out partition coefficients for RNA, as well as equilibrium constants and the Gibbs free energy.

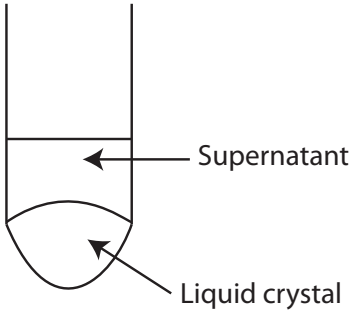

Figure 22: Diagram showing phase separation of transcription samples. The supernatant (15 µl) was removed and recovered to a new tube when the samples were split.

The RNA concentrations from the above separation can be used to work out the "real" concentrations in the supernatant and liquid crystal phases (when the supernatant is removed only 15 µl are taken which means a small residue, of around 1 µl will remain).

$$[RNA]_{TOT} = [RNA]_{LC}^{\exp} + [RNA]_{SN}^{\exp} \quad \textbf{(2.1)}$$

$$[RNA]_{SN}^{real} = [RNA]_{SN}^{\exp}\left(1 + \frac{(v-x)}{x}\right) \quad \textbf{(2.2)}$$

$$[RNA]_{LC}^{real} = [RNA]_{LC}^{\exp} - \left(\frac{v-x}{x}[RNA]_{SN}^{\exp}\right) \quad \textbf{(2.3)}$$

Where $[RNA]_{TOT}$ represents the maximum concentration of mRNA, $[RNA]^{exp}$ and $[RNA]^{real}$ are the recovered and true concentrations of mRNA in the liquid crystal (LC) and supernatant (SN) phases respectively. The true concentrations of mRNA, termed $[RNA]^{real}$ are calculated from the experimentally derived concentrations using a correction factor, which allows for a small amount of supernatant being left with the liquid crystal phase, where *v* represents the total assay volume remaining after transcription, estimated to be 16 µl, and *x* represents the volume of supernatant removed for purification (15 µl). The coefficient for partitioning of RNA into the supernatant phase (*K*) may then be calculated as follows:

$$K = \frac{[RNA]_{SN}^{real}}{[RNA]_{TOT}} \quad \textbf{(2.4)}$$

These parameters were calculated for buffers without spermidine, triton X-100 or either as follows:

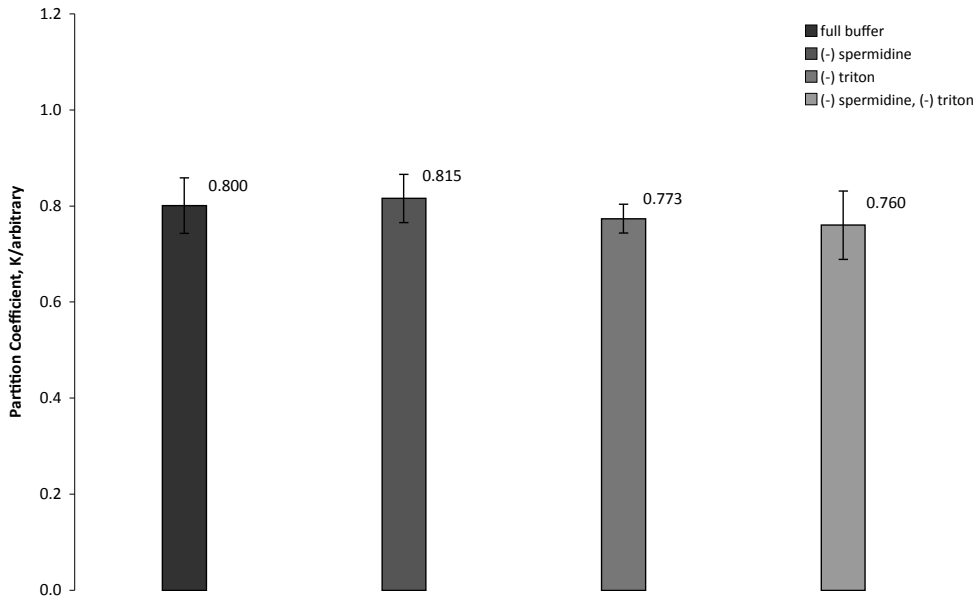

Figure 23: Graph showing the partition coefficient, *K*, for each buffer system, as calculated in equation (2.4). L-R: full buffer, buffer deficient in spermidine, buffer deficient in triton X-100, buffer deficient in spermidine and triton X-100. For data see appendix B, table 24.

It can be seen from figure 23 that the partition coefficient, *K*, as calculated in equation (2.4) is the same for all buffer systems, at around 0.8. This value shows there is a preference for RNA to be partitioned into the supernatant phase rather than the liquid crystal phase. These results are in good agreement with results in the literature from systems where mRNA is added to a liquid crystal phase rather than being transcribed from the phase itself; in this case the partition coefficient for H_{II} DOPE, in full buffer, was calculated as 0.79 ± 0.06.

2.7.2 Calculating the Gibbs free energy of the system

The "real" values for RNA concentration in the liquid crystal and supernatant calculated in equations (2.2) and (2.3) can then be used to calculate the equilibrium constant of the system (K_{eq}):

$$K_{eq} = \frac{[RNA]_{SN}^{real}}{[RNA]_{LC}^{real}} \quad \textbf{(2.5)}$$

This allows the Gibbs free energy (ΔG) to be calculated as per equation (2.6), where R is the ideal gas constant and T is the temperature in Kelvin.

$$\Delta G = -RT \ln K_{eq} \quad \textbf{(2.6)}$$

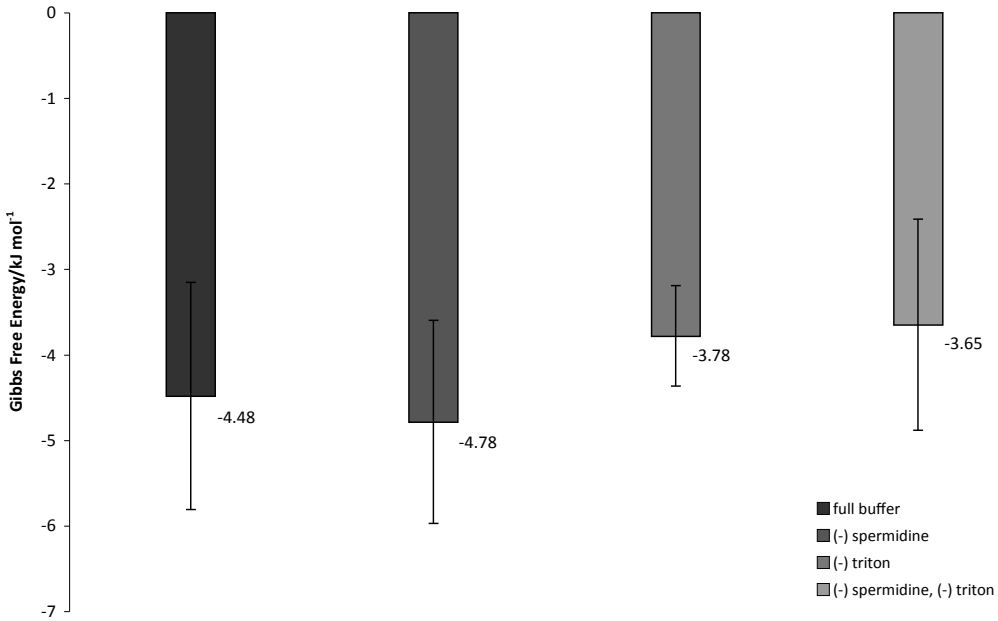

Figure 24: ΔG values calculated for the partitioning of mRNA into the supernatant phase of transcription experiments from the inverse hexagonal phase of DOPE/DNA. L-R: full buffer, buffer deficient in spermidine, buffer deficient in triton X-100, buffer deficient in spermidine and triton X-100.

Figure 24 shows that the Gibbs free energy for the system is negative for all buffers tested, showing that in all cases that partitioning of the RNA into the supernatant phase is a spontaneous and favourable process. The ΔG values for all samples overlap within error.

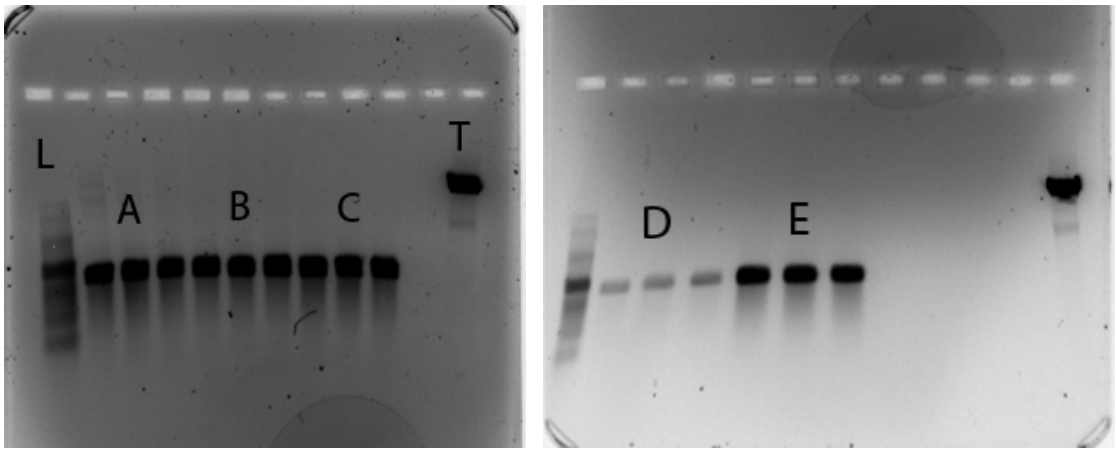

Figure 25: Gel electrophoresis of samples taken from partitioning experiments. Samples A and B represent positive controls (6 lanes in total); C: transcription from H_{II} lipid/DNA, whole sample; D: transcription from H_{II} lipid/DNA, liquid crystal phase only; E: transcription from H_{II} lipid/DNA, supernatant phase only.

The observed partitioning of the mRNA into the supernatant phase is mirrored by the gel electrophoresis image presented as figure 25. The faint bands labelled as 'D' represent mRNA recovered from the liquid crystal phase, while the darker bands (labelled 'E') show mRNA recovered from the supernatant.

2.7.3 Explanation of observed partition coefficients of RNA and DNA

As mentioned previously, the partition coefficient for linearised EGFP DNA (the same plasmid with the luciferase gene removed and replaced with the gene for GFP) was calculated to be ($8x10^{-3}$), with a ΔG value of roughly 15.4 kJ mol^{-1}.[75] It is clear that this partition coefficient and related change in Gibbs free energy is significantly different to those calculated for RNA and listed in the literature,[76] suggesting that in contrast to RNA, partitioning of DNA into the supernatant phase is energetically unfavourable.

In order to show why the partition coefficients of RNA and DNA between the H_{II} phase and the supernatant are so different the enthalpic and entropic contributions must be considered. To establish why it is favourable for DNA to be located in the pores of the liquid crystal phase we must consider three separate states: bulk water, DNA in bulk water and DNA associated with the H_{II} phase (see figure 26). The first two states create a negative change in entropy, ΔS, which results in a positive value for ΔG, as discussed in section 1.5 of this report. The third state can be split into two possible outcomes; the DNA in the pores or the DNA on the surface of the phase (figure 26 B and C respectively)[19]. In case C the DNA is held on the surface by electrostatic interactions between the surface and the phosphate backbone of DNA, releasing a small amount of water (and bound counterions) which produces a small increase in the disorder of the system[30, 77]. As DOPE is a zwitterion and has no net charge, interactions between the

DNA and the lipid are assisted by cations provided in the isotonic saline used in sample preparation, and in the transcription buffer. Literature sources suggest that screening of lipid headgroup phosphates by divalent magnesium ions causes a net positive charge to be placed over the surface of the channels. It is also suggested that this overall positive charge is balanced by chloride ions. DNA in solution is likely to be sheathed by sodium cations, with a theoretical maximum of 8.67×10^3 ions on each strand of lin-pT7*luc* DNA.[76] Scenario B results in increased disorder of the system as the sodium counterions and water molecules that were spatially constrained around hydrophobic minor groove of the DNA molecules are released. In this case enthalpic contributions are much smaller than entropic factors; a decrease in the conformational entropy of the system is offset by a larger increase in the configurational entropy resulting from the release of ions and water.[76] This positive change in entropy results in a negative value for the Gibbs free energy, proving that partitioning of DNA into the aqueous channels of the inverse hexagonal topology is a spontaneous and favourable process, thus explaining the low partition coefficient[19] for DNA in solution.

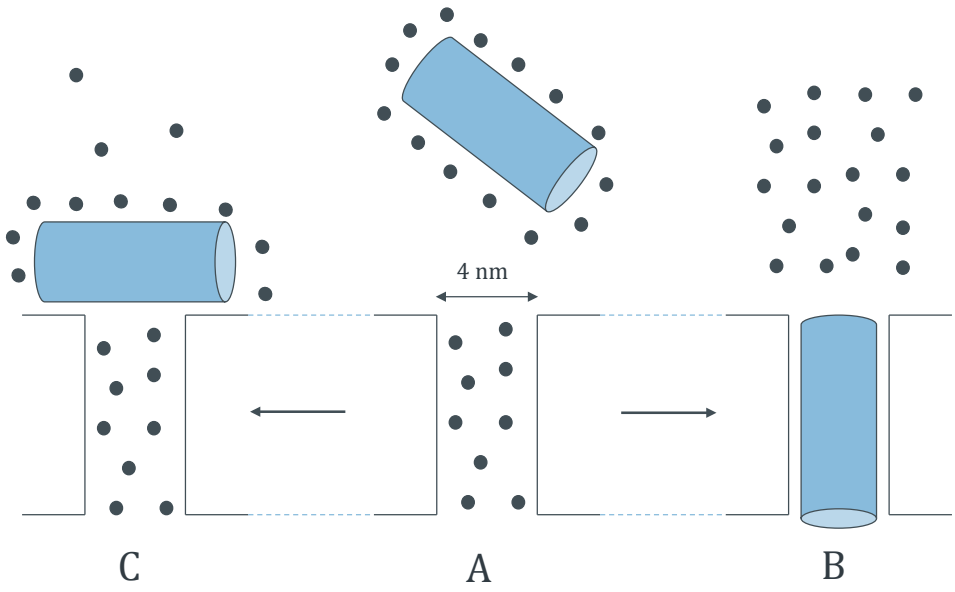

Figure 26: diagram showing possible conformations of DNA with the inverse hexagonal phase, grey cylinders represent DNA, black dots represent water, line structure represents H_{II} phase of DOPE. A: DNA dissociated from the hexagonal phase, surrounded by solvent cage. B: DNA situated in 2nm pore, with water molecules displaced. C: DNA associated with the top of the phase, releasing few water molecules.

With RNA, which is single stranded and much more flexible than DNA, the enthalpic contributions that arise from the conformation changes between primary and secondary structure (where the RNA binds to itself, in an intramolecular fashion via base pair interactions) must be accounted for. The secondary structure arises because the coherence length of RNA is 0.8 nm and much shorter than that of DNA (roughly 50nm)[19]; the coherence length of a polymer is defined as the distance over which the cosine of the angle from the origin becomes 1. This means that RNA is much more coiled than its rigid counter-part. As with DNA, when studying the partitioning into the inverse hexagonal phase of DOPE we must consider RNA in the bulk water alongside possible conformations of RNA associated with the inverse hexagonal phase, while also accounting for the secondary structure. This finding is in good agreement with the literature.[75]

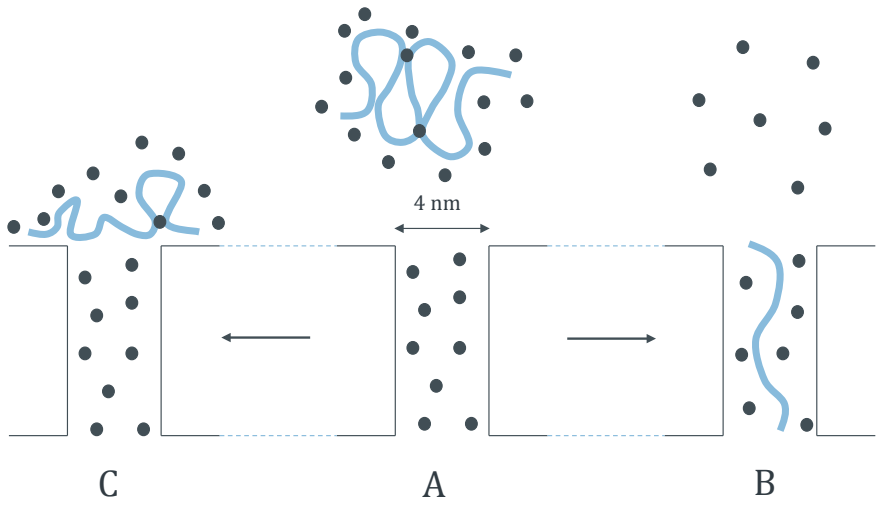

Figure 27: Schematic showing possible conformations of RNA with the liquid crystal phase; grey lines represent RNA, black dots represent water molecules and the line drawing represents the hexagonal phase. A: RNA dissociated from the phase in its secondary structure. B: RNA in the pores of the phase in its primary structure, with water molecules present. C: RNA associated with the surface of the phase.

Figure 27 shows the three possible states of RNA to be considered: A represents RNA dissociated from the pore, in a secondary structure surrounded by a solvent cage; B represents single stranded mRNA in the pores of the inverse hexagonal phase, displacing some (but not all) of the water from the pore; C shows the messenger RNA

associated with the surface of the phase. In case B there is a positive entropic contribution from the water leaving the pore although this is outweighed by a decrease in entropy caused by confining the RNA to a pore and breaking its secondary structure; this means that the value for the change in entropy is small and negative. The enthalpic contribution to the process is derived from the energy requirement to break the bonds formed in the mRNA secondary structure; this also gives a positive value, resulting in a positive change in the Gibbs free energy, suggesting that it is unfavourable for the RNA to be located in the pores of the H_{II} phase.

2.8 Effect of DTT on transcription

The effect on transcriptional yield of DTT, a redox agent that is commonly used in biochemical reactions, were evaluated. When DTT was removed from the transcription buffer a loss in activity was observed which could then be partially recovered by addition of DTT; this loss of activity was exploited to study the whereabouts of T7 RNA polymerase with regards to the liquid crystal and supernatant phases.

2.8.1 Recovering transcriptional activity with DTT – whole lipid sample

T7 RNA polymerase, in a 20µl volume containing buffers with and without DTT, was added to the H_{II} phase (which contained template DNA) and incubated at 37 °C for 2 hours. Transcription was then initiated in the samples by adding a solution of mixed ribonucleotides. Adding extra ingredients to the standard transcription assay will, of course, cause minor alterations to the buffer concentrations, these are recorded in appendix

Figure 28 shows that in the absence of the inverse hexagonal phase of DOPE, removing DTT from the buffer does not cause a significant decrease in transcriptional yield, and may therefore be considered non-essential for transcription. In the presence of a liquid crystal phase, however, transcriptional activity is inhibited when DTT is not included in the transcription buffer. Addition of DTT to the transcription mixture causes some recovery of the transcriptional yield although not to levels observed when DTT is included in the buffer as standard. It is therefore evident that some component of the liquid crystal phase causes reversible denaturation or inhibition of the polymerase in the absence of DTT in the buffer. It is not clear why the presence of liquid crystalline DOPE would have this effect, and whether this effect is the result of dissolved species in the supernatant or a phenomenon related to the bulk liquid crystalline phase itself. Experiments involving the incubation of T7 RNA polymerase with the inverse

hexagonal phase and then splitting the samples into liquid crystal and supernatant phases immediately prior to transcription were carried out to give insight into whether the polymerase is denatured and fixed to the liquid crystal phase or becomes inactive in the supernatant. The series of experiments listed in this section involved incubation of various species vital to transcription (namely DNA or polymerase) with the DOPE liquid crystal phase in the presence and absence of DTT. Full details of each experiment can be found in the appendix.

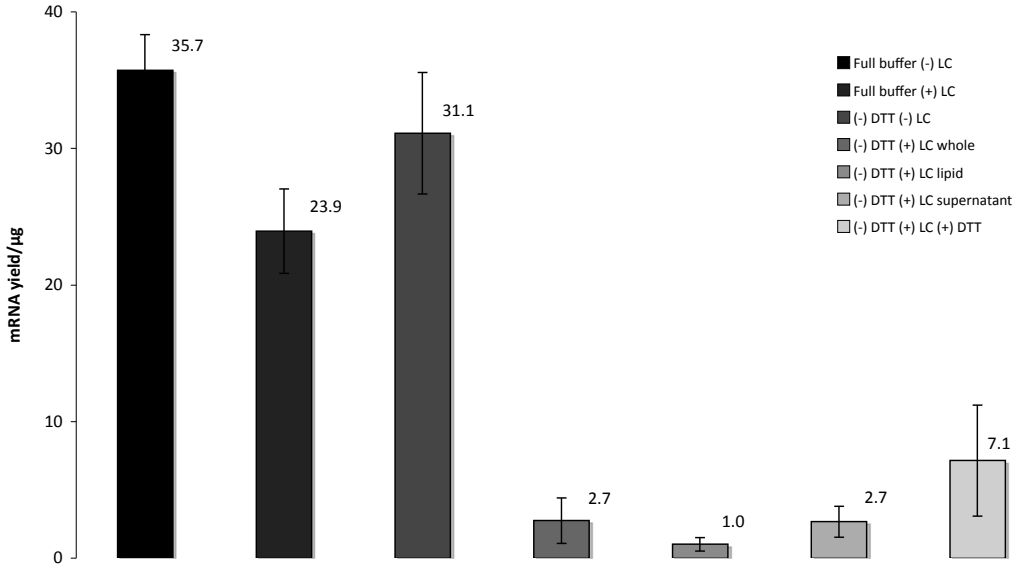

Figure 28: The effect of DTT on transcription. L-R: full buffer without H_{II} DOPE, full buffer with DOPE (note how familiar decrease in transcription is seen), buffer – DTT without DOPE (comparable to positive control within error), buffer – DTT with DOPE (whole sample), buffer – DTT with DOPE (lipid sample), buffer – DTT with DOPE (supernatant sample), buffer – DTT with DOPE (0.2µl DTT added for transcription to give a total assay concentration of 10 mM DTT). For data see appendix B, tables 28 and 30.

2.8.2 Locating the denaturant of T7 RNA polymerase

It is unclear whether the polymerase is inactivated by the phase itself or dissolved species in the buffer as a result of contact with the inverse hexagonal phase. In order to understand more about the location of the denaturant an experiment was devised in which the transcription buffer was left in contact with the phase before being removed and prepared for transcription.

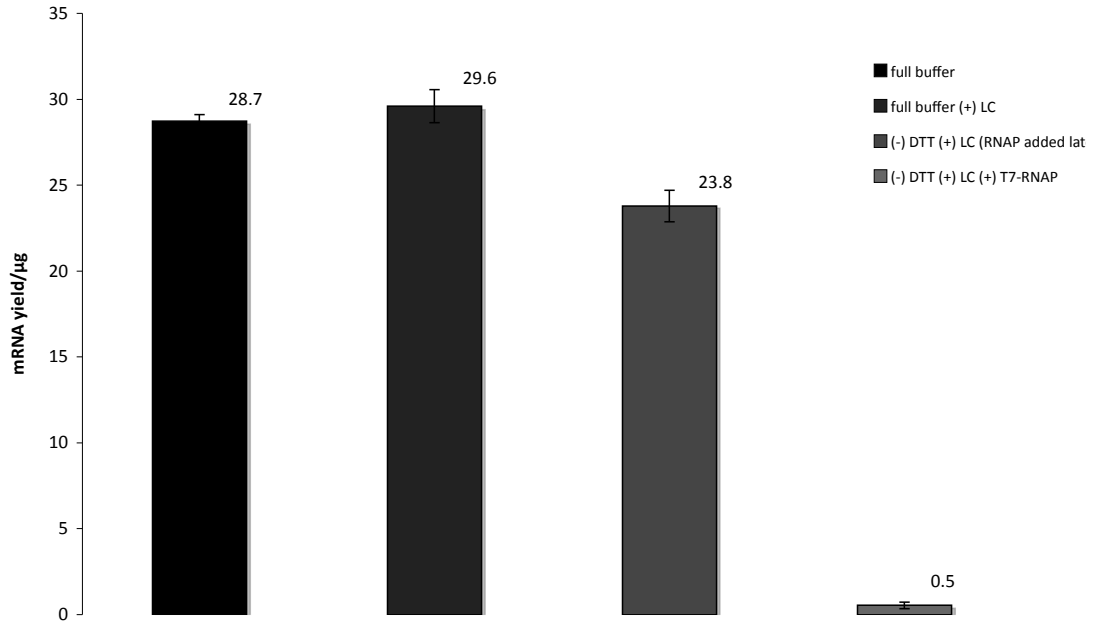

Figure 29: Graph showing transcription using T7 RNA polymerase and transcription buffer incubated in the presence of H_{II} DOPE for 2 hours at 37 °C

Figure 29 shows that the denaturing agent of T7 RNA polymerase is part of the phase itself and not dissolved species. The mRNA yield from experiments where the buffer had been in contact with the phase was 23.8 ± 2 µg compared with 0.5 µg for experiments where the T7 RNAP had been incubated with the lipid phase in addition to the transcription buffer.

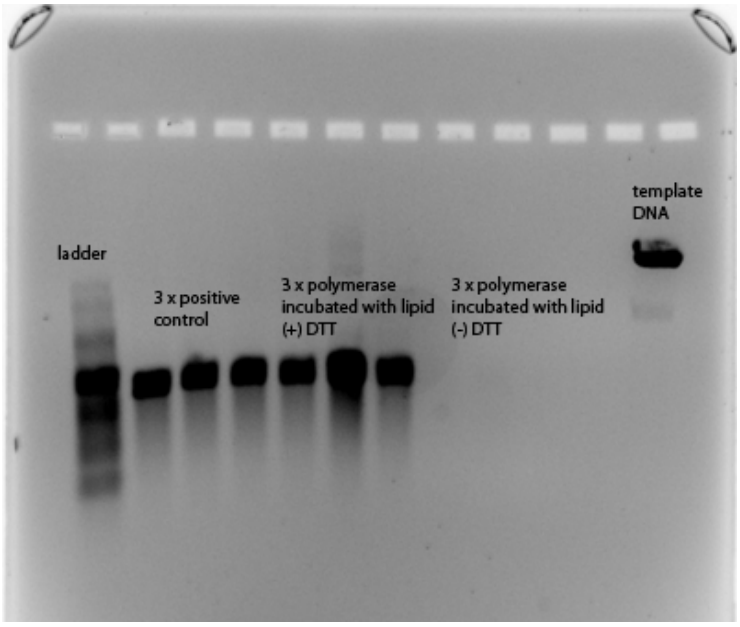

Figure 30: Gel electrophoresis image of mRNA production from DOPE/DNA H_{II} phases in the presence and absence of DTT.

2.8.3 Recovering transcriptional activity by adding DTT – supernatant studies

T7 RNA polymerase was incubated with the inverse hexagonal phase consisting of DOPE only (2 hours, 37 °C). The supernatant was then recovered (15 µl of the estimated 16µl total remaining after incubation) and prepared for transcription by adding template DNA (1µg) and mixed ribonucleotides. For details on the buffer concentrations resultant from these additions see appendix B.

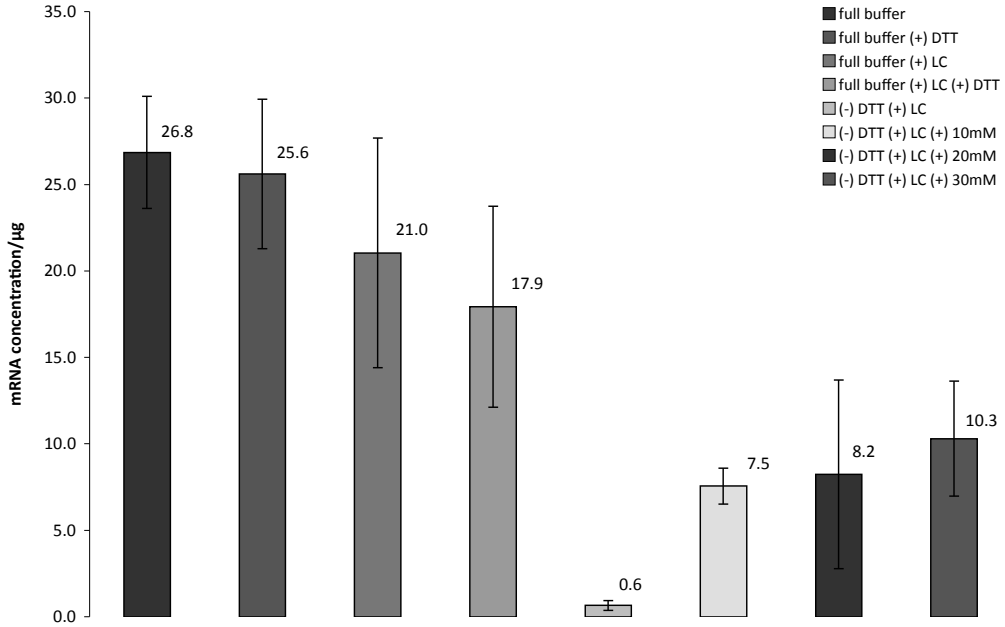

Figure 31: Effect of adding DTT to supernatant samples of T7 RNA polymerase denatured by contact with H_{II} DOPE. L-R: full buffer 10 mM DTT, 20 mM DTT; full buffer with H_{II} DOPE 10 mM DTT, 20 mM DTT; buffer without DTT with H_{II} DOPE and added DTT (0 mM, 10 mM, 20 mM). For data see appendix B, tables 29 and 30.

It can be seen in figure 31 that adding extra DTT to transcription buffers that already contain DTT does not cause an increase in transcription and, in fact, appears to cause the transcriptional yield to decrease. Adding DTT to those samples where it had not already been included caused transcriptional activity to be recovered, although the levels observed when DTT is included in the buffer from the beginning were not achieved. This shows that there is inactivated polymerase present in the supernatant phase of the sample, and that it is unlikely that the polymerase becomes bound to the surface, although to ensure that this is the case transcription from the liquid crystal phase itself must also be attempted and the mRNA produced analysed.

2.8.4 Recovering transcriptional activity with DTT – liquid crystal phase studies

If denaturation of the polymerase in the absence of DTT causes binding to the liquid crystal phase, inducing transcription by addition of DTT along with substrates (ribonucleotides and template DNA) would cause transcript RNA to be produced from the liquid crystal phase. The liquid crystal phases remaining when the supernatant is removed were prepared for transcription according to appendix A2 and analysed for transcript RNA production.

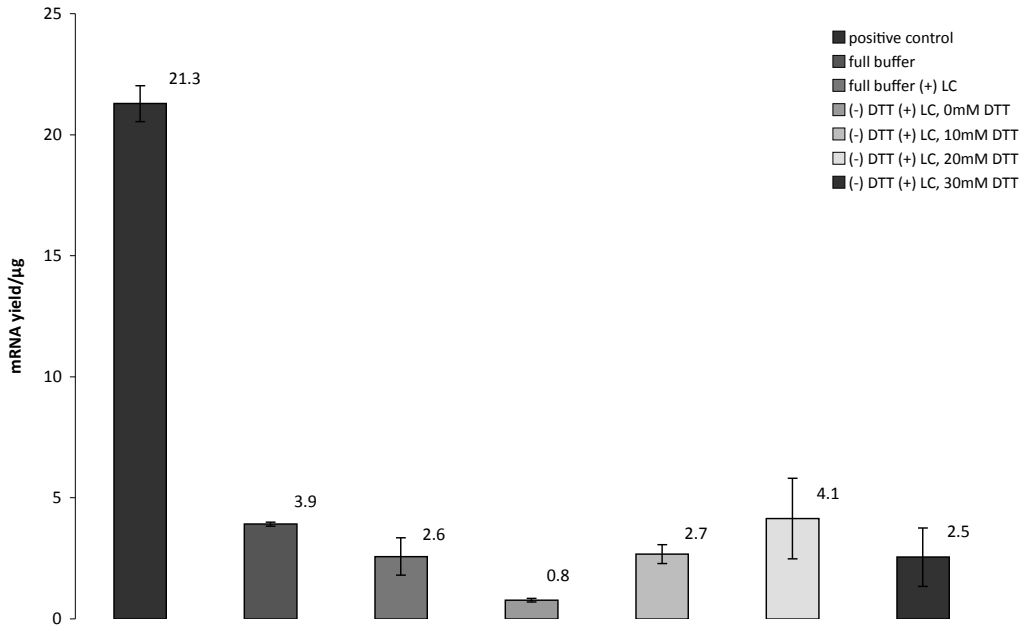

Figure 32: Transcription from liquid crystal phase with and without DTT. L-R: positive control (full reaction); positive control (15 µl removed, with no liquid crystal); full buffer with LC (15 µl supernatant removed); buffer without DTT, LC phase (15 µl supernatant removed, 0 mM DTT added); buffer without DTT, LC phase (15 µl supernatant removed, 10 mM DTT added); buffer without DTT, LC phase (15 µl supernatant removed, 20 mM DTT added); buffer without DTT, LC phase (15 µl supernatant removed, 30 mM DTT added). For data see appendix B, table 35.

Figure 32 shows that when DNA is not included in the liquid crystal phase, it is possible to recover transcription with the addition of DTT. When examining columns 4 through 7 of figure 32 an increase in mRNA yield is observed when the transcription mixture added to the liquid crystal phase is supplemented with DTT. There also appears to be an optimum concentration for DTT in terms of recovery of transcription, at 20 mM DTT. This suggests that polymerase is associated with the liquid crystal phase in a reversible fashion, as the levels of transcription recovered (4.1 ± 1.7) µg at 20 mM added DTT) are comparable, within error, to those of the full buffer (3.9 ± 0.1) µg.

2.9 Including DNA in the liquid crystal phase

It was suggested that when the DNA is present as part of the liquid crystal phase that recovering the transcriptional activity of the system may not be possible. It is possible that the presence of DNA in the phase would cause stronger binding of inactivated polymerase to the inverse hexagonal phase. Experiments were conducted in which the polymerase was incubated with the H_{II} phase of DOPE/DNA, in buffers with and without DTT, split into liquid crystal and supernatant components and prepared for transcription.

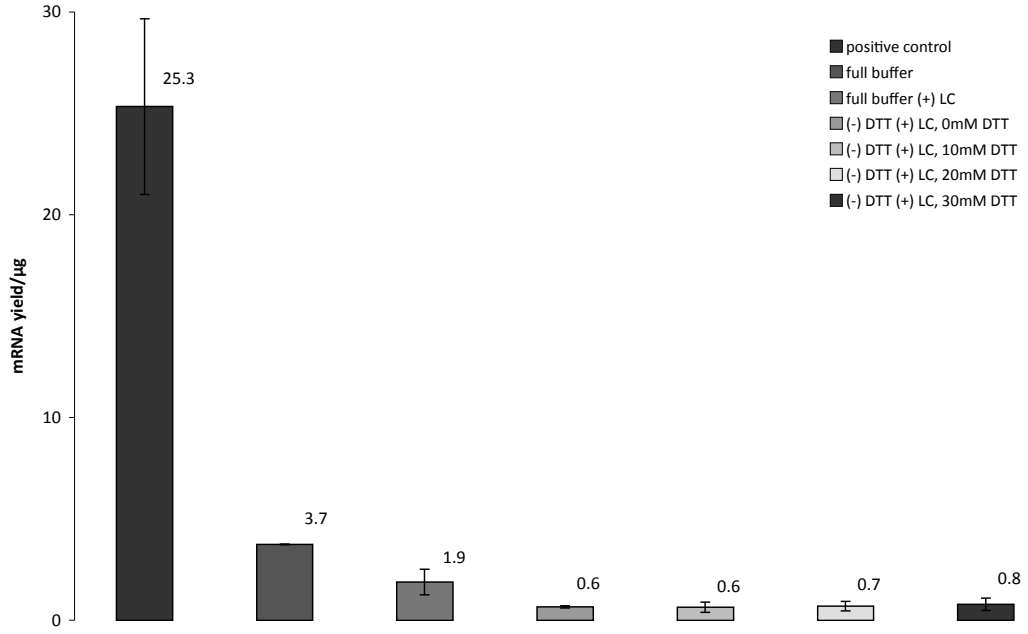

Figure 33: Recovery of transcriptional activity by adding DTT to T7 RNA polymerase denatured by DOPE/DNA, liquid crystal studies. L-R: positive control, full buffer, no LC phase; full buffer, no LC phase, 15 µl removed; full buffer + LC, 15 µl supernatant removed; buffer without DTT + LC, 15 µl supernatant removed, 0 mM DTT added; buffer without DTT + LC, 15 µl supernatant removed, 10 mM DTT added; buffer without DTT + LC, 15 µl supernatant removed, 20 mM DTT added; buffer without DTT + LC, 15 µl supernatant removed, 30 mM DTT added. For data see appendix B, table 40.

Figure 33 demonstrates that when DNA is associated with the inverse hexagonal phase, the transcriptional activity of polymerase inactivated by the lipid may not be recovered. For comparison, when 10 mM DTT is added to the denatured polymerase on the liquid crystal phase in the presence of DNA the transcriptional yield of RNA is (0.6 ± 0.3) µg, when DNA is not included as part of the inverse hexagonal phase but added later the concentration of RNA recovered is (2.6 ± 0.4) µg. This implies that denatured polymerase could be irreversibly bound to the liquid crystal phase by interaction with

the DNA. To reinforce this hypothesis the transcriptional yield of the supernatant samples must also be compared with those obtained from the liquid crystal phase.

2.9.1 Comparison of reactivation of T7 RNA polymerase – H_{II} DOPE and DOPE/DNA

The data from experiments where transcription was performed on the liquid crystal and supernatant components of experiments involving denaturation of T7 RNA polymerase denatured by DOPE and DOPE/DNA were normalised and compared.

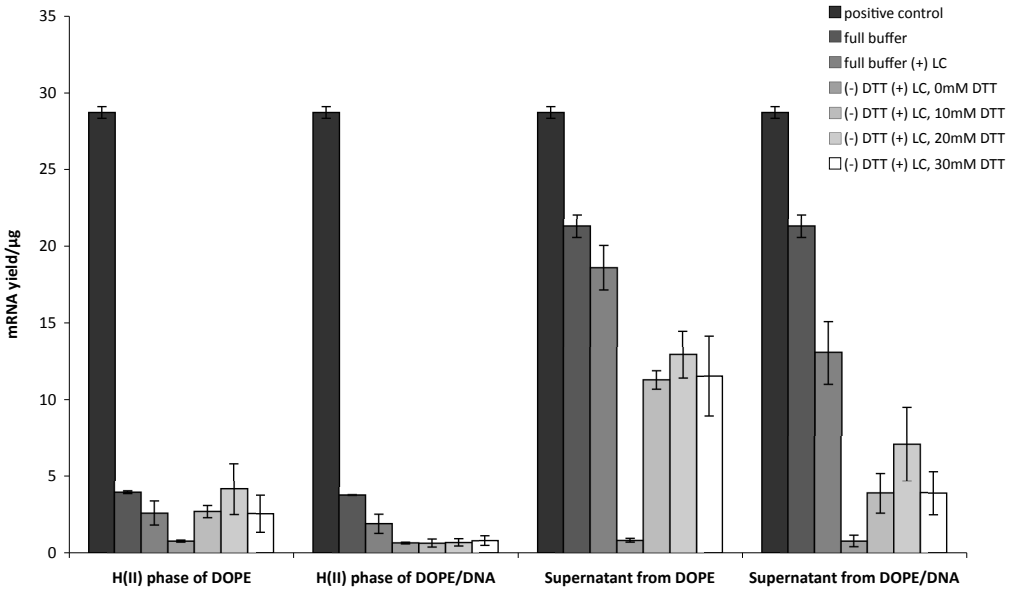

Figure 34: Normalised data comparing transcript RNA recovered from liquid crystal and supernatant components of reactions containing T7 RNA polymerase denatured by DOPE and DOPE/DNA. L-R (x-axis): liquid crystal component of DOPE only (15 µl supernatant removed); liquid crystal component, DOPE/DNA (15 µl supernatant removed); supernatant component, DOPE only (15 µl supernatant recovered for transcription); supernatant component, DOPE/DNA (15 µl supernatant recovered for transcription). L-R (each data set): positive control (full reaction); full buffer, no lipid phase present; full buffer + LC phase; buffer without DTT + LC, 0 mM DTT added for transcription; buffer without DTT + LC, 10 mM DTT added for transcription; buffer without DTT + LC, 20 mM DTT added for transcription; buffer without DTT + LC, 30 mM DTT added for transcription. For data see appendix B, tables 35 and 40

Figure 34 shows that levels of transcription are greater in those samples where the template DNA was not included as part of the DOPE inverse hexagonal phase. This implies that the T7 RNA polymerase is not as available for recovery when it has been denatured by DOPE with DNA in it, suggesting that the polymerase is more strongly and perhaps irreversibly bound to the DOPE/DNA phase. It is also apparent that there

is an optimum level of DTT addition to the system; the maximal transcriptional activity is observed when 20 mM DTT is added to the transcription mixture, which then drops as the DTT concentration is increased to 30 mM. This is mirrored by a fall in mRNA yield as the concentration of DTT was increased to 30 mM in experiments carried out in the full standard buffer in figure 23.

2.10 Explanation of observed effects of DTT on the system

DTT (1,4-dithio-DL-threitol; 1,4-dimercapto-2,3-butanediol; Cleland's reagent) is a powerful reducing agent first synthesised in 1949[78], and whose biological significance wasn't discovered until 1964 when its advantages as a protecting agent of sulfhydryl groups in proteins became apparent[79]. Since this time DTT has been used extensively in the reduction of disulfide bonds, with a standard search in a single database of biomedical journals returning over 10,000 references in the last quarter of a century[80]. The key characteristic of DTT is its unusually negative redox potential of -0.332 V at pH 7 and -0.366 V at pH 8.1; the transcription buffer (full buffer) used in this investigation is measured as having a pH of 7.6[79]. The reaction of DTT in the protection of sulfhydryl groups is driven by formation of a thermodynamically favourable six-membered ring[79, 81] formed by a 6-exo-dig cyclisation, as permitted by Baldwin's rules[82]. This reaction occurs as detailed in figure 35 and is complete in a few minutes at pH 8.

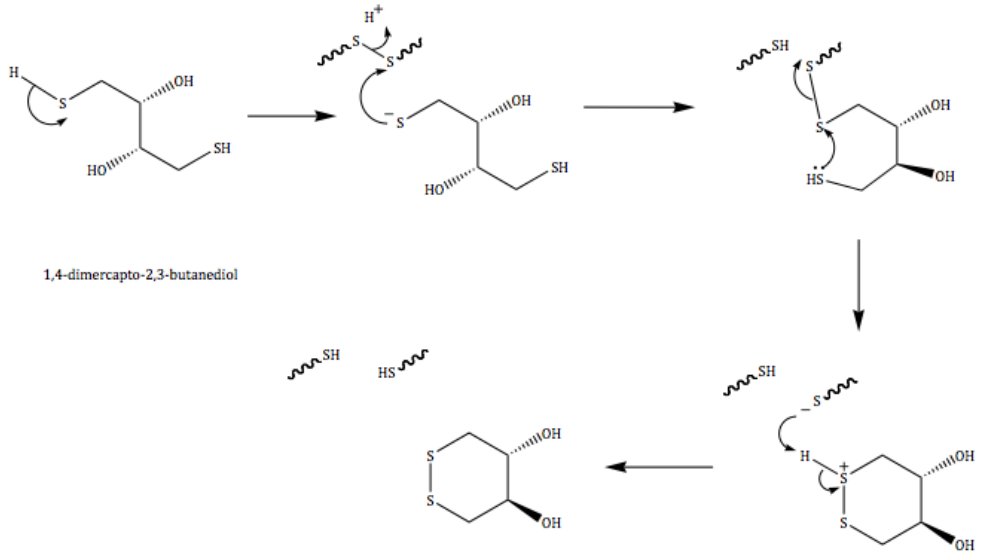

Figure 35: Mechanism of preservation of sulfhydryl groups by DTT (1,4-dimercapto-2,3-butanediol) by formation of a six-membered cyclic disulfide; reaction obeys Baldwin's rules as cyclisation is 6-exo-dig. Scheme adapted from mechanism propsed by Cleland, 1964.

The T7 RNA polymerase loses activity in the presence of DOPE and the absence of DTT; reasons for this are likely to be linked to the effect of the DOPE on the pH of the buffer at the surface of the liquid crystal phase. The pK_a of the ethanolamine head group is given as 11.25 (for DMPE)[5]; this suggests that the interface between the liquid crystal phase and the supernatant could be much more alkaline than the bulk solution. Under these conditions it would be expected that there was some effect on the structure of the protein; it is likely that important disulfide links may be broken and others formed, rendering the polymerase inactive.

As mentioned previously, transcription of template DNA by T7 RNA polymerase involves two conformations, the initiation complex, where a short DNA-RNA hybrid exists in the active site of the enzyme, which transforms into the elongation complex, with an exit pore for the messenger RNA by rearrangement of subdomains. There are two disulfide links that are implicated in the transition between the initiation and elongation complexes, the first is between residues D147 and R292, where the alpha-carbons are located 5.4 Å apart in the initiation complex and 43 Å in the elongation complex. The second disulfide link of interest is formed between K179 and M750 are widely separated in the initiation complex, at a distance of 60 Å but become close in the elongation complex at 5.7 Å[37].

The evidence suggests that the decrease in polymerase activity observed in the presence of lipids and its recoverability by addition of DTT is caused by disruption of the protein structure, most likely a consequence of formation of unwanted disulfide links. It is possible that the presence of DTT aids the transformation between initiation and elongation complex in the presence of DOPE; if the enzyme is unable to move out of the initiation complex the result would be abortive cycling and release of many short transcripts. This hypothesis could be tested by the use of polyacrylamide gel electrophoresis, which would show the presence of single-stranded oligonucleotides of less than 9 bases in length.

2.11 Effects of DNA concentration

The effect of DNA concentration on transcriptional yield was explored to show that DNA leaching from the liquid crystal phase was not responsible for transcription levels observed. Investigations into the partitioning of DNA into the inverse hexagonal phase of DOPE show that the partition coefficient of DNA in the supernatant phase is ≤ 8 x 10^{-3}. This indicates that the amount of linearised GFP DNA present in the supernatant is roughly 0.008 µg of a 1 µg sample[76]. As the two DNA templates used in the lab are of similar length and structure, it is reasonable to assume that this would be the case for the luciferase gene, and indeed this has been shown to be the case. This means that the quantity of template DNA present in the supernatant phase is much lower than that of the liquid crystal phase or included in a standard transcription reaction. This evidence suggests that transcription occurs from DNA that is located within the inverse hexagonal channels, and would not be possible from DNA in the supernatant (see figure 36).

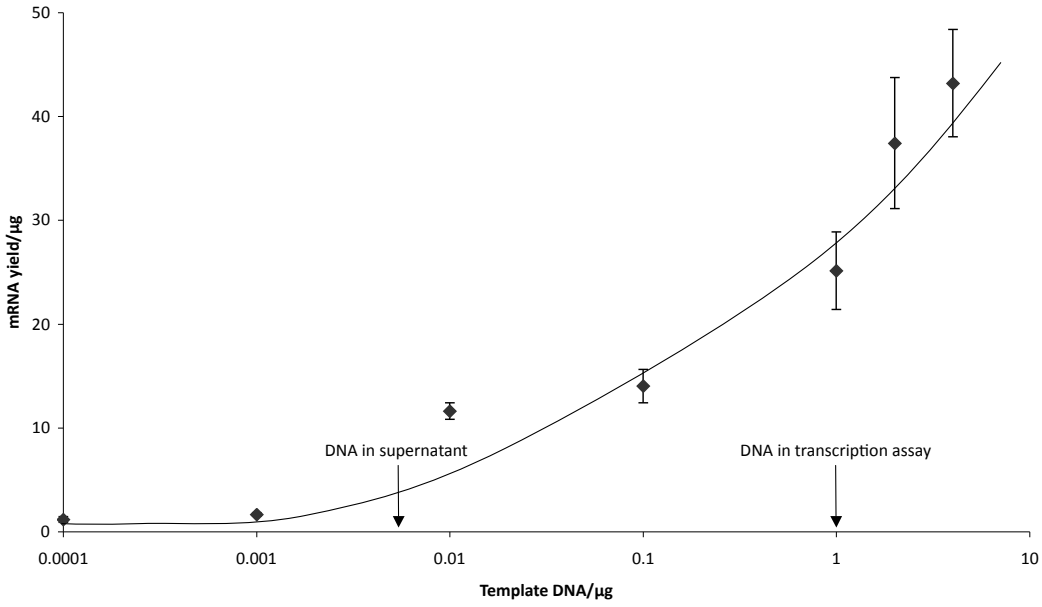

Figure 36: Transcript RNA produced from increasing quantities of template DNA. The quantities in the standard transcription reaction and in the supernatant of the heterogeneous liquid crystal transcription samples are clearly marked on the x-axis. For data see appendix B, table 41.

That the DNA is physically associated with the liquid crystalline phase is also evident from other reports in the literature: DOPE and DNA form stable mesophases[1, 13, 16, 18-20, 23, 60-74] and, as reported in the literature, the DNA does not partition into the supernatant phase upon addition of transcription buffers, nucleotides or polymerase[1,

[83, 84]. In addition to this, several control experiments have shown that transcription mixture that had been incubated for 2 hours with DOPE/DNA buttons could not sustain transcription when removed from the H_{II}-DOPE/DNA system and added to fresh ribonucleotides and polymerase[1, 83, 84]. Similarly, when transcription buffer containing DNA was incubated with H_{II} DOPE for 2 hours and then removed, before mixing it with ribonucleotides and polymerase, no transcript RNA was detected, even after the sample has been incubated for several hours[1, 83, 84].

Several studies have shown the formation of inverted hexagonal systems of DOPE with long stretches of double stranded DNA in the aqueous channels (for reviews see refs. 5, 75,78). As the diameter of these channels is typically only slightly larger than that of the DNA itself, electrostatic interactions are important in these structures, and in the case of neutral (zwitterionic) lipids such as DOPC and DOPE these interactions are mediated by cations[19]. The optimum equilibrium geometry of a lipid/DNA mixture is determined by a balance of the elastic (spontaneous curvature) and electrostatic properties of the system[85, 86]; the formation of an inverse hexagonal phase occurs by cylindrical wrapping of the DNA by lipid molecules, as the DNA is comparatively rigid[19]. In the case of DOPE, which has a high negative spontaneous curvature, the inverse hexagonal phase is observed with and without DNA[1, 16, 18, 19, 85-87].

2.12 Time-course experiments

Time-course experiments were undertaken to establish the kinetic properties of T7 RNA polymerase transcribing from DNA in and out of the inverse hexagonal phase of DOPE. Experiments were set up and removed for purification at regular time intervals, giving insight into how the production of mRNA varies over the course of the reaction.

2.12.1 Time-course experiments without DOPE

A time course experiment was set up such that transcription in the solution phase, without DOPE was prepared and triplicate samples were removed and purified at measured intervals. The transcript RNA was isolated and purified and the concentration was measured using the absorbance of light of wavelength 260nm. The mRNA yield was calculated in μg.

Figure 37 shows that the concentration of RNA produced increases linearly over the first hour of the experiment. The rate of production of RNA may be calculated as the

gradient of the graph in the kinetic region of the experiment (45 minutes) and is found to be 0.31 μg minute^{-1}. It is apparent from this experiment that after the first hour of incubation at 37 °C the reaction has reached saturation with no further RNA being produced. As the mRNA extracted from experiments that had been incubating for 2.5 hours was shown by gel electrophoresis to be of the correct length the transcription experiments which were allowed to progress for 2.5 hours are therefore representative of the total mRNA production of the system under varying conditions.

2.12.2 Time-course experiments – H_{II} DOPE/DNA

The inverse hexagonal phase of DOPE/DNA was prepared as standard and set up for transcription under standard conditions (full buffer, 20 mM total [rNTP], 1μg linearised T7 luciferase DNA). Individual samples were incubated at 37 °C and removed from the water bath at various time intervals for processing. The yield of mRNA was calculated from the A_{260} values obtained using the Nanodrop ND-1000.

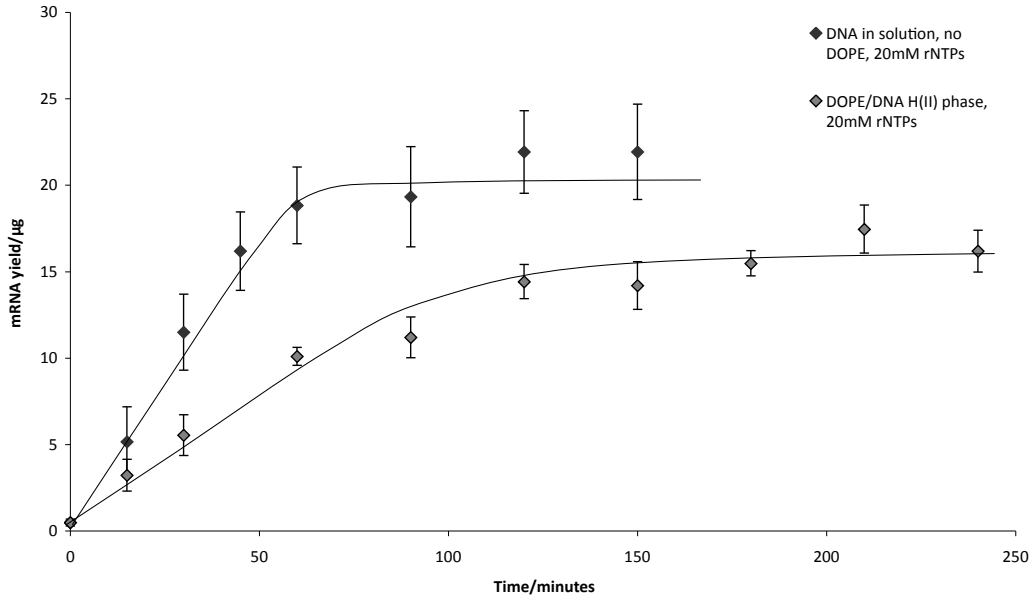

Figure 37: graph showing how the rate of transcription is affected by the inclusion of template DNA in the inverse hexagonal phase of DOPE. For data see appendix B, tables 45 and 47.

It can be seen in figure 37 that the rate of production of mRNA from template DNA in the inverse hexagonal phase of DOPE occurs at roughly half the rate of transcription in the absence of lipid, with a calculated rate of 0.16 μg minute^{-1}, compared with 0.31 μg minute^{-1}. It is important to note that for the experiments where the effects of buffer components were compared in the presence and absence of DOPE that all samples

were transcribed for 2.5 hours (150 minutes) and that samples with and without inverse hexagonal DOPE appear to have been at saturation, although when the DNA is associated with the lipid the total mRNA produced is lower than when DOPE is not present. This drop in activity could be caused by the fact that T7 RNAP abortively cycles through the initiation stages of transcription when conditions are not optimum. Such abortive cycling would result in an overall depletion of the nucleotide concentration, with particular effect on the concentration of rGTP as the initiation sequence of transcription by T7 RNA polymerase has been shown to be rich in rGTP. This is in good agreement with observations that the mRNA produced from DNA in the inverse hexagonal phase of DOPE is consistently lower than comparable experiments that do not contain a liquid crystalline phase.

2.12.3 Time-course experiment – buffer without spermidine

The buffer deficient in spermidine was used to assess transcriptional activity over time, in the absence of DOPE. Transcription was set up in buffer JC/5221/22/2R and transcribed at 37 °C over a time period of 5 hours, with samples being removed and processed at regular time intervals.

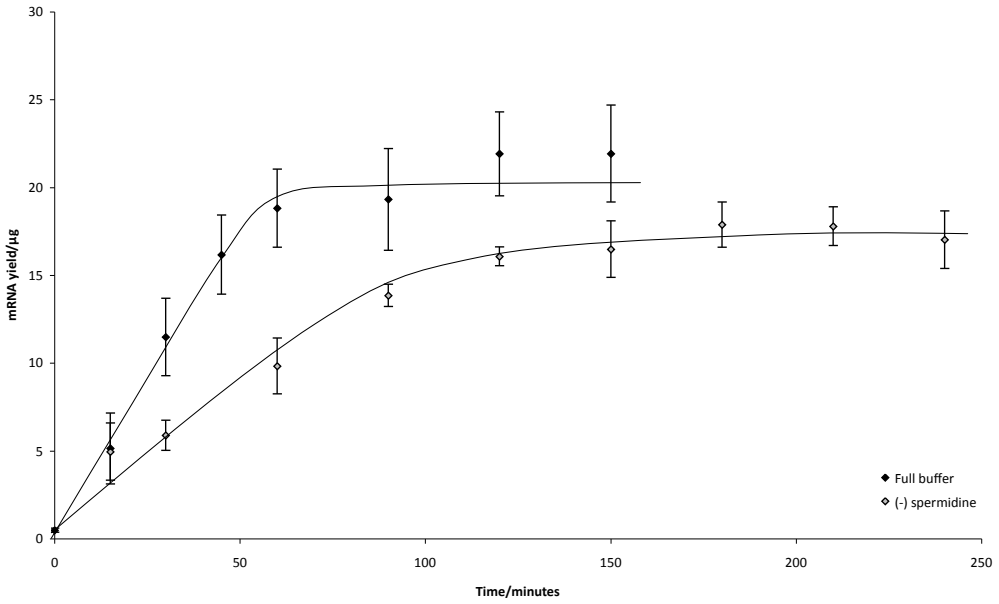

Figure 38: Time course experiment from transcription in buffer deficient in spermidine, 20 mM total ribonucleotide concentration, no lipid present. Transcription time variable, from groups of samples in triplicate. Data retrieved from experiment JC/5221/82. For data see appendix B, tables 45 and 49.

Figure 38 shows that removing spermidine from the transcription reaction slows the rate of transcription from 0.31 μg minute^{-1} to 0.16 μg minute^{-1}. The reaction also reaches saturation at a lower mRNA concentration that when spermidine is included in the transcription buffer at 17 μg compared with roughly 26 μg for the full buffer.

2.13 Effect of varying ribonucleotide concentration

The concentration of ribonucleotides was varied to show how transcriptional yield is related to substrate concentration. Initially the total [NTP] of 20 mM was chosen, as it was the concentration to produce transcript RNA most consistently by gel electrophoresis, although detailed kinetic studies of this must be obtained.

2.13.1 Varying rNTP concentration without a liquid crystal phase

In the absence of a liquid crystal phase, the ribonucleotide concentration was varied across a concentration gradient from 5 mM to 40 mM in 5 mM increments. Transcription was carried out for 2.5 hours at 37 °C in full buffer. Transcript RNA was processed and purified using the RNeasy lipid tissue mini kit from Qiagen and yields were calculated from absorbance values at 260 nm obtained using the Nanodrop ND-1000.

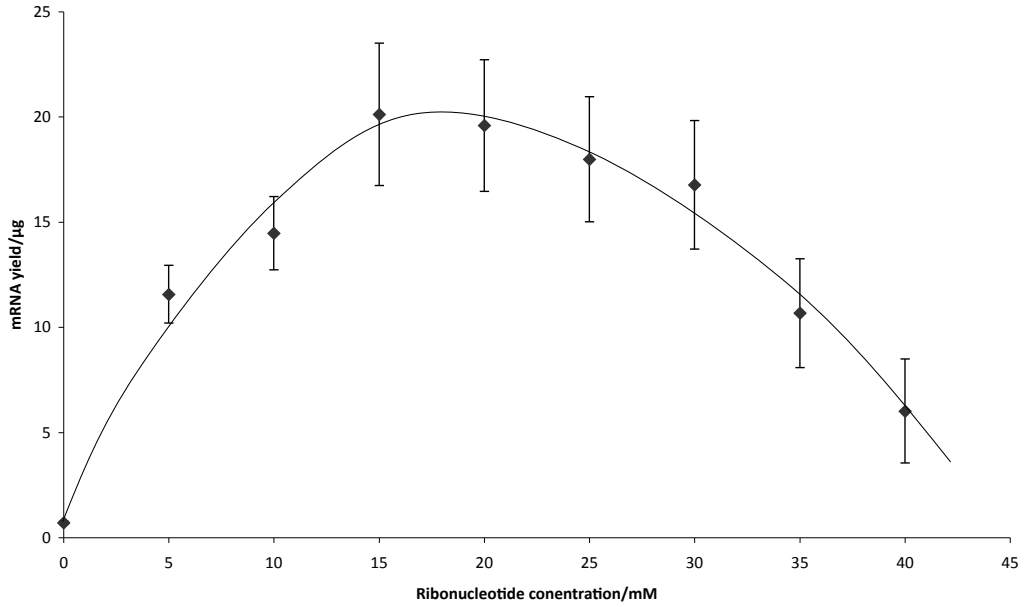

Figure 39: Transcript RNA yields produced from a concentration gradient of ribonucleotides over 2.5 hours at 37 °C . For data see appendix B, table 51.

It can be seen in figure 39 that there is an optimum nucleotide concentration in the range of 15-30 mM, suggesting that the chosen nucleotide concentration of 20 mM is at the maximal activity of the enzyme. It is therefore suggested that the transcriptional levels observed are limited by DNA concentration and polymerase concentration. Analysis of the transcript RNA produced in the system after a shorter transcription time could show more clearly how the production of messenger RNA varies with nucleotide concentration.

2.13.2 Varying rNTP concentration with the H_{II} phase of DOPE/DNA

The same nucleotide gradient was assembled and used to transcribe from DNA in the inverse hexagonal phase of DOPE.

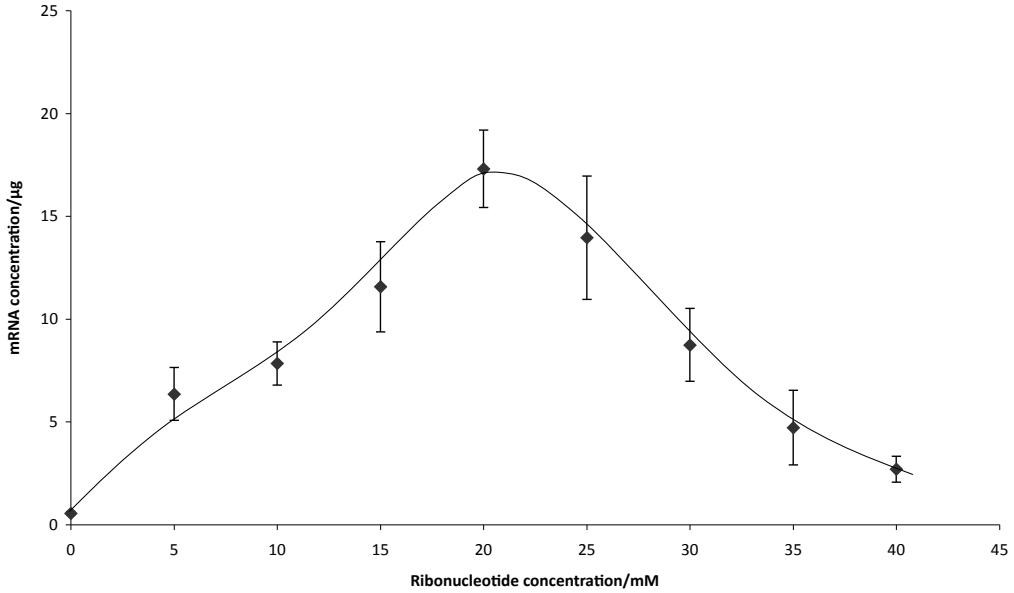

Figure 40: transcript RNA yield from DNA in the inverse hexagonal phase of DOPE over 2.5 hours at 37 °C . For data see appendix B, table 53.

Figure 40 shows a clear maximum transcriptional yield associated with a total nucleotide concentration of 20 mM. As with the time course experiments it can be seen that the presence of the liquid crystalline phase slows the reaction down; this is represented by the low amounts of RNA recovered at ribonucleotide concentrations lower than 20 mM. At concentrations greater than 20 mM the transcriptional yield falls again, this could be caused by inhibition of polymerase by excess ribonucleotides.

2.13.3 Varying rNTP concentration without a liquid crystal phase, short transcript time

A transcription identical to that outlined in 5.3.1 was assembled and allowed to incubate at 37 °C for 30 minutes. Transcription was then halted by addition of Qiazol lysis reagent and the transcript RNA purified using the RNeasy kit as standard. Transcript RNA was then analysed using the Nanodrop ND-1000 UV-visible spectrometer.

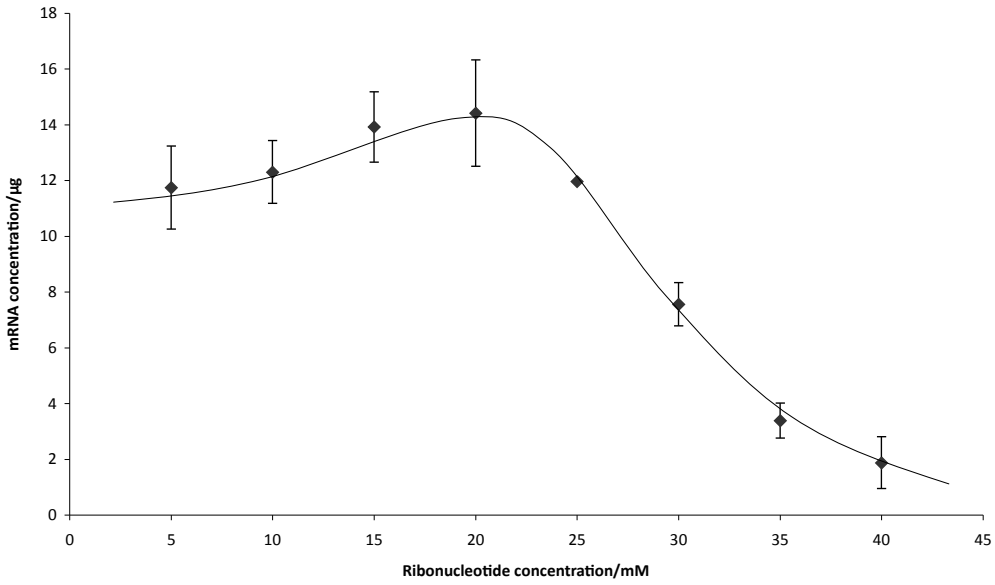

Figure 41: Transcript RNA yields produced from a concentration gradient of ribonucleotides over 30 minutes at 37 °C . For data see appendix B, table 55.

It is observed in figure 41 that the transcription from concentrations of mixed ribonucleotides lower than 20 mM produce similarly high yielding results over a time period of 30 minutes (11.7 ± 1.5 µg at 5 mM compared with 14.4 ± 1.9 µg at 20 mM). The slope of the graph in this region, however, combined with results observed over longer time periods, suggests that the lowest concentration of ribonucleotides may have reached saturation at this point. Levels of transcription from concentrations such as 20 mM over longer time periods are higher, with an expected transcriptional yield of around 25 µg, suggesting that the transcription reaction is still ongoing; indeed, we know from the time course experiment outlined in section 5.2.1 that the reaction at this concentration doesn't reach saturation within the first hour. In contrast to the

transcriptional yields obtained from concentrations of rNTPs lower than 20 mM, the transcriptional activity observed above 40 mM falls sharply, and is observed to be 1.9 ± 0.9 µg after 30 minutes. This graph suggests that the lower concentrations of ribonucleotides are transcriptionally active but reach saturation more quickly than the reaction at 20 mM, as a result of running out of substrate. The sharp fall in activity at higher ribonucleotide concentration is suggestive of enzyme inhibition at high nucleotide concentrations. These effects were tested by running time-course experiments at the highest and lowest concentrations of ribonucelotides observed above, i.e. 5 mM and 40 mM.

2.13.4 Time-course experiment, 5 mM rNTPs

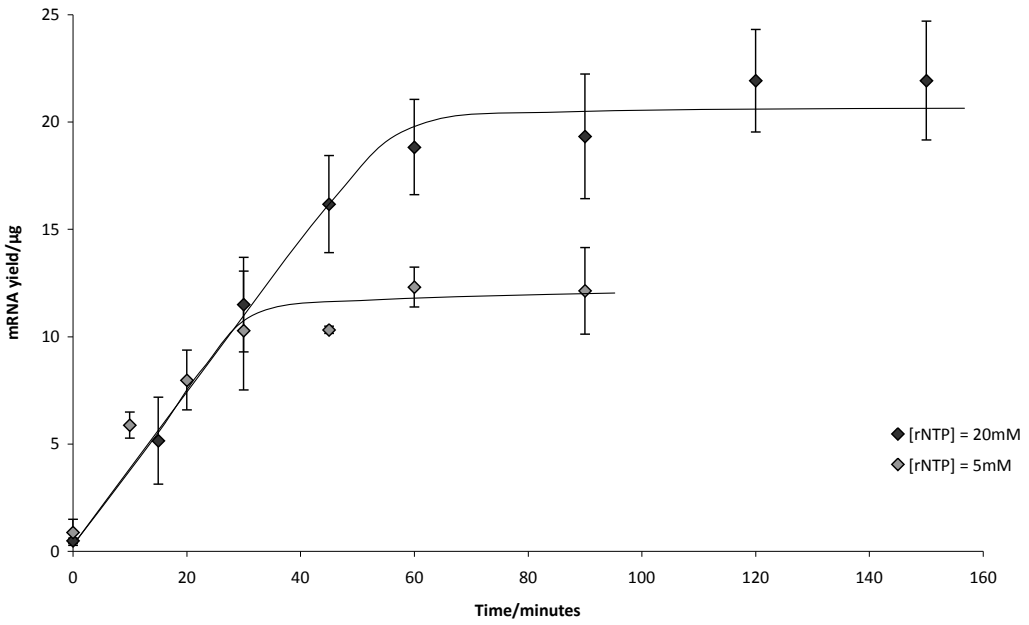

Figure 42: Comparison of transcript RNA production over time for total ribonucleotide concentrations of 20 mM and 5 mM. For data see appendix B, tables 45 and 56.

Figure 42 shows that the rate of transcription within the first 30 minutes is comparable at both 5 mM and 20 mM ribonucleotide concentrations. The reaction at 5 mM reaches saturation after this point while the reaction observed at 20 mM continues to proceed for a further 30 minutes, reaching saturation after a transcription time of 1 hour. The saturation point at 5 mM is likely to be caused by insufficient nucleotides to continue transcription.

2.13.5 Time-course experiment, 40 mM rNTPs

Transcription from a ribonucleotide concentration of 40 mM was set up and run over 4 hours, with triplicate groups of samples being removed at regular time intervals and processed to assess the yield of messenger RNA. As shown in figure 37, the level of transcription after four hours is (2.1 ± 0.5) μg and therefore still within the noise of the system. This is suggestive of inhibition by high concentrations of ribonucleotides and can be seen below.

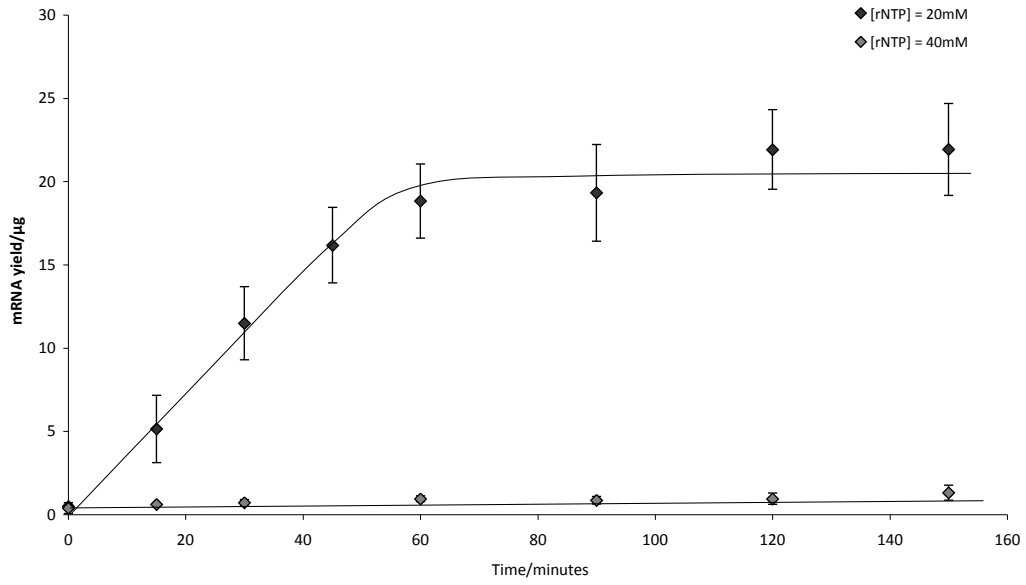

Figure 43: Comparison of transcript RNA production over time for total ribonucleotide concentrations of 20 mM and 5 mM. For data see appendix B, tables 45 and 57.

2.14 Explanation of trends observed in kinetic studies

The experiments outlined in this section have shown that the amount of DNA partitioned into the supernatant of the transcription reaction (0.008 μg)[83] could not produce significant levels of transcript RNA, which means the template DNA for transcription must be in the phase. Earlier experiments using SAXS showed that a 2.5mg sample of DOPE containing 1μg of linearised T7-luciferase DNA produced a d-spacing of 6.2 nm and a suggested hexagonal phase with the DNA occupying between one in 500 and one in 700 of the aqueous channels[1]. These observations suggest that that the DNA molecules are associated with the DOPE phase, which is in an inverse hexagonal geometry and, based on extensive structural studies in the literature, are likely to be in an extended conformation and inserted into the pores of the phase.

2.15 Summary of Transcription Experiments

Results showed that both the introduction of the DOPE/DNA inverse hexagonal phase (in full buffer) and the removal of spermidine from the transcription buffer (in the absence of lipids) caused the rate of transcription to fall by approximately half. It is not clear whether, in the case of DOPE/DNA, the reaction has reached saturation after four hours or is still progressing to reach transcriptional yields similar to those of the standard reaction without a liquid crystal phase. This has been discussed previously as a possible effect of triton X-100 sequestering cations and partitioning them from the transcription mixture. To this end, kinetic experiments involving the H_{II} phase should be repeated in buffers deficient in triton. The effects of spermidine on transcription are believed to be complex; several studies have shown a requirement for spermidine in transcription but the ubiquitous nature of polyamines in cells and their known interactions with nucleic acids and proteins make their precise role in transcription unclear. Spermidine is known to condense DNA and also promote transformation of the DNA double helix from the B-form to the Z-form[88]. This is indicative of an ability to stabilise Z-DNA, the transition to which can happen as a result of negative supercoiling upstream of the transcription bubble[89]. It could be that these actions of spermidine on DNA stabilise the transcription complex, so that removing spermidine from the transcription reaction causes decreased production of messenger RNA.

Exploring the effects on nucleotide concentration showed that there was an optimum ribonucelotide concentration of 20 mM for DNA associated with DOPE, and that this corresponded to a high yield in the experiments without lipids. Time course experiments showed that at nucleotide concentrations lower than 20 mM, a similar rate of reaction was observed but that saturation occurred earlier and at a lower yield of mRNA. A time course experiment at a ribonucleotide concentration of 40 mM showed inhibitory effects of high ribonucleotide concentrations.

Chapter 3

Experimental phase behaviour of DOPE and DOPE/DOTAP lipoplex systems

In this chapter the effect of including dioleoyl trimethylammounium propane (DOTAP) on the phase behaviour of DOPE systems, with and without DNA, is studied. Samples such as those used for transcription studies in chapter 2 of this thesis were explored alongside those with higher DNA contents, under a variety of different buffer conditions.

Phase maps were created by compiling data obtained through study of samples with varying composition by polarised light microscopy and X-ray diffraction. The phase transition from inverse hexagonal to lamellar was observed as a function of hydration, DOTAP content and temperature.

3.1 Experimental phase behaviour

In addition to what is known about DOPE/DNA and DOPE/DOTAP/DNA systems from previous studies detailed in the literature[16, 72], experimental studies on comparable samples were undertaken to create a phase diagram of DOPE/DOTAP mixtures in the presence of DNA, water, saline and transcription buffer. Studies of these lipids have been both numerous and varying throughout the last few decades; the phase diagram of DOPE has been extensively explored although many studies are limited to the use of deionised water as the hydrating agent. The mixtures in question are routinely used during transfection as part of the diverse area of research on using cationic lipids as gene delivery systems. Few studies examine the phase behaviour of DOPE/DNA and DOPE/DOTAP/DNA mixtures under physiological conditions. This use, combined with the studies on transcription of DNA in the inverse hexagonal phase of DOPE[1] outlined earlier in this thesis mean that it is therefore more appropriate to study these systems under more realistic conditions, for example, at physiological temperature and in a buffer system that is more reflective of the cellular environment. The aim of these studies was to ensure that the phase architecture of the inverse hexagonal DOPE/DNA samples is conserved during the transcription studies already carried out and to evaluate the limits of the inverse hexagonal phase for future experiments.
For the reasons outlined above, mixtures of lipid in water, saline and buffer have been examined using polarising light microscopy and small angle x-ray diffraction to create a phase diagram for the DOPE/DOTAP and DOPE/DOTAP/DNA systems. The sample preparation listed in previous studies by members of the Safinya group[16, 90] differs from what would be an appropriate protocol for comparison to the work undertaken in this study (such as the transcription, simulation and transfection studies detailed in chapters 2, 4 and 5 of this thesis), with particular relevance to the water content of the samples. The structural studies carried out by members of the Safinya group use dispersions of lipid and DNA, and the DNA used is not always linear, and the sample preparation resulted in a lipid content of 0.1 mg ml^{-1} in aqueous solution, which is not comparable to the bulk-phase samples used here.. Previous work on the DOPE/DOTAP mixtures also fails to provide in the literature a complete phase diagram across the whole range of DOPE and DOTAP concentrations, even upon examination of the supplementary information available in the literature.

3.2 Polarised Light Microscopy

Phase maps were constructed by comparing the phase behaviour observed under the polarised light microscope with the data obtained from x-ray diffraction experiments.

Phase identification was determined based on classical characteristics of the main phases displayed by lyotropic liquid crystals[91, 92], for example the high degree of birefringence, faceted bubbles, feathery texture and high viscosity exhibited by the inverse hexagonal phase,[1] which is dominant in DOPE mixtures. Where characteristics of more than one phase were observed, the mixture was designated as biphasic, and where possible descriptions of the different components of the biphase were identified. One example of this would be the hexagonal/lamellar biphasic system, where 'islands' of inverse hexagonal phase are observed with areas of material with predominantly lamellar characteristics flowing between them. A system such as this has an appearance reminiscent of 'crazy paving' under the microscope. Phase maps were examined for mixtures with varying DOPE and DOTAP content, at a series of hydration levels, in water and in transcription buffer.

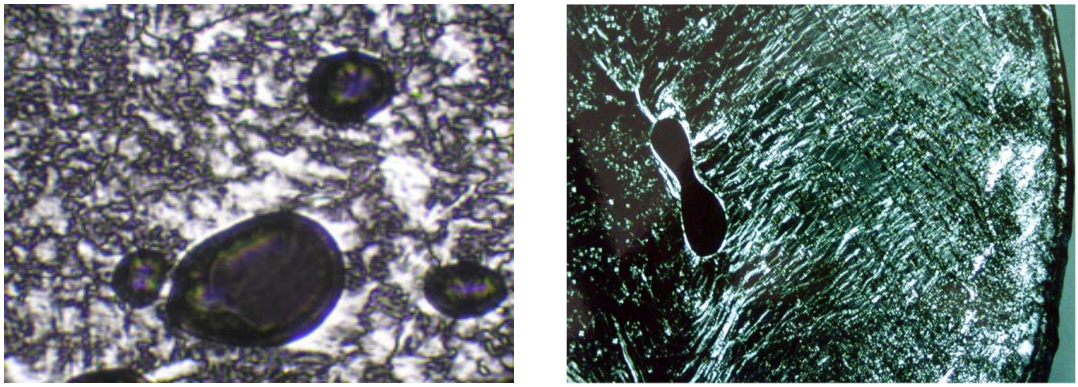

Figure 44: inverse hexagonal (L) and lamellar (R) phases as viewed under the polarised light microscope. Note the 'feathery texture' and faceted bubbles in the inverse hexagonal phase, and the 'oily streak' texture and rounded bubbles of the lamellar phase.

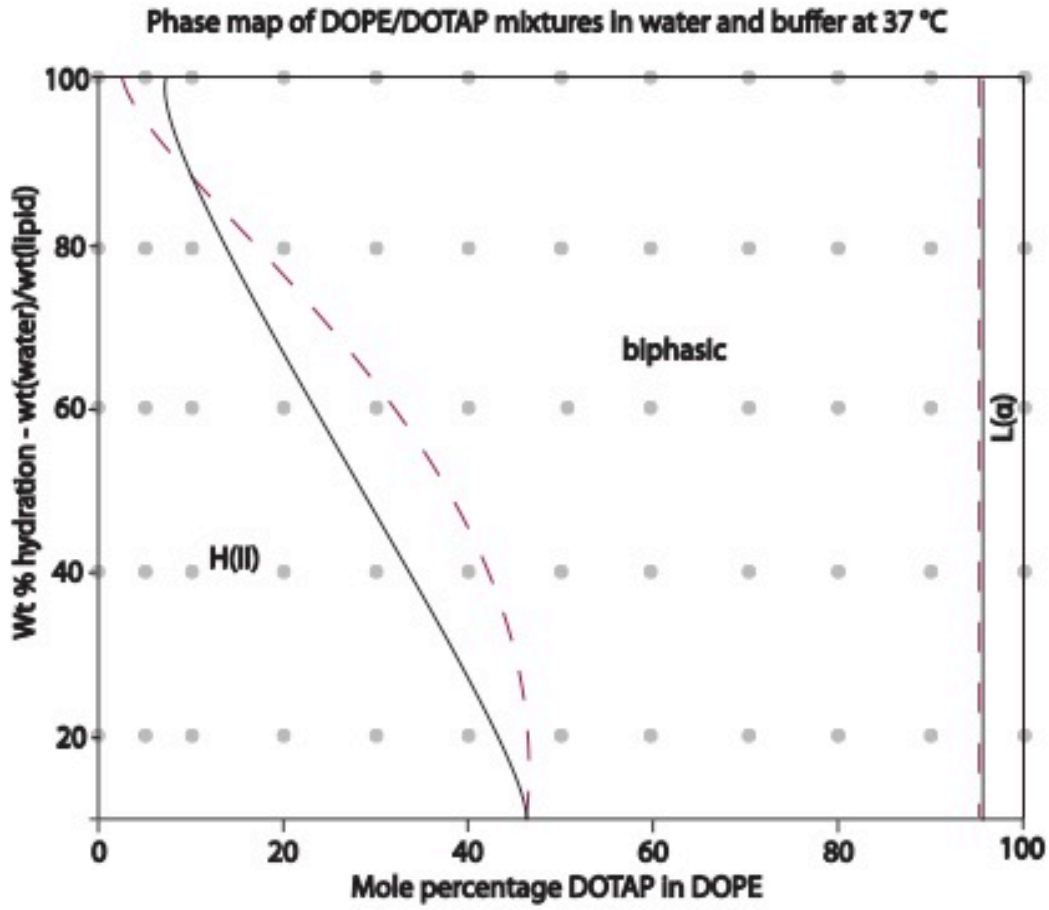

Figure 45: Overlay of phase diagrams of DOPE/DOTAP/water mixtures (black) and DOPE/DOTAP/buffer mixtures (red, dashed) at 37 °C.

The phase diagram displayed in figure 45 is an overlay of the phase behaviour of DOPE/DOTAP mixtures in water and in buffer at 37 °C. It is clear from this phase diagram, and all others compiled during this project, that the monophasic inverse hexagonal and lamellar regions occur for relatively small portions of the phase diagram. Monophasic regions occur where the dominant lipid species present favours formation of the monophase, for example samples with a large DOPE content favour the H_{II} phase, while samples with a high DOTAP content exhibit lamellar behaviour. For mixtures of intermediate concentration of DOPE and DOTAP the phase behaviour observed is that of a mixed-phase system, with regions that are dominated by the inverse hexagonal phase yet containing some lamellar character, and then a predominantly lamellar system with small regions retaining hexagonal character. At above 90% DOTAP the true lamellar phase is observed, and is characterised by the classic 'oily-streak' texture associated with lamellar phases and the appearance of 'Maltese cross' motifs. The above phase diagram detailed in figure 45 was compiled

using microscope observations at the points displayed as grey dots, and groups of phase behaviour with similar appearance have been outlined and labelled accordingly. Figure 45 displays the effect of transcription buffer on the phase behaviour of the system, in comparison with the same system in water. The transcription buffer contains a number of different salts, in addition to the rehydration of the sample with 1 µl isotonic saline, in a method identical to the one used to create the lipid samples for transcription. It is clear that the concentration of salts present preserves the inverse hexagonal character, both through the single phase hexagonal region, and also through the biphasic regions. The region labelled L_α/L_I in the water phase diagram has completely disappeared upon addition of buffer. These trends are something that is preserved across the phase diagrams at the temperatures studied (25 °C, and 37 °C). Possible explanations for this behaviour are effective screening of the positive charge of DOTAP by counterions present in the buffer solutions, or dehydration effects, again as a result of the ions present in the system. The difference in structure between zwitterionic DOPE and positively charged DOTAP causes a difference in the spontaneous curvature of the system, as discussed in previous sections of this thesis. The DOPE lipid with its comparatively small headgroup and bulky cis-unsaturated chains shows a propensity for a high degree of negative curvature. Conversely, the positive charge of DOTAP makes its effective headgroup size considerably larger than that of DOPE, despite being slightly smaller in terms of atomic structure. The charged headgroups of multiple DOTAP molecules will actively repel each other, causing swelling and, at high enough DOTAP contents eventual disruption of the internal honeycomb structure of the inverse hexagonal phase. Where samples were prepared with transcription buffer, the presence of ions, in particular negatively charged chloride ions could provide screening of the charge within the internal hexagonal stucture, preventing the disruption of the inverse hexagonal phase until higher DOTAP contents. The other possibility, effective dehydration would preserve the inverse hexagonal phase by drawing water out of the bulk lipid phase and preserving the negative curvature favoured by the DOPE.

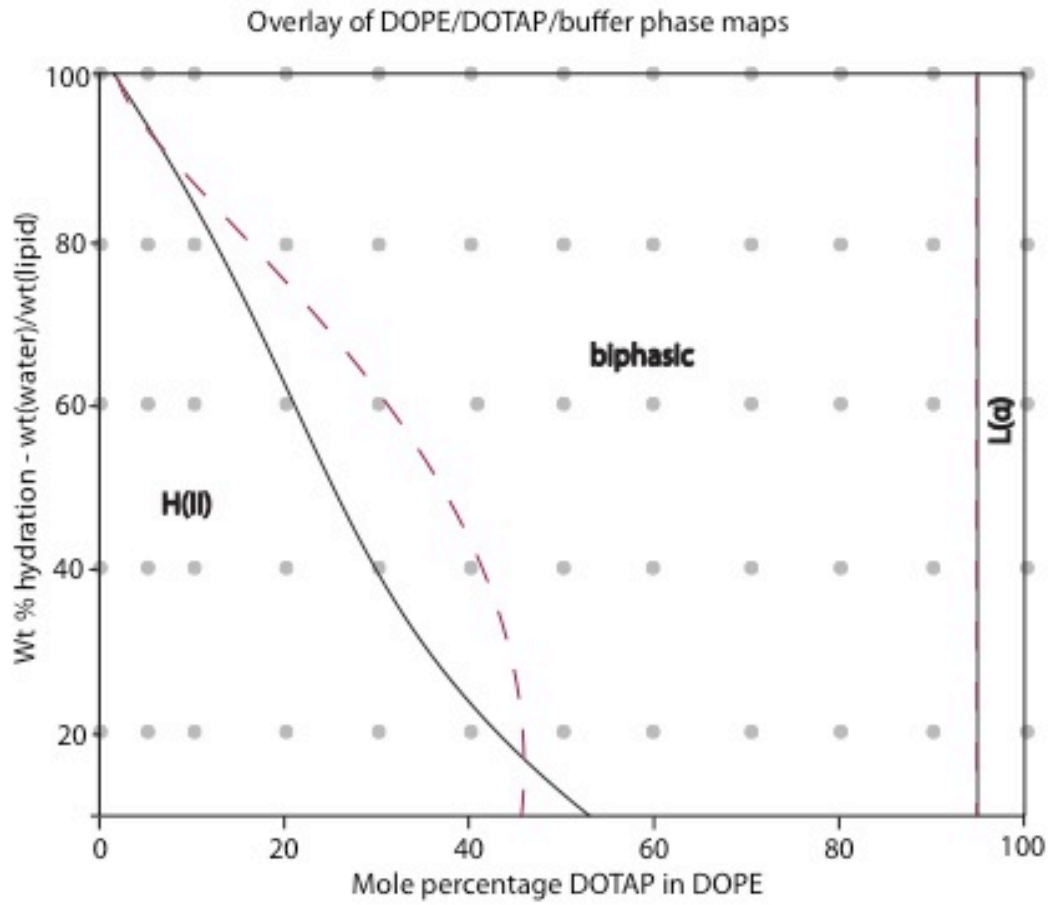

Figure 46: Phase diagram of DOPE/DOTAP systems in transcription buffer at 25 °C (black, solid) and 37 °C (red, dashed)

Figures 46 and 47 show that the inverse hexagonal regions of the phase diagrams are preserved with increasing temperature. This is in good agreement with the literature on lipid and DNA complexes. Two equilibrium structures are reported, the L_{α}^{C} and H_{II}^{C} geometries discussed previously. Under conditions in which the spontaneous curvature of the lipid, c_0, is low (zero) and the bending modulus of the phase, κ, is high ($k>k_BT$) the lamellar complex is favoured. When the lipid has a large (negative) spontaneous curvature, as in the case of DOPE, and the bending modulus is low ($k<k_BT$) the inverse hexagonal complex is formed. Upon raising the temperature the value of k_BT is raised, changing the conditions such that the inverse hexagonal geometry may be favoured.[16, 93]

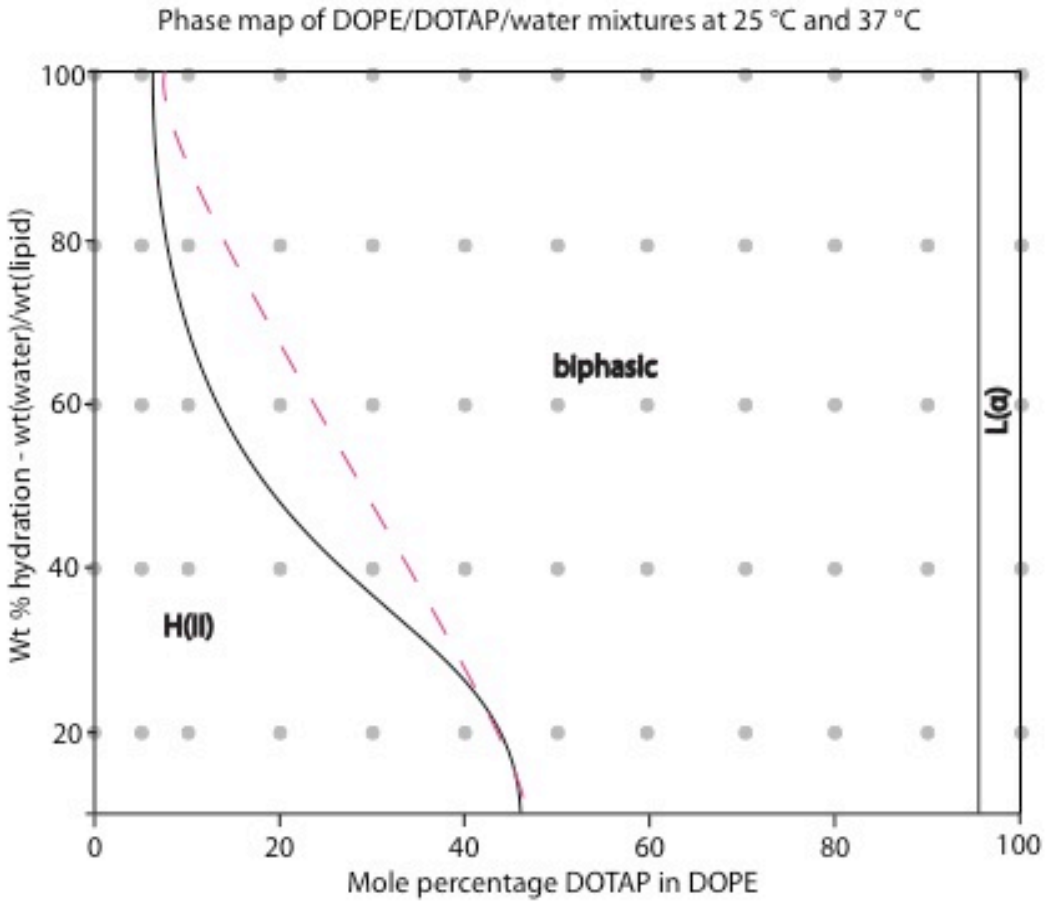

Figure 47: Phase diagram of DOPE/DOTAP systems in water at 25 °C (black, solid) and 37 °C (red, dashed)

3.3 X-ray determined structure of crystals

While it is true that the orientational ordering of atoms may be studied using NMR techniques, the study of translational ordering requires study by diffraction of radiation scattered by atoms in a sample. When an x-ray beam passes through a sample, the waves scattered by the atomic sites combine and, through the phenomena of constructive and destructive interference produce a diffraction pattern.

X-ray diffraction utilises the ability of atomic electrons to scatter electromagnetic radiation with wavelength of 1.54 Å; this scattering power increases with atomic number, such that hydrogen has a very low scattering ability when compared with heavier atoms. The diffracted x-rays may not be focussed using lenses and as such the structure must be deduced mathematically from analysis of the resultant diffraction pattern. For detailed detailed descriptions on x-ray diffraction please see works by Bragg[94] and Guinier.[95, 96]

The peaks observed as part of an x-ray diffraction pattern arise from Bragg's Law. Repeating planes within the structure cause elastic scattering of the incident rays, such that constructive interference between reflected x-rays occurs only when Bragg's Law is satisfied.

$$n\lambda = 2d\sin\theta \qquad \textbf{(3.1)}$$

The directions of incident and diffracted beams are specified by their wavevectors, $\underline{k}_i$ and $\underline{k}_s$, whose moduli are given by

$$\left|\underline{k}_i\right| = \left|\underline{k}_s\right| = \frac{2\pi}{\lambda} \qquad \textbf{(3.2)}$$

where the magnitudes are equal as the scattering is elastic. The peak positions of the scattered rays are often described in terms of their scattering vector, Q, which represents the change in wavevector of the scattered beam.

$$Q = \left(\underline{k}_s - \underline{k}_i\right) \qquad \textbf{(3.3)}$$

$$|Q| \equiv Q = \frac{4\pi\sin\theta}{\lambda} \qquad \textbf{(3.4)}$$

The scattering vector can be related back to Bragg's Law as follows

$$Q_n = n\frac{2\pi}{d} \qquad \textbf{(3.5)}$$

In this fashion, the scattering vector for a set of equidistant planes has intensity of zero, except for those cases where Bragg's Law is satisfied.

3.3.1 Powder x-ray diffraction and lipid samples

Techniques used in the x-ray diffraction of powder samples yield a powerful analytical tool for analysis of lipid structure. Like the powder sample, a lipidic sample contains many microdomains, with random orientation.[6, 19] This means that the Bragg equation is satisfied for all values of *n*, and all diffraction peaks are simultaneously observed. Each diffraction spot is averaged to give Bragg rings, rather than peaks, which can also be used to deduce the overall structure of the sample. The appearance of rings identifies the sample as being formed of differently oriented domains; during the construction of a phase diagram from x-ray data, samples at certain mixtures may display evidence of alignment, in the appearance of bright spots along the Bragg rings.[6]

3.3.2 Lyotropic liquid crystals and phase identification

There are many different phases observed in lipidic systems, all driven by the hydrophobic effect, partitioning of the hydrophilic and hydrophobic components, and hydration of the lipid molecules. The DOPE/DOTAP system studied as part of this PhD exhibits predominantly inverse hexagonal and lamellar phase behaviour; the x-ray diffraction patterns of these lyotropic phases are distinct and easily identifiable. Bragg rings from a lamellar complex form according to the ratios 1, 2, 3, 4; while Bragg rings resulting from an inverse hexagonal structure have the ratio 1, $\sqrt{3}$, 2, $\sqrt{7}$.[6]

3.3.3 X-ray diffraction experiments

X-ray diffraction experiments were carried out in collaboration with the Membrane Biophysics Research Group at Imperial College London. A Bede Microsource generator with a copper anode and nickel filters was used to produce the x-rays which were then passed through a custom designed, peltier driven temperature controlled sample chamber and detected by a CCD detector supplied by Photonic Science. The data for each sample was collected as a TIFF image file, and then analysed on custom software called AXcess.[93] From this software it is possible to obtain the *d*-spacing, which corresponds directly to the lattice parameter for a lamellar phase and is easily converted to lattice parameter for the hexagonal phase.[6]

In good agreement with the polarised light microscopy experiments, the x-ray diffraction experiments show a hexagonal system that gives way to a biphasic system, at intermediate DOPE and DOTAP concentrations, before displaying a lamellar phase at higher DOTAP concentrations. Unfortunately, the x-ray diffraction patterns of all components of the biphasic regions are not always visible, most often displaying only

the dominant phase. That said, phase parameters can still be calculated from them, allowing insight into what happens to the phase dimensions with altered lipid content and hydration. As with the microscopy studies, samples were allowed to equilibrate at 37 °C for several days before being inserted into capillaries; samples with high hexagonal character were inserted into capillaries using the plunger from a Hamilton-style syringe to gently ease the sample to the bottom of the shaft, while samples with a greater degree of lamellar character were inserted into the capillaries using centrifugation.

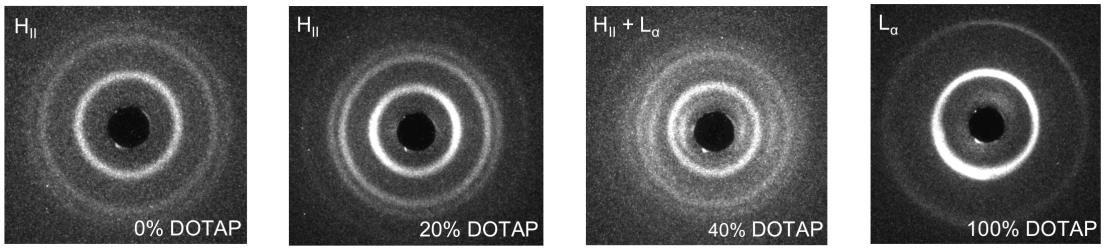

Figure 48: Diffraction patterns from DOPE/DNA samples in water. Note the Bragg peaks at 1, √2 and √3 for the H_{II} diffraction pattern, and the peaks at 1 and √4 for the L_α pattern.

3.3.4 The effect of hydration medium on hexagonal d-spacing

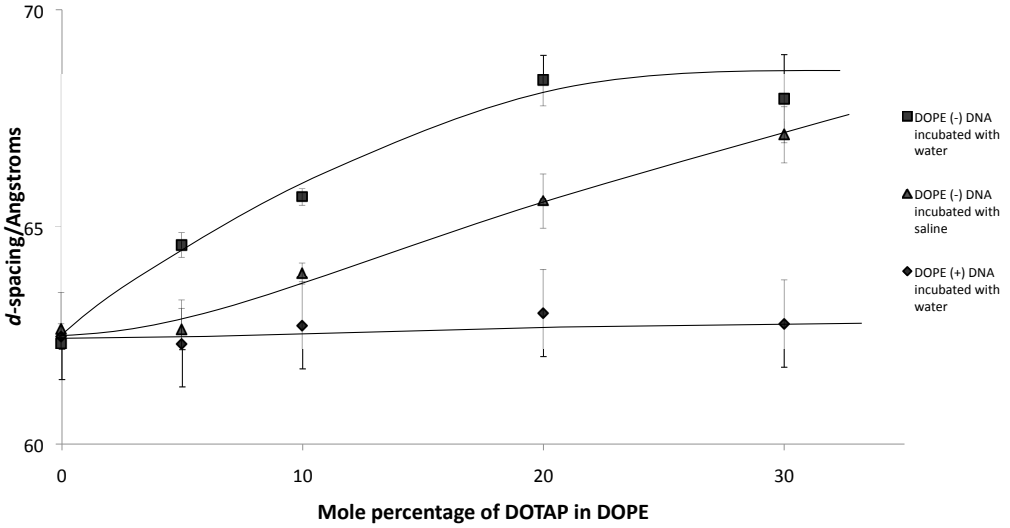

Figure 49: variation of *d*-spacing with increasing DOTAP content after incubation in water, isotonic saline and a solution of salmon sperm DNA (10 mg ml^{-1})

Figure 49 shows how the *d*-spacing of the inverse hexagonal phase varies with hydration medium over the inverse hexagonally dominant region of the phase diagram (i.e. at lipid content less than 30 % DOTAP in DOPE, and from samples in excess water, above 60 wt % hydration). It was found that a *d*-spacing of ~ 62.5 Å was observed for

pure DOPE, whether the sample was rehydrated with water, isotonic saline or a 10 mg ml^{-1} solution of salmon sperm DNA. This value corresponds to a unit cell lattice parameter of 72.2 Å, which is in good agreement with literature sources. It can be seen from the data that increasing the DOTAP content of the phase causes a swelling of the phase, to a *d*-spacing of roughly 68 Å, that is screened to some extent by the isotonic saline solution. The addition of salmon sperm DNA to the lipid samples shows a preservation of the inverse hexagonal *d*-spacing of ~ 62.5 Å all the way through the inverse hexagonal region to a lipid composition of 30 mole percent DOTAP in DOPE. At DOTAP concentrations higher than this the x-ray diffraction pattern no longer shows a clear hexagonal correlation for any sample, regardless of which solution is used to hydrate it. These observations are, however, in very good agreement with both the simulation and the polarising light microscope studies. The preservation of the inverse hexagonal *d*-spacing in the presence of isotonic saline is in keeping with the observed preservation of the hexagonal character of the system at increased salt concentration (by microscopy), and the stabilisation of the inverse hexagonal phase by salmon sperm DNA is in good agreement with the simulated data.

The DNA concentration in both the studies involving DOPE/DOTAP/DNA (salmon sperm) and the simulated systems is highly comparable. In the simulation, twelve out of the seventeen channels are occupied, while the experimental systems were constructed so that 0.6 mg DNA was added to each 5 mg lipid sample. This corresponds to 2.8 x 10^{15} molecules of DNA 200 base pairs in length. If the cross-sectional area of the DOPE headgroup is between 48 and 65 $Å^2$,[1] this gives a value of between 16.5 and 19.0 lipid molecules arranged around a channel of diameter 47.2 Å, as found in the inverse hexagonal phase of DOPE. The number of DNA molecules that can be accommodated by 5 mg lipid lies between 4.8 and 6.5 x 10^{15} molecules, giving a channel occupation of between 1 in 1.7 and 1 in 2.3 channels filled. The occupation of the system studied by simulation was 1 in 1.4 channels, which is comparable with those systems studied experimentally. The simulated system consists of a simulations box infinitely replicated in all directions, and is not wholly reflective of the bulk state of the lipid. In a real system the inverse hexagonal phase of the lipid system consists of a number of microdomains that are oriented randomly within the bulk sample. Indeed, this behaviour gives rise to the classic feathery birefringence observed in this type of sample during polarised light microscopy. This arrangement of domains means that some channels within the sample may not be available for occupation by DNA molecules as both ends of the channel will be located within the bulk phase. It is therefore suggested that this level of DNA occupation is as close to saturation as is

realistically possible in an experimental system; increasing the DNA content of the system by just a fraction of a milligram would mean that there was an excess of DNA molecules when compared with the DNA-condensing properties of the lipid. In terms of comparability of the experimental and simulated systems, the occupation of DNA within the channels is clearly comparable, when compared with biologically active samples used for the transcription and transfection elements of this thesis, which have a DNA concentration several orders of magnitude lower.

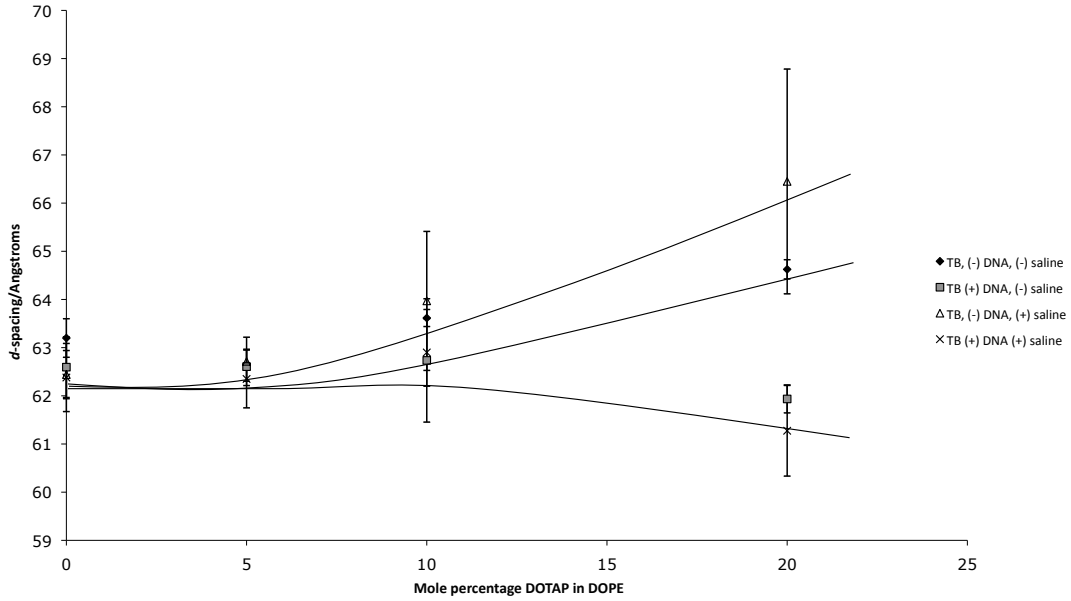

Figure 50: Graph showing d-spacing of transcription samples of lipid and transcription buffer with and without 1 µg linearised-T7-luciferase DNA, varying lipid composition, with and without incubation with isotonic saline as part of the sample preparation.

It is clear from the above figure that even small amounts of DNA add stability to the inverse hexagonal phase with increasing DOTAP content. The samples contributing to figure 50 have about 300 times less DNA in them (by mass) than the samples used in figure 49 yet this low concentration of DNA still appears to have the ability to preserve the inverse hexagonal character of the lipoplex. Preservation of the hexagonal *d*-spacing is observed at DOTAP contents of 20 %, even though the channel occupancy of DNA in this system would be several orders of magnitude lower. The samples used in transcription experiments were shown to have a channel occupancy of roughly 1 in 600 channels, which is vastly different to the high-concentration DNA samples where occupancy was roughly 1 in 2 channels. It is also clear from figure 50 that the preservation of the hexagonal lattice parameter cannot be attributed to the buffer salts alone, as while some degree of structural preservation is observed in the DNA-free

samples at DOTAP concentrations of less than 10 mol %, it is clear that at 20 mol % any screening effect observed as a result of the transcription buffer is overcome by the curvature preferences of the DOTAP.

3.3.5 Effect of saline on x-ray diffractogram

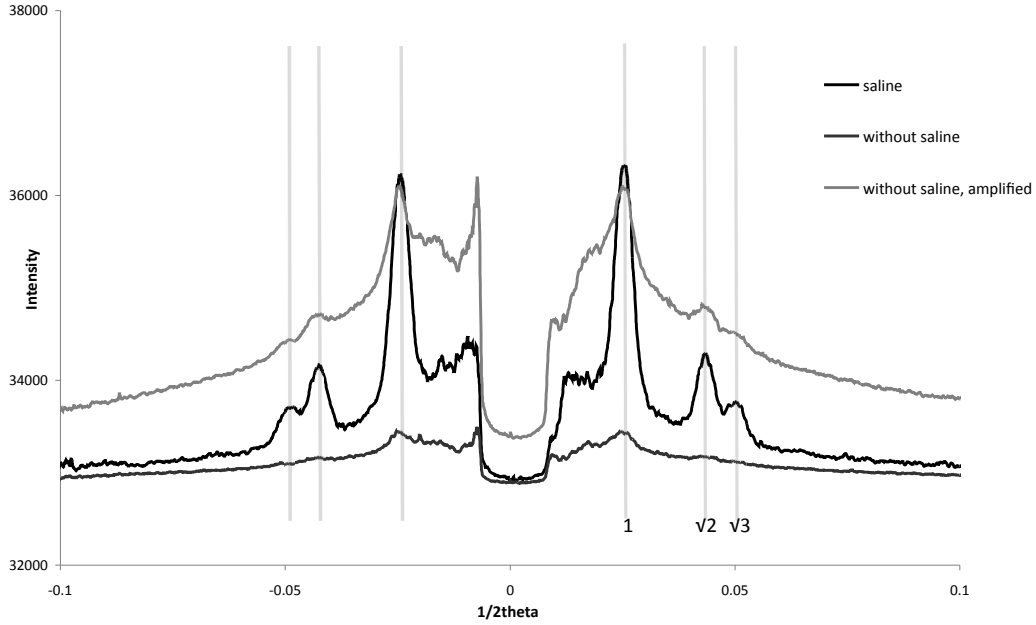

Figure 51: x-ray diffraction patterns for a sample of DOPE incubated with transcription buffer with and without 1 µl isotonic saline

It is clear from the experiments carried out in this chapter that the increased salt concentrations and the presence of DNA in biologically relevant samples may affect the phase behaviour. This must be considered when designing experiments to be carried out under both *in-vitro* and *in-vivo* conditions. The temperature of these systems is also of concern; this is once again highlighted by the differences in phase behaviour observed between 25 °C and 37 °C and the general trend that preservation of the hexagonal character of the system is observed with increasing temperature. It is also important to note the implications of measurements taken on a bulk-phase system and then applied to a cellular experiment carried out at a much lower lipoplex concentration. This is not a great concern when the system in question is known to form dispersions of solid lipid nanoparticles as both synchrotron SAXS[97] and cryo-TEM[98] studies have show preservation of the bulk phase properties within the dispersed samples. It is more problematic, however, when the system studied becomes vesicular at lower concentrations, such as the mixtures containing 20 mole percent DOTAP, which exhibit a great degree of hexagonal character when in the bulk phase but

are dispersed into a predominantly lamellar arrangement by addition of pluronic F-127 in 1% ethanol. Such systems will be discussed further in chapter 5 of this thesis.

3.4 Conclusions of the Structural Studies

The main purpose of the structural studies was to identify regions of the phase diagram of DOPE and DOTAP mixtures that were inverse hexagonal, and how these regions were affected by additives such as DNA and buffer. The inverse hexagonal phase is observed and DOTAP contents that are below 20 mol %, and this is preserved by raising including buffer (such as transcription buffer) and DNA. The SAXS experiments showed that the lattice parameter of the inverse hexagonal phase was also preserved by addition of salt, buffer and DNA, at both high and low DNA concentrations (representing the simulated system and biologically active samples used in this study, respectively). This indicates that a DOPE/DOTAP/DNA system of less than 20 mol % DOTAP in DOPE, that contains DNA and is under isotonic conditions is likely to have an inverse hexagonal architecture and be suitable for investigating the transfection properties of inverse hexagonal phase gene delivery vehicles.

Chapter 4

Coarse-grained Molecular Dynamics Simulation of DOPE/DNA and DOPE/DOTAP/DNA complexes

This chapter explores the use of coarse-grained molecular dynamics simulation to assess the equilibrium structure of DOPE/DNA and DOPE/DOTAP/DNA mixtures with varying hydration and DOTAP content. Systems containing 5660 lipids and twelve 30-mers of DNA were examined at a variety of hydration levels, to show the process of formation of an equilibrium structure from a non-equilibrium starting conformation. The topologies obtained through these simulations were used to gather key information about the morphology of the system, such as the lattice parameter. Structural dimensions gathered through simulated and experimental approaches were compared in order to evaluate the use of CGMD computational techniques as a method for phase prediction in lipoplex systems. The simulated systems detailed in this chapter were designed to be comparable to the samples used for the transcription experiments through the phase diagrams outlined in chapters 2 and 3 of this thesis.

4.1 A review of the literature on simulation of lipid systems

Simulation is a powerful tool for studying chemical interactions at the molecular level. Advances in the field have made the study of lipid aggregation possible on appropriate size (thousands of lipid molecules) and timescales (within a few weeks) that allow direct comparison with experimental observations.[99] In addition to this they allow tracking of individual particles and groups, yielding much more detail than is possible under experimental conditions. The experimental study of biologically relevant states derives measurements from a large number of conformations that arise from the high degree of disorder present in natural systems. For this reason the theoretical study of such systems is advantageous, particularly where the systems may be difficult to study experimentally; this is especially relevant when considering bilayer structures which are difficult to set up experimentally.

The development of the field of lipid simulations has, over the past two decades, moved from the self-assembly of surfactant and phospholipid bilayers to collective events. The current state of the art in the field of biomolecular simulations ranges from experiments with vesicles (such as formation of vesicles from a monolayer under compression[100] and vesicle fusion) to membrane domain[101-103] and pore formation, as well as remodelling of membranes by curvature-inducing proteins.[104] Simulations of up to 50,000 coarse-grained, or 5,000 atomistic lipids are possible with timescales routinely being of the order of several hundred nanoseconds.

Several examples of the study of phase formation exist in the literature, and the creation of complete phase diagrams of a number of systems is now possible.[105-107] The first lipid simulations, involving spontaneous self-assembly of bilayers from randomly dispersed lipids[108, 109] highlights a mechanism by which this process is likely to occur. The intermediate stages of self-assembly towards an equilibrium structure were shown to be aggregation to form micelles, which then extend to form rod-like micelles, before formation of a pore-containing bilayer, which then seals to form a single bilayer. This mechanism is reflective of what is already known of the phase behaviour of amphiphilic mixtures and is likely to describe the process by which this process occurs in “real” systems.[99]

The formation of inverse phases has also been explored as the importance of non-bilayer states in natural processes has long been realised.[9] Inverse phases may be implicated in

various membrane events, such as pore formation, membrane genesis, viral entry, and intermediates of fusion and fission in endocytosis and exocytosis.[4]

4.1.1 An Introduction to Molecular Simulation

A detailed source of information on the background to computational methods may be found in Leach[110] and Allen and Tildesley[111] while discussions of thermodynamic concepts in biological systems are found in works by Haynie,[112] and Bromberg and Dill.[113]
Molecular simulations use computational methods to study systems of atoms and molecules as a way of determining the structures and energies related to those systems. Simulated systems typically involve 10^3 – 10^6 particles and allow an assessment of the interactions between these particles, and calculating thermodynamic properties. Simulations produce information about a system at the molecular level, generating velocities and positions of individual atoms. In order to convert this into observable thermodynamic properties, such as pressure, temperature, energy and heat capacity, it is necessary to use statistical mechanics. In this way statistical thermodynamics uses rigorous mathematical expressions to link microscopic and macroscopic properties; without statistical mechanics, thermodynamics is a phenomenological theory. The microscopic state of a system is described using the atomic positions, q, and momenta, p, of all components of the system. These properties can be considered as coordinates in a multidimensional space, known as phase space. A single point in phase space is known as a microstate, Γ.
A collection of microstates that satisfy the conditions of a particular themodynamic state is known as an ensemble; the microstates of an ensemble will all be different but their macroscopically observable thermodynamic state is identical. Possible ensembles include microcanonical (where NVE are conserved), canonical (NVT), isothermal-isobaric (NPT), grand canonical (μVT), where N represents number of molecules, V represents volume, P stands for pressure and μ is the chemical potential. The postulate of equal a priori probabilities states that two microstates that are equal in energy are equally probable. Different microstates are useful for simulating different things, for example a process involving a change in volume may be better simulated using an isothermal-isobaric rather than a canonical ensemble (i.e. NPT rather than NVT). The statistical thermodynamical properties of a system at equilibrium are encoded by the partition fuction, Q, and this varies depending on the type of ensemble.

There are two main branches of simulation within classical molecular mechanics: Molecular Dynamics (MD) and Monte Carlo (MC). Molecular dynamics (which is the type of simulation used in this study) generates the approximate dynamics of a system and can be used to generate time-dependent properties, while the Monte Carlo method generates configurations by imposing random moves of atoms (or groups of atoms). MC simulations are combined with an energy bias, which defines whether the new configuration is acceptable; MC cannot, therefore, give dynamical information. Monte Carlo simulations are typically combined with an acceptance test, for example, the Metropolis test, to ensure that the most statistically likely states are sampled.

The Ergodic hypothesis states that if the system is allowed to evolve in time for an indefinite period that all possible microstates will occur. This is one of the most fundamental concepts of statistical mechanics and its implications are that over infinite time both MC and MD simulation will yield the same results as the ensemble and time averages of the system are equal.

4.1.2 Molecular Dynamics

As molecular dynamics involves integration of Newton's Laws of motion over all the particles in the system, it can be used to calculate any position from the past or future from any point in the simulation. An MD simulation therefore consists of a system propagated through phase space from step-to-step over a large number of closely spaced timesteps, t_{obs}, length $dt = t_{obs}/\tau_{obs}$

$$A_{obs} = \langle A \rangle_{time} = \frac{1}{t_{obs}} \sum_{t=1}^{t_{obs}} A(G(t)) \qquad \textbf{(4.1)}$$

In order to move the system $\Gamma(\tau)$ to $\Gamma(\tau+1)$ the positions, momenta and forces for all atoms must be taken into account and used to generate a new configuration a short timestep later. Common algorithms used to propagate the system through space are based on a Taylor series expansion, for example the Verlet algorithm.[111] Possibly the most widely used algorithm for the integration of the equations of motion in an MD simulations, the Verlet algorithm involves calculation of new atomic positions at $t + \delta t$ and $r(t + \delta t)$ from the accelerations and positions at time t, termed $\mathbf{a}(t)$ and $\mathbf{r}(t)$ respectively, and the positions from the previous step $r(t - \delta t)$. The Verlet algorithm is written as follows[111]

$$\mathbf{r}(t+\delta t) = \mathbf{r}(t) + \delta t\mathbf{v}(t) + \frac{1}{2}\delta t^2\mathbf{a}(t) + \ldots$$
$$\mathbf{r}(t+\delta t) = \mathbf{r}(t) - \delta t\mathbf{v}(t) + \frac{1}{2}\delta t^2\mathbf{a}(t) - \ldots \quad \textbf{(4.2,3)}$$

These equations can be added to give

$$\mathbf{r}(t+\delta t) = 2\mathbf{r}(t) - \mathbf{r}(t-\delta t) + dt^2\mathbf{a}(t) \quad \textbf{(4.4)}$$

The Verlet algorithm is simple to use, with relatively low storage requirements of only two sets of positions and accelerations. Disadvantages of using the Verlet algorithm arise from the fact that positions are generated by addition of a small term *($\delta t^2 a(t)$)* to the difference of two much larger terms, (*$2r(t) - r(t - \delta t)$*), resulting in a loss of precision. It is also difficult to obtain velocities from the Verlet algorithm, as there is no explicit term for velocity in the equations. Velocities can be calculated from the Verlet algorithm using a number of methods, for example, dividing the difference in positions at times *$t + \delta t$* and *$t - \delta t$* by *$2\delta t$*, as follows:

$$\mathbf{v}(t) = \left[\frac{\mathbf{r}(t+\delta t) - \mathbf{r}(t-\delta t)}{2\delta t}\right] \quad \textbf{(4.5)}$$

To overcome the issues outlined above, several variations of the Verlet algorithm have been developed. An exampled of this is the Leapfrog algorithm,[111] in which the velocities are first calculated at *$t + (1/2)\delta t$* and then used to calculate the positions at time *$t + \delta t$*.

$$\mathbf{r}(t+\delta t) = \mathbf{r}(t) + \mathbf{v}\left(t + \frac{1}{2}\delta t\right)\delta t$$
$$\mathbf{v}\left(t + \frac{1}{2}\delta t\right) = \mathbf{v}\left(t - \frac{1}{2}\delta t\right) + \mathbf{a}(t)\delta t \quad \textbf{(4.6,7)}$$

The velocities at time t can be approximated by the relationship:

$$\mathbf{v}(t) = \frac{1}{2}\left[\mathbf{v}\left(t - \frac{1}{2}\delta t\right) + \mathbf{v}\left(t + \frac{1}{2}\delta t\right)\right] \quad \textbf{(4.8)}$$

The leap-frog algorithm is named for the way that the velocities and positions are calculated at a constant phase difference of ± *½δt,* and are continually leap-frogging over one another. It is an improvement on the standard Verlet algorithm in that it contains and explicit term for the velocity, and also does not require the differences of large numbers in its calculation. The most obvious limitation of the leap-frog algorithm is that the velocities and positions are calculated at different times, which means that it is not possible to calculate the kinetic energy contribution to the total energy of the system at the time that

the positions are defined. Other advantages of the leapfrog algorithm include the fact that conservation of energy is respected, even at large timesteps.[111]

4.1.3 The timestep

The timestep, δt, is a significant source of errors in calculation; a small timestep may help eliminate errors. The full length of simulation is related to the number and size of the timestep, but too large a timestep leads to a large error when collisions between particles in the system are not smooth, resulting in atomic overlap (which is, obviously, unfavourable) and a rapid increase in energy before the system "blows up". The timestep should be at least an order of magnitude smaller than the fastest vibration; in atomistic simulation this would usually be the vibration of hydrogen bonds, in which case an appropriate timestep would be ~1 fs. Coarse-grained simulations do not include hydrogen atoms and can, therefore, use a timestep that is considerably larger than this. A typical timestep for a coarse grained simulation is 0.01 ps, which means that a greater amount of simulated time can be achieved on the same physical timescale.

4.1.4 Periodic Boundary Conditions

Molecules at the edge of a simulation box which is surrounded by hard boundaries or vacuum would experience different forces to those positioned at the centre, resulting in properties that are not reflective of a bulk material. This issue can be overcome by the use of periodic boundary conditions, under which the simulation box is surrounded on all sides by infinitely continuing replicas of itself. When a molecule leaves the box on one side, it is replaced by a replica molecule entering on the opposite side, meaning that the number of molecules remains constant. To overcome the possibility of artificial long-range order the minimum image convention is employed; that is that the molecule is not permitted to "see" itself entering the box on the other side. The minimum image convention is created by truncating the long-range forces to less than half the length of the shortest dimension of the cell. This method saves calculating infinite numbers of pair interactions but can lead to incorrect summation of forces.[111]

4.1.5 Force fields

There are three things needed to set up a simulation: the starting position for all particles in the system, an algorithm to generate new positions and a force field. Starting

coordinates may be randomly generated, or taken from experimental findings, e.g. X-ray crystallographic data. The algorithm often depends on the software being used, although the choice of force field is up to the operator. Choosing the right force field is important, however, as force-fields are a main source of discrepancy between simulated and experimentally gained results.

The generation of an accurate trajectory for an MD simulation depends on the accurate solution of Newton's equations of motion. The force acting on each particle must be known, in order to calculate the inter-atomic potential energy (U, the sum of the potential energies of all bonds, angles, torsions, electrostatics and non-bonded terms in the system).

$$U_{tot} = U_{bonds} + U_{angles} + U_{VdW} + U_{Coulomb} + U_{torsions} \quad \textbf{(4.9)}$$

An important feature of large-scale molecular simulation is that the ability of the model to reproduce the properties being simulated is much more important than the "absolute correctness" of the model.[111]

4.1.6 Intra-molecular Interactions

It is often more convenient and computationally easy to describe two covalently-bonded atoms as masses on either end of a spring, using Hooke's Law

$$U(r_{i,j}) = \frac{1}{2}k(r_{i,j} - r_0)^2 \quad \textbf{(4.10)}$$

Where $U(r_{i,j})$ is the chemical bond energy between two atoms, i and j, and k is the force constant of the spring and the square of the comparison between the distance between the atoms ($r_{i,j}$) and the ideal bond length r_0.

An alternative method would involve implementing rigid bond constraints, where the force is directed along the bond and the magnitude of said force ensures that the bond length does not stretch during simulation.

4.1.7 van der Waals Interactions

van der Waals interactions are typically modelled using the Lennard-Jones potential:

$$U_{VdW} = 4\varepsilon\left[\left(\frac{\sigma}{r}\right)^{12} - \left(\frac{\sigma}{r}\right)^{6}\right] \quad \textbf{(4.11)}$$

where σ represents the inter-atomic distance at which point the overall potential is equal to zero and ε represents the depth of the potential energy well.[111] The attractive term in

the equation (which is proportional to r^{-6}) rapidly tends towards zero with increasing atomic separation; for this reason a cut-off distance can be applied, beyond which the potential is zero. van der Waals interactions provide a negligible contribution to the total energy of the system for a single pair of atoms but can become significant after summation over all pairs. This means that a long-range correction factor is required…. For non-identical pairs of atoms, Lennard-Jones parameters are applied using mixing rules, such as the Lorentz-Berthelot rules[111]

$$\sigma_{AB} = \frac{\sigma_{AA} + \sigma_{BB}}{2} \qquad \varepsilon_{AB} = \sqrt{\varepsilon_{AA}\varepsilon_{BB}} \qquad \textbf{(4.12,13)}$$

4.1.8 Electrostatic Interactions

The electrostatic potential due to charge-charge interactions between two atoms, i and j, can be calculated through

$$U_{ij} = \frac{q_i q_j}{4\pi\varepsilon_0 r_{ij}} \qquad \textbf{(4.14)}$$

as the 1/r term dictates that the electrostatic potential decays only slowly with distance, the potential cannot be truncated at half the length of the box and so all surrounding boxes must be considered.

$$U = \frac{1}{2}\sum_{n}\sum_{i=1}^{N}\sum_{j=1}^{N}\frac{q_i q_j}{4\pi\varepsilon_0\left|r_{ij}+n\right|} \qquad \textbf{(4.15)}$$

where n represents the sum over periodic cells at cubic lattice points $n=(n_xL,n_yL,n_zL)$ and n_x, n_y, and n_z are integers. The above equation can be split into two parts (representative of real and reciprocal space) that converge quickly using the Ewald summation.[111]

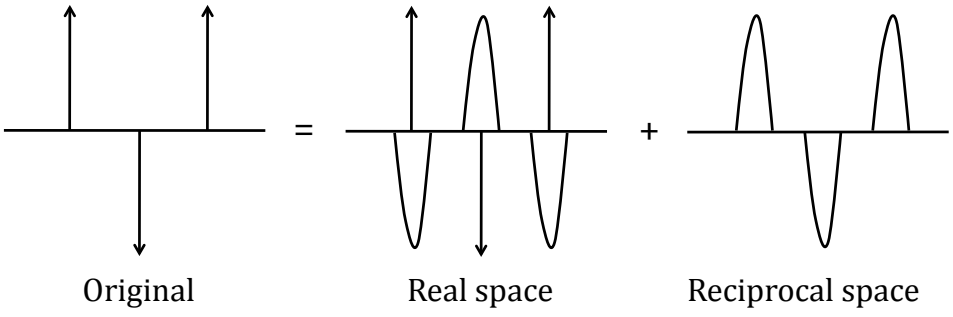

Figure 52: Schematic of the Ewald summation

In real space the charges are considered to be point charges, surrounded by a diffuse region of charge density with the opposite charge. This diffuse region has a Gaussian distribution, which effectively screens the point charge, and allows pairwise summation. The reciprocal space component removes the effect of screening the charge and involves another set of Gaussian distributions, exactly opposite to the first set allowing the summation to converge much more quickly.[111]

4.1.9 Coarse Graining

Coarse graining is a tool used in simulation where groups of atoms are modelled by a single interaction site. Examples of this include the United Atom Model, where groups such as CH_n are combined into one particle in order to minimise computational time; this technique should not be used for hydrogen atoms that are considered "chemically interesting," i.e. those that are directly involved in the chemical reactions being studied. The coarse grained technique involved in this study uses the MARTINI force-field, where coarse grained centres are used to represent groups of four "heavy" atoms (i.e. ignoring hydrogen). This allows much larger systems to be simulated, e.g. simulations containing thousands of lipids, in a much shorter timescale (days rather than weeks) and using less computational power than would be possible using an atomistic approach.[114-116]

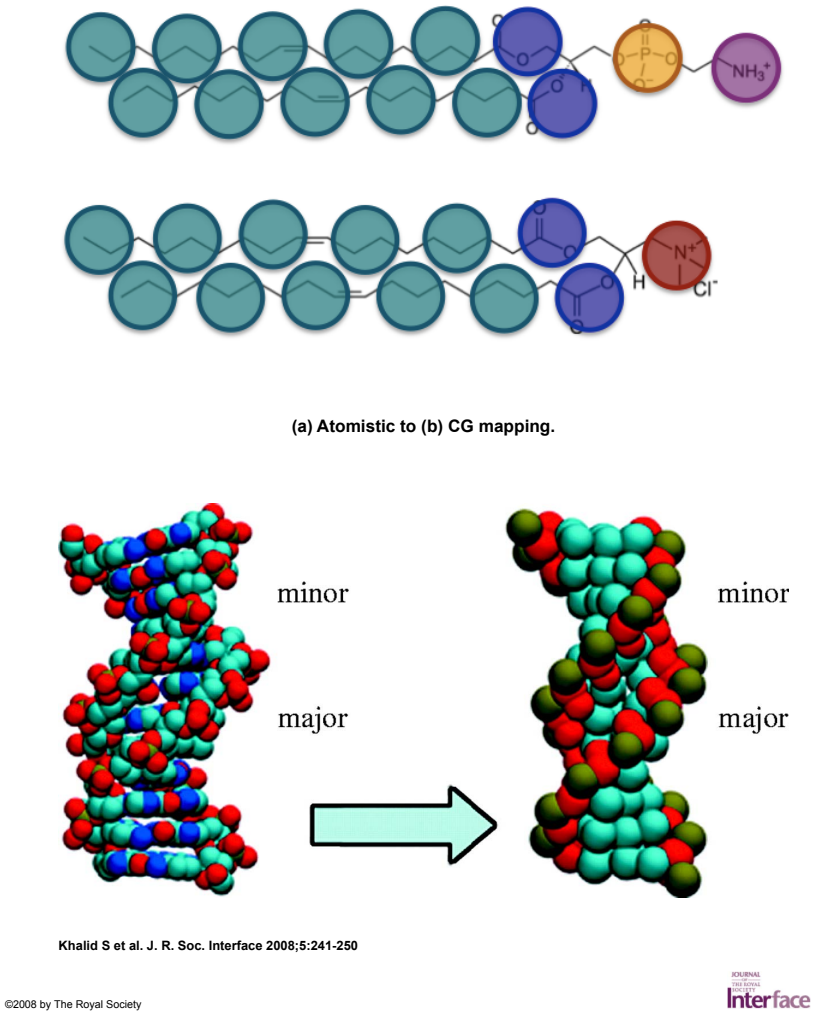

Figure 53: Top: schematic of coarse-grained DOPE and DOTAP lipids using the MARTINI force field; Bottom: schematic of the DNA model used[117]

4.2 Simulating Lipid and DNA Phases using the MARTINI Force-field

Complexes of lipid and DNA are routinely delivered to cells as gene delivery vehicles in *in vitro* transfection studies, while the lipids and DNA that make up these complexes are important components of the cells themselves. Although the array of lipid phases predicted and observed using experimental techniques may not be routinely observed in the lipid of the cell membrane, there is evidence to suggest that non-bilayer phases are implicated in a number of membrane events, such as endocytosis. Experimental studies of lipoplexes include X-ray and Neutron diffraction, solid-state NMR and microscopy, which give information that must be extrapolated and solved to the structure of the lipoplex. None of these techniques are able to show the complete structure at the level of detail that can be

extracted from a simulation. This computational study of lipoplex equilibrium phase formation was undertaken alongside experimental studies of lipid and DNA mixtures of ratios approximate to the simulated system in order to compare the dimensions of the phases formed and study the phase formation from the movement of individual molecules.

4.2.1 The MARTINI force field

The MARTINI (MARrink Toolkit INItiative) force field is a coarse-grained force field designed for simulation of lipidic systems.[114] It uses four main types of interaction site: polar (P), non-polar (N), apolar (C) and charged (Q). These are split into different subtypes according to their capacity for hydrogen bonding (donor, d; acceptor, a; both donor and acceptor, da; and none, 0) or by their degree of polarity (numbered from one to five where one is low polarity and five is high polarity).[114]

The non-bonded interactions are described by a shifted Lennard-Jones (12-6) potential energy function where σ_{ij} represents the closest difference of approach between the two particles and ε_{ij} represents the strength of their attraction (as shown in equation 4.11 on page 95). The size of each interaction pair is set at σ = 0.47 nm, in all but a few special cases. There are ten different types of interaction, each with differing interaction strengths allowing for greater reproduction of experimental solubilities. Interaction of charged particles bearing a full charge (type Q) is modelled using a shifted Coulombic potential energy function with relative dielectric constant, ε_r = 15 for explicit screening, (as shown in equation 4.14 on page 96). Bonded interactions are described using a weak harmonic potential (see equation 4.10) with an equilibrium distance, $R_{bond} = \sigma$ = 0.47 nm and a force constant, K_{bond} = 1250 kJ mol^{-1} nm^{-2}. The Lennard-Jones interaction is excluded between bonded particles, which are closer to each other than non-bonded particles whose equilibrium distance is $2^{1/6}\sigma$. The underlying chemical structure may be better represented using different values of R_{bond} and K_{bond}, and for this reason use of a single equilibrium bond distance and force constant is not necessary and these may be adjusted accordingly. The hydrocarbon chain stiffness of the phospholipids the bond angles are represented using a weak harmonic potential of the cosine type

$$V_{angle}(\theta) = \frac{1}{2}K_{angle}\left\{\cos(\theta) - \cos(\theta_0)\right\}^2 \qquad \textbf{(4.16)}$$

where LJ interactions between second nearest neighbours are not excluded. The magnitude of K_{angle} is 25 kJ mol^{-1} for aliphatic chains and 45 kJ mol^{-1} for both cis- and trans-

unsaturated bonds. The equilibrium angle, θ_0, is set at 180° and 120° for aliphatic and unsaturated chains respectively. [114]

4.2.2 Timescales

The interpretation of the time scale represented by a coarse-grained simulation is not straightforward, when compared to an atomistic simulation and indeed experimental results. The larger particle sizes and loss of detail of a coarse-grained system results in a much smoother energy landscape, devoid of the friction that results from atomic degrees of freedom. It is therefore found that coarse grained systems exhibit dynamics that are faster than atomistic simulation. It was found that scaling of the rates by a factor of four (so that one simulated MARTINI second is equivalent to four 'real' seconds) brought events in a MARTINI simulation in line with the same events observed in atomistic systems, including the movement of water molecules across a DPPC bilayer and the formation of vesicles.[114]

4.2.3 Solvents and Ions

The MARTINI force field is parameterised for a number of different traditional solvent molecules although for biological phenomena water is the only choice. Coarse graining of water is achieved by the representation of water molecules by a single P_4 interaction site. Ions are coarse grained using Q type particles. When considering single atom ionic species the first solvation shell is included within the coarse grained representation; ions within the MARTINI forcefield are considered to be only *qualitatively* accurate. This means that the MARTINI forcefield may only be successfully used to add counter ions to a system rather than create an accurate buffer system as used in physiologically relevant experiments.

4.2.4 The GROMACS Simulation Package

GROMACS (GROningen Machine for Chemical Simulation) is a software package designed for running MD simulation on parallel computing systems.[118, 119] It was developed by a group of collaborators at the University of Groningen in the Netherlands in the early 1990s, as a successor to their previous GROMOS program. Although originally designed for systems containing complex biomolecules, such as proteins, lipids and nucleic acids, it is suitable for all kinds of simulation based on pair potentials, as a result of effective implementation of non-bonded force calculations. GROMACS does not have a force field of

its own, but is compatible with a number of different force fields, including CHARMM and AMBER (for atomistic simulation) and the MARTINI force field used in the coarse grained simulations in this study. Additional versatility of the GROMACS package comes from the fact that there is a high degree of customisability built into the software, allowing interfacing with popular quantum mechanical packages to create mixed QM/MM simulations. GROMACS is written in the programming language C and uses the MPI (Message Passing Initiative) method of communication between processors.

4.3 The experiments carried out in this study

The experiments carried out in this study are split into two groups; a study of the phase behaviour of a system of DOPE and DNA with respect to hydration and the study of the effect of DOTAP concentration on the same system. These groups were designed to find the limiting hydration of the DOPE/DNA system in order to compare it to experimental values, and to assess the effect of DOTAP on the inverse hexagonal structure. Experiments were set up such that 5440 lipids and twelve pieces of DNA (each 30 base pairs in length) were fixed in a forced lamellar phase (i.e. a lamellar phase that would not be expected to be found as an equilibrium state of the system). The DNA helices were arranged so that when viewed cross-sectionally they occupied the vertices of a 4x3 grid. Hydration of the system was carried out using the GROMACS genbox function with different hydration levels achieved by altering the van der Waals radius of the water molecules (how close the water molecules are allowed to come to each other). Where systems contained an unbalanced charge (either as a result of the negatively charged phosphate backbone of the DNA or from the cationic DOTAP lipids) this was neutralised by addition of appropriate numbers of sodium or chloride ions, using the GROMACS genion command. Energy minimisations were carried out both after solvation of the lamellar phase, and after addition of ionic species. Simulations were initiated by short runs of 50 steps of molecular dynamics with increasing timestep from 0.0001 ps to 0.015 ps before being set up to run $4x10^6$ steps on a parallel system. To get the 300 ns duration used for the analysis in this study the MPI simulation was extended to six parts (each covering approximately 50 ns) for each system studied.

4.3.1The hydration study

The behaviour of the DOPE:DNA system was observed to be significantly different to the pure DOPE system. A simulation of 6400 DOPE molecules was found to undergo transition from a lamellar to an inverse hexagonal phase at a water content of ~15000 MARTINI waters (equivalent to 60000 "real" waters, from herein the number of real waters will be quoted). This corresponds to a water/lipid molar ratio of 9.4, which is below the experimentally-derived limiting hydration of DOPE,[12] and the observation of lipid stalk formation in simulations where the water content is < 12 waters/lipid.[120] When DNA is included in the lipid phase, the behaviour observed is somewhat different; at ~60,000 water molecules a system containing 5440 lipids and 12 DNA helices results in a continually undulating lamellar phase (water/lipid ratio of 11.0). The transition to an inverse hexagonal phase is not observed until the water content is reduced to ~20,000 water molecules (via a mixed phase at 40,000 water molecules). This corresponds to 3.7 waters/lipid for the hexagonal phase, and 7.4 waters/lipid for the biphasic sample. This reduction of water content in the presence of the DNA helices is expected and consistent with displacement of water within the H_{II} aqueous channels.

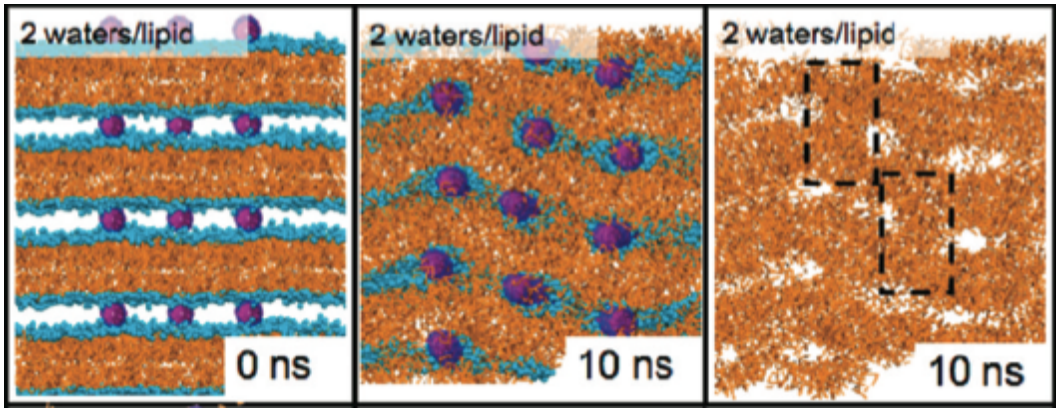

Figure 54: Phase transition of a DOPE:DNA system at low hydration from lamellar to inverse hexagonal over the first 10 ns of simulation. L-R: starting conformation of a forced lamellar phase; rearrangement of DNA helices within the first 10 ns; arrangement of the lipid tails after the first 10 ns of simulation

The first panel of figure 54 details the 'forced' starting conformation of the lipid-DNA complex; although this snapshot is taken from the low hydration simulation, this arrangement was observed at the start of all simulations containing DNA. It is clear from the middle panel that the initiation of phase transition occurs within the first 10 ns of simulation, through movement of the DNA helices to the hexagonal formation expected

from this mixture; this is indicated both by the rapid movement of the helices and also the fact that the helices do not move further over the course of the simulation. This immediate movement of the DNA is indicative of some long-range ordering of the DNA helices. The remainder of the simulation (up to 300 ns) involves rearrangement of the lipids to complete the transition. The third panel of the aforementioned figure details the positioning of the lipid tails after the first ten nanoseconds of simulation. The formation of lipid stalks is clearly visible and is highlighted by the boxes drawn over the simulations image. This is an important observation as it confirms the believed mechanism for such phase transitions,[121, 122] and has been observed in simulations of similar lipidic systems.[120]

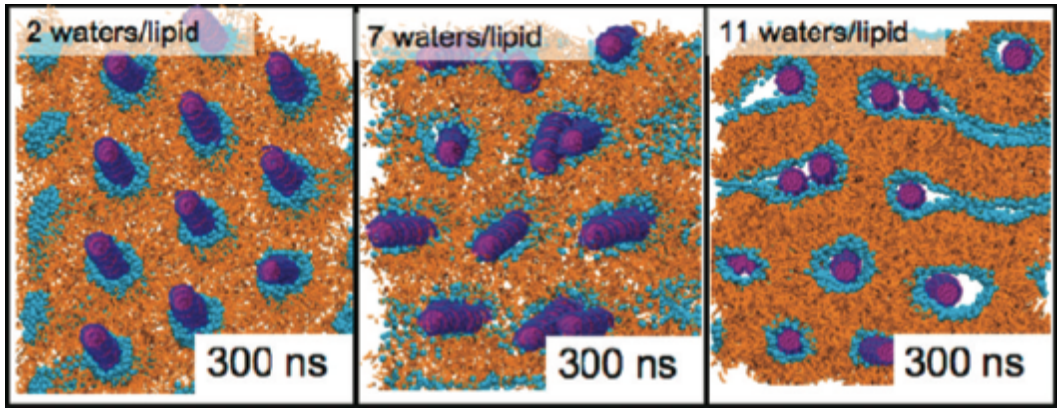

Figure 55: The effect of hydration on phase transition of a DOPE:DNA system from lamellar to inverse hexagonal over the first 10 ns of simulation. L-R: a 'perfect' hexagonal phase formed at low hydration; at 7 waters/lipid an imperfect hexagonal phase is observed; a biphasic system is observed at 11 waters/lipid

Figure 55 highlights the inability of the DOPE:DNA phase to accommodate water. The 'perfect' hexagonal phase observed at the low hydration level of 2 waters/lipid is disrupted by an increase in hydration. At 7 waters/lipid distortion is observed in the inverse hexagonal phase geometry such that the lipid headgroups are more disperse and there is multiple occupation of DNA molecules in the pores. At the yet higher hydration of 11 waters/lipid, further swelling of the hexagonal phase is observed, with further incidences of multiple occupation of pores by DNA molecules. There are also pores that are substantially wider than the DNA molecules, and evidence of lamellar-type regions within the simulation box. A degree of hexagonal character is retained in that lattice parameters are identifiable and calculable, although they are not uniform as observed previously at lower hydration.

4.3.2 Lipid composition study

Three DOTAP concentrations were studied in order to observe the effect of DOTAP on the inverse hexagonal phase of DOPE and DNA.

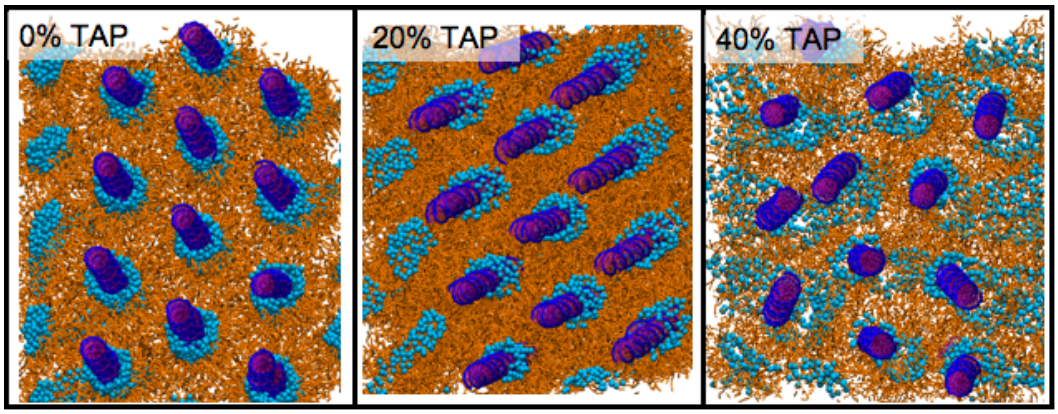

Figure 56: The effect of DOTAP content on phase transition of a DOPE:DNA system at low hydration from lamellar to inverse hexagonal over the first 10 ns of simulation. L-R: a 'perfect' hexagonal phase formed on the absence of DOTAP; when the DOTAP content is increased to 20% of the total lipid content the phase is still hexagonal; at 40% DOTAP peturbation of the inverse hexagonal geometry is observed

Figure 56 shows the effect of adding the cationic lipid DOTAP to the inverse hexagonal phase observed at low hydration (2 waters/lipid) detailed in the previous section. Conversion of DOPE lipids to DOTAP lipids, so that the overall DOTAP content of the lipid sample is 20 mol % shows retention of the inverse hexagonal geometry, which is in good agreement with microscopy and small angle X-ray diffraction studies also carried out in this study. Each of the twelve DNA molecules is aligned in the same direction, with even spacing between duplexes. The inverse hexagonal phase is, however, significantly disrupted on increasing the DOTAP content of the phase to 40 mol %. This is highlighted by the manner in which the DNA helices are no longer aligned or evenly spaced, with the ends of the duplexes pointing in different directions. There is also visible disruption of the lipids themselves, with the reduction of neatly distributed head groups around the DNA as seen at lower DOTAP concentrations. The orientation of the lipids is not as uniform as observed at lower DOTAP concentrations and evidence for a transition to a lamellar phase is displayed. This distortion is in excellent agreement with experimental results, where at a DOTAP content of 40 mol % evidence of both lamellar and inverse hexagonal character is observed by x-ray diffraction and under the microscope.

The distribution of the lipid headgroups in relation to the phosphate groups of the DNA backbone was further analysed by calculation of the radial distribution function between these species. This gives information about the probability of finding a particular species in the first and second solvation shell surrounding a group of molecules of interest. This information is an example of the type of information that cannot be found by traditional experimental techniques.

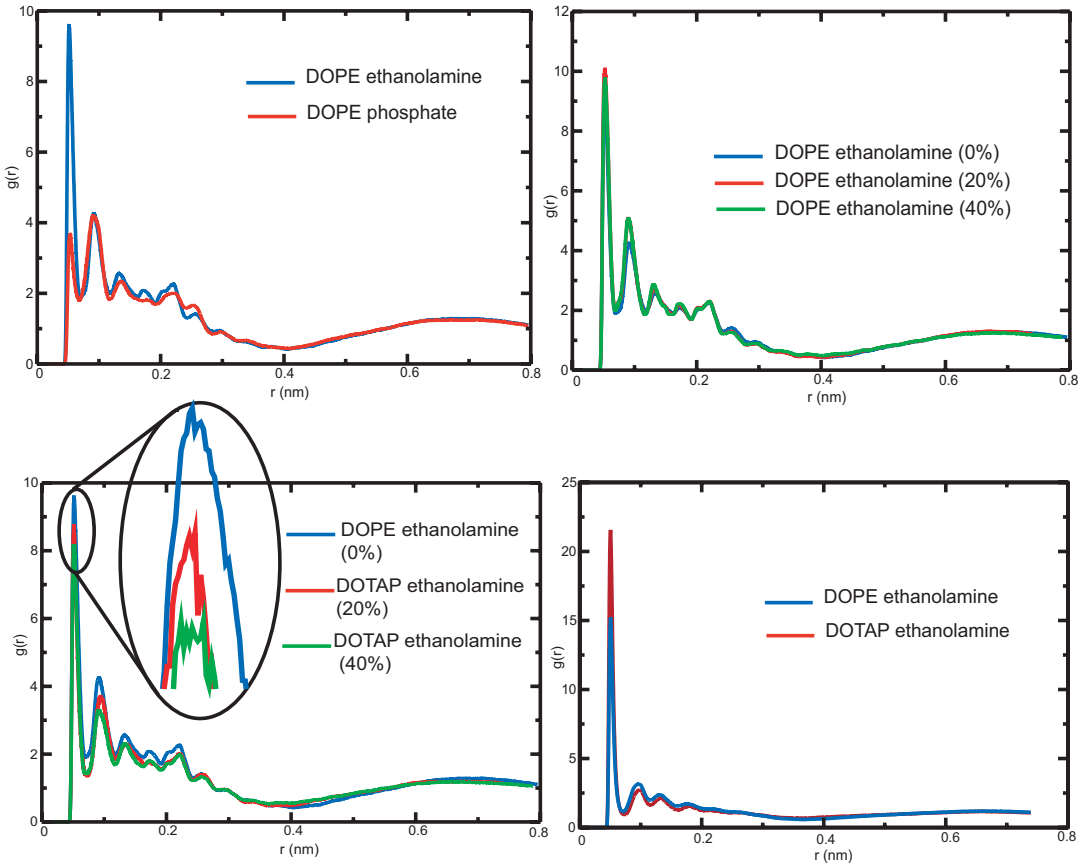

Figure 57: Radial distribution functions between DNA phosphate groups and lipid headgroups. Clockwise from top left: DOPE ethanolamine and DOPE phosphate; DOPE ethanolamine at different DOTAP contents; comparison of DOPE ethanolamine (at 0% DOTAP) and DOTAP ethanolamine groups at different DOTAP concentrations;

The radial distribution functions, as detailed in figure 57 indicate the relative positions of coarse-grained particles representing DOPE ethanolamine, DOPE phosphate and DOTAP ethanolamine groups within the system. The proximity of DOPE lipids to the DNA backbone is outlined in figure 57a; as expected the probability of finding the ethanolamine group of DOPE within the first hydration shell of the DNA molecule (at a distance of roughly 0.52 nm) is greater than the probability of finding the DOPE phospate group in this

position. Conversely, the DOPE phosphate group is much more likely to be found in the second hydration shell of the DNA phosphate groups, at a distance of roughly 0.92 nm. This arrangement is likely to be driven by the electrostatic repulsion between DOPE and DNA phosphate groups and the attraction of the ethanolamine group of DNA to the negatively charged DNA backbone. Interestingly, the equilibrium distance of the DOPE ethanolamine group to the DNA backbone is not affected by the addition of the cationic DOTAP, as observed in figure 57b. When studying the system containing 2 waters/lipid (the lowest hydration considered in the previous section), it is observed that the shapes of the RDFs at 0 mol %, 20 mol % and 40 mol % DOTAP in DOPE are identical, as displayed in figure 57c. The main peak undergoes a slight shift, from an equilibrium distance of 0.52 nm to 0.53 nm on addition of DOTAP but it is not possible to determine from these simulations whether this difference is significant. A similar trend is observed in the distances between the DNA phosphate backbone and the ethanolamine group of DOTAP; at 20 mol % DOTAP, the peak corresponding to the first hydration shell is observed at 0.51 nm, but at 40 mol % DOTAP this peak has broadened to cover the distance 0.50 to 0.52 nm. From these data it is possible to suggest a slight preference for the closer proximity of the DNA backbone to the DOTAP headgroups when compared with the headgroups of DOPE, although the small differences observed here warrant further investigation with a more detailed, atomistic force field. The final pane of figure 57 indicates that there is tight packing between the headgroups of the two types of lipid included in this study. There appears to be a slightly higher probability of finding a DOTAP headgroup within the first solvation shell of a DOPE phosphate group that a DOPE ethanolamine group (figure 57d). This is similar to previously observed behaviour concerning headgroups of DOTAP and DOPC from a lamellar phase simulation of this binary mixture.[117, 123, 124]

4.3.4 Calculating the lattice parameter from simulated systems

The *d*-spacing of the inverse hexagonal phase was calculated using a trigonometric approach. Thin slices of the final structure (after 300 ns of simulation) were taken using vmd, and individual atoms from the centre of the DNA helices were selected. The three-dimensional coordinates of these atoms were taken and then used to calculate *d*-spacings using basic trigonometry. The identification of individual atoms by eye introduces bias, which can increase the error of the system. An attempt to limit this was made by ensuring that the coordinates of the atom in the z direction were broadly similar, and by choosing particles that formed the DNA bases. Distances were then calculated from multiple parts of the simulated box (at differing positions along DNA length) and the mean distance was taken. The error represents the standard deviation over all distances calculated for each system (20 in total).

Mol % DOTAP in DOPE	DNA	Visual Inspection of Phase			Lattice Parameter/Å	
		Microscope	SAXS	Simulation	SAXS	Simulation
0	no	H_{II}	H_{II}	H_{II}	62 ± 2	62 ± 5
	yes	H_{II}	H_{II}	H_{II}	62 ± 2	62 ± 5
20	no	H_{II}	H_{II}		68 ± 2	
	yes	H_{II}	H_{II}	H_{II}	63 ± 2	64 ± 5
40	no	H_{II} and L_{α}	H_{II} and L_a		69 ± 2	
	yes	H_{II} and L_{α}	H_{II}	Distorted H_{II}	68 ± 5	69 ± 12

Table 2: Phase behaviour and *d*-spacing values from experimental and simulated approaches.

4.3.5 Channel Geometry – Dr S. Khalid

The stability of the inverse hexagonal phase is likely to be connected to both the geometry and flexibility of the pores. An average radius profile was calculated for two separate channels, with the channel circumference being determined by the positioning of the phosphate head groups of the DOPE. The average channel radius was found to be in the region of one nanometre, although the radius was not uniform along the entire length. The pore radius exhibited fluctuations measured between 0.93 ± 0.05 nm and 1.08 ± 0.05 nm, which along with deviations from the average radius during the latter 50 ns of the simulation, are indicative of an undulating channel. Whilst it is not possible to confirm this from a single snapshot, such undulations in the channel are likely to be reflective of a high degree of flexibility in the channel.

The channel geometries were compared to those gained from simulation of a DOPE/water system at 10 waters per lipid. In the absence of DNA, the channels were found to be just as flexible, but with a radius that varied between 1.02 ± 0.05 nm and 1.18 ± 0.05 nm. This shows that in the absence of DNA, the channels are slightly wider than when DNA is present, suggesting that there is an attraction between the ethanolamine head groups and the negatively charged phosphate backbone of the DNA.

The two systems studied are comparable in terms of hydration, as the DNA-containing system with water content of two waters per lipid is comparable to the limiting hydration case of DOPE, which was found to be roughly eleven waters per lipid. This allows for some water molecules to be displaced by the DNA duplexes. The water molecules in the simulation were assessed for their association with lipid species; it was observed that individual water particles were not bound to specific lipid phosphate groups, but rather, free to move, with longitudinal and lateral movement in the region of 0.6 nm in the last 5 ns of simulation.

Figure 58 shows the radius profiles of both channels, with the DOPE/water system being displayed in black and the DOPE/DNA/water system represented in red. The top of the figure displays an isolated channel, where the channel surface is shown in blue and the ethanolamine particles are represented in grey.

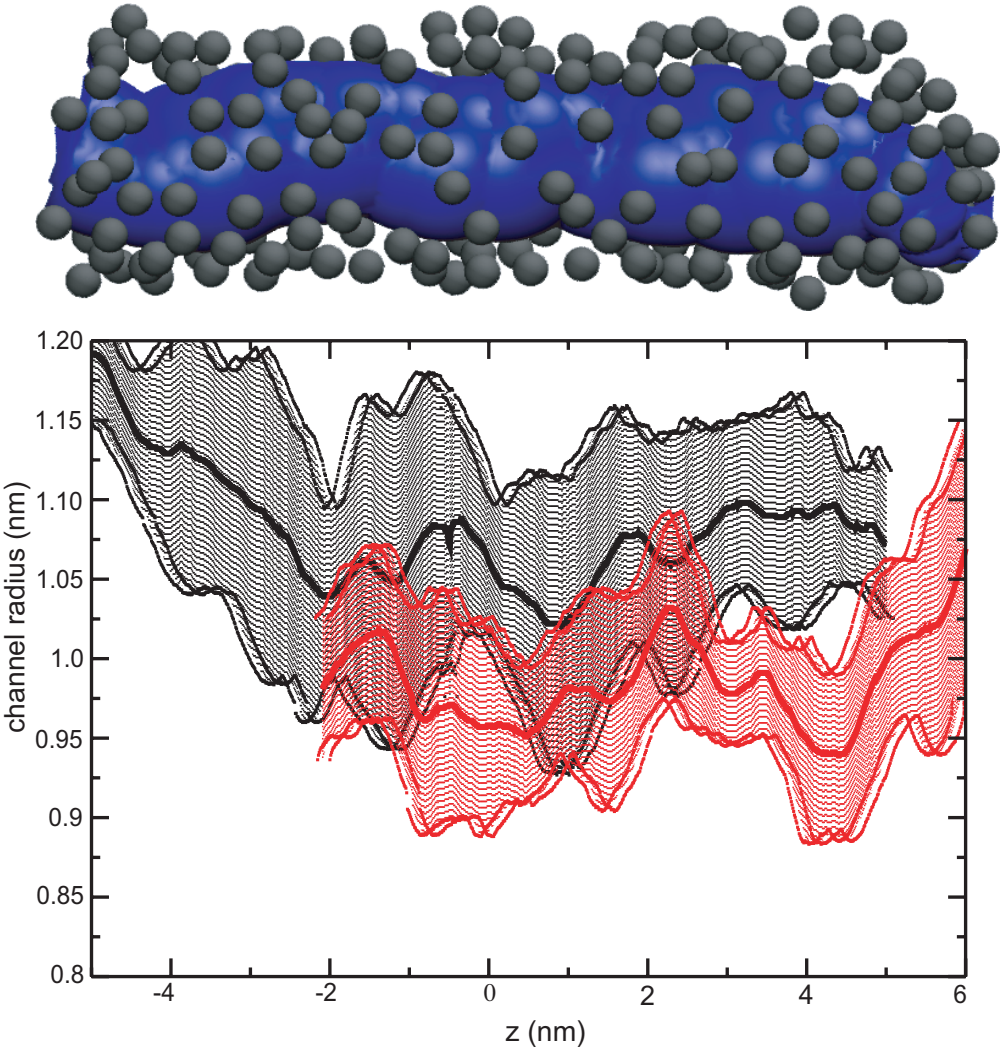

Figure 58: Representation of the channel geometry of the DOPE/water system (black) and the DOPE/DNA/water system (red). The surface of an isolated channel (blue) and the associated lipid ethanolamine groups (grey) are displayed above

4.4 Impact and relevance of the simulated system

The simulation study detailed in this thesis represents the observation of the formation of the inverse hexagonal phase from a pre-set, non-equilibrium geometry. It follows a series of other studies monitoring inverse hexagonal phase formation on a variety of lipid mixtures but in the absence of DNA. Marrink *et al*[125] studied the formation of the inverse hexagonal phase from bilayers of DOPE and DOPE/DOPC, while other studies use a mixture of DOPA, DOPE and LPA.[126] Other simulation studies used to assess the molecular view of phase formation are not directly comparable to experimentally studied mixtures, in that in previous studies comparisons were drawn indirectly from similar studies in the literature for the experimental field. Not all simulations of lipid-DNA complexes use the MARTINI force field; many previous simulations use systems that are even more coarsely grained than this one, sometimes using just two coarse-grained sites for lipid head and tail groups. Unlike other studies, for example Farago *et al* whose work covers the formation of complexes by condensation of vesicles and DNA,[127-130] or May *et al* who provide a highly detailed theoretical description of DNA-lipid phase behaviour,[60, 131] the aim of our study is to predict bulk phase stability in lipid-DNA mixtures.

The models used in our study allow a greater degree of detail than comparable pieces of work, even in their coarse grained state. The DNA model,[117] in particular, is much more detailed than included previously (other scientists have traditionally modelled the DNA duplex as rods). Thus study of different DNA conformations, such as the A and B forms, as well as major and minor groove interactions are possible.[132] The lipid models are part of the well-validated MARTINI forcefield,[114, 120] which allows the study of lipids with varying chain lengths and a wide variety of headgroup possibilities. Previous work on lipid simulation often uses highly coarse-grained species, which preclude the modelling of saturated and unsaturated acyl chains, and asymmetric chains. Further increased detail comes from the use of an explicit solvent and counter ion system, which allows the study of water and ion confinement within the different phases. Implicit solvent models prohibit the analysis of specific DNA and lipid interactions with water.

The results of this study yield an unprecedented view of the molecular processes that occur during the formation of an equilibrium structure from forced non-equilibrium geometries. The detail displayed is an exciting complement to experimental techniques that provide information about the bulk structure but cannot give detail at the molecular level. From an experimental point of view, conclusive experimental proof of the occupation

of the pores of the inverse hexagonal phase by DNA duplexes relies on the absence of detection of DNA anywhere other than the bulk phase (i.e. in the supernatant). This still leaves the onus of proof on the experimental scientist to differentiate between possible positions for the DNA, which in addition to being in the pores could also be associated with the surface of the bulk phase (see chapter 2 of this thesis). Studies such as the computational approach outlined here, combined with work related to counterion release, provide theoretical proof for the location of the DNA.

There are, however, limitations associated with the system studied here. The first is that the hydration of the system must be taken into account. When water greater than the limiting hydration of DOPE was used, the system reached a perpetually undulating lamellar phase. This might give the impression that DOPE forms a lamellar phase at high water content. Experimentally this is not the case, as DOPE has such a high preference for negative curvature that even at very high hydrations the inverse hexagonal phase is the preferred equilibrium geometry. It is likely that this observation is a direct result of using the periodic boundary conditions approach, as the simulation box is infinitely replicated in all directions, and excess water molecules may not be expelled from the bulk phase as they would in a "real" system.

This means that although the simulated system does provide a useful tool for equilibrium phase prediction, a caveat must be applied that covers only the use of 'known' systems, i.e. those for which the experimental phase behaviour is well documented. Any observations made on previously unexplored or under-developed systems, such as one of the many non-natural synthetic lipids that emerge in the literature each year, should therefore be used with caution. The limitations of the system also extend to the ability to study only the bulk phase properties of the lipid system of choice, and not the interfacial phenomena that may be displayed. Even taking these disadvantages into account, however, it is easy to see how such a system could be employed to the multitude of lipid and lipid/DNA systems that have already been extensively studied experimentally.

Chapter 5

Interfacing DOPE-derived DNA-containing Inverse Hexagonal Phases with Mammalian Cells

The ability for DOPE/DNA complexes to transfect cells was assessed using samples that were comparable to those used for transcription studies in chapter 2 of this thesis, and for which the bulk phase behaviour had been explored.

To overcome difficulties in handling the complexes, and therefore introducing them to cells, dispersions of inverse hexagonal phases of DOPE/DNA and DOPE/DOTAP/DNA, so-called hexosomes, were used to transfer both linear and plasmid DNA templates containing the gene for the fluorescent protein AmCyan into HeLa cells. The ability of these hexosomes to successfully transfect cells was assessed in the presence and absence of serum. The uptake of complexes, colocalisation of fluorescently-tagged lipid and DNA and expression of a fluorescent coral reef protein was monitored using laser-scanning confocal microscopy.

5.1 An introduction to transfection using solid lipid nanoparticles

Since the pioneering work of Felgner *et al* showed the potential of cationic lipid-mediated gene therapy[133] there has been a great effort to develop efficient methods of delivering DNA to cells. The concept of delivering a new piece of DNA to replace an imperfect and non-functional one is beautiful in its simplicity, although the reality of doing so is experimentally rather challenging. The main routes for gene delivery fall into two categories: virally mediated transfection,[134-138] and cationic lipid-driven transfection.[13, 17, 18, 20] The former has the advantage of being relatively efficient, although the clinical risks associated with undesirable immune responses limit its therapeutic use. The use of cationic lipid to deliver DNA has the advantage of a reduced immune response, but is hampered by low transfection efficiencies arising from poorly understood cellular mechanisms for gene delivery. The generalized mechanism by which all DNA delivery must occur may be split into three different stages: binding to and entry into the cell; dissociation of DNA from the delivery complex; and entry of the DNA into the nucleus. The structure of lipoplex systems has already been extensively covered in earlier chapters of this thesis, but the mechanisms by which lipoplexes have been observed to interact with cells have been thus far neglected.

5.1.1 Interaction with cells in vivo

Cationic lipid is used to drive the interaction between lipoplexes and cells, and in the absence of a driving ligand, the binding between lipoplex and cell is largely electrostatic.[139] To this end, the charge ratio of the lipoplex (defined as lipid/DNA) has been shown to be important, with complexes with higher charge densities exhibiting greater transfection efficiencies. The main mechanism for cellular entry appears to by through endocytosis, although there is an apparent size limit,[140-142] which governs this process. Small lipoplexes in polyanionic medium have been observed to enlarge to form granules on the cell surface, prior to entry by membrane-directed movement.[140] The duration of incubation is also an important parameter, as longer incubation times result in a greater uptake of lipoplex.[22] Also (as discussed previously in this thesis), the 'helper lipid' employed also affects the transfection efficiency.[143]

5.1.2 Escape of DNA into the cytoplasm

It has been shown that DNA cannot be expressed when complexed with lipids,[22] indicating that dissociation of the lipoplex is a crucial step in the process of transfection. Some studies have shown that DNA is released into the cytoplasm from the early endosome, potentially through destabilization of the endosomal membrane[142, 144] as a result of interaction with the lipoplex.[145] In cases where DOPE is used as the 'helper lipid', chosen for its fusogenic properties, the endocytic pathway is still observed. This is thought to be caused by aggregation of DOPE lipoplex systems in transfection medium[143], resulting in inefficient binding to the cell surface.[26, 133, 141, 146] While the endocytic pathway is considered dominant for the majority of lipoplex systems, it is impossible to rule out a mechanism involving spontaneous fusion.[147]

5.1.3 Entry of DNA into the nucleus

The process by which DNA enters the nucleus is necessary for gene expression but is believed to be inefficient. Pores in the nuclear envelope allow diffusion of small macromolecules (<70 kDa), but larger species require active transport.[148] Experiments involving the microinjection of intact lipid-DNA complexes into *Xenopus* oocytes showed poor transfection efficiencies,[22] indicating that release of DNA from the lipoplex is crucial. The relatively short half-life (1-2 hours) of naked DNA in the cytoplasm[149] highlights the delicate nature of this process, although providing a nuclear localization signal at one end of the DNA strand resulted in a 1000-fold increase in transfection efficiency.[150] It is possible that variations in the nuclear envelope over the cell cycle could provide optimised timescales for transfection, with evidence for nuclear envelope breakdown as the cell approaches mitosis.[151] This breakdown of the nuclear membrane could result in an increased transfection efficiency.

5.1.4 Cytoplasmic expression

There is evidence to show that cytoplasmic expression systems that employ T7 RNA polymerase to transcribe a gene under T7 promoter control show a promising solution for the improved delivery of genes. Expression is, however, linked to the co-delivery of T7 RNA polymerase, which is not trivial. Methods for doing so include delivery of viruses modified to produce T7 RNAP, mature mRNA sequences for T7 RNAP and delivery of the polymerase itself.[152]

5.1.5 Liquid crystal nanoparticles (LCNs)

The use of LCNs to deliver DNA has shown promise in recent years. Dispersions of lipoplex systems are easier to handle than bulk phases, and may be delivered to cells in their cell culture medium. The transfection experiments described in this thesis use inverse hexagonal dispersions, termed hexosomes. Aqueous dispersions of the DOPE/DOTAP mixtures designed to fall within the inverse hexagonal region of the phase diagram were created by dissolving a 9:1 (wt/wt) lipid:Pluronic-F127 mixture in 1% ethanol. Particles were dispersed by sonication for 2 hours, and then left to equilibrate overnight at 37 °C. Samples were then incubated with DNA in cell culture medium and allowed to equilibrate at 37 °C for several days. Lipoplexes were then delivered to HeLa cells via incubation.

5.2 Particle sizing data

The size of the hexosomes formed by sonication was assessed using dynamic light scattering (DLS). Sometimes referred to as photon correlation spectroscopy, DLS is one of the most popular methods of sizing particles, and works by shining a laser light source at a solution of spherical particles in Brownian motion. The motion of the particles causes a Doppler shift of the light source, which is related to the size of the particles. Advantages of DLS include the relatively short acquisition time and the fact that commercial particle sizers are available.

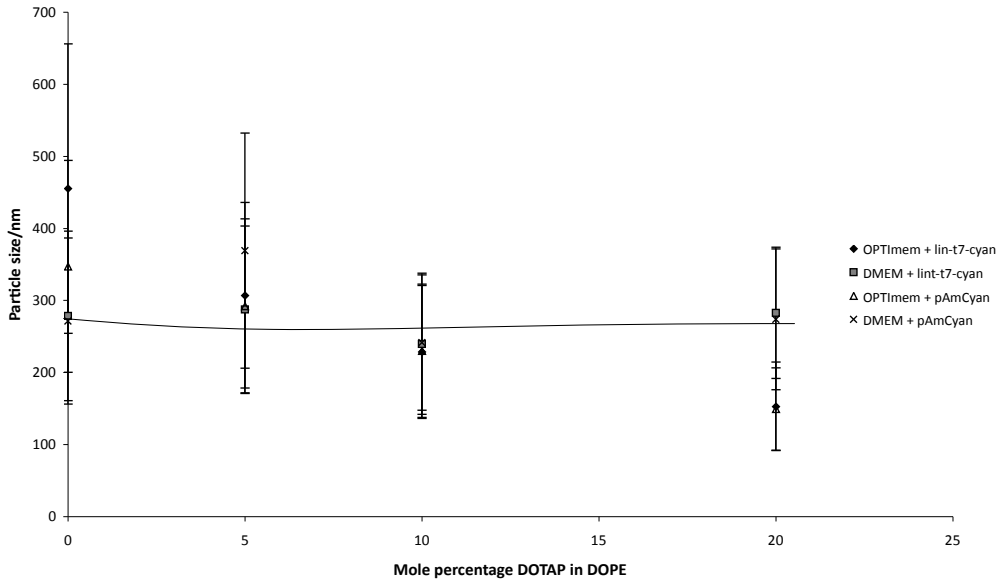

Figure 59: Particle size of hexosome and DNA solutions in cell culture medium as determined by DLS

Figure 59 shows DLS data from a variety of different hexosome and DNA combinations in both serum-containing and serum-free medium; as the hexosome solutions measured were from the transfection experiments carried out they did not contain antibiotics. It is clear from the graph that particle size is not significantly altered by increasing DOTAP content of the particle, whether equilibrated in serum-free medium (Opti-MEM), or medium containing traditional fetal calf serm (DMEM supplemented with 5 % FCS). The range of particle sizes observed decreases with increasing DOTAP content, suggesting that the paticle size becomes more uniform, but at all DOTAP concentrations the measured particle sizes overlap within error, indicating that any perceived difference in particle size is not statistically significant. It is possible that with increasing DOTAP content the hexosomes gain a greater proportion of molecules able to shield the oil/water interface, as the DOTAP molecules contain a highly hydrophilic and positively charged headgroup. In the serum-free medium this would likely mean that as the DOTAP content is increased there is an increased quantity of lipid molecules with a preference for lower curvature, which allows for greater shielding of the hydrophobic regions of the inverse hexagonal particles. If this were so, an increase in the lattice parameter of the inverse hexagonal phase would be observed. This increase is certainly the case for bulk phase samples, but in order to measure the structural parameters of the particulate dispersions, a synchrotron x-ray source must be used. Such experiments have been carried out on DOPE/DOTAP/DNA mixtures by members of the Safinya group and have shown an increase in the inverse hexagonal lattice parameter to be the case.[16]

5.3 Transcription from DNA in hexosomes

In order to show that transcription *in vitro* is possible in the presence of hexosomes, in a similar manner to the transcription in the bulk inverse hexagonal phase of DOPE that was described in chapter 2 of this thesis, transcription assays were set up. The assay was identical to those used in chapter 2 but the incubation time was 40 minutes rather than the 2 hours used for some previous experiments, so that measurements were taken before the experiment reached saturation, in keeping with the kinetic data.

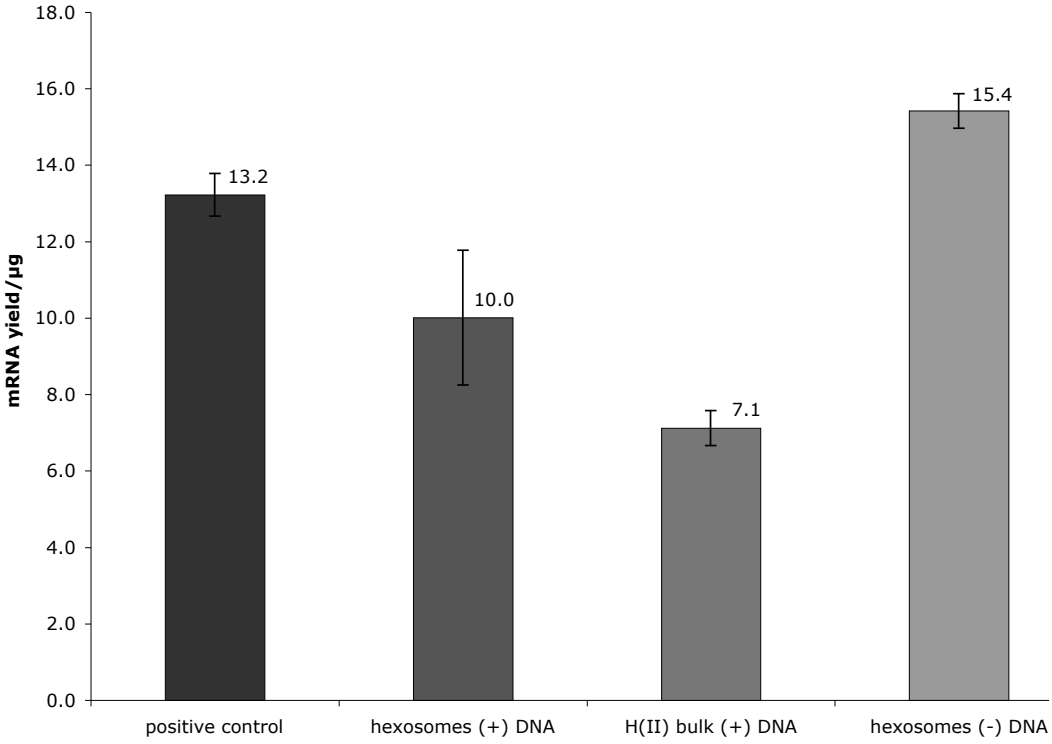

Figure 60: Graph showing in vitro transcription from DNA associated with hexosomes and the bulk-phase inverse hexagonal phase of DOPE (incubation time 40 minutes). L-R: positive control (standard); hexosomes and DNA incubated at 37 °C for several days; bulk H_{II} phase of DOPE with DNA; hexosomes added to standard transcription reaction (no colocalisation).

Figure 60 shows that the mRNA yield produced from hexosomes colocalised with DNA is slightly higher than that obtained from DNA associated with the bulk inverse hexagonal phase of DOPE. The fact that there is a reduction in transcriptional activity when comparing the hexosome-associated DNA with the standard positive control is suggestive that the DNA partitions into the hexosomes and is therefore less available in solution (and

in keeping with the data from chapter 2). The fact that the transcriptional activity of hexosome-associated DNA is greater than that of DNA associated with the bulk inverse hexagonal phase could be a result of the fact that the hexosomes form a dispersion rather than a bulk phase, as this would present a greater surface area of lipid. This would not only provide a greater surface area for DNA partitioning but also a greater interface with the solution component of the transcription reaction and therefore the polymerase and nucleotides necessary to produce messenger RNA.

As the transcription experiments undertaken as part of work towards this chapter investigate the effect of DOTAP content on transfection efficiency, it was important to understand how including DOTAP in the lipid phase affected transcription. Bulk phase lipid mixtures of DOPE/DOTAP/DNA were prepared and used for transcription reactions similar to those carried out in chapter 2 of this thesis.

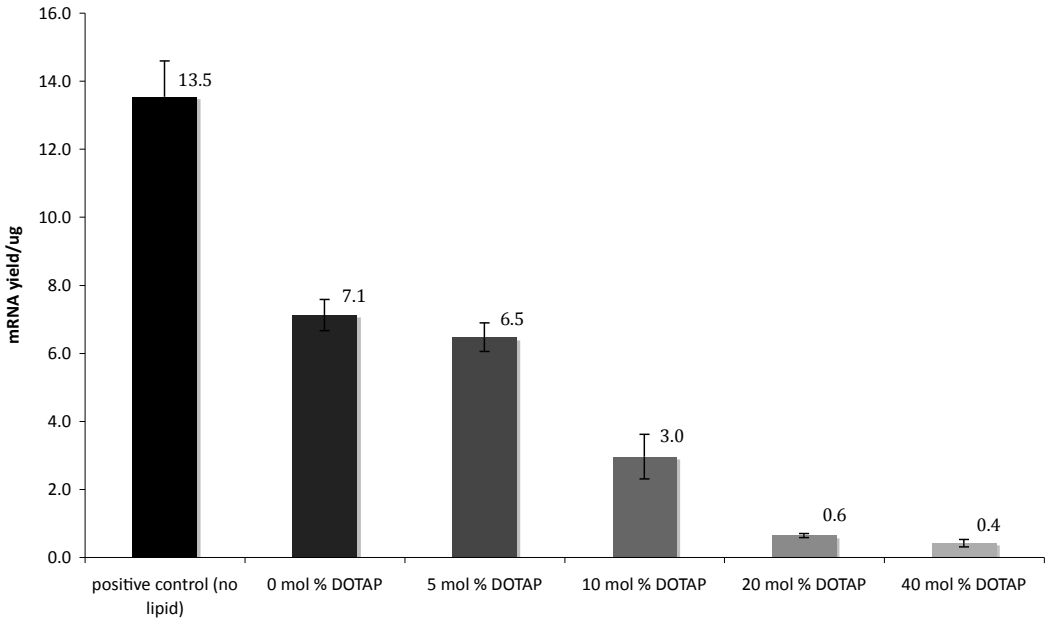

Figure 61: effect of DOTAP concentration on in vitro transcriptional yield of mRNA

Increasing the DOTAP content of the bulk lipid phase causes a decrease in transcriptional activity of the DNA. At a DOTAP concentration of 5 mol % there is only a slight decrease in transcriptional activity (6.5 μg compared with 7.1 μg for DOPE) when compared with a lipid phase of pure DOPE; the error bars for these samples overlap, showing that this difference is not significant. This is possibly because the addition of this low concentration of DOTAP does not cause significant disruption of the inverse hexagonal phase. At 10 mol

% DOTAP the transcriptional activity of the phase has fallen by roughly half when compared with the activity of DNA associated with DOPE, and at DOTAP concentrations of 20 mol % and greater the DNA is no longer transcriptionally active. There are several possible reasons for this drop in activity, but the most obvious ones being an increased attraction between the lipid and DNA as the net positive charge of the bulk phase has increased, or denaturation of the polymerase by the DOTAP. In order to investigate these possibilities, T7 RNA polymerase was incubated with the lipid phase, over a range of different DOTAP concentrations. In columns 3-5 of figure 62 the DNA was added with the polymerase and incubated with the phase, while in columns 6-8 of figure 62 the DNA was added after the polymerase had been incubated with the phase prior to transcription. Both sets of data (those where the DNA was included in the polymerase incubation and those where DNA was added later) show the same behaviour. The yield of mRNA decreases with increasing DOTAP content, although transcription is not totally inhibited at 20 mol % DOTAP, as was observed in figure 62, when the DNA was included in the bulk lipid phase.

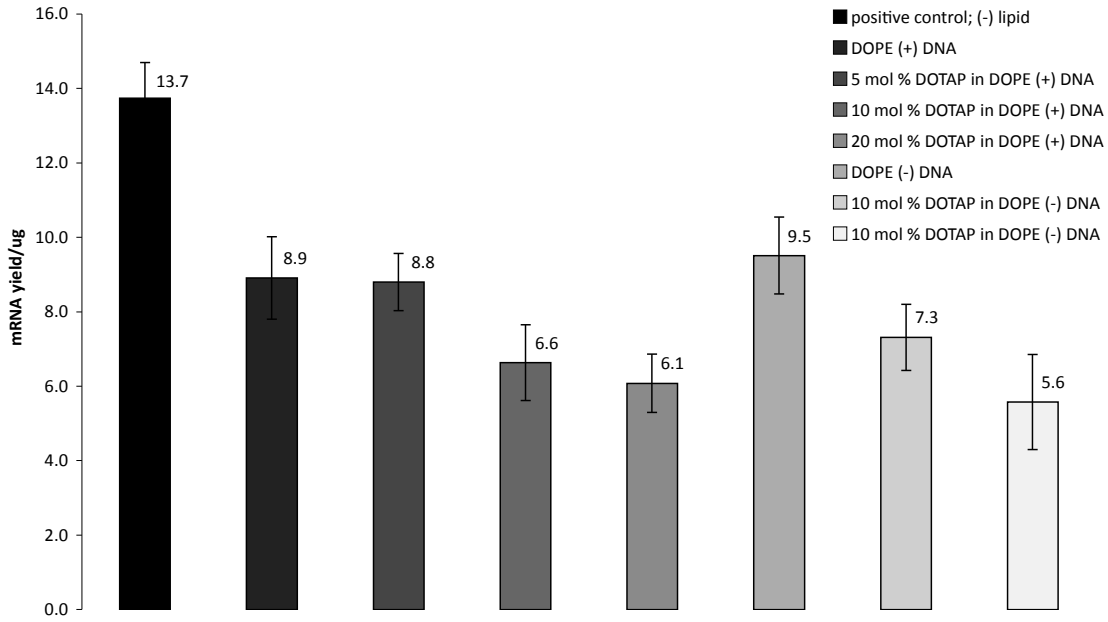

Figure 62: Incubation of T7 RNA polymerase (+) DNA and T7 RNAP (-) DNA with bulk phase DOPE/DOTAP mixtures. Incubation was carried out for a period of two hours in transcription buffer prior to transcription at 37 °C for 40 minutes. Initiation of transcription was achieved by the addition of rNTPs, and template DNA in those samples where DNA was not included in the incubation of the polymerase with the bulk lipid phase.

Figures 61 and 62 show that the loss in transcriptional activity observed on adding DOTAP to the inverse hexagonal phase of DOPE has two causes. There is some inactivation of the

T7 RNA polymerase enzyme caused by the increasing DOTAP concentration (see figure 61). It is possible that this effect is similar to the deactivation of T7 RNAP by DOPE observed in the absence of DTT in the transcription buffer, as detailed in section 2.8 of this thesis. This hypothesis could be tested by increasing the DTT content of the transcription buffer, although results detailed in chapter 2 of this thesis showed that DTT concentrations of 30 mM and greater actually caused a decrease in transcriptional activity so this may not work. Figure 61 shows complete deactivation of transcription once a DOTAP content of 20 mol % is achieved. As these samples contained DNA within the inverse hexagonal structure, and there is evidence in the literature for increased partitioning of DNA into the inverse hexagonal phase at a DOTAP content of 5 mol % in DOPE,[75] it is likely that at 20 mol % the partition coefficient is sufficiently high to prevent transcription.

5.4 Laser Scanning Confocal Microscopy (LSCM)

The LCSM study carried out as part of this work involved using separate laser light sources on the Leica SP5 microscope to excite individual fluorophores. Cells were cultured in microscope chambers, with bottoms of coverslip thickness. To begin each session, untreated cells were used to set the gain values on the microscope channels, such that no natural autofluorescence was detected. This ensured that any signal detected from cells treated with transfection agents was directly caused by the experimental setup. Samples were viewed through the confocal microscope eyepiece, and when cells showing a positive transfection result (i.e. the production of AmCyan), an image was collected using the microscope software. This provided the best method for scanning each whole well of the microscope chamber for positive cells. Typical cell length for a culture of HeLa cells that are well-adhered and in good health is roughly 40-50 μM.

	Label	Excitation λ_{max} /nm	Emission λ_{max} /nm	Laser line /nm
Lipid	**Lissamine Rhodamine B**	557	571	561
DNA	**Alexa 488**	495	519	488
	Label-IT Cy5	649	670	633
Protein	**AmCyan**	458	491	458

Table 3: Fluorophores used in the transfection experiments

5.5 Uptake of DOPE hexosomes by HeLa cells

Preliminary experiments involving the incubation of DOPE hexosomes doped with 0.1 mol % lissamine rhodamine-B headgroup-labelled DOPE with HeLa cells we carried out. Cells were incubated with hexosomes for different lengths of time between 1 and 8 hours, and were fixed for microscopy (using 4 % paraformaldehyde solution, chosen for its non-precipitating properties) at the end of their incubation time.

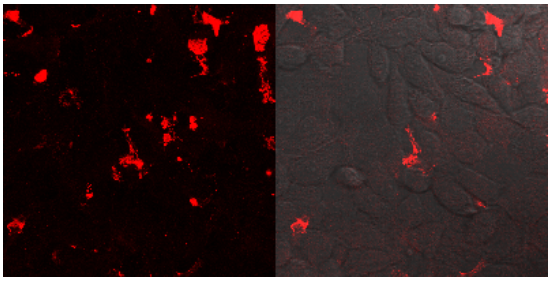

2 hour incubation, Opti-MEM

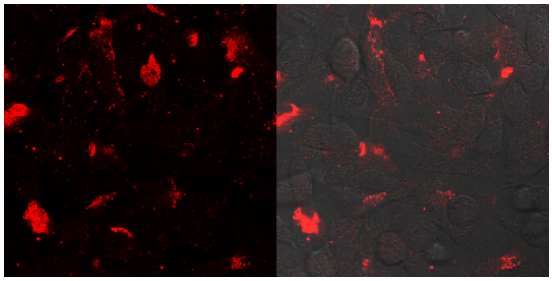

2 hour incubation, DMEM

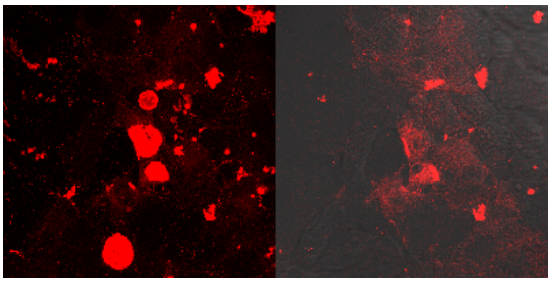

3 hour incubation, Opti-MEM

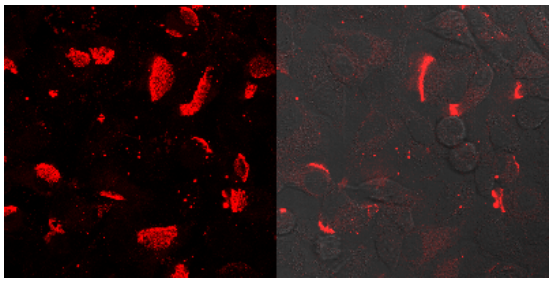

3 hour incubation, DMEM

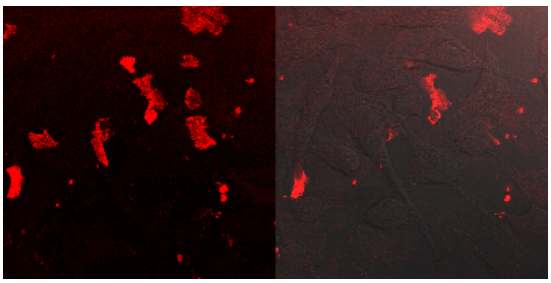

4 hour incubation, Opti-MEM

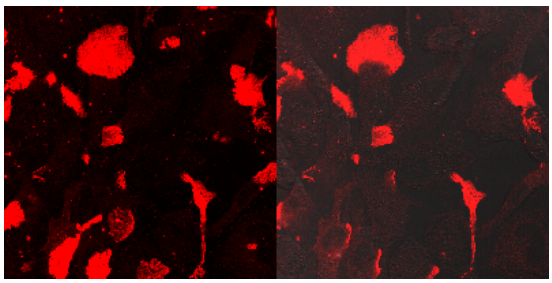

4 hour incubation, DMEM

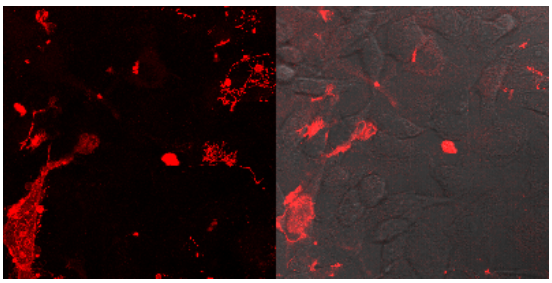

5 hour incubation, Opti-MEM

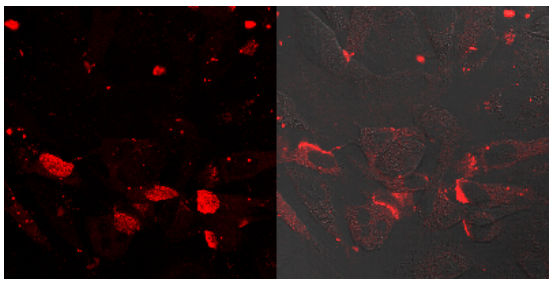

5 hour incubation, DMEM

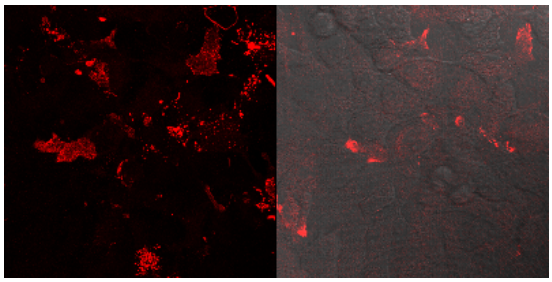

6 hour incubation, Opti-MEM

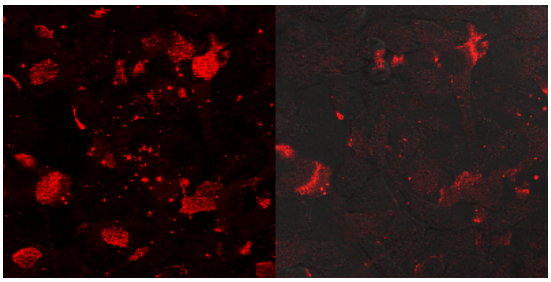

6 hour incubation, DMEM

Figure 63: Uptake of DOPE hexosomes by HeLa cells in Opti-MEM reduced serum medium and DMEM 5% FCS. In each image the left-hand pane represents the maximum projection image for the lipid channel, while the right-hand pane shows a single slice of the lipid channel superimposed on the DIC cellular image.

Figure 63 shows that the hexosomes are internalised by the cells within two hours of incubation. At around 5 hours of incubation networks within the cells appear to be labelled by the fluorescent lipid; this is particularly visible in the maximum projection image of the experiment carried out in Opti-MEM (see figure 64). It is also apparent from this set of images that, even after a long incubation, where a large amount of lipid is deposited on the cells, that cytotoxicity is not an issue at the concentration of lipid used (4 mg ml^{-1}), which is four times the concentration that was used in subsequent experiments. The appearance of vesicular structures after incubation at 37 °C for eight hours (see figure 65) further supports the suggestion that lipid is taken up from the hexosomes and repackaged within cells. Lipids are clearly visible in many parts of the internal cellular structure, although never the nucleus (as is supported by these, and other images forming part of this study, see figures 64 and 65) before leaving the cell as vesicles.

Figure 64: hexosomes (DOPE:pluronic F-127; 9:1) incubated with cells for 5 hours in Opti-MEM reduced serum media, before fixation with a 3.7 % paraformaldehyde solution.

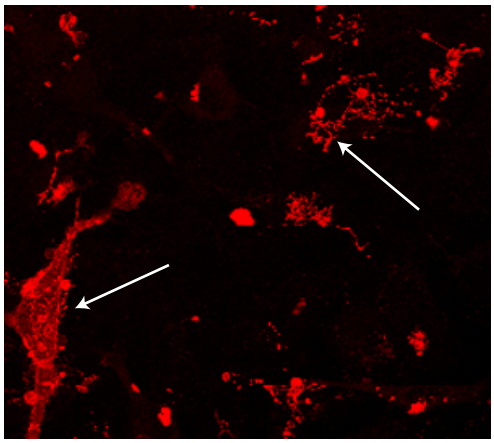

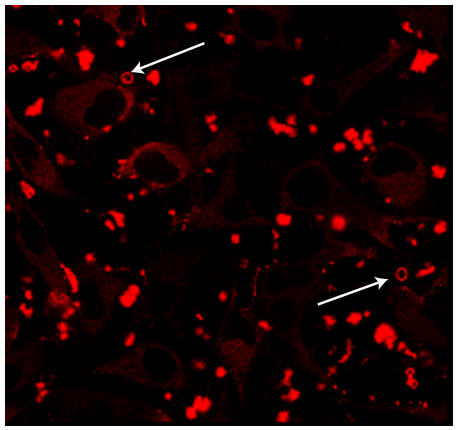

Figure 65: hexosomes (DOPE:pluronic F-127; 9:1) incubated with cells for 8 hours in Opti-MEM reduced serum media, before fixation with a 3.7 % paraformaldehyde solution. Note how the nuclei are clearly visible in the cells, by their absence of lipid (displayed in red). Arrows have been used to highlight vesicular structures of fluorescent lipid that have left the cells. These are visible as small rings of red pigment.

5.6 Colocalisation of lipids and DNA

There are many publications on the structures formed from lipids and DNA, and in particular the driving forces behind, and evidence of, DNA partitioning into the inverse hexagonal phase of phospholipids. In order to show that the DNA is located within the inverse hexagonal phase in hexosome form, the DOPE portion of the hexosomes was doped with 0.1 mol % lissamine rhodamine B (LRB) headgroup-labelled DOPE, while linearised DNA was also fluorescently labelled.

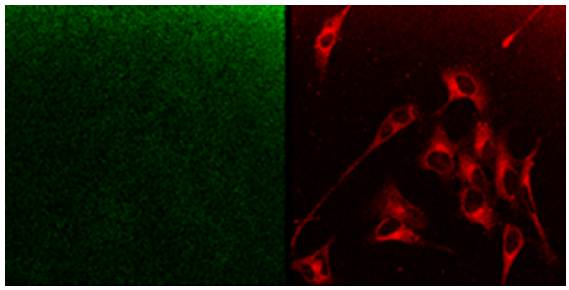

A: 2h DOPE, Opti-MEM

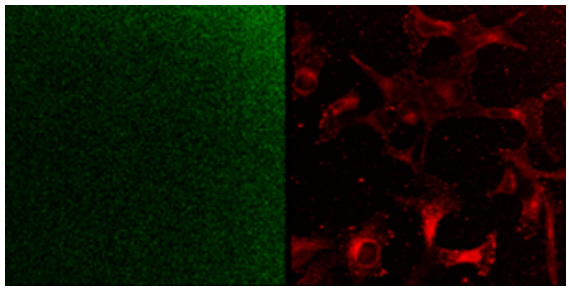

E: 4h DOPE Opti-MEM

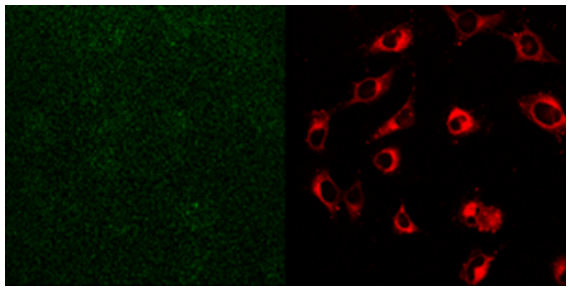

B: 2h DOTAP 5 mol % in DOPE, Opti-MEM

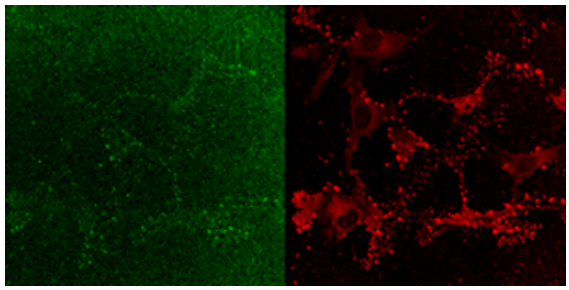

F: 4h DOTAP 5 mol % in DOPE, Opti-MEM

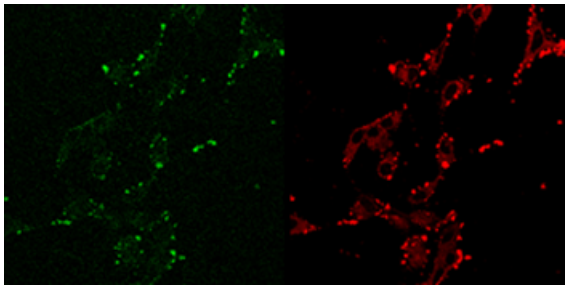

C: 2h DOTAP 10 mol % in DOPE, Opti-MEM

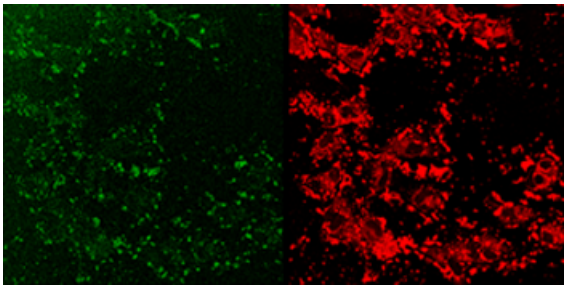

G: 4h DOTAP 10 mol % in DOPE, Opti-MEM

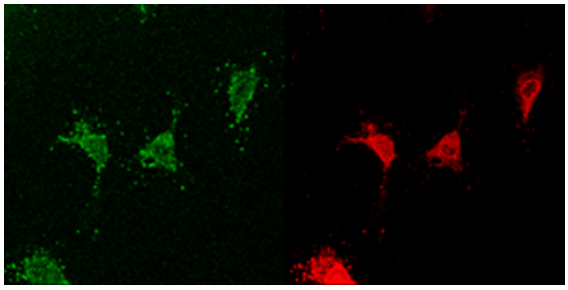

D: 2h DOTAP 20 mol % in DOPE, Opti-MEM

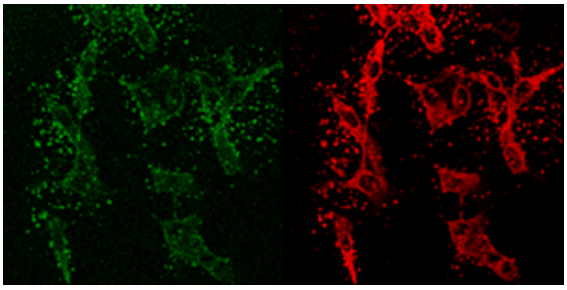

H: 4h DOTAP 20 mol % in DOPE, Opti-MEM

Figure 66: Colocalisation of DNA that is fluorescently labelled by PCR-driven incorporation of an Alexa-488 tagged aminoallyl dUTP nucleotide (green) and hexosomes labelled with lissamine-rhodamine B headgroup labelled DOPE (red). On the left hand side of the table (images A-D) are cells that have been incubated with the hexosomes for 2 hours, while on the right (images E-H) show cells incubated with hexosomes for 4 hours. Moving down the table represents and increase in DOTAP content of the hexosomes, over the hexagonal region determined for DOPE and DOTAP mixtures by SAXS and polarising light microscopy as outlined in other chapters of the thesis.

Figure 66 shows images of LRB labelled hexosomes doped with linearised-t7-cyan DNA labelled by PCR incorporation of a fluorescent Alexa-488 labelled aminoallyl-dUTP analogue. The images show a high degree of colocalisation of the lipid and DNA species in serum-free medium, which increases with increasing DOTAP content. The colocalisation of the DNA appears to be visible for the samples where a great degree of aggregation occurs, which is suggestive that even in samples appearing to show no colocalisation, it may be that the signal from the Alexa-488 is too weak to be detected.

The concentration of labelled DNA was increased (from 0.4 μg DNA per mg lipid, as was used in the transcription experiments of chapter 2, to 2 μg DNA per mg lipid) and a slight improvement in visibility of the DNA was observed, but it was still not possible to see the location of the DNA in situations other than where large aggregates had formed. It is worth noting from these pictures, however, that even with relatively high concentrations of

hexosomes (2 mg ml^{-1} total lipid) the cells are adhered, flat and evenly spread with no sign of rounding, and appear in general good health. The pictures in figure 66 were taken of cells fixed approximately 24 hours after addition of lipid, suggesting a relatively low level of toxicity that likely results from the fact that DOPE is a naturally occurring lipid.
Incubations of these fluorescent hexosomes and HeLa cells have been carried out for time periods of up to eight hours; during these experiments the general health of the cells appears to be good, and movement of the fluorescently tagged lipid within the cell can be observed, with structures such as the endoplasmic reticulum becoming visible, before fluorescent vesicles are observed leaving the cells as part of exocytosis (see figure 65). It is also apparent that within two hours of incubation the lipid has entered the cell, although results in serum-containing medium suggest that a more appropriate incubation time may be four hours, as there is less aggregation in these samples and uptake of lipid complexes appears to be slower. Cells incubated with lipoplexes in DMEM are less bright under the microscope, with less lipid visible on the cell surface.

Figure 67: The Mirus Label IT DNA labelling kit. The fluorophore (cy5) is attached to the DNA by a covalent bond with the reactive group at the end of the linker molecule. Reproduced with permission from Mirus Bio

Improved results from the colocalisation studies were sought using an alternative method of fluorescently labelling DNA. The Label-IT nucleic acid labelling system from Mirus Bio aims to label an intact piece of DNA (either linear or plasmid), rather than through enzymatic incorporation. This method has been successfully used in studies similar to this to highlight the use of hexosome species to deliver plasmid DNA, although the study showed that DNA and lipid were not colocalised inside cells.
The main advantage of the Mirus Label-IT tagging system over the PCR incorporation of fluorescent nucleotide analogues is that the density of the label may be greatly increased in

the label-IT protocol. PCR incorporation uses an aminoallyl-dUTP analogue, which can only replace a maximum of 1 in 4 nucleotides in the PCR sequence (in reality the reaction conditions dictate that the number of fluorophores included the PCR product is far lower than this). The Label-IT procedure involves covalent bonding of a fluorophore to the DNA duplex, anywhere along its length. The result of this is that the visibility of labelled DNA is far greater when using the Label-IT protocol, with visibility of DNA at small concentrations that were not visible using DNA labelled by PCR incorporation.

5.7 Evidence of colocalisation of lipid and DNA outside and within cells

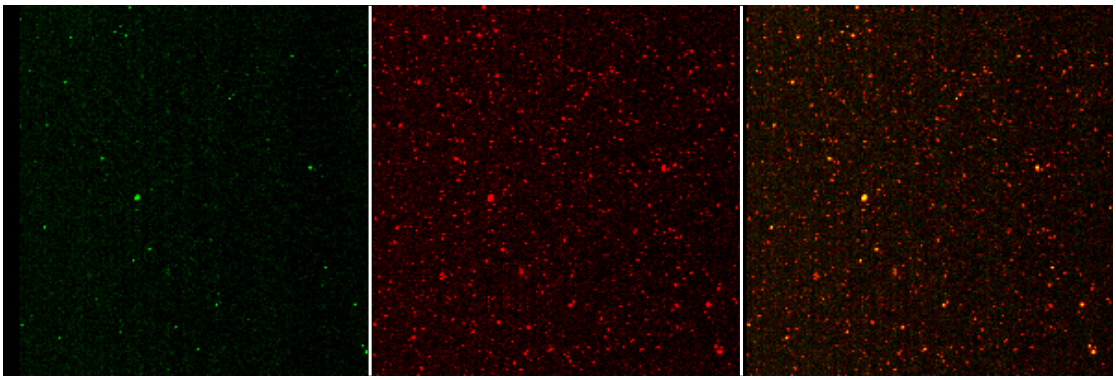

A: DOPE hexosomes and cy5 labelled DNA in DMEM

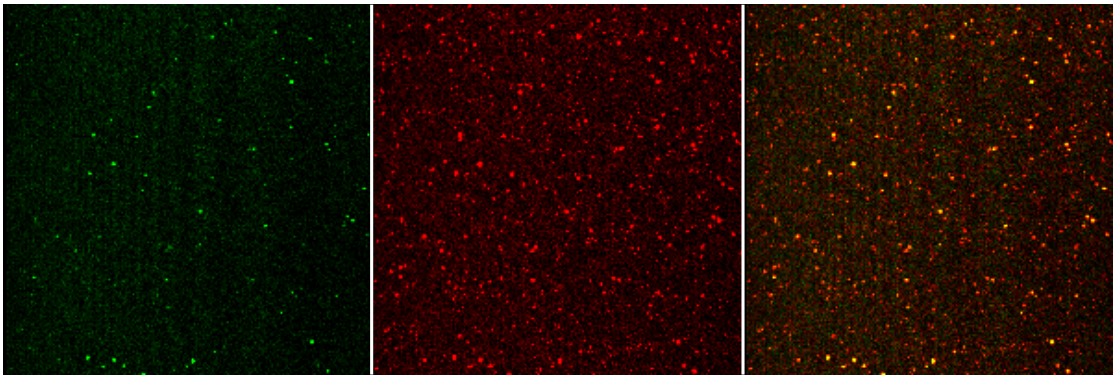

B: 5 mol % DOTAP in DOPE hexosomes and cy5 labelled DNA in DMEM

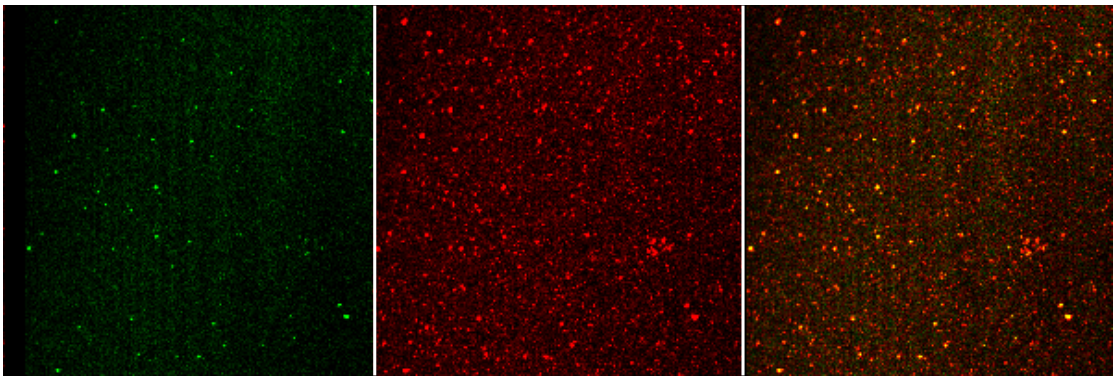

C: 10 mol % DOTAP in DOPE hexosomes and cy5 labelled DNA in DMEM

Figure 68: Images showing colocalisation of hexosomes and Label-IT cy5 tagged linearised-T7-cyan DNA incubated for several days in DMEM supplemented with 5 % fetal calf serum, in the absence of cells. The green channel (left) represents the DNA, the red channel (middle) represents hexosomes and the right hand channel shows both red and green channels, colocalisation is observed as yellow dots in the right hand channel.

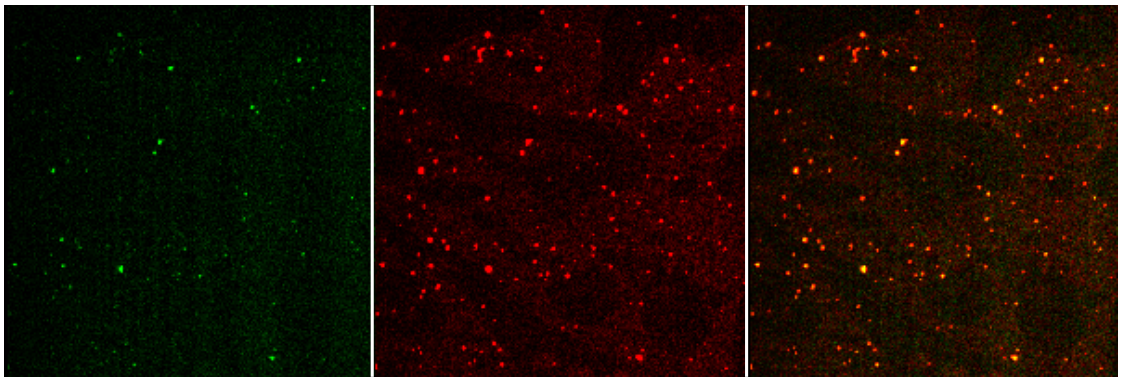

A: DOPE hexosomes and cy5 labelled DNA in Opti-MEM

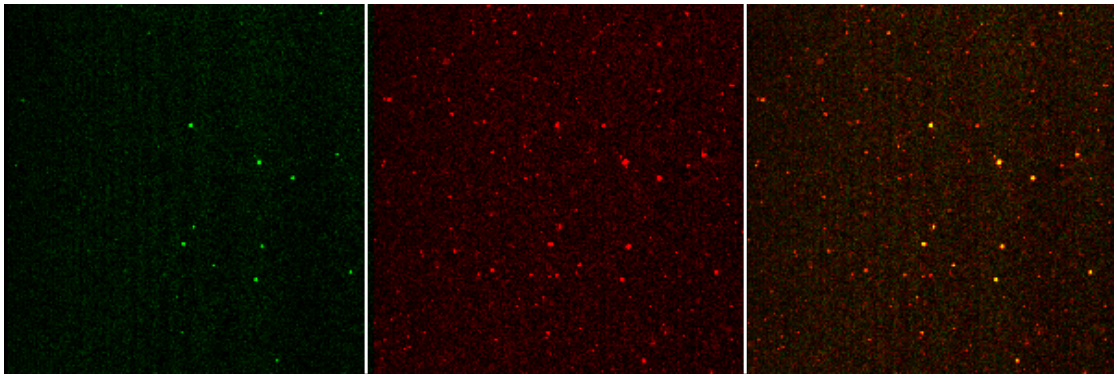

B: 5 mol % DOTAP in DOPE hexosomes and cy5 labelled DNA in Opti-MEM

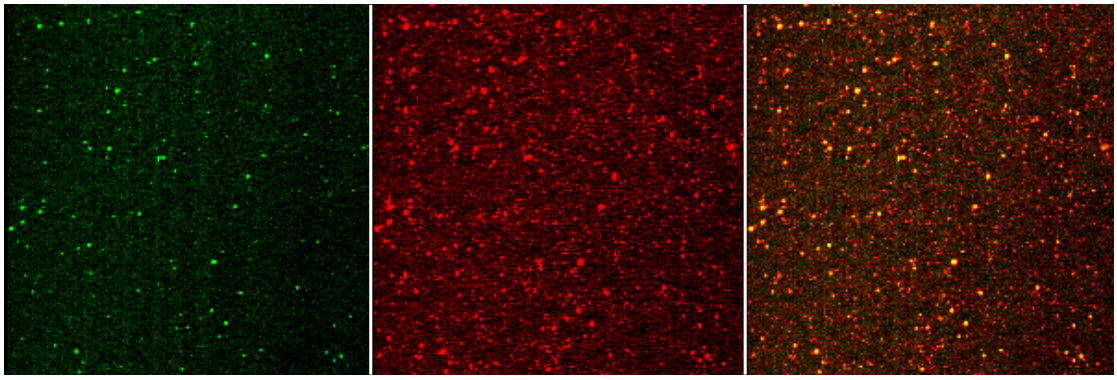

C: 10 mol % DOTAP in DOPE hexosomes and cy5 labelled DNA in Opti-MEM

Figure 69: Images showing colocalisation of hexosomes and Label-IT cy5 tagged linearised-T7-cyan DNA incubated for several days in Opti-MEM serum-free medium, in the absence of cells. The green channel (left) represents the DNA, the red channel (middle) represents hexosomes and the right hand channel shows both red and green channels

Figures 68 and 69 show that for a DOTAP concentration of up to 10 mol %, in serum-containing and serum-free medium there is a great degree of colocalisation between the DNA and the hexosomes. The number of green spots appears to increase with increasing DOTAP content, suggesting that there may be a higher degree of colocalisation with increasing DOTAP content. In all cases green spots representing DNA can be matched to

their red lipid counterpart, suggesting that there is no aggregated lipid-free DNA in the system. All samples appear to be particulate, in that both channels show discreet signals rather than a general glow.

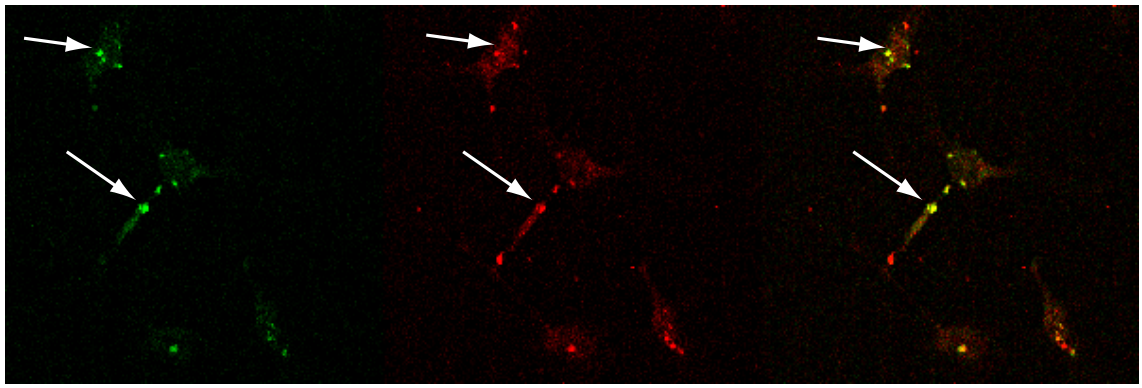

A: DOPE hexosomes, 4 hours incubation with cells in DMEM

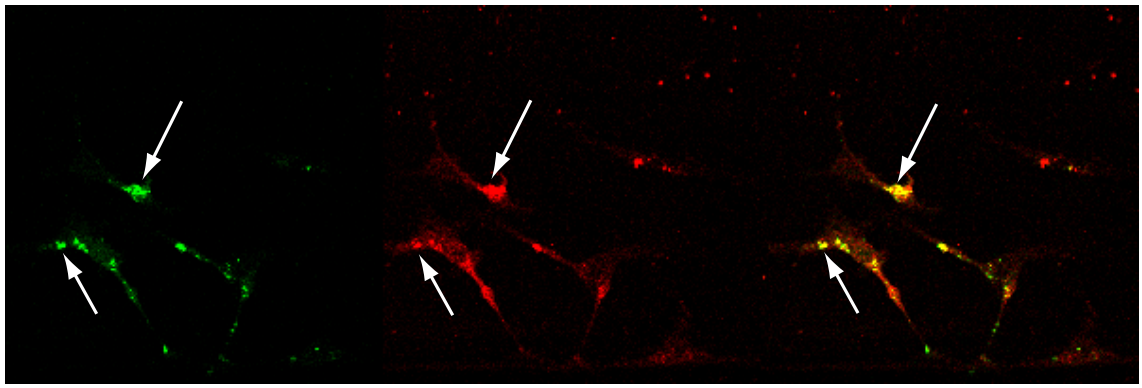

B: 5 mol % DOTAP in DOPE hexosomes, 4 hours incubation with cells in DMEM

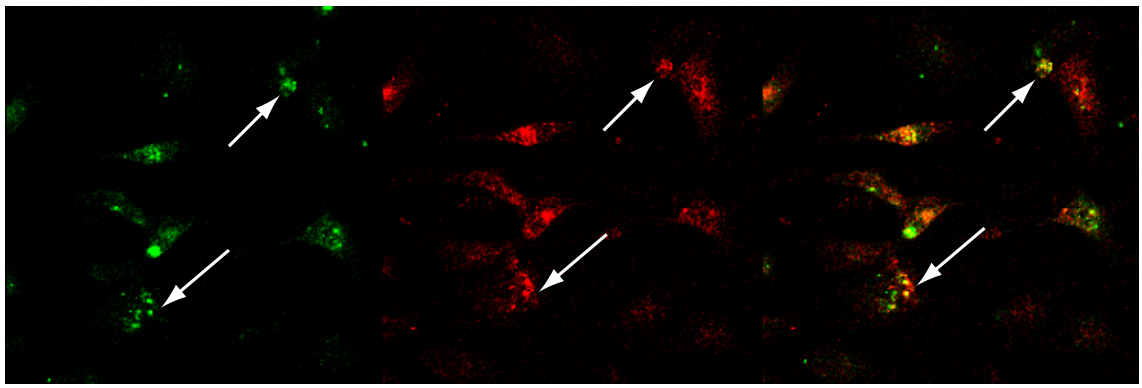

C: 10 mol % DOTAP in DOPE hexosomes, 4 hours incubation with cells in DMEM

Figure 70: Images showing colocalisation of hexosomes and Label-IT cy5 tagged linearised-T7-cyan DNA incubated for several days in DMEM supplemented with 5 % fetal calf serum, in the presence of cells (image taken 24 hours after a 4 hour incubation with cells). The green channel (left) represents the DNA, the red channel (middle) represents hexosomes and the right hand channel shows both red and green channels. Arrows are used to highlight some of the areas of colocalisation of lipid and DNA within cells, there are several examples in each picture.

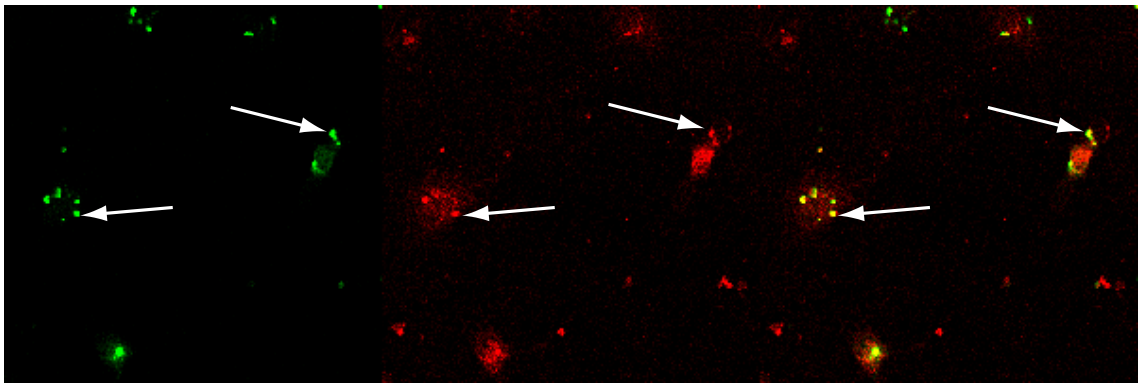

A: DOPE hexosomes, 4 hours incubation with cells in Opti-MEM

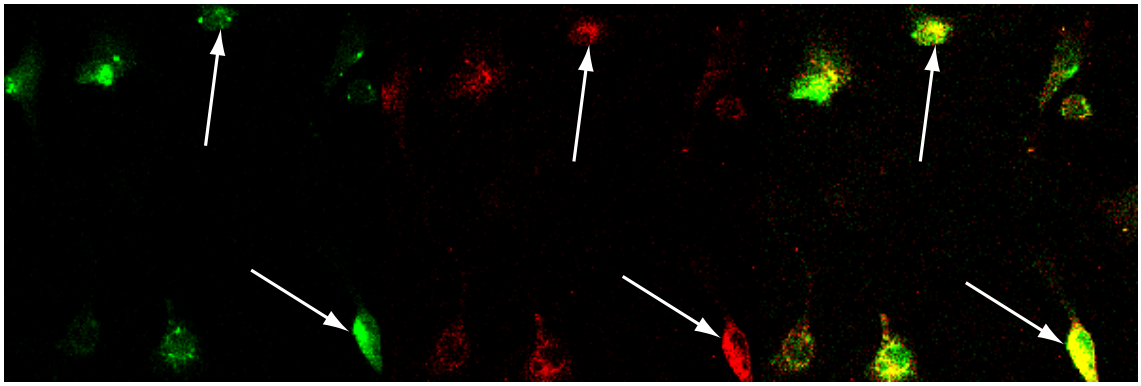

B: 5 mol % DOTAP in DOPE hexosomes, 4 hours incubation with cells in Opti-MEM

Figure 71: Images showing colocalisation of hexosomes and Label-IT cy5 tagged linearised-T7-cyan DNA incubated for several days in Opti-MEM serum-free medium, in the presence of cells. The green channel (left) represents the DNA, the red channel (middle) represents hexosomes and the right hand channel shows both red and green channels. Arrows are used to highlight some of the areas of colocalisation of lipid and DNA within cells, although there are several examples in each picture.

It is clear from figures 70 and 71 that there is a good degree of colocalisation of lipid and DNA within the cells. This is apparent from the fact that at lower DOTAP contents (up to 5 mol % DOTAP in DOPE) there are no areas of DNA (in green) that cannot be matched to an area of lipid (red). As the DOTAP content is increased to 10 mol % (figure 70C) areas of green are seen that are not colocalised with red, suggesting that some of the DNA is dissociated from the lipid inside the cell. It is also visible that, for the most part, lipoplexes are located within the cytoplasm or at the edge of the nucleus and not within the nucleus itself.

Previous experiments detailed in the literature used mixtures of DOPE and DOPC with cationic lipids DOTAP, DOSPA and DMRIE to transfect mouse fibroblast cells with plasmid

DNA.[23, 153] It was shown that for L_{α}^{C} complexes some colocalisation of lipid and DNA was observed within cells, but that a significant amount of DNA was present in the cytoplasm as a lipid-free aggregate. This study was extended to a DOPE weight fraction of 0.7 (defined as DOPE/(DOPE + DOTAP)), which corresponds to a DOTAP concentration of 30 mol % in DOPE using the nomenclature employed in this thesis. The DNA used in the study by Lin *et al* was a plasmid encoding the luciferase gene, with no evidence of it having been linearised in the paper. The transfection study outlined in this thesis differs from the Lin *et al* study in that the lipid mixtures used ventured deeper into the inverse hexagonal region of the phase diagram, at higher DOPE contents, and used a linearised DNA template for formation of the inverse hexagonal complexes.

5.8 Transient transfection to produce T7 RNA polymerase

In order to link the transfection experiments to the transcription of DNA located in the inverse hexagonal phase of DOPE (see chapter 2), hexosomes of DOPE with DNA containing the gene for the protein AmCyan under T7 control were introduced to cells.

In order to promote production of the AmCyan protein under T7 control in the hexosomes colocalised with linearised-T7-cyan DNA, the HeLa cells first had to be manipulated to produce T7 RNA polymerase. There are several options in the literature, including introduction of modified viruses that contain the genetic sequence for T7 RNA polymerase,[134, 135, 137, 154] introduction of mRNA coding for T7 RNA polymerase,[155] or transient transfection from a plasmid vector. Two of these methods were evaluated using the AmCyan gene to assess their efficiency. The messenger RNA method was attempted, using Transmessenger RNA transfection reagent (Qiagen), but production of sufficient mRNA (by *in vitro* transcription) that contained both the ^{7}mG cap and poly(A) tail required for efficient translation was difficult. The ^{7}mG cap was incorporated by doping the ribonucleotide mixture with cap analogue in a standard T7 RNA polymerase transcription and the tail was added subsequently, using *E. coli* poly(A) polymerase. The transfection reagent (Transmessenger, by Qiagen) proved incredibly cytotoxic, causing apoptosis in 90% of cells at the specified concentration after an incubation time of less than two hours, and as such transfection efficiency was poor. Transient transfection was first attempted using the commercially available pAmCyan plasmid (Clontech) and Attractene transfection reagent (Qiagen). Attractene was also found to be quite cytotoxic but a titration was performed to find the most appropriate concentration for the cells, in terms of lower cytotoxicity and greater protein production in all cells. Concentrations of Attractene used in the titration are shown in table 4, with an value of transfection efficiency given for successful concentrations. Higher concentrations were not assigned transfection efficiencies as the cell density had decreased by too much (by greater than 50%, and at the highest concentrations greater than 90%) to give a representative value. The health of the cells was assessed by monitoring their general morphology; as adherent cells undergo apoptosis, they become rounded and raised, before detaching from the surface. Transfection is quantified using the transfection efficiency; this maybe be gathered using fluorescence assisited cell sorting (FACS) where facilities allow, or by expressing the number of cyan cells relative to the total number of cells as a percentage.

Concentration Identification	Volume of Opti-MEM/µl	Volume of pAmCyan DNA/µg	Attractene (µl)/ Vol. Opti-MEM (µl)	Attractene (µl)/ Vol. Opti-MEM (µl) when added to cells	Transfection Efficiency/%
1*	**60**	**0.4**	**25×10^{-3}**	**4.2×10^{-3}**	n/a
2	**120**	**0.4**	**13×10^{-3}**	**2.1×10^{-3}**	n/a
3	**180**	**0.4**	**8.3×10^{-3}**	**1.4×10^{-3}**	n/a
4**	**240**	**0.4**	**6.3×10^{-3}**	**1.0×10^{-3}**	n/a
5	**300**	**0.4**	**5.0×10^{-3}**	**0.8×10^{-3}**	34.8
6	**360**	**0.4**	**4.2×10^{-3}**	**0.7×10^{-3}**	14.4
8	**500**	**0.4**	**3.0×10^{-3}**	**0.5×10^{-3}**	12.3
10	**600**	**0.4**	**2.5×10^{-3}**	**0.4×10^{-3}**	7.7

Table 4: reaction conditions for concentration gradient of attractene transfection reagent. *denotes advised concentration for 2 cm^2 dish, **denotes corresponding advised concentration for 1 cm^2 growth area used in this study. Where the transfection efficiency is not given, the cytotoxicity of the Attractene reagent was too great to judge the efficiency

The DNA solution was diluted in the appropriate amount of Opti-MEM serum free medium, before addition of the attractene transfection reagent. The complexes were incubated at room temperature (20 minutes) before addition to cells in fresh DMEM (with 10% FCS but no antibiotics). Cells were incubated for 24 hours under normal culture conditions.

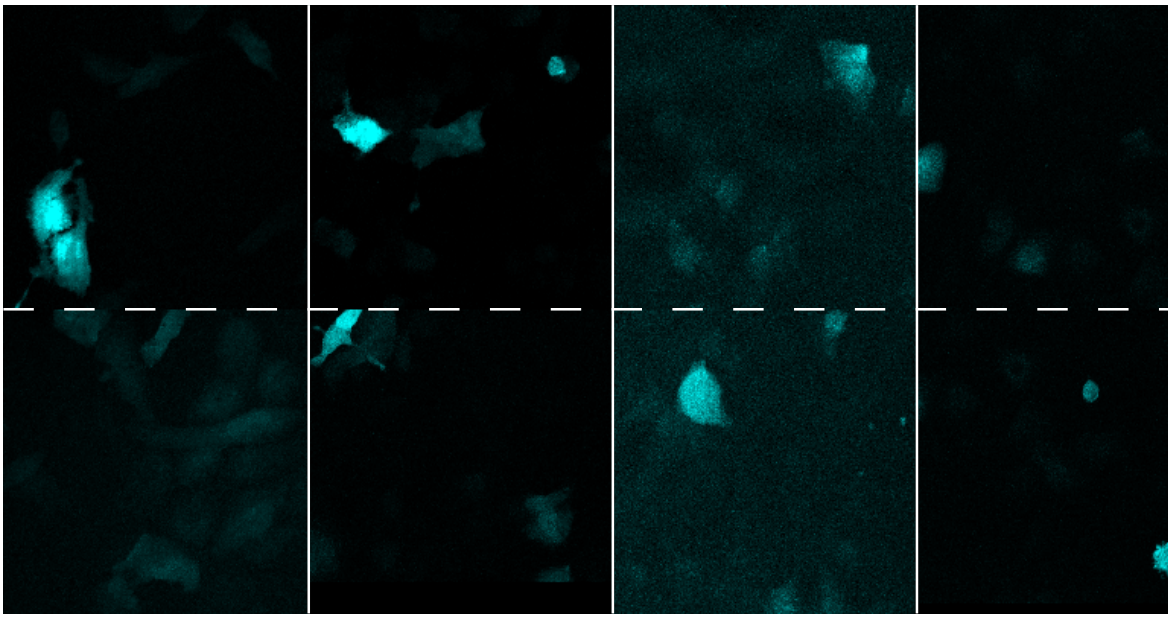

Figure 72: Concentration gradient of Attractene transfection agent and pAmCyan in cells produced with varying concentrations of Attractene transfection reagent. L-R: concentrations 5, 6, 8 and 10 (see table…)

Once it was established that transient transfection could be reliably used to produce AmCyan fluorescent protein, the AmCyan gene was excised from the plasmid and replaced with the gene coding for T7 RNA polymerase, which had been excised from the TargeTron pAR1219 vector (Sigma), built by Davanloo *et al.* in the 1980s.[156] This plasmid was analysed using gel electrophoresis and then amplified by transformation in *E. coli.* This plasmid, termed pAmT7Pol was used to transfect cells approximately 24 hours prior to introduction of the hexosome complexes, in keeping with the recommended protocols for both the Attractene reagent and the pAmCyan vector.

A concentration gradient of Attractene using the pAmCyan plasmid was carried out to ascertain the optimal conditions for transient transfection in this way (i.e. best production of protein, in the most cells with least toxicity). It was discovered, as shown in figure 72 that the best concentration for production of AmCyan using Attractene was concentration 5 (in table 4). It is worth noting, however, that the pAmCyan plasmid sourced from Clontech contains genes that are mammalian codon optimised, which would possibly mean that production of the T7 RNA polymerase gene product may be less efficient than the fluorescent gene. It is apparent, however, from the observation of cyan protein produced from the pAmT7/T7cyan system that T7 RNA polymerase produced as a result of transfection using Attractene (see figure 73).

5.9 Production of AmCyan from the T7-based system

Hexosomes were prepared by dispersing dried lipid samples (10 mg total lipid) in 300 µl pluronic-F127 coblock polymer solution (3.3 mg ml^{-1} in 1% ethanol) in an ultrasonic bath. Hexosome solutions were then stored at 37 °C until use (hexosomes were made fresh for each experiment and stored overnight at 37 °C before dilution in cell culture medium, although there is evidence to suggest that they are stable for periods of six months or more). Prior to transfection into cells, hexosomes were diluted in appropriate cell culture medium (either with or without serum) and lin-pT7Cyan DNA was added. Twenty-four hours after transient transfection of the HeLa cells to produce T7 RNA polymerase, the hexosomes were incubated with cells for 4 hours. The hexosome-containing medium was then removed from the cells, which were washed with PBS and resuspended in serum-containing medium. Cells were left to produce cyan fluorescent protein for 48 hours before being fixed with 3.7% paraformaldehyde solution and stored in PBS:glycerol (10:90) for imaging.[157]

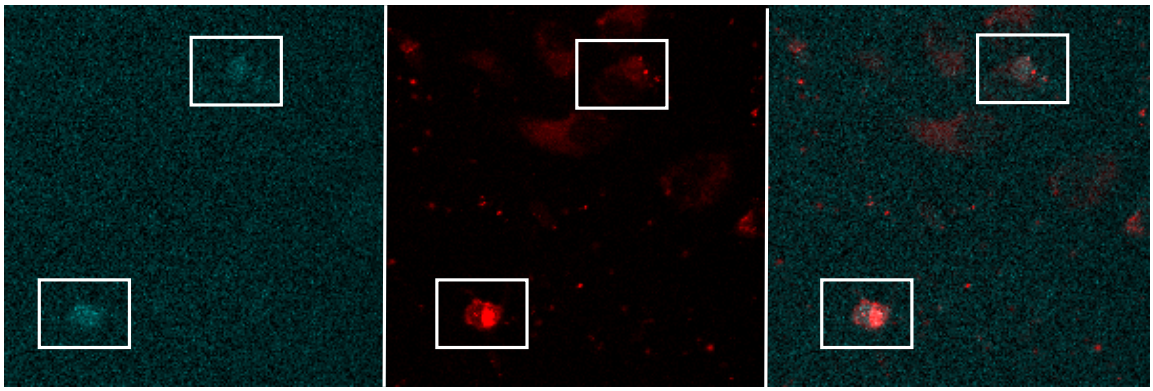

DOPE hexosomes with the AmT7/T7cyan system in Opti-MEM

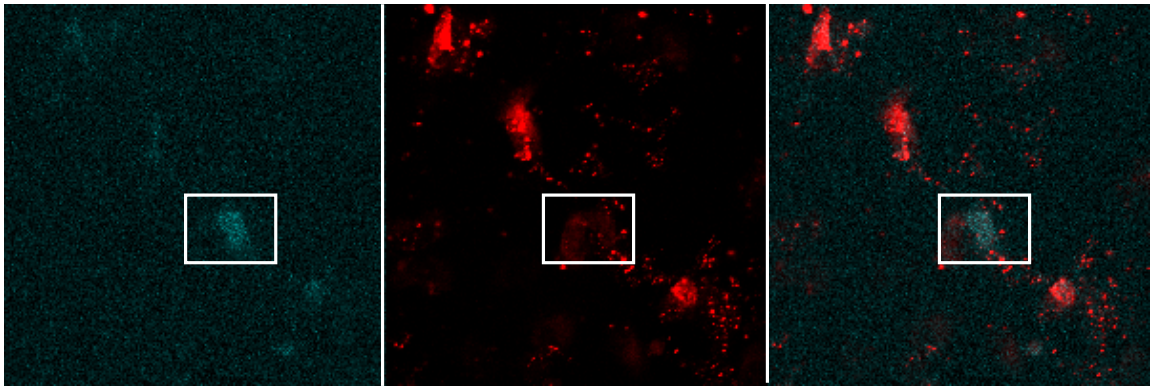

5 mol% DOTAP in DOPE hexosomes with the AmT7/T7cyan system in Opti-MEM

Figure 73: Transfection of HeLa cells with AmCyan using the AmT7/T7cyan double transfection method. Cells expressing detectable levels of cyan protein are highlighted.

The images displayed in figure 73 highlight cells that are producing the AmCyan protein from a linearised piece of DNA containing a T7 promoter inside HeLa cells producing T7 RNA polymerase. The efficiency of transfection, defined as the number of cells expressing AmCyan relative to the total number of cells, is low (22% for DOPE hexosomes, 55 % for hexosomes of 5 mol % DOTAP in DOPE) but it is worth noting that the concentration of attractene transfection reagent was concentration 8 (referred to in table 4 and as detailed in figure 72). Efficiency of transfection at this concentration is relatively low. Even so, there are still a few blue cells visible in this small image (two in the case of DOPE, six for hexosomes made of 5 mol % DOTAP in DOPE). It is also worth mentioning the fact that the DNA containing the protein sequence is linearised, and that this may well affect the efficiency of transcription and translation of the gene product. There is some evidence to show that transcription from plasmid templates is more efficient than that from linear

templates because the polymerase may stay on the plasmid, instead of disassociating with the DNA and having to once again find the correct place on the same strand, or another strand of DNA. In this manner, the association of the polymerase with the T7 promoter sequence would likely become the rate-limiting step of the process. The detectable production of AmCyan protein from some cells is accompanied by a marked, visible change in the autofluorescence of the remaining cells when viewed through the eyepiece of the confocal microscope. This change is not, however, picked up by the detector. It is therefore clear that production of the AmCyan gene using this method is possible, although subject to a degree of possible optimisation that was not undertaken during this study. That the levels of protein production in cells, and the incidence of protein-producing cells appears to be similar when the hexosomes consist entirely of DOPE, or of 5 mol% DOTAP in DOPE is to be expected, as the levels of *in vitro* transcription are not affected by the introduction of 5 mol % DOTAP both in the format of a bulk phase, or a dispersion, as shown previously in figures 61 and 62.

5.10 Control Experiments

Several control experiments were carried out to establish the limitations of using this double-transfection method of gene delivery. The primary concern was that the cells would take up the DNA presented to them without the need for hexosomes, although this proved to be unfounded, with multiple experiments showing that the cells did not produce the AmCyan protein in the presence in solution of either plasmid or linear DNA containing the relevant gene. Similarly, introducing hexosomes containing the AmCyan gene under T7 control did not yield the gene product in cells that had not first been transiently transfected to produce T7 RNA polymerase.

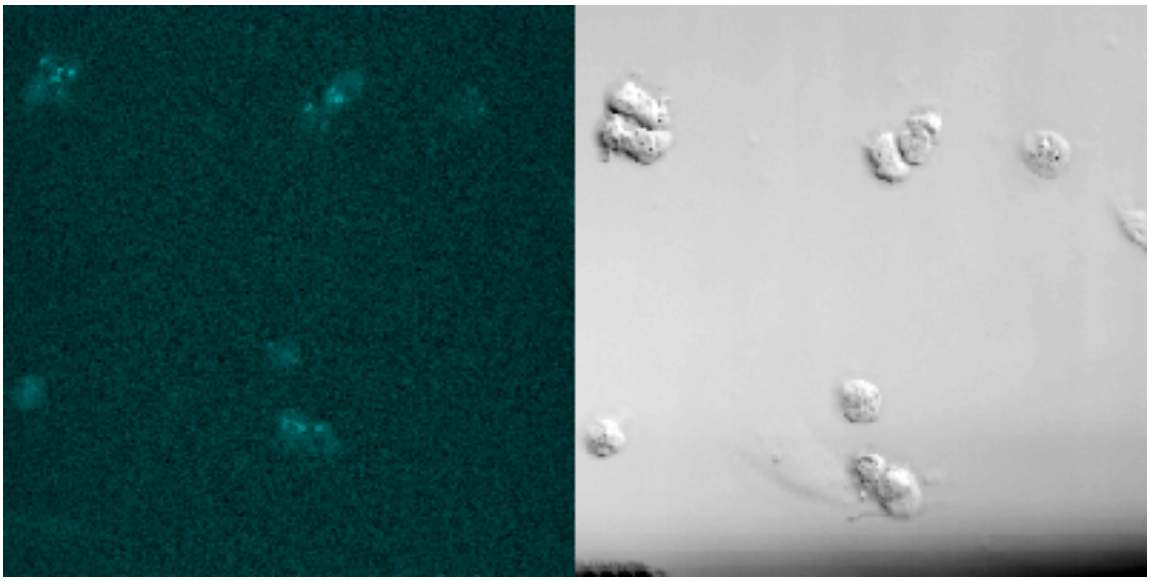

Figure 74: AmCyan production in cells transfected twice with Attractene transfection agent. Transfection one: Attractene with pT7pol; transfection two: Attractene with lin-pT7Cyan

Figure 74 shows that T7 RNA polymerase is produced in all cells visible. This indicates that the method of double transfection to produce T7 RNA polymerase and AmCyan under T7 control is possible and works well using commercial transfection reagents. It is worth mentioning, however, that the cell density in the above image is very low, at about one tenth of the cell density seen from other experiments (10,500 cm^{-2}, compared with over 100,000 cm^{-2} for a single transfection with DOPE hexosomes). This is because of the cytotoxic effects of Attractene experienced when attempting to deliver DNA to HeLa cells. Cells that take up too much of the Attractene compound frequently become rounded and fall off, leaving healthy cells that appear to be expressing less protein. The relative amount

of AmCyan compared with positive controls using a single-transfection of pAmCyan (see figure 72) appears to be much lower. It is likely that this is because the T7-cyan system uses a linear piece of DNA, from which the transcription would be much less efficient when compared with a plasmid template, resulting in less protein being produced and cells that are not as bright under the microscope.

It is also possible that production of T7 RNA polymerase is itself problematic for the HeLa cells. This is suggested because of the lack of a stable HeLa cell line transfected with T7 RNA polymerase. As HeLa cells and T7 RNA polymerase represent two systems that are frequently studied in biochemical and biophysical experiments, it would be expected that a stable cell line would have been deposited in one of the cell repositories available worldwide. This, plus the fact that other methods of T7 RNA polymerase expression in HeLa cells, such as the modified Vaccinia system reported by Bernard Moss and colleagues,[134] in which the HeLa die 72 hours post transfection are suggestive of instability. For these reasons further experiments were carried out, using the hexosome system to introduce both plasmid and linear DNA containing the AmCyan gene under mammalian promoter control, using the commercially available pAmCyan vector used for control experiments described earlier in this chapter.

5.11 Production of AmCyan from plasmid DNA

The ability of hexosomes to incorporate plasmid DNA into cells was assessed using the pAmCyan plasmid purchased from Clontech. The plasmid was incubated in cell culture medium with the hexosomes at 37 °C for three days, as in other experiments. Hexosomes were then introduced to cells and incubated for the standard 4 hours, or overnight and then removed from the cells. Cells were incubated under normal cell culture conditions for 48 hours to allow production of the AmCyan protein.

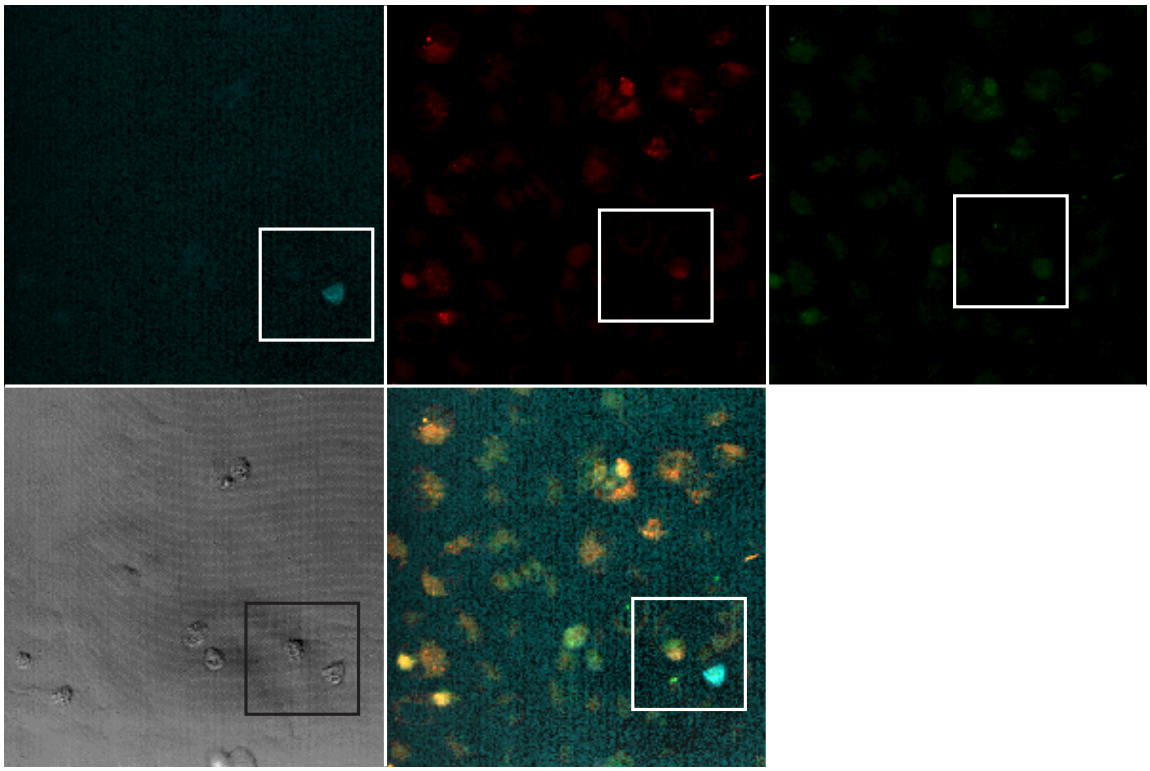

A: 5 mol % DOTAP in DOPE hexosomes, pAmCyan DNA, incubation 4 h in Opti-MEM, 48 h post-transfection

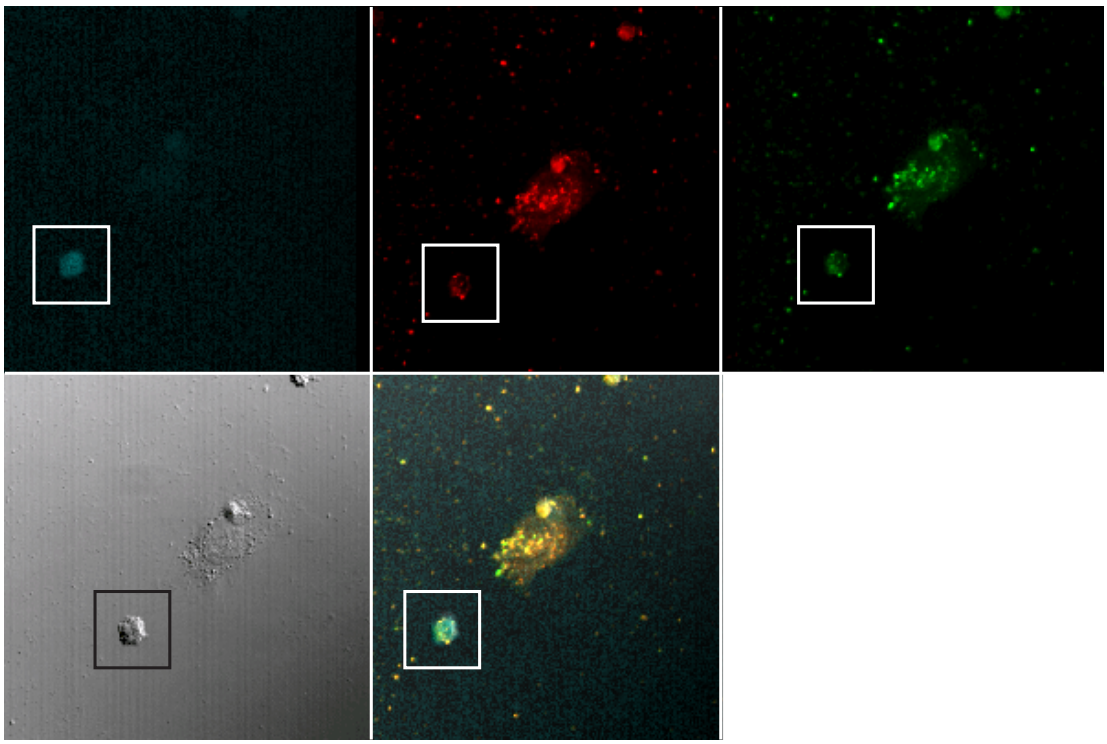

B: 10 mol % DOTAP in DOPE hexosomes, pAmCyan DNA, incubation 4 h in Opti-MEM, 48 h post-transfection

Figure 75: Tramsfection with pAmCyan and DOPE/DOTAP hexosomes, incubation 4h at 37 °C, 48 h post transfection

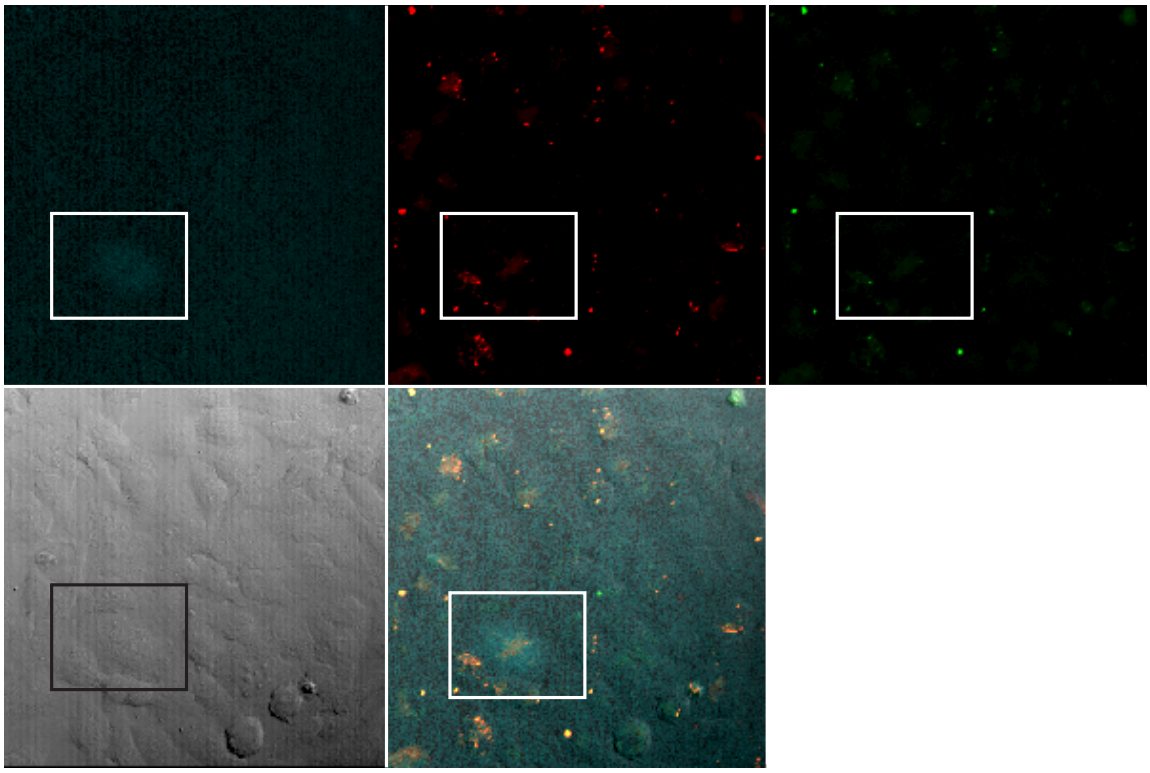

A: DOPE hexosomes, pAmCyan DNA, incubation 4 h in DMEM + 5% FCS, 48 h post-transfection

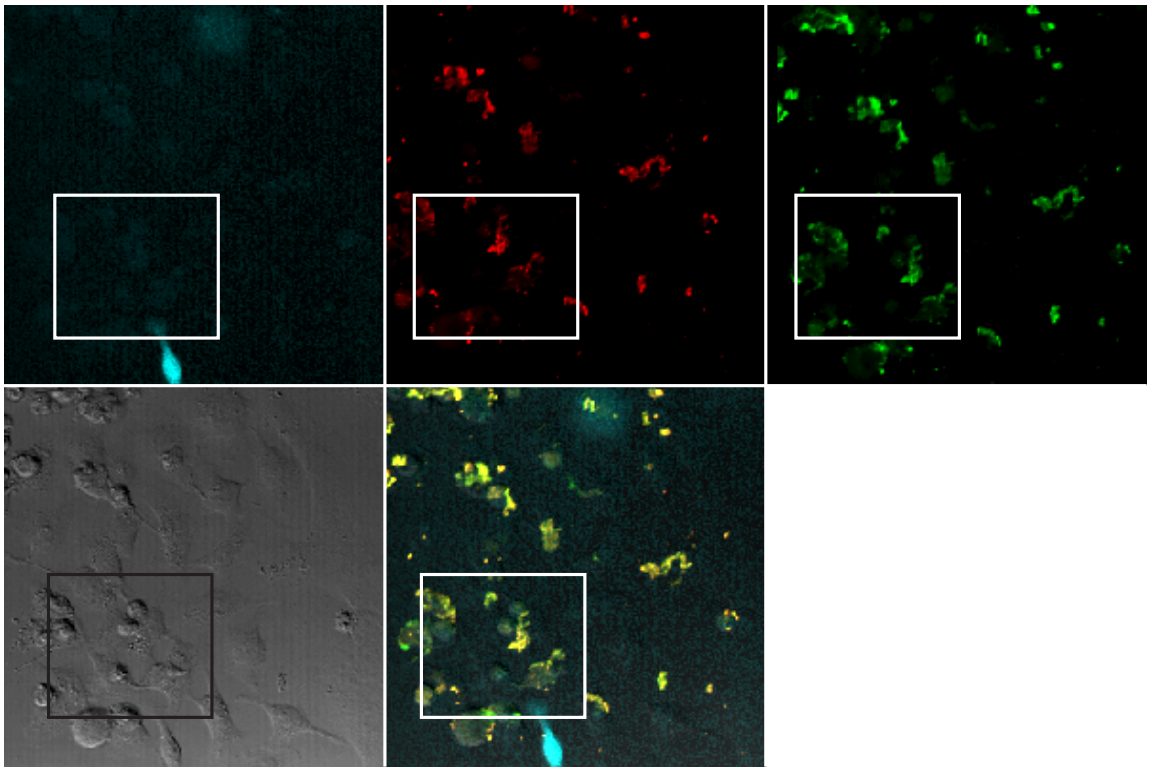

B: 10 mol % DOTAP in DOPE hexosomes, pAmCyan DNA, incubation 4h in DMEM + 5% FCS, 48 h post-transfection

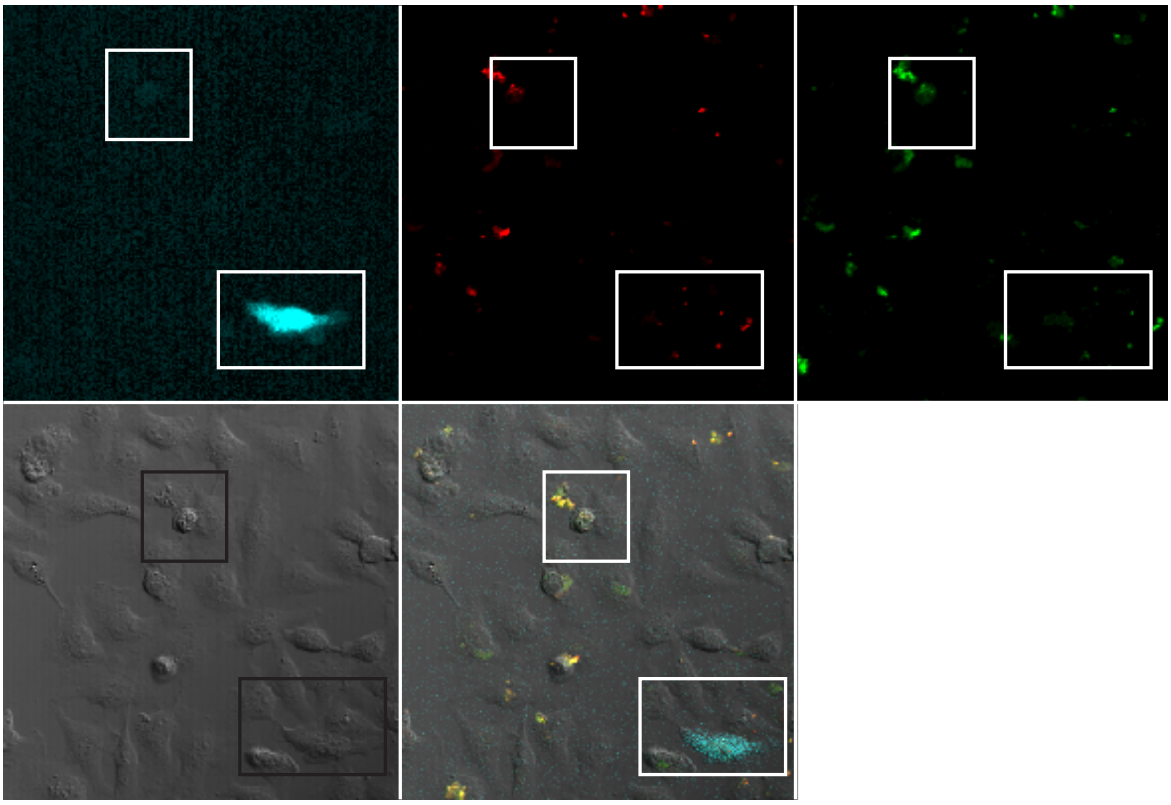

C: 20 mol % DOTAP in DOPE hexosomes, pAmCyan DNA, incubation 4h in DMEM + 5% FCS, 48h post-transfection

Figure 76: Transfection with pAmCyan and DOPE/DOTAP hexosomes in DMEM, incubation 4h at 37 °C, 48h post transfection

Figures 75 and 76 represent the transfection data for cells transfected with hexosomes accompanied by plasmid DNA. Figures of this type (including these and figures 78 amd 79) should be analysed according to the presence of AmCyan protein in cells that contain both lipid (red) and DNA (green), identifiable from their respective channels and the overlay image. It is clear that AmCyan protein is produced from the plasmid, which is incorporated into cells in the presence of hexosomes. It is also apparent that the incorporation of plasmid DNA is possible in the presence and absence of serum, although appears to be slightly better in the cells and hexosomes incubated in DMEM substituted with 5 % FCS. Greater proportions of DOTAP in the hexosome appear to increase the transfection efficiency of the system, in line with experiments carried out in the literature. It has been previously shown that a mixture of DOPE and DOTAP, where the ratio of DOPE:DOTAP is firmly in the lamellar region of the phase diagrams of bulk phase preparations studied in chapter … of this thesis, have been used to deliver plasmid DNA with a moderately high transfection efficiency. Considering this information, and the appearance of hexosomes

consisting of 20 mol % DOTAP in DOPE as a clear solution, compared with the turbidity of other hexosome preparations with lower DOTAP contents, it is concluded that at 20 mol % DOTAP the dispersion could be vesicular rather than hexosomal. It is thought that the inverse hexagonal phase may not be able to accommodate a plasmid DNA (even when supercoiled), as easily as a linear template, as the structural dimensions would be greater than those of a linear DNA duplex, although this warrants further investigation. Indeed, most of the structures of lipid-DNA inverse hexagonal phases in the literature include linear rather than plasmid DNA.

It is also worth noting that in figure 76 the transfection efficiencies of hexosomes made only of DOPE and those consiting of 5 mol % DOTAP in DOPE are poor, resulting in one cell expressing AmCyan across each whole experiment. The incubation time with hexosomes and plasmid DNA was increased from four hours to overnight, in an effort to improve the transfection efficiency.

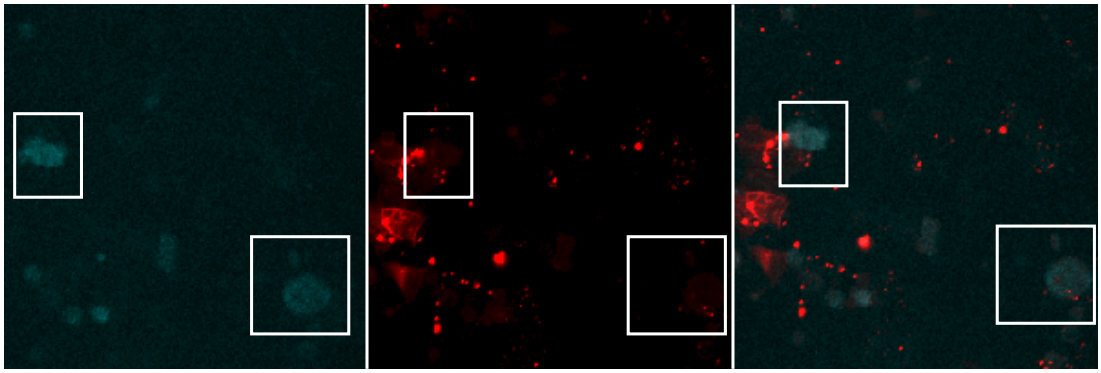

pAmCyan + DOPE hexosomes in DMEM/5% FCS, overnight incubation

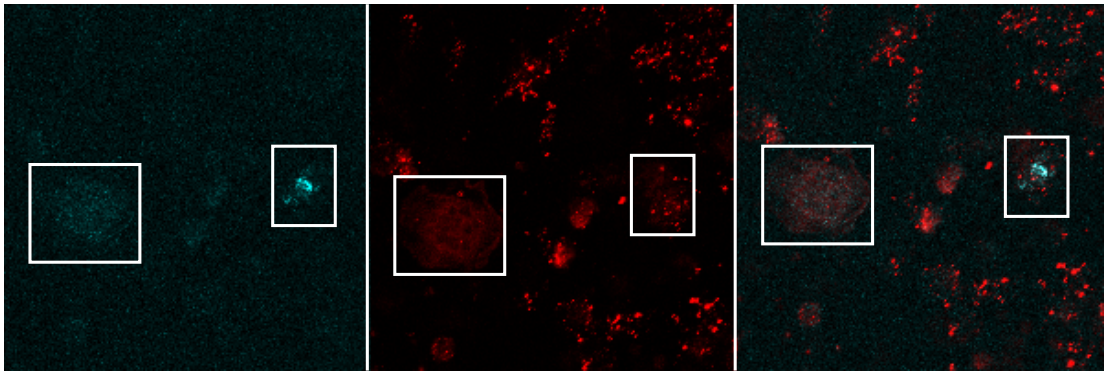

pAmCyan + 5 mol% DOTAP in DOPE hexosomes in DMEM/5% FCS, overnight incubation

Figure 77: AmCyan fluorescent protein produced by cells containing pAmCyan introduced by hexosomes from an overnight incubation.

After ovenight incubation with hexosomes containing only DOPE and 5 mol % DOTAP in DOPE with pAmCyan DNA, transfection was observed in a number of cells (see figure 77). This increase in transfection efficiency with longer incubation time is something that could be explored when using the linear DNA template, possibly resulting in higher transfection efficiency.

5.12 Delivery of linear pAmCyan DNA using Hexosomes

To overcome problems experienced in the manipulation of the T7-cyan double-transfection protocol (namely the cytotoxic effects of Attractene) transfection was attempted with the linearised version of the pAmCyan plasmid to produce the AmCyan protein from a linear template under mammalian promoter control.

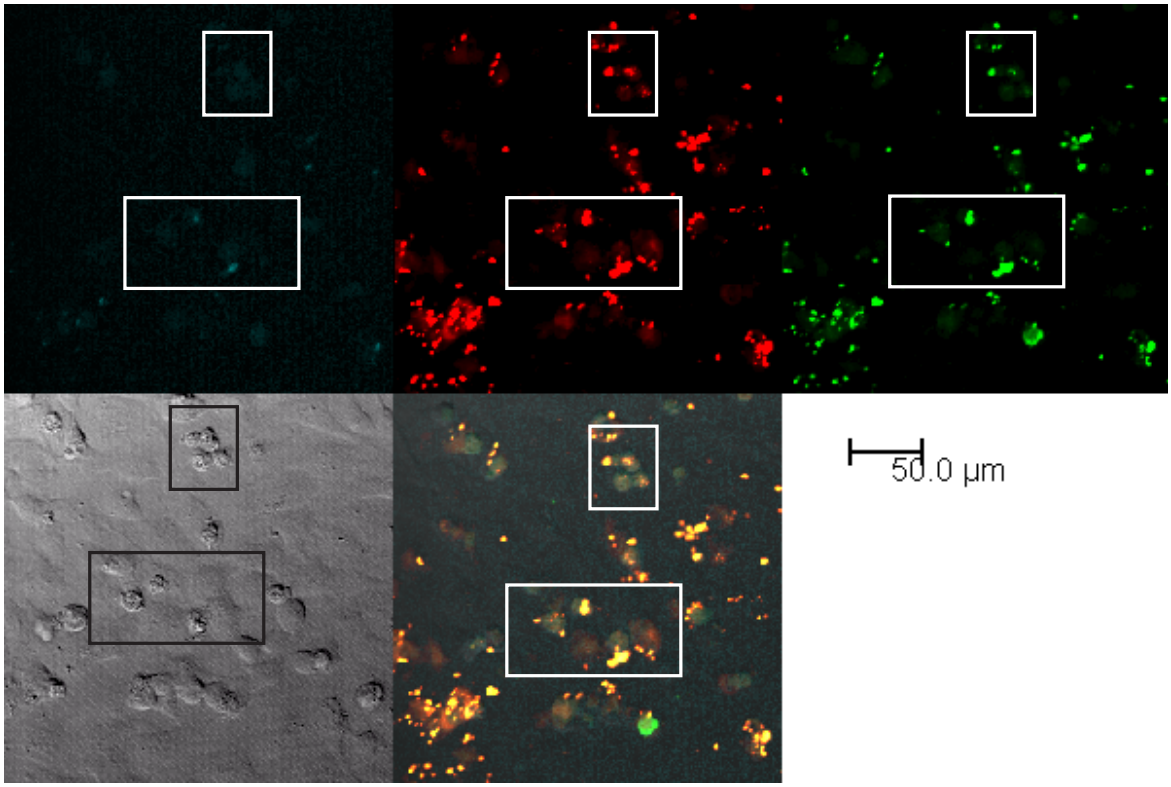

A: DOPE hexosomes, linearised AmCyan DNA, incubation 4 hour Opti-MEM, 48 hours post-transfection

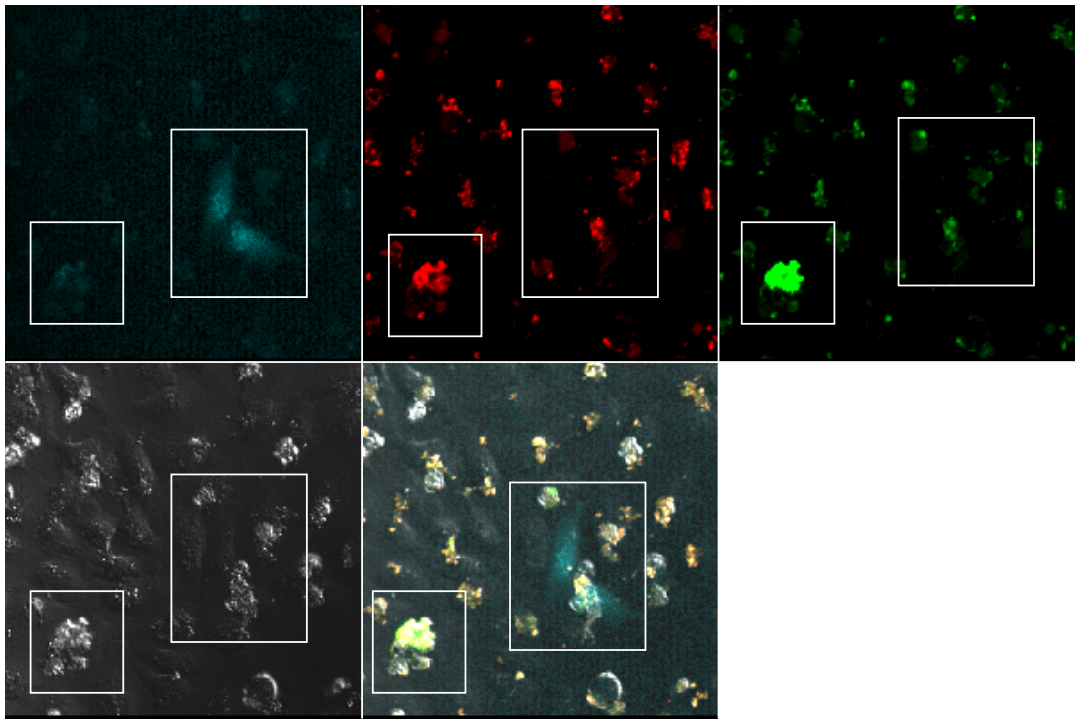

B: DOPE:DOTAP (95:5) hexosomes, linearised AmCyan DNA, incubation 4h in Opti-MEM, 48h post-transfection

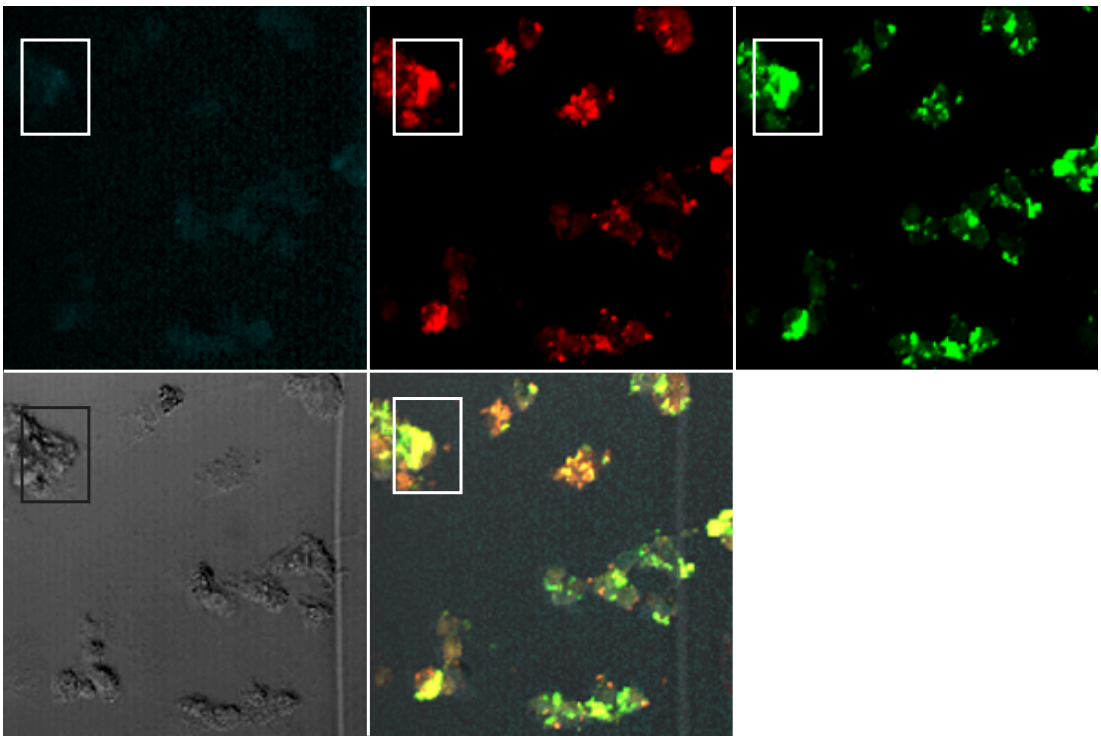

C: DOPE:DOTAP (90:10) hexosomes, linearised AmCyan DNA, incubation 4h in Opti-MEM, 48h post-transfection

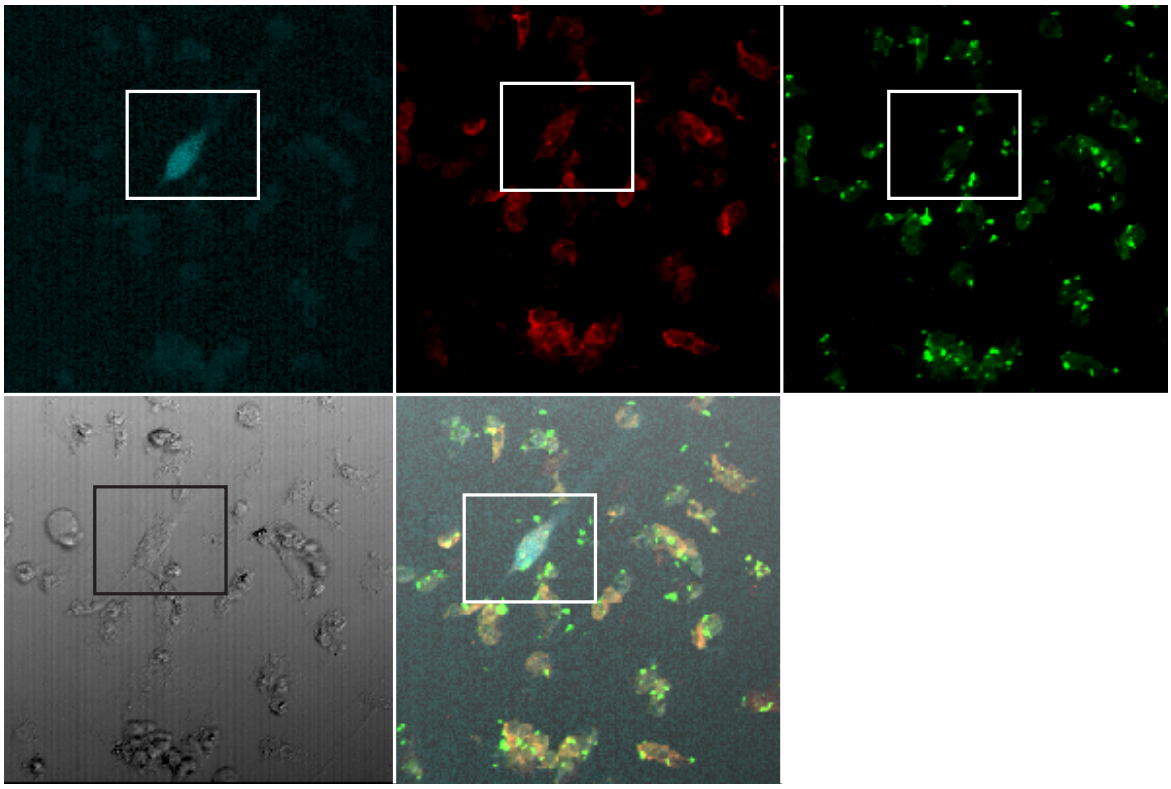

D: DOPE:DOTAP (80:20) hexosomes, linearised AmCyan DNA, incubation 4h in Opti-MEM, 48h post-transfection

Figure 78: Linear pAmCyan DNA delivered by hexosomes with varying DOPE and DOTAP content, with 4 hour incubation in Opti-MEM reduced serum medium, before 48 hours growth in DMEM + 5 % FCS and Antibiotic-Antimycotic solution. Individual points of interest are highlighted in each channel. For each image, L-R (top): AmCyan, lipid (LRB labelled), DNA (cy5 labelled); L-R (bottom): DIC cellular image, overlay of all channels

Mol % DOTAP in DOPE	Cyan cells /image	Total cells /image	Area surveyed /μm^2	Cyan cells /cm^2	Total cells /cm^2	Transfection efficiency/%
0	23	82	75931	29937	108060	27.7
5	30	52	78975	36980	64545	57.5
10	15	22	68171	21274	31352	67.9
20	26	35	80744	31879	43284	73.8

Table 5: Calculation of mean transfection efficiency from cells transfected with lin-pAmCyan in hexosomes, using Opti-MEM reduced serum medium. Individual data sets can be found in appendix …

It is clear from the images displayed in figure 78 that all four hexosome compositions studied produce significant transfection with linear pAmCyan DNA. This follows on from the experiments carried out on the T7 double transfection system reviewed earlier in this chapter, and reinforces the notion that DNA that is located with the inverse hexagonal

phase of DOPE-containing lipid mixtures is available for biological processes. The overlay images for each set of results suggest that the colocalisation of lipid and DNA outside the cell is greater at lower DOTAP contents, with a large amount of non-colocalised DNA visible in figure 78D, (hexosomes formed from 20 mol % DOTAP in DOPE). As you increase the DOTAP content of the hexosomes, more areas are observed in the DNA (green) channel that cannot be matched to points in the lipid (red) channel. Section 5.7 of this thesis explored the colocalisation of lipid and DNA within cells, and the images taken at 10 mol % DOTAP in DOPE are also suggestive that colocalisation of lipid and DNA within the cell decreases with increasing DOTAP content. It is, of course, entirely possible that by the point at which these images were taken, 48 hours post transfection, that a large amount of lipid had in fact been processed by the cells, in keeping with the time-course data displayed in section 2.12 of this thesis. This would account for the faint appearance of the lipid channel. Should the DNA not be included within the pores of the inverse hexagonal structure it may not be easily incorporated into cells alongside the lipid. This would be the case if the increase in DOTAP content caused the morphology of the lipid dispersion to switch from hexosomal to liposomal. That considered, at all DOTAP concentrations the transfection efficiency, in terms of the number of expressing cells and their relative brightness appears constant, suggesting that similar quantities of DNA were taken up by the cells. There does appear to be a marked difference in the number of cells present after experiments containing different quantities of DOTAP; for cells incubated with hexosomes of DOPE the cell count is 108,060 cm^{-2}, which falls to 43,284 cm^{-2} at a DOTAP content of 20 mol %. This is worth mentioning, considering that the cell density was constant at the time of transfection. The density of cells appears to have dramatically increased upon introduction of DOPE hexosomes when compared with the untreated control samples, yet this effect is not observed in those experiments containing 10 and 20 mol % DOTAP. Further analysis of this is undertaken in section 5.3.

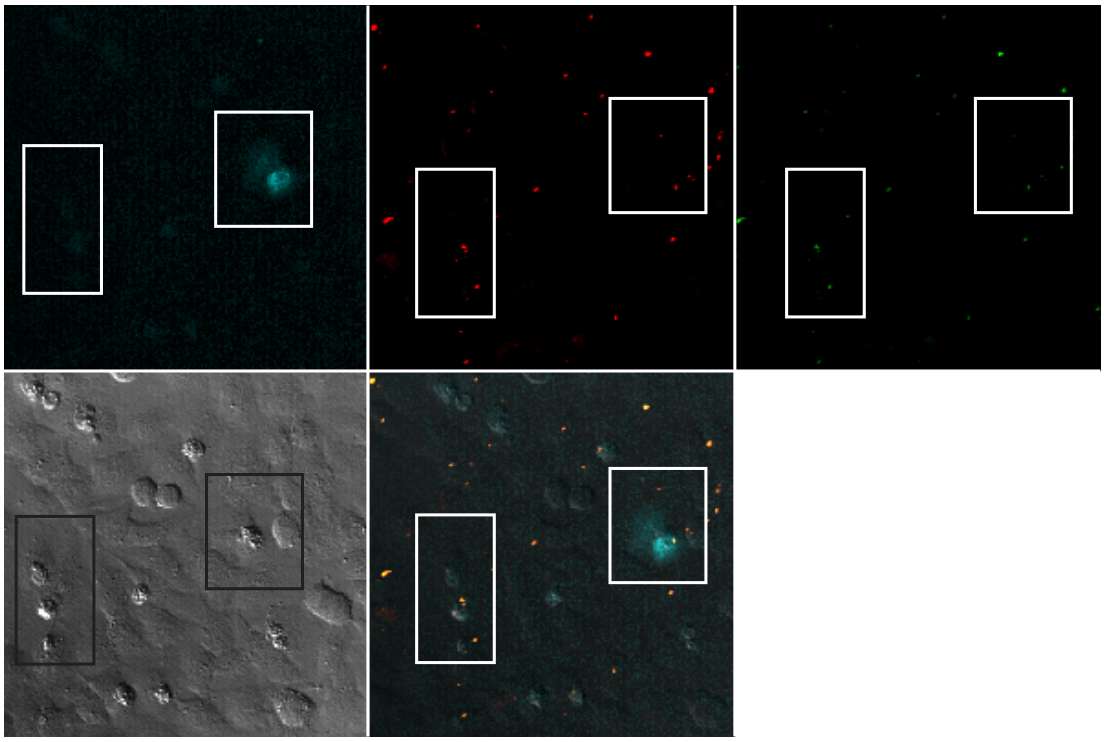

A: DOPE hexosomes, lin-AmCyan DNA, incubation 4h DMEM + 5% FCS, 48h post-transfection

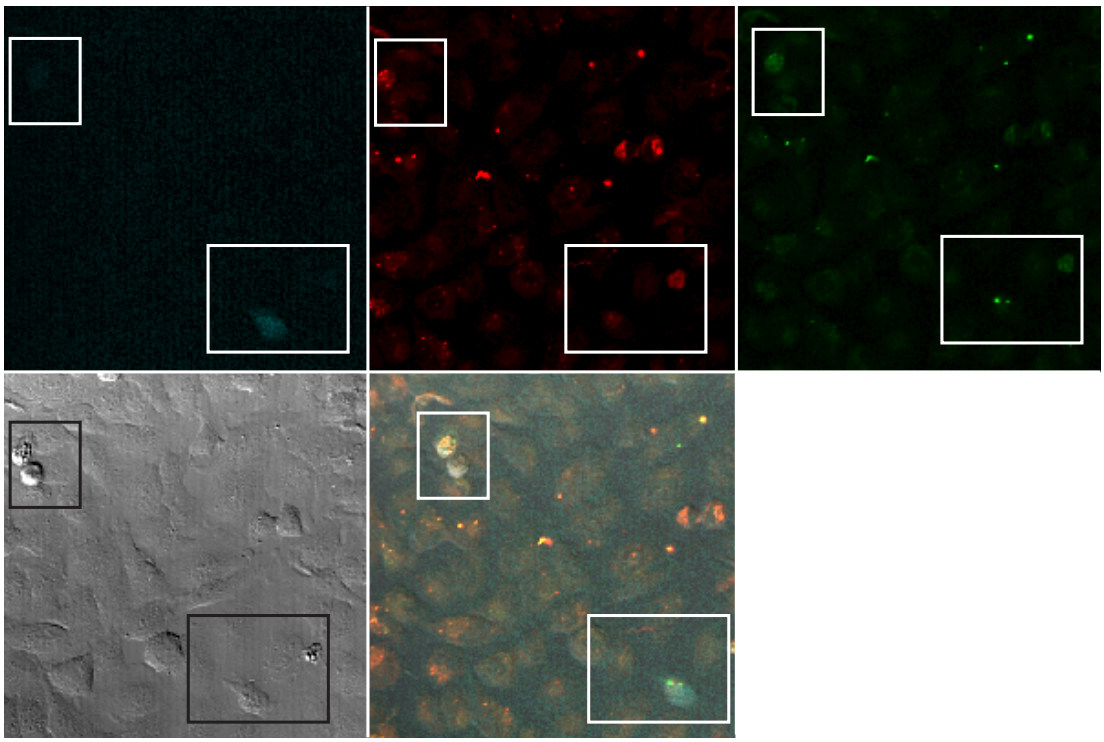

B: 5 mol % DOTAP in DOPE hexosomes, lin-AmCyan DNA, incubation 4h in DMEM + 5% FCS, 48h post-transfection

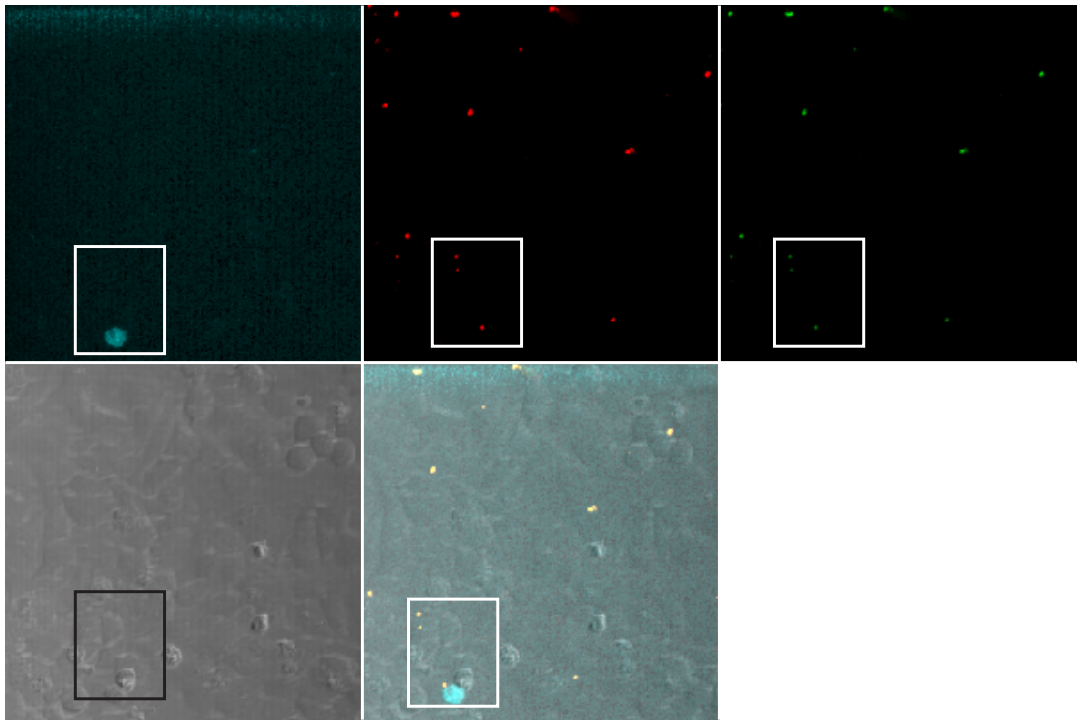

C: 10 mol % DOTAP in DOPE hexosomes, lin-AmCyan DNA, incubation 4h in DMEM + 5% FCS, 48h post-transfection

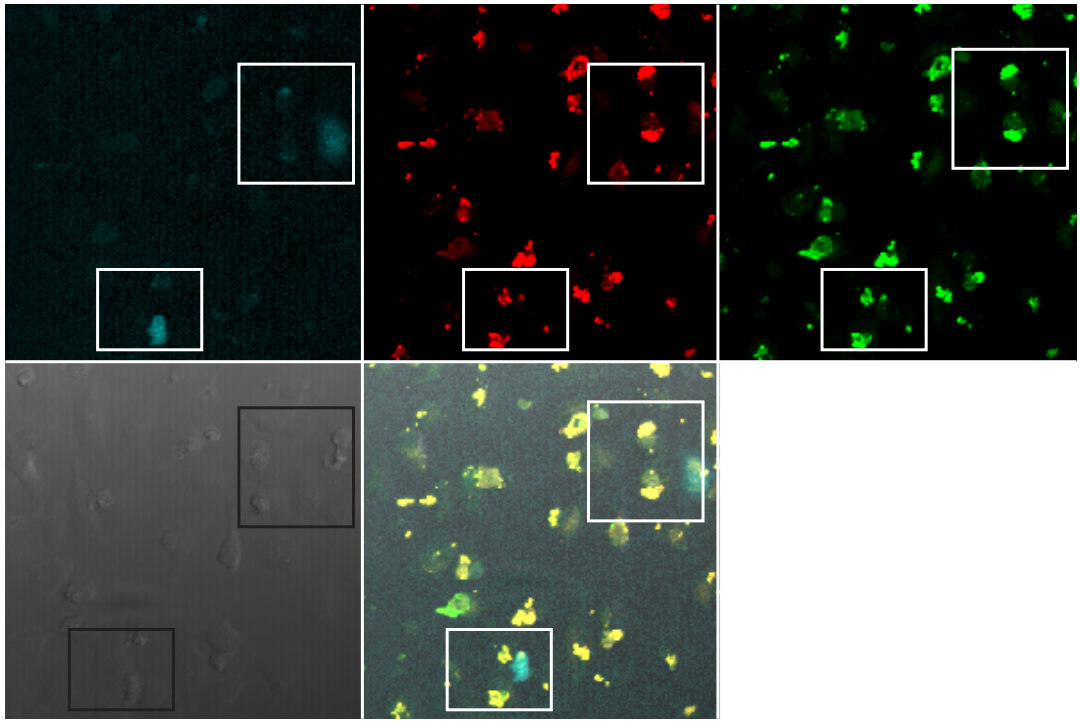

D: 20 mol % DOTAP in DOPE hexosomes, lin-AmCyan DNA, incubation 4h, DMEM + 5% FCS, 48h post-transfection

Figure 79: Linear pAmCyan DNA delivered by hexosomes with varying DOPE and DOTAP content, with 4 hour incubation in DMEM + 5 % FCS, before 48 hours growth in DMEM + 5 % FCS and Antibiotic-Antimycotic solution. Individual points of interest are highlighted in each channel; L-R (top): AmCyan, lipid (LRB labelled), DNA (cy5 labelled); L-R (bottom): DIC cellular image, overlay of all channels

Mol % DOTAP in DOPE	Cyan cells /image	Total cells /image	Area surveyed /μm^2	Cyan cells /cm^2	Total cells /cm^2	Transfection efficiency/ %
0	12	89	75931	15723	115902	13.6
5	9	77	79139	12153	97188	12.4
10	12	59	67376	17768	86766	20.4
20	30	67	80744	37478	83024	45.3

Table 6: Calculation of mean transfection efficiency from cells transfected with lin-pAmCyan in hexosomes, using Opti-MEM reduced serum medium. Individual data sets can be found in appendix …

Transfection of hexosomes complexed with lin-pAmCyan in the presence of serum appears to be less efficient than observed from experiments carried out in reduced serum medium. The only difference between the two sets of experiments detailed in figures 78 and 79 is that the incubation of the hexosome-DNA complexes and cells was carried out in serum-deficient (Opti-MEM) and serum-containing (DMEM) culture medium.

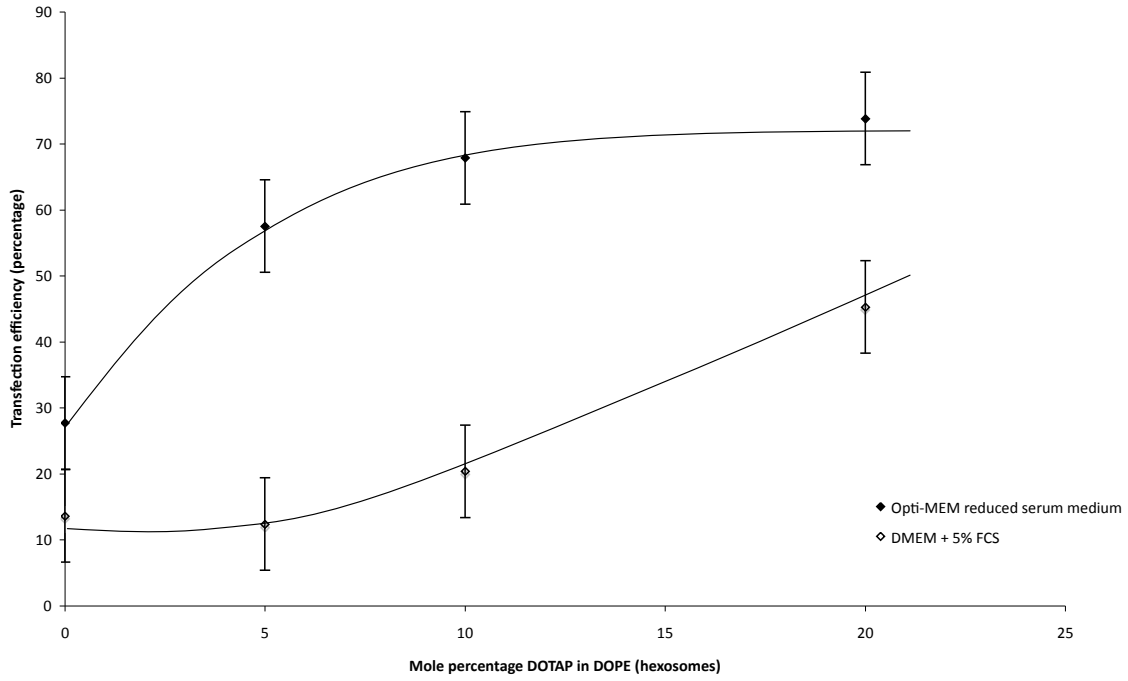

Figure 80: Transfection efficiency in cells incubated with hexosomes containing lin-pAmCyan DNA. Incubation time was 4 hours, in either Opti-MEM reduced serum medium or DMEM + 5% FCS.

5.13 Effect of DOTAP on cells

It was observed that DOTAP concentrations of 10 mol % or greater caused a decrease in cell number. This was more pronounced in those cells that had been incubated with hexosomes in the absence or serum.

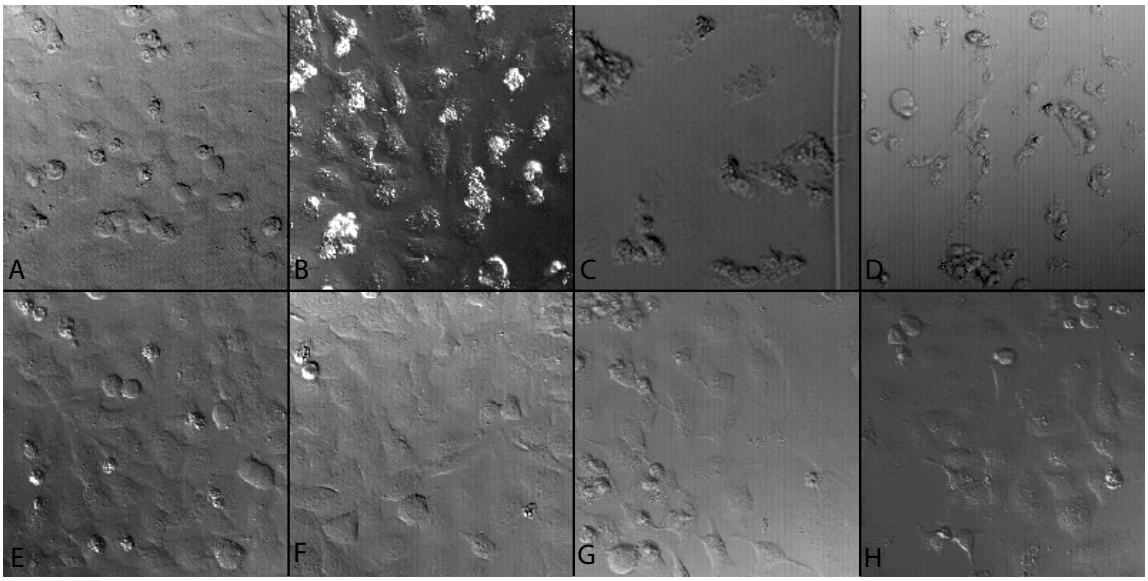

Figure 81: DIC images of cells incubated with hexosomes with varying dotap content. L-R: DOPE, 5 mol % DOTAP in DOPE, 10 mol % DOTAP in DOPE, 20 mol % DOTAP in DOPE; top: incubation in Opti-MEM reduced serum medium; bottom: incubation in DMEM + 5 % FCS. After hexosome incubation all cells were returned to the incubator in DMEM + 5 % FCS + Antibiotic-Antimycotic solution and grown for 48 hours at 37 °C and 5 % CO_2

It is clear that increasing the DOTAP concentration results in a lower cell density, and that this effect is more pronounced in cells that were incubated with hexosomes in Opti-MEM reduced serum medium. This could be a result of the aggregation that is observed when samples that contain higher concentrations of DOTAP are incubated in cells. Aggregation is clearly visible in the upper row of figure 81 as the globular structures visible on top of the cells. Indeed, the DIC image of hexosomes of 5 mol % DOTAP in DOPE incubated in media containing serum (figure 81F) shows a greater number of cells that are smooth and healthy looking when compared with its low serum counterpart (figure 81B).

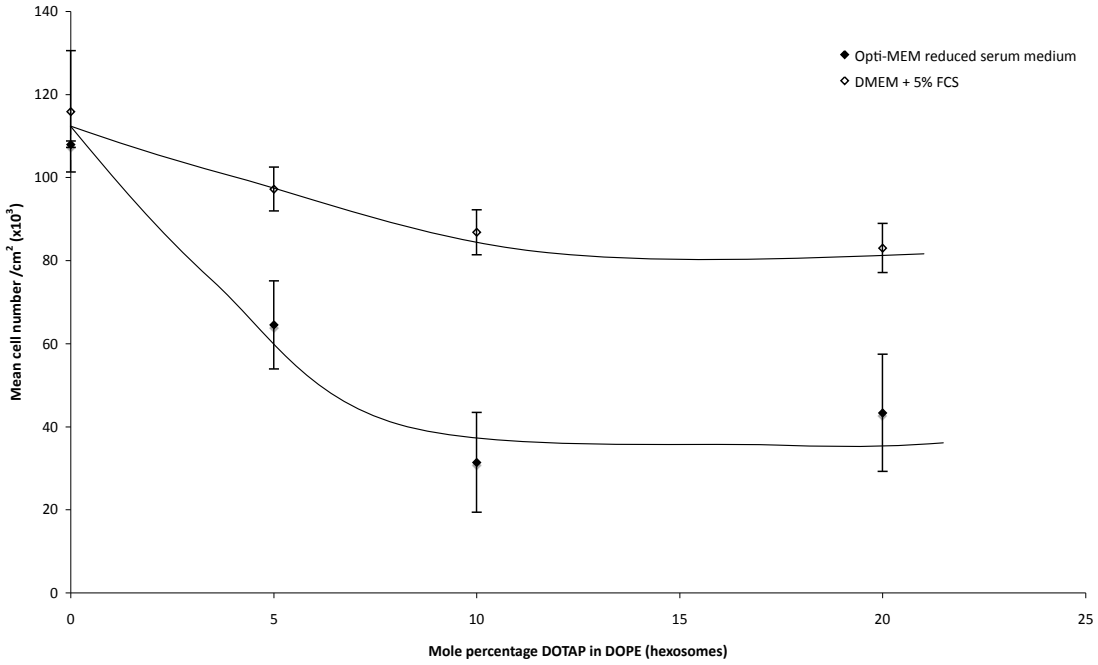

Figure 82: Cell density per cm^2 for transfections carried out in Opti-MEM reduced serum medium and DMEM substituted with 5% FCS

As previously mentioned in this thesis the cytotoxicity could be caused by a greater uptake of hexosomes that is possible in the absence of serum, either through the cells' own uptake mechanisms or as a result of the increased aggregation observed under reduced serum conditions. Serum contains, among other things lipids, carrier proteins and growth factors. The literature shows that HeLa can be successfully cultured in a lipid-free, chemically defined environment, which would be chemically similar to that produced by Opti-MEM. It is possible that although HeLa cells are hardy enough to be cultured in this way, that the culture conditions do not entirely meet the requirements of the cells, resulting in uptake of available lipid species in the form of hexosomes. Regardless of the reason, it is apparent that more of the hexosome species are taken up during incubation in reduced serum medium than traditional serum-containing medium, resulting in the increased cytotoxicity observed in figures 81 and 82 and the increased transfection efficiency displayed in figure 80. It is not, however, true that transfection in serum-containing medium does not work; other experiments displayed in figures 77 shows the promise of increased incubation time when considering transfection using plasmid DNA at low DOTAP concentrations in the presence of serum. Optimising the system for use with sera is advantageous as it ensures

that the DOPE-based hexosome system is compatible with *in vivo* conditions. For applications under true *in vivo* conditions it is likely that the hexosomes will not be removed from the target cells, as they have been in this study. It would therefore be prudent to optimise the system such that the dose of hexosome is sufficient not to cause toxicity, yet produce a high yield of target protein, without the lipid species being removed from the cells.

In light of this observed cytotoxicity it is advantageous to investigate the transfection efficiency of hexosomes with increasing DOTAP content in terms of the total number of cells per unit area.

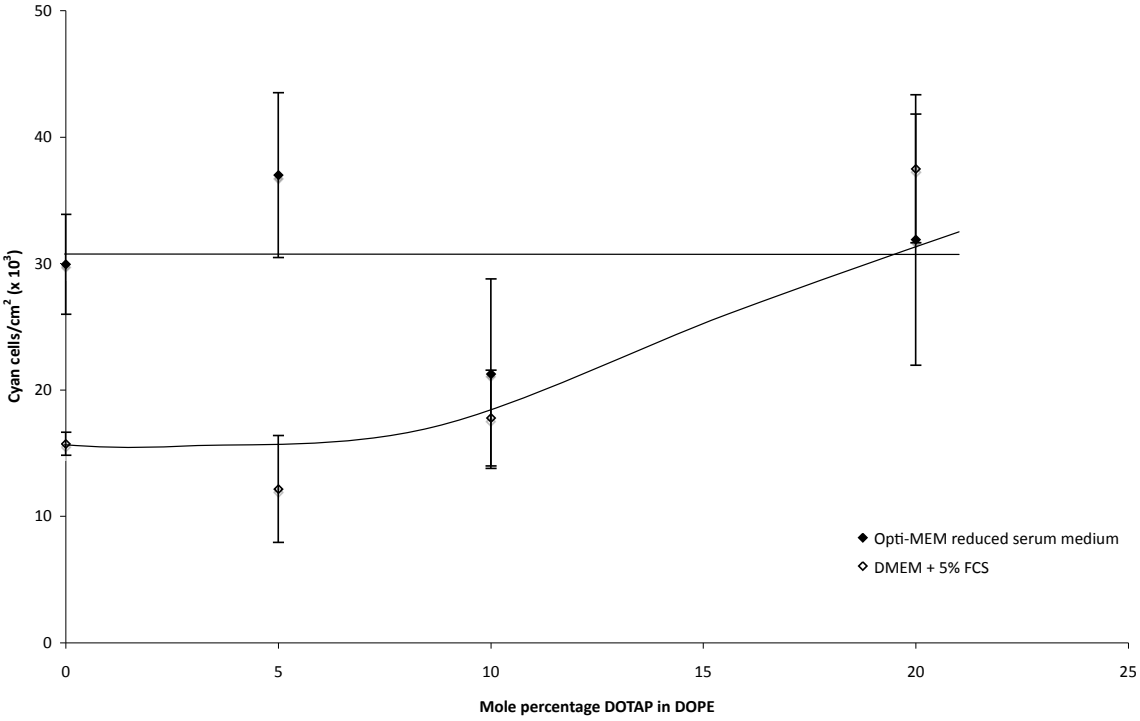

Figure 83: Number of cyan cells per cm^2 from transfections carried out in Opti-MEM reduced serum medium and DMEM substituted with 5% FCS.

The total number of cyan cells per unit area remains constant at around 30,000 cells cm^2 across all DOTAP concentrations when transfection is carried out with a 4 hour incubation in Opti-MEM reduced serum medium. When transfection complexes are incubated with cells in DMEM substituted with 5% FCS the number of cyan cells per unit area increases by more than double, from (15700 ± 900) cells cm^{-2} for hexosomes made of DOPE to (37300 ± 5900) cells cm^{-2} at 20 mol % DOTAP in DOPE.

5.13 Discussion

It is apparent from data presented in this report and elsewhere that DOPE/DOTAP lipoplex systems offer a viable delivery system for DNA in the context of gene therapy. Few studies have focussed on the use of DOPE itself as a transfection agent, with the majority of works centering on cationic lipids, i.e. DOTAP, for gene delivery. It has been shown in this study that DOPE has much more to offer to the field of gene delivery in terms of its ability to deliver viable DNA to cells.

Experiments in this study showed that DOPE-based hexosomes systems are able to deliver both plasmid and linearised DNA to HeLa cells in the presence and absence of serum. Experiments in the absence of serum showed greater transfection efficiencies than those carried out in serum-supplemented medium, however, the overall cell number was much higher in the presence of serum, indicating a lower toxicity for complexes under these conditions. Densities of cyan cells per cm^2 were within error for complexes with 20 mol % DOTAP, although the increased cell density as a result of serum presence resulted in a lower calculated transfection efficiency.

The experiments detailed in this thesis have indicated that the concept of delivering DNA using systems where the lipid component is comprised entirely of DOPE is not only possible, but that with some optimization (e.g. increased incubation time) the process should be reliable in serum-containing medium, under reaction conditions that are more similar to those encountered *in vivo* than are often used. The advantages of using a DOPE-based system (i.e. that the lipid material is naturally occurring and therefore easily processed by cells) present a promising solution to the toxicity issues associated with cationic lipid-mediated gene delivery.

Chapter 6

Conclusions and Further Work

6.1 Transcription studies

The transcription experiments described in chapter 2 of this thesis describe how DNA that is located within the inverse hexagonal phase of DOPE can be used to produce mRNA through transcription with T7 RNA polymerase. The mRNA produced has been shown to be of the expected length (by gel electrophoresis) and of reproducible quantities (through A_{260} values). The essential components for the transcription buffer were shown to be Trizma, $MgCl_2$, spermidine, RNasin, and DTT, with triton X-100 being deemed a non-essential component. It was also shown that the partitioning of mRNA into the supernatant phase of the liquid crystal system remains constant under a variety of different buffer conditions. The optimal ribonucleotide concentration was found to be 20 mM both in the presence and absence of a liquid crystal phase, and the optimal incubation time for transcription was shown to be 45 minutes.

That the DNA is incorporated into the inverse hexagonal phase is generally accepted by several members of the experimental and theoretical field, and corroborated by partitioning studies published recently. Inverse hexagonal systems of lipid and DNA offer scope for development of commercial protein production methods. It could be possible to exploit the transcription methods studied here and couple them to a translation system to create a microfluidic device for protein production.

6.2 Phase behaviour of DOPE/DOTAP and DOPE/DOTAP/DNA systems

Experimental study on the phase behaviour of mixtures of DOPE and DNA, and DOPE/DOTAP and DNA showed that at even low concentrations, the DNA helped stabilise the inverse hexagonal phase. This was observed through the preservation of the lattice parameter of samples with DOTAP content ≤ 20 mol % in DOPE. The SAXS data presented represents the total that was accumulated during experiments in the Membrane Biophysics research group, at Imperial College London. Unfortunately, the beamline being used suffered a breakdown part way through the study and some experiments were only repeated once. It would be prudent to repeat these experiments.

It is also apparent from the polarised light microscopy work that large areas of the phase diagram consist of a mixture of phases. This is not always detected in the SAXS results, so it is important to use both methods as a means of phase identification. Another solution would be to try synchrotron SAXS, which is more powerful, and may detect all of the phases present in the mixture.

6.3 Coarse grained molecular dynamics simulation

In order for a simulation to be considered valuable, the system (forcefield, code, and protocol) must first, where possible be used to generate results that agree with experimentally derived answers to the same problem. The simulations discussed in this thesis were able to reproduce behaviour observed experimentally, and give structural parameters for lipoplex systems that are in good agreement with experimentally derived ones. That said, there were numerous simulations carried out that did not produce the architectures expected; this is not wholly unexpected as the MARTINI model was developed to study bilayers, rather than lipoplex systems. An extension to this work is already being carried out within the group, exploring the optimization of the MARTINI forcefield to produce inverse phase architectures.

6.4 Transfection experiments

Experiments were undertaken to explore the possibility of DOPE-based lipoplex systems as gene delivery vehicles. It was postulated that DOPE (which is commonly used as a helper lipid) may be suitable for gene delivery without the requirement of a cationic lipid. Transfection from hexosomes of DOPE and DNA were shown to transfect cells, with less cytotoxicity than mixtures containing greater proportions of DOTAP. The incorporation of DOTAP in the hexosomes caused an increase in transfection efficiency, although this was accompanied by a marked and undesirable increase in the cytotoxicity of the lipoplexes. It is postulated that the optimal formulation for lipoplexes of this type may be 5 mol % DOTAP in DOPE, as an increase in transfection efficiency was observed, but without the cytotoxic effects of hexosomes with higher DOTAP contents.

There are a great deal of experiments that could be carried out to optimize the hexosome system explored in this work, including optimizing the lipid concentration and incubation time of the mixtures. Time-lapse microscopy could be employed to view transfection in 'real time,' providing vital information on the timescale of this process.

Appendix A - Protocols

This section covers all protocols used in experiments associated with this thesis. Protocols are arranged by chapter, in the order that they are referred to in the text.

A1 Lipid preparation

Almost every experiment undertaken as part of this thesis uses lipid samples, either in the form of a sample of pre-determined mass, a hydrated sample for loading into capillaries or onto microscope slides, or prepared as hexosomes. Lipids were supplied by Avanti Polar Lipids, other reagents from Sigma-Aldrich unless otherwise stated.

A1.1 Samples of pre-determined mass

Lyophilised lipid was weighed out and dissolved in chloroform, such that the final concentration of lipid was 0.5 mg μl^{-1}. The chloroform mixture was then vortexed, centrifuged for 30 seconds and allowed to stand for roughly 10 minutes, in order to produce a homogeneous sample. Samples were then separated into clean, sterile, RNAse-free microcentrifuge tubes by using a positive displacement pipette to separate individual aliquots of 5 µl (2.5 mg). Chloroform was removed using a sample concentrator, with the heating block set to 40 °C and nitrogen flow switched on. Samples requiring DNA were then incubated with an appropriate amount of DNA (usually 1 µg), for two hours, before lyophilisation. Water (100 µl)was added to each sample, which was then flash-frozen in liquid nitrogen before being placed under high vacuum overnight. To ensure complete lyophilisation, samples were placed in metal blocks that were also immersed in liquid nitrogen, and the cold fingers of the freeze-drying apparatus were filled with cardice. Once dried, samples were removed and stored at 4 °C until required.

A1.2 Hexosomes

Hexosomes were created by dissolving a 9:1 mixture of DOPE:pluronic F-127 in a water and ethanol mixture (99% water, 1% ethanol). Lipid and pluronic samples were created as 9 mg and 1 mg aliquots respectively, by solvation in chloroform and drying under vacuum. The pluronic was then dissolved in water (300 µl) and ethanol (3 µl), at 37 °C for 2 hours. This mixture was then transferred to the lipid sample and the vial was sonicated for 2 hours. Samples were then stored at 37 °C. In the event that after sonication some lipid

remained, the sample was returned to the incubator and sonicated for a further two hours the following day.

A1.3 Samples with mixed lipid content

When samples with mixed lipid content were required, for example samples used in x-ray diffraction and polarising microscopy structural studies, pure lipids were dissolved in chloroform as outlined above, and then solutions were mixed together in the appropriate ratios. This mixed lipid solution was then used to create individual samples. The formula weight of each lipid was taken into account, such that for every 100 mg DOPE used, 94 mg DOTAP was used to create samples with a known mole percentage of DOTAP in DOPE. This method was used to create samples between pure DOPE and pure DOTAP.

A1.4 Fluorescent lipid samples

Fluorescent lipid samples, in particular hexosomes, were made by incorporating 0.1 mol % lissamine rhodamine B labelled DOPE (Avanti), in the DOPE chloroform mixture. All subsequent steps were carried out as normal, although care was taken to limit exposure of the fluorophore to ambient light, with the use of aluminium foil.

A2 Transcription

All transcription experiments were carried out using buffers created in-house, with ribonucelotides and T7 RNA polymerase supplied by NEB, unless otherwise stated. Individual buffer components were supplied by Sigma, with molecular biology grade/certified RNAse-free reagents used wherever available. Messenger RNA prepared for transfection experiments, with the m^7G cap was created from ribonucleotides supplied by Promega, as a deficient concentration of rGTP was required.

A2.1 Transcription buffers

Transcription buffers with the following components were assembled in deionised, RNAse-free water. Buffers were stored at 4 °C as loss of activity can be linked to decreased spermidine solubility following repeated freeze-thaw cycles. The estimated shelf-life of a buffer solution is in the region of a month to six weeks, and when a drop in activity was observed, buffers were refreshed from the frozen stock solutions listed in table 7

Component	Stock Conc.	Volume/µl	Conc. in 10x buffer solution	Working conc. in assay
Trizma*	2 M	193.8	400 mM	40 mM
$MgCl_2$	1 M	250	250 mM	25 mM
Spermidine	0.25 M	100	25 mM	2.5 mM
Triton X-100	16 mM	100	1.6 mM	0.16 mM
RNasin	1600 units/ml	50	80 units/ml	40 units/ml
DTT*	1 M	99.4	100 mM	10 mM
Nuclease-free water	-	206.8	-	-
Total		**1000**		

Table 7: preparation of 10x buffer solutions from stock solutions

***denotes adjusted quantities to allow for storage conditions of ribonucleotides (NEB)**

Several variants of this transcription buffer were created, to ascertain the necessity of key components in the transcription reaction. The end goal of this was to create a defined buffer system, with the effects of all components understood.

Component	Full buffer JC/5003/82/1	(-) Spermidine JC/5003/82/2	(-) Triton JC/5003/82/3	(-) Spermidine, (-) Triton JC/5003/82/4
Trizma	193.8 µl	193.8 µl	193.8 µl	193.8 µl
$MgCl_2$	250 µl	250 µl	250 µl	250 µl
Spermidine	100 µl	-	100 µl	-
Triton X-100	100 µl	100 µl	-	-
DTT	99.4 µl	99.4 µl	99.4 µl	99.4 µl
RNasin	50 µl	50 µl	50 µl	50 µl
Water	206.8 µl	306.8 µl	306.8 µl	406.8 µl
Total	1000 µl	1000 µl	1000 µl	1000 µl

Table 8: preparation of buffers deficient in spermidine and triton X-100

A2.2 Transcription Assay

Transcription reactions were carried out as a 20 µl assay at 37 °C over 2.5 hours or 45 minutes, as detailed in the details of individual experiments.

Component	Volume added
Mixed rNTPs	1.25 µl
Linear T7 luciferase DNA	α µl (1 µg)
10x reaction buffer	2 µl
T7 RNAP	0.8 µl
Nuclease-free water	(15.95 – α) µl
Total assay volume	**20 µl**

Table 9: Components used in transcription reactions

Transcription reactions were set up by mixing together appropriate volumes of all components, except the T7 RNA polymerase together for all samples, plus one surplus, to allow for pipetting error. Aliquots of 19.2 µl were then pipetted out into single microcentrifuge tubes. Initiation of the reaction occurred with addition of T7 RNA polymerase, using a fine pipette tip and taking care not to add excess. Reactions were then placed in a water bath set to physiological temperature.

A2.3 Purification of transcript RNA

RNA purification was carried out using RNeasy kits provided by QIAGEN. Lipid-containing samples were purified using and adapted protocol the RNeasy lipid tissue mini kit, which couples a phenol-chloroform extraction to the standard spin column RNeasy protocol. Samples that did not contain lipid, for example, those transcription experiments used to produce mRNA used in the transfection experiments in later parts of this thesis, were purified using the standard RNeasy protocol.

A2.3a RNeasy lipid tissue (mini) kit

The protocol used in purifying mRNA from the lipid samples was adapted from the RNeasy lipid tissue kit. QIAZOL lysis reagent (500 µl) was added to each sample, followed by chloroform (100 µl). Samples were then shaken, and centrifuged for ten minutes at room

temperature. The upper, colourless, aqueous phase (300 µl) was then removed from the pink organic phase and mixed with an equal volume of 70 % ethanol. Samples were vortexed briefly before being transferred to RNeasy spin columns. The columns were centrifuged for 30 seconds before the flow-through was discarded. A series of washing steps followed, with buffer RW1 (750 µl) and buffer RPE (500 µl, twice) being used to remove salt from the RNA. The columns were allowed to dry by centrifugation into a new collection tube for 10 minutes at room temperature. Columns were then transferred to labelled microcentrifuge tubes, and the RNA was eluted in water (50 µl, twice) during centrifugation for 1 minute. Transcript RNA was analysed by UV-visible spectrometry on the Nanodrop ND-1000 and gel electrophoresis.

A2.3b Standard RNeasy protocol

The standard RNeasy protocol is designed to "clean up" < x µg RNA in 100 µl buffer, a modified version was used to purify smaller volumes than this. The sample was made up to 50 µl with RNase-free water, before buffer RLT (175 µl) and ethanol absolute (125 µl) were added. The sample was then placed on an RNeasy column, centrifuged (10000 rpm, 30 seconds, RT) and the flow-though discarded. The column was washed twice with buffer RPE (500 µl), before being dried by removal to a clean collection tube and centrifuged (10000 rpm, 2 minutes, RT). Elution of the RNA was carried out as in the RNeasy lipid protocol outlined in 2.3a.

A2.4 RNA gel electrophoresis

RNA samples were prepared for gel electrophoresis using 2x RNA sample loading buffer (NEB), deionised RNAse-free water, and mRNA sample in the ratio 5:4:1. This sample was then incubated at 65 °C for 10 minutes before 2 µl was loaded onto a precast 1.25% agarose gel impregnated with ethidium bromide (Sigma). The gel was run in TBE buffer, at 100V for 40 minutes and stained with Sybr II green nucleic acid stain (Invitrogen).

A2.5 UV-visible spectrometry

The yield of mRNA was analysed using the Nanodrop ND-1000 spectrophotometer (Labtech). The nucleic acid concentration was defined as a function of the A_{260} value, using the Beer-Lambert relationship. Purity of RNA samples was assessed using A_{260}/A_{230} and

A_{260}/A_{280} ratios. The messenger RNA yield was then converted into a total yield (in μg), rather than a concentration.

A3 Structural studies

Lipid samples used in structural studies were prepared from dried chloroform solutions, as outlined in section 1 of this chapter. Samples were then rehydrated and loaded into capillaries or placed onto microscope slides.

A3.1 Loading capillaries

Glass capillaries with an external diameter of 1.5 mm were purchased from Capillary Tube Supplies. Samples were mixed mechanically and allowed to equilibrate at 37 °C for several days. For loading into capillaries, samples were manipulated using the metal plunger from a Hamilton syringe and carefully coaxed into the capillary. Samples with a high DOPE content, and therefore more hexagonal character, were gently pushed to the base of the capillary, while those with a high DOTAP content, and therefore more lamellar character were introduced to the capillary and centrifuged to the bottom (2000 rpm, 2 minutes, room temperature). Samples were flame-sealed to prevent dehydration and taken to Imperial College London for x-ray scattering experiments.

A3.2 SAXS experiments

Small angle x-ray diffraction experiments were carried out at the Membrane Biophysics research group at Imperial College. The beamline used consists of a BEDE Microsource generator, with a copper anode and nickel filter. This is then connected to a custom built, peltier-driven temperature controlled sample chamber. The diffraction pattern is detected on a CCD photomultiplier tube (Photonic Science). The diffraction data is acquired as a tiff image and analysed using AXcess, a custom designed software package, produced by Andrew Heron, formerly of the membrane biophysics group. Bragg rings were assigned and the *d*-spacing was defined using the AXcess package. Where a structural phase was assigned from the x-ray data it was done so from at least three peaks.

A3.3 Polarising light microscopy

Samples for light microscopy studies were placed on a glass slide and covered with a cover slip. Samples were then heated to 70 °C and cooled before being studied. The phase

properties of each sample were studied at 37 °C, 55 °C and 70 °C and recorded according to appearance and texture from observation and manipulation.

A4 Simulations

All simulations were performed using the Gromacs 3.3.3 simulation package. Production simulations were performed in the NPT ensemble. The temperatures of the DNA and lipids were coupled separately to the water using the Berendsen algorithm at 323 K, with a coupling constant of 0.5 ps. The simulations were performed at 323 K as, while it is known that the inverse hexagonal phase of pure DOPE will form at temperatures above 295 K, on a simulation time scale this is best captured at elevated temperatures and low hydration levels.(13) The system pressure was coupled anisotropically using the Berendsen algorithm at 1 bar, with a compressibility of 1×10^{-5} bar^{-1}. Orthorhombic periodic boundary conditions were applied in all three dimensions. Lennard–Jones interactions were smoothly shifted to zero between 0.9 and 1.2 nm to reduce the cutoff noise, and electrostatics were smoothly shifted to zero between 0 and 1.2 nm. Analyses were performed using GROMACS tools, HOLE,[158] and locally written scripts. VMD was used for visualization. *d*-Spacings were calculated by measuring the distances between the centers of the channel cross sections using standard trigonometric methods.[2]

A5 Interfacing lipid structures with mammalian cells

It was decided that the hexosome is the simplest form of the inverse hexagonal phase of DOPE to introduce to living cells, owing to its relative ease of manipulation and greater likelihood of uptake by the cells, a result of the theorised entry mechanism for lipidic gene delivery vehicles involving granulation and endocytosis. A transfection system was designed to include fluorescently labelled hexosomes, and DNA carrying the gene for cyan fluorescent protein.

A5.1 Building the gene systems for T7 RNAP and AmCyan

The hexosome transfection system was designed to deliver a linearised piece of DNA containing the gene for AmCyan under control of a T7 promoter, similar to the DNA used in the early *in vitro* transcription experiments. In order to achieve successful expression of the AmCyan protein the cells were first stably transfected with a mammalian promoter carrying the gene for T7 RNA polymerase. This was achieved by using the polymerase

chain reaction (PCR) to remove the gene of choice from its existing plasmid and inserting it into a new plasmid, under the control of the desired promoter.

A5.1.1 PCR copying of a gene from its plasmid

Primers were designed such that the gene was copied from the original plasmid, flanked by the Kozak sequence and restriction sites appropriate for the destination plasmid. Three commercially available plasmids were utilised to generate the plasmids required for the transfection experiments: T7 luciferase control (Promega), Targetron pAR1219 (Sigma), and pAmCyan-N1 (Clontech). Both genes were copied from their original plasmids by PCR using Phire polymerase (New England Biolabs), which was chosen for its superior speed of copying and high fidelity.

Gene/plasmid	Primer sequence		Restriction site
AmCyan/ pAmCyan-N1	**F**	GTTGTTGGATCCGCCACCATGGCCCTGTCCAACAAGTT CATCGGCG	BamHI
	R	GTTGTTGAGCTCTCAGAAGGGCACCACGGAGG	SacI
T7 RNA polymerase/ pAR1219	**F**	GTTGTTGGATCCGCCACCATGAACACGATTAACATCGC TAAGAACG	BamHI
	R	GTTGTTGCGGCCGCTTACGCGAACGCGAAGTCCGACT CTAAG	NotI

Table 10: Primer sequences for PCR-driven amplification of genes for AmCyan and T7 RNA polymerase

PCR reactions were assembled to the following specification:

Component	Concentration	Volume added/µl
Reaction Buffer	5x	10
Template DNA	1 ng μl^{-1}	1
Forward Primer	10 pM	2
Reverse Primer	10 pM	2
dNTPs	10 mM	1
Phire Polymerase		0.4
Water	-	34.6
Total assay volume	**-**	**50**

Table 11: Components included in PCR reaction to amplify genes for AmCyan and T7 RNA polymerase

The reaction was carried out in a thermocycler over the course of the following program (note that this protocol does not include an annealing step; this is a special feature of Phire polymerase):

Step	Temperature/° C	Duration/s	Number of Cycles
Initial denaturation	98	30	1
Denaturation	98	5	30
Extension	72	20/kb	
Final extension	72	60	1
Preservation	4	∞	1

Table 12: Thermocycler program for PCR amplification of genes for AmCyan and T7 RNA polymerase

PCR product was analysed by Gel electrophoresis and by UV-visible spectrometry. Using a 2-log DNA ladder (New England Biolabs), the DNA band for AmCyan was identified near to the 1000 bp band, and the gene for T7 RNA polymerase between the 2000 and 3000 bp bands.

A5.1.2 Restriction of PCR products and vectors

For all restriction reactions carried out, high fidelity versions of the enzymes were available from New England biolabs; this enabled double digests to be carried out, saving time.

A5.1.3 Gel purification of the restriction products

Once the restriction had been carried out the digested DNA was separated and purified using gel electrophoresis. The whole restriction samples were run on agarose gel (1.25%) in TAE buffer, using enlarged sample wells. The gel was then visualised using a UV-transilluminator and the required bands removed using a scalpel. Gel bands were weighed and then purified using the QIAquick gel extraction kit (QIAGEN).

A5.1.4 Dephosphorylation of the vector backbone

In order to prevent self-ligation of the vector, a process that is kinetically very quick as it is an intramolecular process, the vector backbone is often dephosphorylated. Typical dephosphorylation agents are shrimp alkaline phosphatase (SAP), or thermosensitive alkaline phosphatase (TSAP). In this study, TSAP (supplied by Promega) was used as the thermosensitivity of the enzyme means that a separate purification of the vector backbone prior to ligation is unnecessary. The reaction mixture is made up of a DNA solution of known concentration, in MultiCore buffer (1x, Promega). An appropriate amount of enzyme was then added, relative to the total amount of DNA present. The reaction mixture was incubated at 42 °C (30 minutes) before heat inactivation at 74 °C (15 minutes).

A5.1.5 Ligation of the new vectors

The dephosphorylated vector backbone and the restricted insert were ligated together using T4 DNA ligase. Appropriate amounts of each DNA solution were incorporated into an 8 µl volume, such that vector and insert were present in a 1:1 ratio. T4 DNA ligase buffer (1 µl) and T4 DNA ligase (1 µl) were then added and the reaction was carried out at room temperature, for one hour. It is worth noting that the T4 DNA ligase buffer contains ATP and is therefore extremely sensitive to freeze-thaw cycles, new vials of buffer are therefore measured into small aliquots for individual use. A negative control consisting of vector backbone and no insert was also prepared and carried forward to the transformation stage.

A5.1.6 Transformation of the vectors in *E. coli*

Transformation of OneShot DH5α cells (Invitrogen) was carried out as follows. First the cells were allowed to thaw on ice (5 minutes), before addition of the ligation mixture (5 µl) and subsequent incubation on ice (30 minutes). The cells were then heat-shocked (42 °C, 30 seconds) before being returned to the ice for a further 2 minutes. Cells were introduced to antibiotic-free LB media (1 ml) and placed in the incubator (37 °C, 1 hour, with shaking). Cells were centrifuged and resuspended in LB broth (115 µl), before being plated at three different concentrations on LB-agar plates doped with an antibiotic appropriate for the desired plasmid. Plates were placed in the incubator overnight (37 °C) and then stored in the fridge for no longer than two weeks.

A5.1.7 Verification of the transformation process

In order to confirm that the correct vector had been transformed into the *E. coli*, a colony PCR was performed. Individual colonies were marked and selected with sterile pipette tips. They were dissolved in nuclease-free water (100 µl), and heated on the thermocycler (95 °C, 5 minutes). This DNA solution was then incorporated into the PCR reaction detailed in section 5.1.1, i.e. the reaction originally used to copy the gene of interest. The results of the PCR reaction were analysed using gel electrophoresis and UV-visible spectrometry.

A5.1.8 Large-scale plasmid production

As most of the experimental processes used in this study require large amounts of DNA, plasmid-containing *E. coli* were typically grown on a 500 ml scale. First, a 5 ml starter culture was grown, either from an individual colony, or a frozen cell stock. After six hours, starter culture (1 ml) was added to an autoclaved flask of LB media (250 ml). Plasmid-containing cells were grown in media inoculated with appropriate antibiotic to a concentration of 100 µg ml^{-1}. Cells were incubated at 37 °C overnight, for a period of less than 18 hours. Plasmid purification was carried out using the PureYield Plasmid Maxiprep (Promega) and purified plasmid was quantified using gel electrophoresis and UV-visible spectrometry.

A5.1.9 Frozen cell stocks

Cells were frozen at -80 °C, in 1% DMSO for future use.

A5.2 Mammalian cell culture

Mammalian cell experiments were carried out using HeLa cells (ATCC number CCL-2) purchased from ATCC via LGC-standards. Cells were cultured in Dulbecco's modified Eagle's medium (DMEM) containing 5% foetal calf serum (FCS), and with and without antibiotic-antimycotic solution. Cells grown in the absence of antibiotic are preferable for transfection experiments, although in the interest of infection control, a second culture was kept in the presence of antibiotic. Cells were passaged every two to three days and siphoned off for experiments as and when needed.

A5.2.1 Aseptic technique and the laminar flow hood

In the interest of infection control it is important that the laminar flow hood is maintained as a clean environment. The hood works by funnelling air through a sterile filter and down

into the hood, the air coming through the hood is therefore sterile, and with proper use the hood can be considered a clean environment. The hood must be subjected to ultraviolet light before and after use, a period of 15 minutes is sufficient. Before use, the hood is then switched on, and all surfaces and instruments inside the hood are liberally sprayed with ethanol. All items entering the hood (flasks, vials, consumables, bottles, hands) are sprayed with 70% ethanol. Solutions considered sterile must only be opened inside the hood. It is usual to pre-warm solutions in a water bath before use, as water baths are notoriously unclean, decontamination is incredibly important for these items, and the water inside the bath must not be allowed to come into contact with necks or caps of bottles. In addition to this, gloves must be worn when handling cell culture reagents, and when accessing the incubator.

A5.2.2 Passage of HeLa cells

Cells were examined under the inverted light microscope to assess their confluence and readiness for passage; typically cells were passaged when the confluence was greater than 80% but not more than 100%, i.e. not overgrown. Used media was aspirated from the cells using a serological pipette, and disposed of into a beaker containing disinfectant. Cells were then bathed in pre-warmed phosphate-buffered saline (PBS, 10 ml). The saline was aspirated before trypsin-edta solution (0.25%, 5 ml) was added. Cells were returned to the incubator for not longer than five minutes to aid the trypsinisation process. Cells were observed on the inverted microscope to check that they were no longer adhered to the growing surface and returned to the hood. Trypsinisation was stopped by addition of pre-warmed serum-containing media (20 ml). Suspended cells (5 ml) were transferred to a new flask and serum-containing media (25 ml) was added. Cells were grown at 37 °C, with 5% CO_2 and checked daily. During the passage process samples of the growing media were removed at intervals and checked for mycoplasma contamination, as this can be problematic in transfection studies.

A5.2.3 Mycoplasma detection

Detection of mycoplasma was carried out using the LookOut mycoplasma detection kit and JumpStart Taq polymerase (both supplied by Sigma). The kit consists of freeze-dried pellets containing nucleotides and primers. Samples of the growth media were taken from the cells in 100 µl aliquots and heated on the thermocycler to break open colonies and

release DNA (95 °C, 5 minutes). To the resuspension buffer provided, supernatant media and Taq polymerase were added. The reaction mixture (25 µl) was added to the dried pellet and the PCR reaction was run as follows.

A5.2.4 Seeding cells in microscope chambers

Microscope chambers were made by IBIDI and supplied by Thistle Scientific. Each of the eight wells per slide has a growing area of 1 cm^2, which was taken into account when calculating amounts of reagent used in transfection. Cells were first prepared for passage as detailed in section 5.2.2. The remaining cells were then further diluted by adding serum-containing media (30 ml) and then seeded into individual wells in 300 µl volumes. Slides were placed inside sterile petri dishes, to reduce the risk of contamination, and placed in the incubator at 37 °C, with 5% CO_2. Cells in microscope slides were checked daily, with frequent changes of media as the growing environment is not preferable when compared with regular flasks.

A5.3 Transfection with commercial reagents

Two commercial reagents were used for transfection of HeLa cells with DNA, and another was used to introduce coding mRNA to cells. These were Attractene (Qiagen), HeLa monster (Mirus, via Cambridge Bioscience) and Transmessenger transfection reagent for mRNA (Qiagen).

A5.3a Attractene transfection reagent

Attractene was used to introduce plasmid DNA coding for either AmCyan (for positive controls) or T7 RNA polymerase (for transient transfection) to cells. Early experiments with attractene showed a high degree of cytotoxicity, so the amount of attractene was decreased and cells were carefully monitored to overcome this. First DNA, 0.4 µg, was diluted to 60 µl in serum-free media (OPTImem, supplied by Invitrogen). Attractene transfection reagent (0.8 µl) was then added, and the samples were incubated at room temperature for 15 minutes to allow complex formation. During this time, cells seeded in microscope chambers were washed with PBS (300 µl) and rehydrated with pre-warmed serum-containing DMEM. Lipid/DNA complexes were then added to the cells dropwise. The cells were returned to the incubator and monitored for evidence of cytotoxicity. After

2-3 hours the lipoplexes were removed along with the media, cells were washed with PBS and media replaced. Cells were returned to the incubator for 24 hours.

A5.3b Transmessenger mRNA transfection reagent

As well as transient transfection of cells to produce T7 RNA polymerase from a piece of plasmid DNA, it was attempted to produce T7 RNAP from a piece of messenger RNA coding for the protein.

A5.4 Fluorescently-tagged DNA

Several methods were used to fluorescently label the DNA, with the preferred methods being incorporation of a fluorophore-coupled aminoally dUTP nucleotide by PCR, and incubation with a powerful intercalator.

A5.4.1 Incorporation of a fluorescent nucleotide by PCR

DNA was fluorescently tagged using an aminoally-dUTP analogue coupled to the fluorophore Alexa-488 (Invitrogen). Some studies were carried out using Atto-488 (Jena Bioscience) instead of Alexa-488, although supply issues favoured the Alexa analogue. As the spectral properties of both fluorophores are almost identical, both being engineered as alternatives to fluorescein, the labelled nucleotides were, at times, used interchangeably.

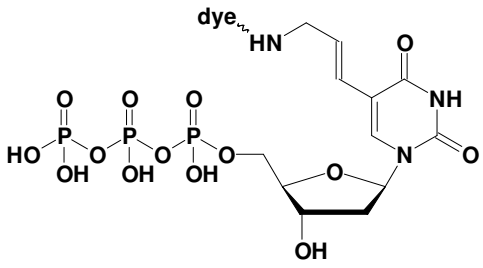

Figure 84: Alexa-488 dUTP

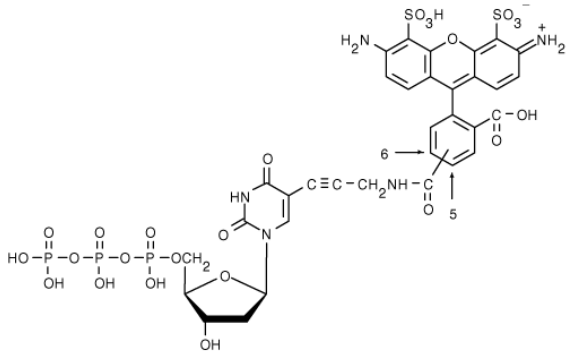

Figure 85: ATTO labelled aminoallyl dUTP

The protocol used for nucleotide incorporation was taken from the instruction sheet for the Alexa-488 nucleotide. The reactions were carried out using LongAmp (New England Biolabs) as some of the PCR reactions entailed copying of large amounts of the plasmid, and efforts to do so with Taq polymerase were unsuccessful. LongAmp is a mixture of Taq

polymerase, for its speed, and Pfu polymerase for its proofreading abilities; this is the gold-standard for copying long pieces of DNA.

Component	Concentration	Volume added/µl
Reaction Buffer	5x	10
Template DNA	1 ng μl^{-1}	1
Forward Primer	10 pM	2
Reverse Primer	10 pM	2
dATP, dGTP, dCTP	10 mM	1
dTTP	2 mM	3.75
Alexa-488-dUTP	1 mM	1
LongAmp		2
Water	-	27.25
Total assay volume	**-**	**50**

Table 13: Components included in PCR incorporation of Alexa-488 dUTP analogue to produce fluorescent DNA

Step	Temperature/° C	Duration/s	Number of Cycles
Initial denaturation	94	30	1
Denaturation	94	20	
Annealing	58	40	30
Extension	65	50/kb	
Final extension	65	10 **minutes**	1
Preservation	4	∞	1

Table 14: Thermocycler program for PCR incorporation of the Alexa-488 dUTP analogue

A5.4.2 Mirus Label-IT nucleic acid labelling kit

The Mirus Label-IT kit provides enough reagents to label 100 µg of DNA.

A5.5 Preparation of hexosome/DNA solutions

Hexosomes were prepared as outlined in section 1.2, with 0.1 mol% lissamine-rhodamine B labelled DOPE incorporated into the DOPE component. Hexosomes were added to cell culture medium in the desired quantities, as detailed for individual experiments, along with DNA that was either coding for the AmCyan gene under T7 control, or a fluorescent

piece of DNA. Hexosome and DNA solutions in cell culture medium were stored in the incubator for several days prior to use, to ensure full colocalisation of lipid and DNA.

A5.6 Transfection with hexosomes

Hexosomes mixed with DNA were introduced to cells in media with and without serum (DMEM and OPTImem, respectively). For all experiments, regardless of the hexosome concentration, the nature of the DNA (i.e. coding or fluorescent), and the incubation time, the protocol for transfection remained the same. Cells pre-seeded in microscop chambers were washed with pre-warmed PBS, and then the hexosome/DNA mixtures in media were added to the cells in 300 µl volumes, in the place of regular culture medium. Cells were then returned to the incubator for the appropriate incubation time, and checked periodically. At the end of the transfection period, cells were removed from the incubator and the hexosome-containing media was aspirated from the cells. The cells were then washed with pre-warmed PBS and the media replaced with appropriate media (i.e. DMEM or OPTImem). Cells were returned to the incubator until fixation.

A5.7 Fixation of cells

Cells were fixed in preparation for microscopy with 3.7% paraformaldehyde solution. The solution was prepared as outlined in table … and then dissolved by heating to 65 °C. Media was aspirated from the cells before washing with pre-warmed PBS. Paraformaldehyde solution (300 µl) was added, and fixaion was carried out at room temperature for 15-20 minutes. Cells were then washed once more with PBS, and then stored at 4 °C in 90% glycerol PBS.

Appendix B Detailed description of experiments

B1 Removing spermidine and triton X-100 from the transcription buffer

Experiments were carried out where spermidine and triton were removed from the transcription buffer. These experiments were carried out with positive and negative controls (complete buffer and lacking in DNA, respectively) alongside buffers deficient in spermidine, triton X-100 and both spermidine and triton X-100. Samples were created in triplicate, creating 15 samples per experiment set.

B2.1 Optimisation of transcription buffers

Reactions were set up to compare the effects of spermidine and triton X-100 in the transcription buffer (for normalised data see sections 3.1 - 3.3 of this report) by compiling buffers deficient in these compounds and testing them in the presence and absence of the DOPE/DNA inverse hexagonal phase.

B2.1.1a Transcription with and without spermidine and triton X-100

The experiments used to generate these results were JC/5140/01, 05, 10, 15, 19 and 29. The buffers were compiled as follows:

	Full buffer JC/5003/82/1	**(-) Spermidine JC/5003/82/2**	**(-) Triton JC/5003/82/3**	**(-) Spermidine, (-) Triton JC/5003/82/4**
Trizma	193.8µl	193.8µl	193.8µl	193.8µl
$MgCl_2$	250µl	250µl	250µl	250µl
Spermidine	100µl	-	100µl	-
Triton X-100	100µl	100µl	-	-
DTT	99.4µ	99.4µl	99.4µl	99.4µl
RNAsin	50µl	50µl	50µl	50µl
Water	206.8µl	306.8µl	306.8µl	406.8µl
Total	**1000µl**	**1000µl**	**1000µl**	**1000µl**

Table 15: preparation of buffers deficient in spermidine and triton X-100

The buffers used above were then incorporated into transcription assays according to the following recipe. The DNA stock used was …. and corresponded to 2.5 µl μg^{-1}.

Component	Volume added
Mixed rNTPs	1.25µl
Linear T7 luciferase DNA	2.5µl
10x reaction buffer	2µl
T7 RNAP*	2µl
Nuclease-free water	12.25µl
Total assay volume	**20µl**

Table 16: Composition of transcription assays JC/5140/01,05,10,15,19,29. *Polymerase was supplied by Sigma; this was later replaced by T7 RNAP supplied by New England Biolabs.

Transcription was carried out at 37 °C for 2.5 hours and purified using the RNeasy lipid tissue mini kit as outlined in appendix A4.1. The resultant RNA samples were quantified by UV-visible spectrometry to give the following data:

Buffer type	Full buffer JC/5003/82/1	(-) Spermidine JC/5003/82/2	(-) Triton JC/5003/82/3	(-) Spermidine, (-) Triton JC/5003/82/4
mRNA yield (µg)	39.70	17.11	44.86	18.28
	37.10	19.12	49.78	13.68
	36.91	22.32	34.75	19.56
	40.04	20.09	36.04	14.22
	38.25	20.22	36.94	17.45
	39.02	16.89	37.58	17.09
	39.41	16.37	38.31	15.98
	36.77	16.44	37.76	16.63
Mean	38.40	19.82	39.50	16.61
Standard deviation	1.33	2.24	5.12	1.96

Table 17: Transcription data from experiments JC/5140/01,05,10,15,19,29; the effect of spermidine and triton X-100 on transcriptional yield.

B2.1.1b Effects of spermidine and triton on transcription in H_{II} DOPE

The effects of spermidine and triton X-100 were assessed in the presence of the inverse hexagonal phase of DOPE and template DNA (lin-T7-luc). Experiments were designed that involved transcription in the presence of a liquid crystal phase (using the same buffers as in those experiments detailed in appendix B1.1.1) which were compared to a positive control sample (which used the full buffer without a liquid crystal phase) as well as a negative control (full buffer with a liquid crystal phase but not DNA). The experiments were assembled so that the standard 20µl transcription assay was placed on top of a liquid crystal phase of DOPE infused with 1µg linearised template DNA.

Component	Volume added
Mixed rNTPs	1.25µl
Linear T7 luciferase DNA	-
10x reaction buffer	2µl
T7 RNAP*	0.8µl
Nuclease-free water	12.25µl
Total assay volume	**20µl**

Table 18: Composition of transcription assays JC/5140/42,50,56,63. *Polymerase for these experiments was supplied by NEB, 0.8µl was used which corresponded to 40 units, or 69nM. Addition of DNA was unnecessary as DNA was present in the inverse hexagonal phase.

Transcription was run at 37 °C for 2.5 hours and purified using the RNeasy lipid tissue mini kit as outlined in appendix A4.1. The resultant RNA samples were quantified by UV-visible spectrometry to give the following data:

Buffer type	Positive control JC/5003/82/1	Full buffer JC/5003/82/1	(-) Spermidine JC/5003/82/2	(-) Triton JC/5003/82/3	(-) Spermidine (-) Triton JC/5003/82/4
mRNA yield (µg)	20.56	16.75	14.04	19.87	15.99
	18.29	18.63	15.77	19.63	14.52
	29.69	11.19	13.82	27.54	12.97
	30.18	26.11	16.31	24.17	14.85
	31.85	16.74	15.97	26.79	11.74
	24.72	19.05	12.47	27.27	
	28.96	15.11		14.68	
	27.75	15.07		18.93	
	30.57	18.48			
Mean	**26.95**	**17.46**	**14.73**	**22.36**	**14.02**
Standard deviation	**4.75**	**4.05**	**1.52**	**4.75**	**1.67**

Table 19: Transcription data from experiments JC/5140/42,50,56,63; the effect of spermidine and triton X-100 on transcriptional yield from template DNA in the inverse hexagonal phase of DOPE.

B2.1.2 Effects of spermidine and triton on the partitioning of mRNA

The aforementioned buffers were used to assess the effects of buffer components on the partitioning of mRNA between the supernatant and liquid crystal phase of the transcription experiment. Transcription experiments were set up as in B1.1.2 but before purification and analysis samples were split into liquid crystal and supernatant components by removing 15 µl supernatant (of an estimated total of 16µl remaining after 2.5 hours at 37 °C) to a clean microcentrifuge tube. Samples were then processed separately alongside positive and negative controls and whole sample extracts.

B2.1.2a Partition coefficient of mRNA in full buffer

Transcription was carried out in buffer JC/5140/22/1R for 2.5 hours at 37 °C and processed to give the following yields of transcript RNA:

Sample type	Positive control	Total extract	Lipid RNA	Supernatant RNA
mRNA yield (µg)	34.21	24.42	5.99	19.48
	30.06	27.24	8.81	18.91
	23.94	26.81	4.39	13.89
	35.43	19.51	2.40	23.99
	28.99	22.87	1.79	19.32
	23.79	27.76	2.19	16.58
	30.29	25.44	2.71	26.75
	30.38	28.16	3.47	19.68
	27.54	28.83	4.66	15.67
	30.83	21.74	6.01	18.36
	29.12	26.61	5.36	19.20
	28.27	19.45	4.14	17.35
	28.42	18.66	2.79	17.05
	27.80	12.62	6.41	15.92
	31.74	17.71	4.98	
	28.67	17.00	4.45	
		19.62	4.73	
			5.65	
Mean	**29.34**	**22.61**	**4.50**	**18.72**
Standard deviation	**3.05**	**4.76**	**1.78**	**3.33**

Table 20: Transcription data from experiments JC/5140/65,73,74,82,86,90; the partitioning of mRNA Between liquid crystal and supernatant phases of DOPE/DNA and transcription buffer.

These data were then used to calculate the partition coefficient of RNA between the liquid crystal and supernatant phases, as outlined in section 3.7 of this report.

Calculation	Assay number	K	Standard deviation
$K = \frac{[RNA]_{SN}^{real}}{[RNA]_{LC}^{\exp} + [RNA$	JC/5140/65	0.834	0.017
	JC/5140/73	0.842	0.059
	JC/5140/74	0.797	0.016
	JC/5140/82	0.798	0.062
	JC/5140/86	0.729	0.059
	Mean	0.800	0.045
	Mean over all data	**0.800**	**0.015**

Table 21: Partition coefficient between liquid crystalline and supernatant phases, full buffer

The nanodrop data were also expressed as a ratio over the positive control value for easy comparison of data:

Mean positive control		Total extract	Lipid RNA	Supernatant RNA
(29.34 ± 3.05) µg	**Ratio: Sample type/ Positive control**	0.832	0.204	0.664
		0.928	0.300	0.645
		0.914	0.150	0.473
		0.665	0.082	0.818
		0.779	0.061	0.659
		0.946	0.075	0.565
		0.867	0.092	0.912
		0.960	0.118	0.671
		0.983	0.159	0.534
		0.741	0.205	0.626
		0.907	0.183	0.654
		0.663	0.141	0.591
		0.636	0.095	0.581
		0.430	0.218	0.543
		0.604	0.170	
		0.579	0.152	
		0.669	0.161	
			0.193	
	Mean	**0.771**	**0.153**	**0.638**
	Standard deviation	**0.039**	**0.014**	**0.030**

Table 22: Transcription data from experiments JC/5140/65,73,74,82,86,90; the partitioning of mRNA Between liquid crystal and supernatant phases of DOPE/DNA and transcription buffer.

B2.1.2b Partition coefficient of mRNA in buffer without spermidine

Transcription was carried out in buffer JC/5140/22/2R for 2.5 hours at 37 °C and processed to give the following yields of transcript RNA:

Sample type	Positive control JC/5140/22/1R	(-)spermidine (-) LC JC/5140/22/2R	Total extract	Lipid RNA	Supernatant RNA
mRNA yield (µg)	24.84	19.68	21.09	2.26	13.71
	21.49	16.31	20.17	2.52	15.82
	27.45	16.19	13.31	2.78	10.29
	25.84	17.17	13.39	3.11	8.59
	26.80	16.71	14.67	2.95	11.90
	34.17	14.23	14.04	2.99	10.45
	31.36	15.63	14.65	4.12	11.36
	31.23	16.62	10.03	2.64	12.40
	37.57	23.09	15.44	2.58	10.71
	22.62	13.80	15.80	2.48	14.65
	25.42	14.85	16.97	2.21	13.94
Mean	**26.95**	**17.46**	**14.73**	**22.36**	**14.02**
Standard deviation	**4.75**	**4.05**	**1.52**	**4.75**	**1.67**

Table 23: Transcription data from experiments JC/5140/65,73,74,82,86,90; the partitioning of mRNA Between liquid crystal and supernatant phases of DOPE/DNA and transcription buffer deficient in spermidine.

These data were then used to calculate the partition coefficient, K:

Calculation	Assay number	K	Standard deviation
$K = \frac{[RNA]_{SN}^{real}}{[RNA]_{LC}^{\exp} + [RNA$	JC/5140/97	0.867	0.011
	JC/5221/03	0.774	0.036
	JC/5221/07	0.779	0.045
	JC/5221/11	0.841	0.031
	Mean	0.815	0.023
	Mean over all data	**0.815**	**0.050**

Table 24: Partition coefficient between liquid crystalline and supernatant phases, buffer deficient in spermidine.

The nanodrop data were then expressed as ratios over the positive control values:

Mean positive control		Positive (–) Spermidine	Total extract	Lipid RNA	Supernatant RNA
(28.64 ± 3.35) µg	Ratio: Sample type/ Positive control	0.704	0.681	0.097	0.426
		0.812	0.817	0.097	0.551
		0.745	0.499	0.109	0.436
		0.821	0.502	0.104	0.592
		0.850	0.549	0.116	0.385
		0.704	0.435	0.110	0.322
		0.606	0.454	0.093	0.446
		0.643	0.541	0.128	0.324
		0.626	0.554	0.082	0.352
		0.441	0.595	0.090	0.384
		0.484		0.087	0.375
		0.515		0.077	0.514
		0.809			0.488
		0.484			
		0.520			
	Mean	**0.665**	**0.563**	**0.099**	**0.430**
	Standard deviation	**0.139**	**0.113**	**0.015**	**0.085**

Table 25: Transcription data from experiments JC/5140/97; JC/5221/03,07,11; the partitioning of mRNA between liquid crystal and supernatant phases of DOPE/DNA and transcription buffer deficient in spermidine.

B2.1.2c Partition coefficient of mRNA in buffer without triton

Transcription was carried out in buffer JC/5140/22/3R for 2.5 hours at 37 °C and processed to give the following yields of transcript RNA:

Sample type	Positive control JC/5140/22/1R	(-) triton (-) LC JC/5140/22/3R	Total extract	Lipid RNA	Supernatant RNA
mRNA yield (µg)	29.49	38.68	25.03	4.94	17.13
	30.00	34.93	23.13	5.76	16.83
	24.16	28.59	23.27	6.12	16.96
	28.84	34.49	25.52	6.76	21.72
	28.84	33.79	25.41	5.50	19.24
	25.98	33.33	27.32	6.35	21.13
Mean	**27.88**	**33.03**	**24.95**	**5.91**	**18.83**
Standard deviation	**2.29**	**2.55**	**1.57**	**0.64**	**2.20**

Table 26: Transcription data from experiments JC/5221/16,18,20; the partitioning of mRNA between liquid crystal and supernatant phases of DOPE/DNA and transcription buffer deficient in triton X-100.

These values were then used to calculate the partition coefficient, K, using the method detailed in section 2.7.1 of this thesis.

Calculation	Assay number	K	Standard deviation
$K = \frac{[RNA]_{SN}^{real}}{[RNA]_{LC}^{\exp} + [RN$	JC/5221/16	0.752	0.022
	JC/5221/18	0.770	0.007
	JC/5221/20	0.798	0.038
	Mean	0.773	0.023
	Mean over all data	**0.773**	**0.030**

Table 27: Partition coefficient between liquid crystalline and supernatant phases, buffer deficient in triton

The nanodrop data were also expressed as a ratio over the positive control:

Mean positive control		Positive (–) T	Total extract	Lipid RNA	Supernatant RNA
(27.88 ± 2.29) µg	Ratio: Sample type/ Positive control	1.387	0.898	0.177	0.614
		1.253	0.829	0.207	0.604
		1.026	0.834	0.220	0.608
		1.237	0.915	0.242	0.779
		1.212	0.911	0.197	0.690
		1.196	0.980	0.228	0.758
	Mean	**1.218**	**0.895**	**0.212**	**0.676**
	Standard deviation	**0.117**	**0.056**	**0.023**	**0.079**

Table 28: Transcription data from experiments JC/5221/16,18,20; the partitioning of mRNA between liquid crystal and supernatant phases of DOPE/DNA and transcription buffer deficient in triton X-100.

B2.1.2d Partition coefficient of mRNA in buffer without spermidine or triton

Transcription was carried out in buffer JC/5140/22/4R for 2.5 hours at 37 °C and processed to give the following yields of transcript RNA:

Sample type	Positive control JC/5140/22/1R	(-) S (-) T (-) LC JC/5140/22/4R	Total extract	Lipid RNA	Supernatant RNA
mRNA yield (µg)	20.74	14.92	9.24	4.67	16.22
	20.43	13.45	10.46	5.67	16.02
	20.39	13.11	10.58	2.14	7.23
	20.33	19.59	13.39	2.22	7.09
	20.46	18.00	13.72	1.66	7.04
	20.18	20.29	13.28	5.33	10.18
	20.32	19.52	13.63	2.11	10.97
	20.34	17.90		5.33	10.16
	20.31	20.12		3.34	10.77
Mean	**20.40**	**17.43**	**10.63**	**3.39**	**10.63**
Standard deviation	**0.16**	**2.87**	**3.50**	**1.58**	**3.50**

Table 29: Transcription data from experiments JC/5221/26,30,32; the partitioning of mRNA between liquid crystal and supernatant phases of DOPE/DNA and transcription buffer deficient in spermidine and triton X-100.

These data were then used to calculate the partition coefficient, K:

Calculation	Assay number	K	Standard deviation
$K = \frac{[RNA]_{SN}^{real}}{[RNA]_{LC}^{\exp} + [RNA}$	JC/5221/26	0.790	0.023
	JC/5221/30	0.729	0.097
	JC/5221/32	0.745	0.094
	Mean	**0.755**	**0.032**
	Mean over all data	**0.760**	**0.071**

Table 30: Partition coefficient between liquid crystalline and supernatant phases, buffer deficient in spermidine and triton X-100

The nanodrop data were also expressed as a ratio over the positive control:

Mean positive control		Positive (-) S (-) T	Total extract	Lipid RNA	Supernatant RNA
(20.32 ± 0.33) µg	**Ratio: Sample type/ Positive control**	0.597	0.370	0.187	0.649
		0.538	0.418	0.137	0.641
		0.525	0.423	0.208	0.289
		0.784	0.536	0.089	0.284
		0.720	0.549	0.066	0.281
		0.812	0.531	0.072	0.407
		0.781	0.545	0.213	0.439
		0.716		0.084	
		0.805		0.213	
				0.086	
	Mean	**0.858**	**0.593**	**0.167**	**0.525**
	Standard deviation	**0.141**	**0.092**	**0.078**	**0.198**

Table 31: Transcription data from experiments JC/5221/16,18,20; the partitioning of mRNA between liquid crystal and supernatant phases of DOPE/DNA and transcription buffer deficient in triton X-100.

B2.1.2e Summary of partition coefficient data

Buffer type		Full buffer	(-) Spermidine	(-) Triton	(-) Spermidine, (-) Triton
Buffer Identity		JC/5003/82/1 JC/5140/22/1R	JC/5003/82/2 JC/5140/22/2R	JC/5003/82/3 JC/5140/22/3R	JC/5003/82/4 JC/5140/22/4R
Mean mRNA yield (µg)	Positive	29.34 ± 3.05	26.95 ± 4.75	27.88 ± 2.29	20.40 ± 0.16
	Deficient +ve	-	17.46 ± 4.05	33.03 ± 2.55	17.43 ± 2.87
	Whole	22.61 ± 4.76	14.73 ± 1.52	24.95 ± 1.57	10.63 ± 3.50
	LC	4.50 ± 1.78	22.36 ± 4.75	5.91 ± 0.64	3.39 ± 1.58
	SN	18.72 ± 3.33	14.02 ± 1.67	18.83 ± 2.20	10.63 ± 3.50
Partition coefficient, K		0.800 ± 0.015	0.815 ± 0.050	0.773 ± 0.030	0.760 ± 0.071
Mean ratios	Def +/pos	-	0.665 ± 0.139	1.218 ± 0.117	0.858 ± 0.141
	Whole/pos	0.771 ± 0.039	0.563 ± 0.113	0.895 ± 0.056	0.593 ± 0.092
	LC/pos	0.153 ± 0.014	0.099 ± 0.015	0.212 ± 0.023	0.167 ± 0.078
	SN/pos	0.638 ± 0.030	0.430 ± 0.085	0.676 ± 0.079	0.525 ± 0.198

Table 32: Summary of partition coefficient data for full buffer and buffers deficient in spermidine, triton X-100 and both spermidine and triton X-100; data from experiments JC/5140/65,73,74,82,86,90,97; JC/5221/03,07,11,16,18,20,26,30,32.

B2.1.3 Gibbs free energies

The values for the Gibbs free energies of the system were calculated using the method discussed in section 2.7.2 of this thesis.

B2.1.3a Full buffer; JC/5140/22/1R

	$[RNA]_{real\ SN}$/µg	$[RNA]_{real\ LC}$/µg	K_{eq}	ΔG/kJ mol^{-1}
$K_{eq} = \frac{[RNA]_{SN}^{real}}{[RNA]_{LC}^{real}}$	14.28	1.63	8.79	-5.60
	8.91	1.32	6.77	-4.93
	10.35	1.65	6.28	-4.74
	22.15	1.20	18.47	-7.52
	17.84	2.16	8.27	-5.44
	15.31	3.40	4.50	-3.88
	21.72	3.60	6.03	-4.63
	15.98	3.41	4.68	-3.98
$\Delta G = -RT \ln K_{eq}$	12.72	2.61	4.87	-4.08
	19.03	1.78	10.70	-6.11
	19.90	5.47	3.63	-3.33
	17.98	4.10	4.38	-3.81
	10.20	4.53	2.25	-2.09
	19.63	4.29	4.57	-3.92
	18.34	5.43	3.38	-3.14
Mean	**16.29**	**3.10**	**6.51**	**-4.48**
Standard deviation	**4.22**	**1.46**	**4.00**	**1.33**

Table 33: Calculation of K_{eq} and ΔG for full buffer, experiments JC/5140/65,73,74,82,86,90; the partitioning of transcript mRNA between H_{II} DOPE/DNA and transcription buffer

B2.1.3b Buffer deficient in spermidine; JC/5140/22/2R

	$[RNA]_{real\ SN}$/µg	$[RNA]_{real\ LC}$/µg	K_{eq}	ΔG/kJ mol^{-1}
$K_{eq} = \frac{[RNA]_{SN}^{real}}{[RNA]_{LC}^{real}}$ $\Delta G = -RT \ln K_{eq}$	16.41	1.27	12.91	-6.59
	13.71	1.45	9.45	-5.79
	15.82	1.59	9.93	-5.92
	10.29	2.17	4.74	-4.01
	8.59	2.60	3.30	-3.08
	11.90	2.25	5.30	-4.30
	10.45	2.37	4.40	-3.82
	11.36	3.45	3.29	-3.07
	12.40	1.91	6.50	-4.83
	10.71	1.95	5.50	-4.39
	14.65	1.62	9.03	-5.67
	13.94	1.39	10.02	-5.94
	11.28	5.87	1.92	-1.68
	14.59	11.25	1.30	-0.67
	11.57	6.81	1.70	-1.36
Mean	**12.51**	**3.20**	**5.95**	**-4.07**
Standard deviation	**2.24**	**2.76**	**3.56**	**1.82**

Table 34: Calculation of K_{eq} and ΔG for experiments JC/5140/97; JC/5221/03,07,11; the partitioning of transcript mRNA between H_{II} DOPE/DNA and transcription buffer deficient in spermidine

B2.1.3c Buffer deficient in triton; JC/5140/22/3R

	$[RNA]_{real\ SN}$/µg	$[RNA]_{real\ LC}$/µg	K_{eq}	ΔG/kJ mol^{-1}
$K_{eq} = \frac{[RNA]_{SN}^{real}}{[RNA]_{LC}^{real}}$	18.65	4.28	4.35	-3.79
	18.32	5.20	3.53	-3.25
	18.46	5.58	3.31	-3.08
	19.80	4.99	3.97	-3.55
	17.54	3.98	4.40	-3.82
$\Delta G = -RT \ln K_{eq}$	19.25	4.66	4.13	-3.66
	21.23	3.60	5.90	-4.57
	16.84	2.56	6.59	-4.86
	16.63	4.41	3.77	-3.42
Mean	**18.52**	**4.36**	**4.44**	**-3.78**
Standard deviation	**1.46**	**0.91**	**1.10**	**0.59**

Table 35: Calculation of K_{eq} and ΔG for experiments JC/5221/16,18,20; the partitioning of transcript mRNA between H_{II} DOPE/DNA and transcription buffer deficient in triton X-100

B2.1.3d Buffer deficient in spermidine and triton; JC/5140/22/4R

	$[RNA]_{real\ SN}$/µg	$[RNA]_{real\ LC}$/µg	K_{eq}	ΔG/kJ mol^{-1}
$K_{eq} = \frac{[RNA]_{SN}^{real}}{[RNA]_{LC}^{real}}$	9.15	2.27	4.03	-3.59
	8.98	1.57	5.70	-4.49
	8.91	1.76	5.07	-4.19
	8.62	4.01	2.15	-1.98
$\Delta G = -RT \ln K_{eq}$	9.30	1.24	7.51	-5.20
	2.31	0.89	2.59	-2.45
Mean	**7.88**	**1.96**	**4.51**	**-3.65**
Standard deviation	**2.74**	**1.11**	**2.01**	**1.23**

Table 36: Calculation of K_{eq} and ΔG for experiments JC/5221/26,30,32; the partitioning of transcript mRNA between H_{II} DOPE/DNA and transcription buffer deficient in both spermidine and triton X-100

B2.1.3e Summary of Gibbs free energies

	$[RNA]_{real\ SN}$/µg	$[RNA]_{real\ LC}$/µg	K_{eq}	ΔG/kJ mol^{-1}
Full buffer JC/5140/22/1R	16.29 ± 4.22	3.10 ± 1.46	6.51 ± 4.00	-4.48 ± 1.33
(-) Spermidine JC/5140/22/2R	12.51 ± 2.24	3.20 ± 2.76	5.95 ± 3.56	-4.07 ± 1.82
(-) Triton JC/5140/22/3R	18.52 ± 1.46	4.36 ± 0.91	4.44 ± 1.10	-3.78 ± 0.59
(-) Spermidine, (-) Triton JC/5140/22/4R	7.88 ±2.74	1.96 ± 1.11	4.51 ± 2.01	-3.65 ± 1.23

Table 37: Summary of of K_{eq} and ΔG for full buffer and buffers deficient in spermidine, triton X-100 and both spermidine and triton X-100; data from experiments JC/5140/65,73,74,82,86,90,97; JC/5221/03,07,11,16,18,20,26,30,32.

B2.1.4 Transcription in the absence of a ribonuclease inhibitor

RNAsin ribonuclease inhibitor was removed from the transcription buffer to assess levels of transcription in its absence. It was found that RNAsin was not essential to produce high yields of mRNA but was necessary for protection of the transcript RNA from RNase degradation. It was also questioned whether the liquid crystal phase itself would protect transcribed mRNA from degradation but this was not the case (see gel electrophoresis, figure …). This suggests that the RNA in the liquid crystal portion is unlikely to be in the pores of the inverse hexagonal phase but associated with the surface instead.

Mean positive control		Positive (-) R	Total extract	Lipid RNA	Supernatant RNA
(36.32 ± 4.24) (µg)	mRNA yield (µg)	44.68	15.19	4.58	21.02
		51.93	16.63	8.13	21.52
		50.36	22.89	8.99	27.27
		40.34	22.57	7.17	20.62
		43.94	28.38	7.44	24.61
		44.65	26.30	9.87	19.15
	Mean	**45.98**	**21.99**	**7.70**	**22.36**
	Standard deviation	**4.34**	**5.21**	**1.82**	**3.00**

Table 38: Transcription data from experiments JC/5221/36,41,55,70; transcription using buffer deficient in RNAsin ribonuclease inhibitor, in the presence and absence of H_{II} DOPE

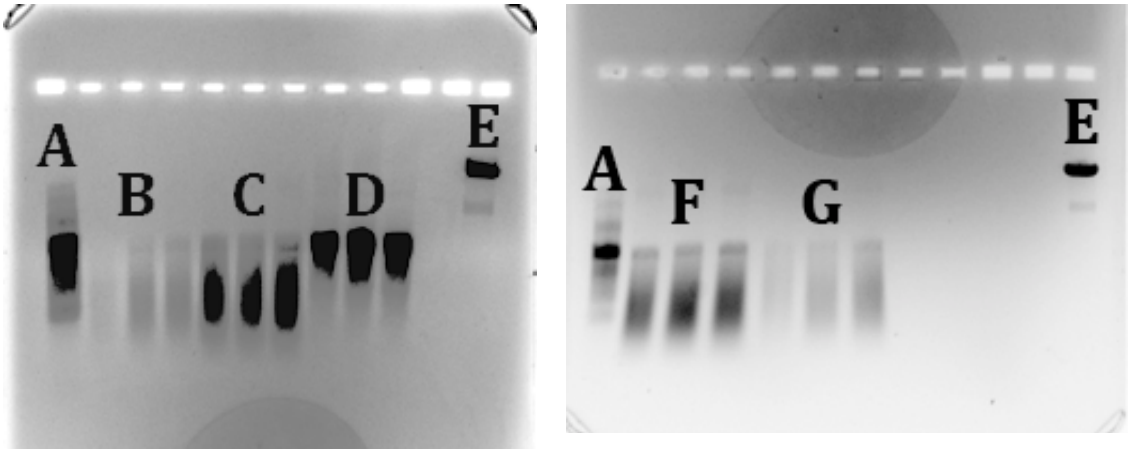

Figure 86: Gel electrophoresis images of transcription from buffers without RNAsin; JC/5140/70. A: ladder, brightest band corresponds to 3000bp RNA; B: transcript RNA from LC phase, note streaking of sample; C: RNA from supernatant, note streaking fo sample; D: positive control (+ RNAsin), with slight overloading of sample; E: template DNA; F: RNA from buffer without RNAsin, no liquid crystal phase; G: RNA from buffer without RNAsin, DOPE/DNA liquid crystal phase, whole sample extract.

B2.2 Mechanistic Studies

The mechanistic studies described in chapter 4 of this report involved exploring the effects of DTT on the transcription system. It was found that DTT was necessary to prevent denaturation of the protein in the presence of the inverse hexagonal phase. Experiments were

designed that exposed the polymerase to the inverse hexagonal phase under the conditions for transcription in the presence and absence of DTT. Samples were then split into liquid crystal and supernatant phases and tested for transcriptional activity by adding measured amounts of DTT. It was found that transcriptional activity could be recovered from denatured polymerase by adding DTT, although the amount of activity recovered varied depending on sample type.

B2.2.1 The effect of DTT on transcription without an H_{II} phase

Experiments were conducted where buffers deficient in DTT were incorporated into a standard transcription on the inverse hexagonal phase of DOPE/DNA. The following data were recovered:

Sample type	Positive control (-) LC JC/5221/36/1J or 2N	(-) DTT (-) LC JC/5221/36/4D
mRNA yield (µg)	35.23	29.76
	37.59	30.04
	36.35	27.96
	34.11	30.92
	30.19	25.26
	36.83	28.75
	33.15	29.92
	38.36	31.54
	37.66	28.82
	32.94	42.68
	38.01	31.60
	38.21	36.00
Mean	**35.71**	**31.10**
Standard deviation	**2.61**	**4.45**

Table 40: Transcription of DNA in full buffer compared with transcription in buffer deficient in DTT, no lipid present; data from experiments JC/5221/36,55,59,62,65.

B2.2.2 The effect of DTT on transcription in the presence of an H_{II} phase

Mean positive control		(–) DTT (–) LC	Total extract	Lipid RNA	Supernatant RNA
(35.72 ± 2.61) µg	Ratio: Sample type/ Positive control	23.79	1.70	1.05	4.23
		27.08	1.58	0.69	1.70
		20.91	2.16	0.61	1.54
			5.63	0.71	3.28
			2.61	1.04	2.52
	Mean	**23.93**	**2.73**	**0.82**	**2.65**
	Standard deviation	**3.08**	**1.67**	**0.21**	**0.50**

Table 41: Data from experiments JC/5221/62,65; the effect of DTT on transcription - DNA in the H_{II} phase of DOPE

B2.2.2a Adding DTT to improve transcription:

Sample type	Full Buffer (–) LC [DTT] = 10 mM	Full Buffer (–) LC [DTT] = 20 mM	Full Buffer (+) LC [DTT] = 10 mM	Full Buffer (+) LC [DTT] = 20 mM
mRNA yield (µg)	28.73	19.97	24.09	24.26
	26.07	28.92	36.69	22.04
	25.74	21.51	22.90	28.82
	31.85	22.54	22.84	20.71
	21.84	25.14	25.12	11.22
	26.95	23.08	20.16	18.77
	24.11	24.88	14.58	16.77
	29.49	20.18	17.31	10.88
	25.50	28.33	14.88	11.06
	28.59	33.03	10.52	14.65
	26.46	30.98	22.29	17.97
	27.68	28.55	21.03	
	25.62			
	27.23			
	33.28			
	19.87			
	27.39			
Mean	**26.85**	**25.59**	**21.03**	**17.92**
Standard deviation	**3.24**	**4.32**	**6.63**	**5.82**

Table 42: The effect of adding DTT to samples already containing DTT, data from experiments JC/5221/65,94; JC/5257/05,11,18.

Table 42 shows that adding extra DTT to buffers that already contain DTT does not cause an increase in transcription, and may be said to be detrimental to transcriptional activity. When DTT was not present in the transcription buffer, and therefore caused the T7 RNA polymerase to become deactivated, adding DTT produced an increase in transcriptional yield.

Mean positive control		(–) DTT (+) LC [DTT] = 0 mM	(–) DTT (+) LC [DTT] = 10 mM	(–) DTT (+) LC [DTT] = 20 mM
		0.74	8.94	15.90
		1.15	11.10	16.86
		0.36	9.34	13.64
		0.42	12.77	12.02
		0.54	14.02	4.48
		0.36	11.07	1.54
(26.85± 3.24) µg	**mRNA yield (µg)**	0.44	4.42	4.02
		0.37	1.74	3.15
		0.44	3.77	6.34
		0.52	5.77	4.31
		0.69	5.64	8.25
		0.92	9.49	
		1.09	3.58	
		0.93	3.98	
	Mean	**0.64**	**7.13**	**8.23**
	Standard deviation	**0.28**	**4.07**	**5.46**

Table 43: Recovery of transcriptional activity by adding DTT to samples where T7 RNA polymerase has been denatured by the DOPE phase in buffer deficient in DTT; data from experiments JC/5221/94; JC/5257/05,11,18

B2.2.2b Recovering transcriptional activity by adding DTT – H_{II} DOPE only

Experiments were set up so that the polymerase was left to incubate in the presence of the inverse hexagonal phase of DOPE for 2 hours at 37 °C , in full buffer or buffer deificient in DTT. After incubation samples were split into liquid crystal and supernatant phases by removing 15 µl supernatant and recovering to a new tube. Transcription was initiated by addition of mixed ribonucleotides and template DNA. Adding DTT to appropriate samples for transcription causes variation in the overall assay volume; the effects of this change on buffer concentrations is outlined below:

Component	Volume added
Mixed rNTPs	-
Linear T7 luciferase DNA	-
10x reaction buffer	2µl
T7 RNAP	0.8µl
Nuclease-free water	17.2µl
Total assay volume	**20µl**

Table 44: preparation of mixture for incubation of T7 RNA polymerase with inverse hexagonal DOPE, experiments JC/5257/30

Component	Supernatant reaction	Liquid Crystal reaction
Mixed rNTPs	1.25µl	1.25µl
Linear T7 luciferase DNA	5.7µl	5.7µl
Reaction supernatant	15 µl	-
Nuclease-free water	-	11.55µl
10x transcription buffer	-	1.5µl
Liquid crystal component	-	whole
Total assay volume	**21.95µl**	**20µl**

Table 45: preparation of liquid crystal and supernatant components for transcription in investigations of the recovery of transcription from T7 RNA polymerase denatured by H_{II} DOPE, experiments JC/5257/30

Effects on transcription buffer concentrations (liquid crystal samples):

Buffer	**Normal assay**	**Full**	**-DTT**	**(-) DTT/ 10 mM added**	**(-) DTT/ 20 mM added**	**(-) DTT/ 30 mM added**
Total Volume	20µl	20µl	20µl	20.2µl	20.4µl	20.6µl
20µl/ volume	1	1	1	0.99	0.98	0.97
Trizma	40 mM	30 mM	30 mM	29.7mM	29.4mM	29.1mM
$MgCl_2$	25 mM	18.75 mM	18.75 mM	18.56mM	18.38mM	18.20 mM
Spermidine	2.5 mM	1.875 mM	1.875 mM	1.856mM	1.838mM	1.820 mM
Triton X-100	0.16mM	0.12mM	0.12mM	0.1188mM	0.1176mM	0.1164mM
DTT	10 mM	7.5 mM	-	9.9mM	19.6mM	29.1mM

Table 46: effect of adding DTT on buffer concentrations in liquid crystal samples, experiments JC/5221/30

Effects on transcription buffer concentrations (supernatant samples):

Buffer	**Normal assay**	**Full**	**(-) DTT**	**(-) DTT/ 10 mM added**	**(-) DTT/ 20 mM added**	**(-) DTT/ 30 mM added**
Total Volume	20µl	21.95µl	21.95µl	22.15 µl	22.35µl	22.55µl
20µl/ volume	1	0.911	0.911	0.903	0.895	0.887
Trizma	40 mM	36.43mM	36.43mM	36.10 mM	35.78mM	35.46mM
$MgCl_2$	25 mM	22.77mM	22.77mM	22.56mM	22.36mM	22.16mM
Spermidine	2.5 mM	2.28mM	2.28mM	2.26mM	2.24mM	2.22mM
Triton X-100	0.16mM	0.146mM	0.146mM	0.144mM	0.143mM	0.142mM
DTT	10 mM	9.1mM	-	9.0 mM	17.9mM	26.6mM

Table 47: effect of recovering supernatant and adding DTT on buffer concentrations in supernatant samples, experiments JC/5221/30

Sample type		Full buffer (-) LC	Full Buffer (+) LC	(-) DTT (+) LC 0 mM DTT added	(-) DTT (+) LC 10 mM DTT added	(-) DTT (+) LC 20 mM DTT added	(-) DTT (+) LC 30 mM DTT added
mRNA yield (µg)	LC	1.32	2.13	0.86	1.50	1.55	2.01
		1.39	2.86	0.70	1.24	1.58	1.41
		1.97	1.67	0.92	1.19	1.70	1.27
		2.76	1.80	0.50	1.65	5.99	1.74
		2.78	1.39	0.59	2.08	3.94	2.85
		2.76	2.53	0.60	2.20	2.19	1.07
	SN	16.27	3.73	1.27	6.45	4.39	6.69
		15.30	7.42	1.23	3.44	3.59	8.86
		11.21	14.55	0.69	4.31	10.64	8.38
		11.19	13.05	0.52	8.15	9.74	6.70
		16.19		0.61	8.10	8.40	10.56
		15.41		0.69	8.88		
LC	**M**	**2.16**	**2.06**	**0.70**	**1.64**	**2.83**	**1.72**
	SD	**0.70**	**0.55**	**0.16**	**0.42**	**1.79**	**0.64**
SN	**M**	**14.26**	**9.69**	**0.84**	**6.56**	**7.35**	**8.24**
	SD	**2.40**	**5.02**	**0.33**	**2.24**	**3.18**	**1.62**

Table 48: Transcription from liquid crystal and supernatant phase of samples incubated with T7 RNA polymerase/transcription buffer before being separated prior to transcription; experiments JC/5257/30

B2.2.2c Adding DTT to recover transcription – H_{II} DOPE/DNA

In experiments similar to those outlined in B2.2.2, the polymerase was left to incubate in the presence of the inverse hexagonal phase of DOPE/DNA for 2 hours at 37 °C , in full buffer or buffer deificient in DTT. After incubation samples were split into liquid crystal and supernatant phases by removing 15 µl supernatant and recovering to a new tube. Transcription was initiated by addition of mixed ribonucleotides, as well as template DNA and additional DTT where appropriate. Adding DTT to the sample for transcription causes variation in the overall assay volume; the effects of this change on buffer concentrations is outlined below:

Component	Volume added
Mixed rNTPs	-
Linear T7 luciferase DNA	-
10x reaction buffer	2µl
T7 RNAP	0.8µl
Nuclease-free water	17.2µl
Total assay volume	**20µl**

Table 49: Description of components included in incubation mixture of polymerase and DOPE/DNA. The concentration of T7 RNA polymerase is 40 units/assay or 69nM.

Component	Supernatant reaction	Liquid Crystal reaction
Mixed rNTPs	1.25µl	1.25µl
Linear T7 luciferase DNA	5µl	-
Reaction supernatant	15 µl	-
Nuclease-free water	-	17.25µl
10x transcription buffer	-	1.5µl
Liquid crystal component	-	whole
Total assay volume	**21.25µl**	**20µl**

Table 50: preparation of liquid crystal and supernatant components for transcription in investigations of the recovery of transcription from T7 RNA polymerase denatured by H_{II} DOPE, experiments JC/5257/34,41

Effects on transcription buffer concentrations (liquid crystal samples):

Buffer	**Normal assay**	**Full**	**(-) DTT**	**(-) DTT/ 10 mM added**	**(-) DTT/ 20 mM added**	**(-) DTT/ 30 mM added**
Total Volume	20µl	20µl	20µl	20.2µl	20.4µl	20.6µl
20µl/ volume	1	1	1	0.99	0.98	0.97
Trizma	40 mM	30 mM	30 mM	29.7mM	29.4mM	29.1mM
$MgCl_2$	25 mM	18.75 mM	18.75 mM	18.56mM	18.38mM	18.20 mM
Spermidine	2.5 mM	1.875 mM	1.875 mM	1.856mM	1.838mM	1.820 mM
Triton X-100	0.16mM	0.12mM	0.12mM	0.1188mM	0.1176mM	0.1164mM
DTT	10 mM	7.5 mM	-	9.9mM	19.6mM	29.1mM

Table 51: effect of recovering supernatant and adding DTT on buffer concentrations in liquid crystal samples, experiments JC/5221/34,41

Effects on transcription buffer concentrations (supernatant samples):

Buffer	**Normal assay**	**Full**	**(-) DTT**	**(-) DTT/ 10 mM added**	**(-) DTT/ 20 mM added**	**(-) DTT/ 30 mM added**
Total Volume	20µl	21.25µl	21.25µl	21.45µl	21.65µl	21.85µl
20µl/ volume	1	0.941	0.941	0.932	0.924	0.915
Trizma	40 mM	37.64mM	37.64mM	37.28mM	36.96mM	36.60 mM
$MgCl_2$	25 mM	23.53mM	23.53mM	23.30 mM	23.10 mM	22.88mM
Spermidine	2.5 mM	2.35 mM	2.35 mM	2.33mM	2.31mM	2.29mM
Triton X-100	0.16mM	0.151mM	0.151mM	0.149mM	0.148mM	0.146mM
DTT	10 mM	9.4mM	-	9.3mM	18.5 mM	27.5 mM

Table 52: effect of recovering supernatant and adding DTT on buffer concentrations in supernatant samples, experiments JC/5221/34,41

Sample type		Full buffer (-) LC	Full Buffer (+) LC	(-) DTT (+) LC 0 mM DTT added	(-) DTT (+) LC 10 mM DTT added	(-) DTT (+) LC 20 mM DTT added	(-) DTT (+) LC 30 mM DTT added
mRNA yield (µg)	LC	1.20	2.08	0.67	0.51	0.87	0.56
		1.65	2.37	0.68	0.46	0.42	0.63
		1.46	1.17	0.59	0.93	0.76	1.14
		2.41	1.45	0.46	0.69	0.82	0.72
		1.74	1.36	0.73	0.99	0.82	0.78
		2.19	1.64	0.41	0.64	0.49	0.77
	SN	26.78	13.19	0.86	4.21	8.52	4.67
		20.45	16.45	0.57	6.05	10.76	5.98
		28.75	16.99	1.30	3.52	5.94	3.18
			9.28	0.63	6.32	4.51	4.92
			9.12	0.63	6.41	7.73	7.41
			16.16	0.48	4.71	5.07	6.97
LC	**M**	**1.77**	**1.68**	**0.59**	**0.70**	**0.70**	**0.77**
	SD	**0.45**	**0.46**	**0.13**	**0.22**	**0.19**	**0.20**
SN	**M**	**25.33**	**13.53**	**0.75**	**5.20**	**7.09**	**5.52**
	SD	**4.34**	**3.61**	**0.30**	**1.22**	**2.37**	**1.58**

Table 53: Transcription from liquid crystal and supernatant phase of samples incubated with T7 RNA polymerase/transcription buffer before being separated prior to transcription; experiments JC/5257/34,41

B2.3 Kinetic Studies

B2.3.1 Effects of DNA concentration

A concentration gradient of DNA was set up so that transcription products could be analysed to show how transcriptional yield is affected by DNA concentration. These experiments were particularly useful in comparing transcript RNA produced from standard reactions and the concentration of DNA estimated in the supernatant phase of transcription samples containing a liquid crystal and supernatant phase.

Amount of DNA added/µg	**4**	**2**	**1**	**0.1**	**0.01**	**0.001**	**0.0001**
mRNA yield (µg)	43.42	43.63	23.89	12.93	12.72	1.78	0.75
	36.68	31.07	28.89	13.63	11.71	1.66	0.93
	50.92	42.00	25.18	16.04	12.00	1.41	1.12
	43.89	32.99	21.79	13.57	12.82	1.78	1.21
	41.10		31.46	13.60	11.47	1.70	1.06
			21.57	11.55	11.71	1.75	1.05
			23.09	16.69	10.76	1.97	1.46
				14.94	10.80	1.56	1.55
				13.26	10.67	1.47	1.44
Mean	**43.20**	**37.42**	**25.12**	**14.02**	**11.63**	**1.67**	**1.17**
Standard deviation	**5.17**	**6.31**	**3.73**	**1.60**	**0.80**	**0.17**	**0.26**

Table 54: transcript RNA concentrations obtained using a concentration gradient of DNA, from experiments JC/5221/48, 51 and 54. Data was used to generate figures 28 and 29. The concentration of T7 RNA polymerase is 40 units/assay or 69nM.

The concentration gradient of DNA was created using a serial dilution from a stock solution of DNA:

Component	Volume added
Mixed rNTPs	1.25µl
Linear T7 luciferase DNA	3.83µl
10x reaction buffer	2µl
T7 RNAP	0.8µl
Nuclease-free water	12.12µl
Total assay volume	**20µl**

Table 55: Assembly of transcription reactions with a concentration gradient of DNA (1µg and below), JC/5221/48,51,54. The concentration of T7 RNA polymerase is 40 units/assay or 69nM.

Solution number	Amount of DNA in assay/µg	from	Volume added/µl	Volume water/µl
1	1	Stock	-	-
2	0.1	Stock	3.83	34.2
3	0.01	Stock	1.60	36.4
4	0.001	(2)	1.60	36.4
5	0.0001	(3)	1.60	36.4

Table 56: Preparation of a concentration gradient of DNA by serial dilution, samples used in experiments JC/5221/48,51,54. The concentration of T7 RNA polymerase is 40 units/assay or 69nM.

B2.3.2 Time course experiments

Experiments were carried out such that identical transcription reactions were stopped at time intervals, processed and analysed for transcript RNA levels. These data were then used to create the graphs shown in sections 5.2 and 5.3 of this report.

B2.3.2a [NTP] = 20 mM, no liquid crystal phase

The standard transcription reaction was carried out over a time course to establish how quickly the reaction reaches saturation in the absence of a liquid crystal phase. The DNA used

was Giga 1 MNT/5222/94 and had a concentration of 572 ng μl^{-1}. The reactions were assembled as follows:

Component	Volume added
Mixed rNTPs	1.25µl
Linear T7 luciferase DNA	1.74µl
10x reaction buffer	2µl
T7 RNAP	0.8µl
Nuclease-free water	14.21µl
Total assay volume	**20µl**

Table 57: Assembly of transcription reactions with a total ribonucleotide concentration of 20 mM; samples were used in time course experiment JC/5257/62 The concentration of T7 RNA polymerase is 40 units/assay or 69nM.

Time/minutes	mRNA yield (µg)			Mean	Standard deviation
	1	2	3		
0	0.48	0.61	0.37	0.49	0.12
15	7.33	4.77	3.34	5.15	2.02
30	10.36	10.09	14.03	11.49	2.20
60	-	14.72	15.04	16.18	2.26
90	16.82	21.22	18.45	18.83	2.22
120	18.79	21.38	17.27	19.32	2.90
150	19.17	23.05	23.54	21.92	2.39
180	21.49	24.88	19.41	21.93	2.76

Table 58: Nanodrop data from transcript JC/5257/62; time-course experiment at 20 mM ribonucleotide concentration.

B2.3.2b [NTP] = 20 mM, H_{II} DOPE/DNA liquid crystal phase

DNA was placed in the inverse hexagonal phase of DOPE and prepared for transcription by addition of 2.5µl isotonic saline followed by incubation at 40°C for 1 hour. Samples were then assembled for transcription and initiated with addition of T7 RNA polymerase (40 units, 69nM) and incubated at 37 °C over 4 hours. Triplicate groups of samples were removed and processed at regular time intervals to assess how the production of messenger RNA varies with reaction time.

Component	Volume added
Mixed rNTPs	1.25µl
Linear T7 luciferase DNA	-
10x reaction buffer	2µl
T7 RNAP	0.8µl
Nuclease-free water	15.95µl
Total assay volume	**20µl**

Table 59: Assembly of transcription reactions with a total ribonucleotide concentration of 20 mM; samples were used in time course experiment JC/5257/65. The concentration of T7 RNA polymerase is 40 units/assay or 69nM.

Time/minutes	mRNA yield (µg)			Mean	Standard deviation
	1	2	3		
0	0.26	0.58	0.63	0.49	0.20
15	3.63	2.18	3.87	3.22	0.92
30	4.20	6.04	6.38	5.54	1.18
60	9.50	10.39	10.41	10.10	0.52
90	12.44	10.11	11.02	11.19	1.17
120	15.25	13.32	14.66	14.41	0.99
150	12.67	14.51	15.38	14.19	1.38
180	-	14.96	15.99	15.47	0.73
210	17.08	18.99	16.29	17.46	1.39
240	16.58	14.83	17.13	16.18	1.20

Table 60: Nanodrop data from transcript JC/5257/65; time-course experiment at 20 mM ribonucleotide concentration, H_{II} DOPE/DNA present.

B2.3.2c [NTP] = 20 mM, buffer deficient in spermidine, no lipid

The standard transcription reaction buffer was exchanged for a buffer deficient in spermidine and transcription assembled without a liquid crystal phase. Transcription was run at 37 °C and triplicate samples were removed at regular time intervals and processed to monitor the production of transcript RNA over a period of time.

Component	Volume added
Mixed rNTPs	1.25µl
Linear T7 luciferase DNA	
10x reaction buffer	2µl
T7 RNAP	0.8µl
Nuclease-free water	15.95µl
Total assay volume	**20µl**

Table 61: Assembly of transcription reactions with a total ribonucleotide concentration of 20 mM; samples were used in time course experiment JC/5140/82. The concentration of T7 RNA polymerase is 40 units/assay or 69nM.

Time/minutes	mRNA yield (µg)			Mean	Standard deviation
	1	2	3		
0	0.26	0.58	0.63	0.49	0.20
15	6.58	4.97	3.32	4.96	1.63
30	6.87	5.26	5.55	5.89	0.86
60	10.10	11.28	8.14	9.84	1.58
90	14.09	13.14	14.34	13.86	0.63
120	16.39	15.46	16.38	16.08	0.53
150	17.48	17.37	14.63	16.49	1.61
180	17.82	19.21	16.65	17.89	1.28
210	17.16	19.06	17.17	17.80	1.10
240	15.84	18.90	16.36	17.03	1.64
300	18.89	16.58	16.02	17.16	1.52

Table 62: Nanodrop data from transcript JC/5140/82; time-course experiment at 20 mM ribonucleotide concentration, buffer deficient in spermidine, no liquid crystal phase present.

B3.3 Transcription using a concentration gradient of ribonucleotides

As one of the substrates of T7 RNA polymerase, ribonucleotides may be used to probe the mechanism of transcription. In the following experiments a concentration gradient of mixed ribonucleotides was set up in order to observe their effects of RNA production. The concentration gradient was between 0 mM and 40 mM total nucleotide concentration, with equal concentrations of each NTP present.

B2.3.3 Effect of rNTP concentration gradient without lipid

Component	Volume added
Mixed rNTPs	αµl
Linear T7 luciferase DNA	2.05µl
10x reaction buffer	2µl
T7 RNAP	0.8µl
Nuclease-free water	(15.15-α)µl
Total assay volume	**20µl**

Table 63: Assembly of transcription reactions across a concentration gradient of ribonucleotides; samples were used in experiment JC/5257/52,53,54. The concentration of T7 RNA polymerase is 40 units/assay or 69nM.

[rNTP] (mM)	5	10	15	20	25	30	35	40
Mixed rNTP (µl)	0.31	0.63	0.94	1.25	1.56	1.88	2.12	2.50
Nuclease-free water (µl)	14.84	14.52	14.21	13.90	13.59	13.27	13.03	12.65
mRNA yield (µg)	10.56	13.86	19.74	17.29	17.78	19.38	12.28	10.61
	13.76	11.17	15.04	15.34	20.24	20.69	15.21	9.06
	12.75	13.92	14.57	18.15	22.77	20.14	10.06	5.23
	12.05	17.54	22.00	20.44	13.56	14.99	8.62	7.60
	9.08	15.71	22.85	20.29	20.42	19.45	6.86	4.57
	10.86	14.77	23.09	20.43	18.01	15.00	12.50	5.13
	12.10	14.34	22.40	25.20	13.86	13.19	9.71	3.63
	10.91	13.58	22.84		17.44	13.95	10.14	4.47
	12.02	15.31	18.53		17.81	14.12		3.88
Mean	**11.57**	**14.47**	**20.12**	**19.59**	**17.99**	**16.77**	**10.67**	**6.02**
Standard deviation	**1.37**	**1.74**	**3.38**	**3.13**	**2.98**	**3.06**	**2.59**	**2.48**

Table 64: transcript RNA concentrations obtained using a concentration gradient of rNTPs, from experiment JC/5257/52,53,54 The concentration of T7 RNA polymerase is 40 units/assay or 69nM.

B2.3.3a Effect of rNTP concentration gradient with lipid

Component	Volume added
Mixed rNTPs	αµl
Linear T7 luciferase DNA	-
10x reaction buffer	2µl
T7 RNAP	0.8µl
Nuclease-free water	(17.20-α)µl
Total assay volume	**20µl**

Table 65: Assembly of transcription reactions across a concentration gradient of ribonucleotides in the presence of the H_{II} phase of DOPE/DNA; samples were used in experiment JC/5257/56 The concentration of T7 RNA polymerase is 40 units/assay or 69nM.

[rNTP] (mM)	5	10	15	20	25	30	35	40
Mixed rNTP (µl)	0.31	0.63	0.94	1.25	1.56	1.88	2.12	2.50
Nuclease-free water (µl)	16.89	16.57	16.26	15.95	15.64	15.32	15.08	14.70
mRNA yield (µg)	4.96	6.63	10.72	19.49	12.11	10.00	4.21	2.20
	8.39	8.83	12.07	15.58	18.25	5.70	4.09	1.90
	6.59	7.54	14.80	15.08	15.11	9.28	4.14	2.90
	5.75	9.05	8.77	18.18	13.93	9.94	7.91	3.17
	6.10	7.18	11.49	18.18	10.37	8.80	3.26	3.36
Mean	**6.36**	**7.84**	**11.57**	**17.30**	**13.95**	**8.74**	**4.72**	**2.70**
Standard deviation	**1.28**	**1.05**	**2.19**	**1.89**	**3.00**	**1.77**	**1.82**	**0.63**

Table 66: transcript RNA concentrations obtained using a concentration gradient of rNTPs, from experiment JC/5257/56 The concentration of T7 RNA polymerase is 40 units/assay or 69nM.

B2.3.3.bEffect of rNTP concentration gradient without lipid, 30 minutes

Component	Volume added
Mixed rNTPs	αµl
Linear T7 luciferase DNA	1.74µl
10x reaction buffer	2µl
T7 RNAP	0.8µl
Nuclease-free water	(15.46-α)µl
Total assay volume	**20µl**

Table 67: Assembly of transcription reactions across a concentration gradient of ribonucleotides; samples were used in experiment JC/5257/60. The concentration of T7 RNA polymerase is 40 units/assay or 69nM.

[rNTP] (mM)	5	10	15	20	25	30	35	40
Mixed rNTP (µl)	0.31	0.63	0.94	1.25	1.56	1.88	2.12	2.50
Nuclease-free water (µl)	15.15	14.83	14.52	14.21	13.90	13.58	13.34	12.96
mRNA yieldr (µg)	12.42	13.57	13.82	12.33	11.94	8.07	2.76	0.97
	12.77	11.94	12.71	16.06	11.99	7.95	3.39	1.83
	10.04	11.40	15.23	14.87	11.97	6.67	4.02	2.83
Mean	**11.74**	**12.30**	**13.92**	**14.42**	**11.96**	**7.56**	**3.39**	**1.88**
Standard deviation	**1.48**	**1.13**	**1.26**	**1.91**	**0.03**	**0.77**	**0.63**	**0.93**

Table 68: transcript RNA concentrations obtained using a concentration gradient of rNTPs, from experiment JC/5221/60

B2.3.3c Time course experiment, [rNTP] = 5 mM

Time/minutes	mRNA yield (µg)			Mean	Standard deviation
	1	2	3		
0	1.58	0.58	0.48	0.88	0.61
10	6.52	5.80	5.30	5.88	0.61
20	8.50	9.02	6.40	7.97	1.39
30	9.36	13.39	8.09	10.28	2.76
45	10.43	10.19	17.17	10.31	0.17
60	11.64	12.96	7.46	12.30	0.93
90	9.83	13.60	12.97	12.13	2.02

Table 69: Nanodrop data from transcript JC/5140/63; time-course experiment at 5 mM ribonucleotide concentration, full buffer, no liquid crystal phase present.

B2.3.3d Time course experiment, [rNTP] = 40 mM

Time/minutes	mRNA concentration (ng μl^{-1})			Mean	Standard deviation
	1	2	3		
0	0.09	0.74	0.36	0.40	0.33
15	0.59	0.62	0.62	0.61	0.01
30	0.74	0.52	0.90	0.72	0.19
60	0.76	1.05	1.05	0.95	0.17
90	1.10	0.66	0.83	0.86	0.22
120	0.87	1.32	0.65	0.95	0.34
150	0.80	1.60	1.55	1.32	0.45
180	1.83	1.89	2.80	2.17	0.55

Table 70: Nanodrop data from transcript JC/5140/64; time-course experiment at 40 mM ribonucleotide concentration, full buffer, no liquid crystal phase present.

B3 Experimental phase behaviour

The phase behaviour of the lipoplex systems was studied using polarising light microscopy. Mixtures of lipid and hydration medium were allowed to equilibrate at 37 °C for three days and examined under the microscope at 25 °C and 37 °C.

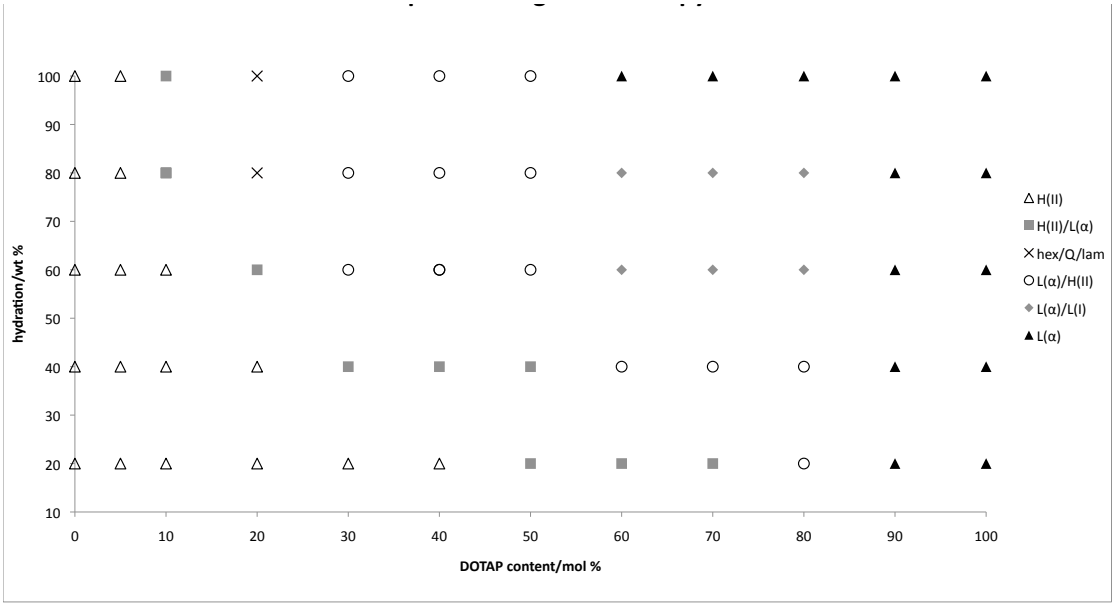

Figure 87: Phase diagram of DOPE/DOTAP mixtures at 25 °C in water

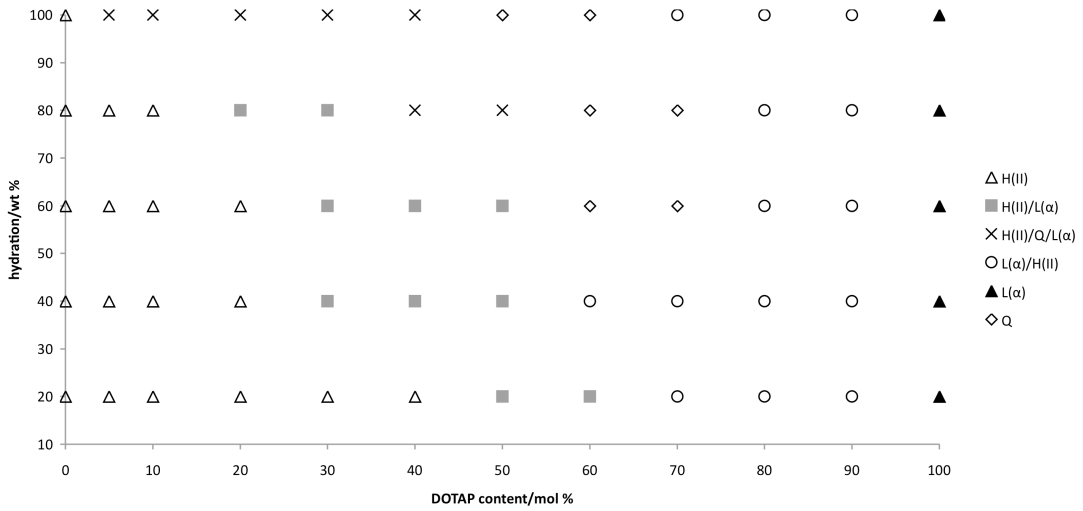

Figure 88: Phase diagram of DOPE/DOTAP mixtures at 25 °C in transcription buffer

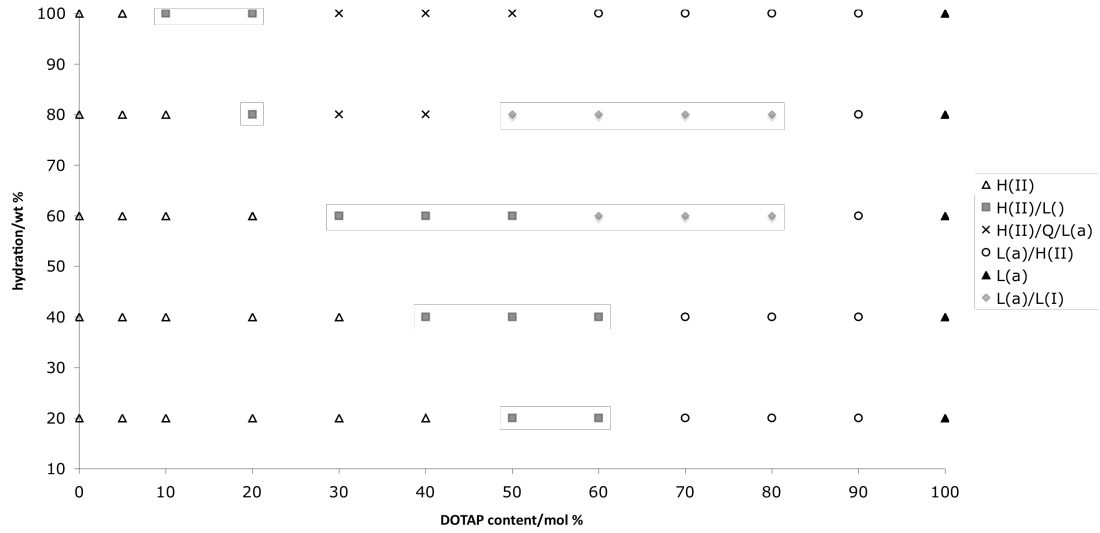

Figure 89: Phase diagram of DOPE/DOTAP mixtures at 37 °C in transcription water

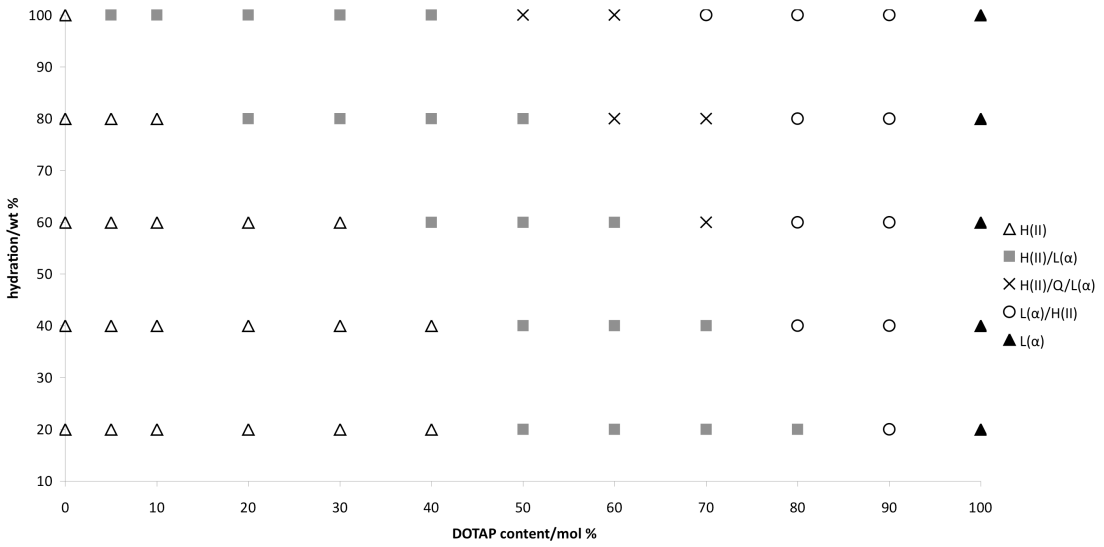

Figure 90: Phase diagram of DOPE/DOTAP mixtures at 37 °C in transcription buffer

The data plotted in figures 87 to 90 represent the basis of the phase diagrams presented in chapter 2 of this thesis.

B3.1 *d*-spacing values from SAXS experiments

SAXS experiments were carried out on lipid mixtures rehydrated with water, isotonic saline, or a solution of salmon sperm DNA (10 mg ml^{-1}). Samples were sealed in glass capillaries and allowed to equilibrate. The x-ray diffraction experiments were carried out at 37 °C using a peltier-driven sample holder. SAXS experiments were carried out using a bench-top system at Imperial College London

	Mol % DOTAP in DOPE				
	0	**5**	**10**	**20**	**30**
***d*-spacing/Å**	62.1 62.5 62.8 62.0 62.3	64.7 65.2 64.5 63.9	65.4 66.1 65.5	69.0 67.8	66.1 68.2 69.6
Mean	**62.3**	**64.6**	**65.7**	**68.4**	**68.0**
Standard deviation	**0.3**	**0.6**	**0.4**	**0.8**	**1.8**

Table 71: *d*-spacing values generated by SAXS for DOPE/DOTAP mixtures hydrated with water

	Mol % DOTAP in DOPE				
	0	**5**	**10**	**20**	**30**
***d*-spacing/Å**	62.7 62.7 62.3 62.9	63.2 63.0 61.7	64.4 63.7 63.6	66.6 66.8 64.7 64.3	65.2 67.7 67.9 67.7
Mean	**62.7**	**62.6**	**63.9**	**65.6**	**67.1**
Standard deviation	**0.2**	**0.8**	**0.4**	**1.3**	**1.3**

Table 72: *d*-spacing values generated by SAXS for DOPE/DOTAP mixtures hydrated with isotonic saline

	Mol % DOTAP in DOPE				
	0	**5**	**10**	**20**	**30**
***d*-spacing/Å**	62.2 62.3 62.2 61.1 64.4	62.4 62.5 62.3 62.1 62.7 61.9	63.5 62.0 62.7	63.1 62.2 63.9 63.4 62.5 63.0	62.77
Mean	**62.5**	**62.3**	**62.7**	**63.0**	**62.8**
Standard deviation	**1.2**	**0.3**	**0.7**	**0.6**	**-**

Table 73: *d*-spacing values generated by SAXS for DOPE/DOTAP mixtures hydrated with salmon sperm DNA (10 mg ml^{-1})

Mol % DOTAP in DOPE	***d*-spacing/Å**		
	Hydration with water	**Hydration with saline (0.15 M)**	**Hydration with salmon sperm DNA (10 mg ml^{-1})**
0	62.3 ± 0.3	62.7 ± 0.2	63 ± 1
5	64.6 ± 0.6	62.6 ± 0.8	62.3 ± 0.3
10	65.7 ± 0.4	63.9 ± 0.4	62.7 ± 0.7
20	68.4 ± 0.8	66 ± 1	63.0 ± 0.6
30	68 ± 2	67 ± 1	62.8

Table 74: Summary of the data displayed in tables … to …; data used to generate figure …

B3.2 *d*-spacing values from transcription samples

SAXS experiments were carried out on samples identical to those used for transcription. The effect of prior hydration with isotonic saline, transcription buffer, and inclusion of 1 µg linearised T7-luciferase DNA were explored.

				Mol % DOTAP in DOPE			
				0	**5**	**10**	**20**
***d*-spacing/Å**	**No prior hydration**	**Transcription buffer**		63.2 63.2	62.2 63.0	- 62.4	61.9 62.9
			M	63.2	62.6	62.4	62.4
			SD	0.0	0.6		0.7
		Transcription buffer + DNA (1 µg)		62.9 62.4	62.6 62.6	62.4 63.1	- 62.4
			M	62.6	62.6	62.7	62.4
			SD	0.3	0.0	0.5	
	Prior hydration (saline)	**Transcription buffer**		63.7 63.5	63.6 61.8	65.0 63.0	- 62.9
			M	63.6	62.7	64.0	62.9
			SD	0.2	1.3	1.4	
		Transcription buffer + DNA (1 µg)		64.6 64.6	61.7 62.1	68.1 64.8	60.6 61.9
			M	64.6	61.9	66.5	61.3
			SD	0.0	0.3	2.3	0.9

Table 75: *d*-spacing values of transcriptionally relevant samples

Mol % DOTAP in DOPE	***d*-spacing/Å**			
	Without prior hydration with saline		**With prior hydration (saline)**	
	Transcription buffer	**Transcription buffer and DNA**	**Transcription buffer**	**Transcription buffer and DNA**
0	63.2 ± 0.5	62.6 ± 0.6	62.4 ± 0.5	62.4 ± 0.7
5	62.6 ± 0.3	62.6 ±0.1	62.7 ± 0.5	62.4 ± 0.6
10	63.6 ± 0.5	63 ± 1	64 ± 1	62.9 ± 0.7
20	64.6 ± 0.2	61.9 ± 0.5	67 ± 2	61.3 ± 0.9

Table 76: Summary of *d*-spacing values from transcriptionally relevant samples. Data used to generate figure …

B4 Simulations

The simulations detailed in chapter 4 of this thesis are summarised in table … Other simulations were carried out, but the data generated was not used in writing this thesis.

Mol % DOTAP in DOPE	**0%**			**20%**			**40%**	
Number of DOPE lipids	5660			4528			3396	
Number of DOTAP lipids	0			1132			2264	
Total number of lipid molecules	5660			5660			5660	
Number of water particles (MARTINI)	15797	9638	3386	16033	10064	4468	16286	3825
W(martini)/lipid	2.79	1.70	0.60	2.83	1.78	0.79	2.88	0.68
Number of water particles (actual)	63188	38552	13544	64132	40256	17872	65144	15300
W(actual)/lipid	**11.16**	**6.81**	**2.39**	**11.33**	**7.11**	**3.16**	**11.51**	**2.70**
Na^+ ions added	864			0			0	
Cl^- ions added	0			268			1400	
Inverse hexagonal phase formation	**biphasic**	**yes**	**yes**	**biphasic**	**yes**	**yes**	**biphasic**	**distorted**
Length of simulation/ns	400	370	300	400	370	300	300	300

Table 77: Summary of data from simulations contributing to this thesis

B4.1 *d*-spacing values calculated from simulated data

The output conformations were used to generate data for the structural parameters of the inverse hexagonal phase. Individual atoms at the centre of the DNA helix were selected and their coordinates noted. The *d*-spacing was then calculated using trigonometric methods. Structural parameters generated in this fashion were found to be in good agreement with the experimental data.

	Mol % DOTAP in DOPE		
	0	**20**	**40**
***d*-spacing/Å (measured from simulated system)**	54.0	56.0	65.0
	58.2	64.4	85.3
	67.9	65.0	72.2
	60.0	64.6	67.5
	66.5	60.2	70.1
	64.4	60.4	66.9
	69.5	60.3	85.0
	61.7	65.9	67.9
	60.1	61.9	54.7
	62.4	75.3	75.0
	63.2	59.9	76.5
	61.9	75.1	54.2
	53.5	64.7	58.9
	51.0	65.0	58.9
	60.1	59.3	57.8
	59.0	61.8	80.5
	68.9	61.7	60.5
	57.5	63.1	69.1
	66.1		60.2
	64.1		72.6
			100.4
Mean	**61.5**	**63.6**	**69.5**
Standard Deviation	**5.1**	**4.9**	**11.6**

Table 78: *d*-spacing values generated from simulated data

B5 Data supporting graphs displayed in transfection chapter

B5.1 Particle sizing data

Solutions of hexosomes and DNA in different cell culture medium were sized using the Coulter N400+ particle sizer. The data generated were plotted graphically.

	Hexosome type	Mol % DOTAP in DOPE			
		0	5	10	20
Particle size/nm	Linear pAmCyan in Opti-MEM	455 ± 201	307 ± 129	228 ± 92	153 ± 61
	Linear pAmCyan in DMEM + 5% FCS	278 ± 118	287 ± 116	240 ± 98	283 ± 91
	pAmCyan in Opti-MEM	347 ± 147	292 ± 121	230 ± 93	149 ± 57
	pAmCyan in DMEM + 5% FCS	271 ± 115	369 ± 163	242 ± 94	274 ± 98

Table 79: Data generated by the Coulter N400+

B5.2 Transcription from DNA in hexosomes

Transcription was carried out under four different sets of conditions, including a standard positive control (full buffer, no lipid), DOPE hexosomes that contained DNA, the DOPE/DNA bulk inverse hexagonal phase, and hexosomes where the DNA was not included within them, but was added with the remaining components at the initiation of transcription.

	Sample Type			
	positive control	**hexosomes (+) DNA**	**H(II) bulk (+) DNA**	**hexosomes (-) DNA**
mRNA yield (µg)	10.80	3.52	15.70	13.89
	10.08	4.69	16.75	4.86
	11.07	5.42	14.86	15.71
	11.82	13.23	14.18	3.34
	11.17	5.82	13.42	3.35
	14.23	5.37	15.30	7.19
	16.42	16.07	16.05	5.34
	12.67	6.43	17.90	7.94
	12.77	14.37	14.61	3.03
	13.72	22.98		
	11.90	7.19		
	13.33	14.98		
	15.95			
	16.37			
	16.04			
Mean	**13.22**	**10.01**	**7.12**	**15.42**
Standard deviation	**0.56**	**1.76**	**0.46**	**0.45**

Table 80: mRNA yield generated from transcription reactions carried out in hexosomes, compared with the bulk inverse hexagonal phase. Transcription was carried out for 40 minutes at 37 °C

B5.3 The effect of DOTAP on transcriptional yield

As some of the hexosomes preparations used for transfection contain DOTAP, the effect of the cationic lipid on mRNA yield was assessed. DOTAP was added to the bulk phase of DOPE and transcription was run for 40 minutes at 37 °C.

	Standard positive control (no lipid)	Mol % DOTAP in DOPE				
		0	**5**	**10**	**20**	**40**
mRNA yield (µg)	191.03	77.38	74.10	42.69	7.41	7.05
	142.41	58.44	53.46	22.38	7.37	2.30
	119.52	99.64	75.84	23.78	7.22	7.59
	182.02	66.03	79.44		4.15	2.76
	110.55	50.62	58.68		4.73	3.87
	121.21	66.12	56.53		8.18	1.31
	128.25	76.87	71.66		9.14	
	126.17	72.37	47.96		4.81	
	97.99	73.03	35.66		4.59	
Mean	**135.46**	**71.17**	**64.71**	**29.62**	**6.40**	**4.15**
Standard deviation	**31.47**	**13.80**	**11.88**	**11.34**	**1.84**	**2.60**

Table 81: mRNA yield generated from transcription reactions carried out in the bulk inverse hexagonal phase of DOPE and DOPE/DOTAP mixtures. Transcription was carried out for 40 minutes at 37 °C

B5.4 Probing the loss of transcriptional activity as a result of DOTAP inclusion

Experiments were carried out such that the polymerase was incubated for 2 hours with DOPE/DOTAP/DNA and DOPE/DOTAP inverse hexagonal phases prior to transcription. The purpose of these experiments was to ascertain whether the loss in activity observed on inclusion of DOTAP in the DOPE/DNA H_{II} system was caused by the unavailability of DNA at increased DOTAP contents, or an inactivation of T7 RNA polymerase in the presence of DOTAP.

	Standard positive control (no lipid)	Mol % DOTAP in DOPE						
		Polymerase Incubation with lipid and DNA				Polymerase incubation with lipid only (DNA added later)		
		0	5	10	20	0	10	20
mRNA yield (µg)	9.48	9.48	9.48	9.48	9.48	9.48	10.45	5.52
	21.80	8.96	8.22	9.66	5.12	9.98	6.43	10.99
	14.81	9.28	7.83	7.86	8.17	13.10	9.41	7.65
	19.10	10.69	10.39	6.57	3.42	10.54	9.69	7.43
	14.24	11.21	7.05		5.87	7.01	8.23	1.18
	11.95	3.64	7.47		5.41	7.98	6.12	2.84
	18.20					12.03	4.14	3.36
	11.06					6.98		
	12.12					4.46		
	12.83							
	12.62							
	9.80							
	10.09							
	22.88							
	9.95							
	12.18							
	12.24							
	11.82							
Mean	**13.73**	**8.90**	**8.80**	**6.63**	**6.07**	**9.51**	**7.31**	**5.57**
Standard deviation	**4.08**	**2.71**	**1.88**	**2.28**	**1.92**	**3.10**	**2.51**	**3.39**

Table 82: mRNA yield generated from transcription reactions carried out after incubation of T7 RNA polymerase with the bulk inverse hexagonal phase of DOPE and DOPE/DOTAP mixtures with and without DNA. Transcription was carried out for 40 minutes at 37 °C

B5.5 Transfection efficiencies of hexosomes in HeLa cells

Experiments involving delivery of hexosomes and DNA containing the gene for AmCyan to HeLa cells were carried. The Transfection efficiency was then calculated using the following formula:

$$\text{Transfection efficiency} = \frac{\text{Number of cyan cells}}{\text{Total number of cells}} \times 100$$

	Number of cyan cells observed	Total number of cells counted	Area surveyed/ μm^2	Cyan cells/ cm^2	Total cells/ cm^2	Transfection efficiency (%)
	18	72	66306	27147	108587	25.0
	28	92	85556	32727	107532	30.4
Mean	**23**	**82**	**75931**	**29937**	**108060**	**27.7**
Standard deviation	**7**	**14**	**13612**	**3946**	**746**	**3.8**

Table 83: Transfection with hexosomes of DOPE and linearised pAmCyan in Opti-MEM reduced serum medium.

	Number of cyan cells observed	Total number of cells counted	Area surveyed/ μm^2	Cyan cells/ cm^2	Total cells/ cm^2	Transfection efficiency (%)
	38	57	85556	44415	66623	66.7
	33	62	85556	38571	72467	53.2
	31	60	85556	36234	70130	51.7
	17	29	59231	28701	48961	58.6
Mean	**30**	**52**	**78975**	**36980**	**64545**	**57.5**
Standard deviation	**9**	**15**	**13163**	**6504**	**10664**	**6.8**

Table 84: Transfection with hexosomes of 5 mol % DOTAP in DOPE and linearised pAmCyan in Opti-MEM reduced serum medium

	Number of cyan cells observed	Total number of cells counted	Area surveyed/ μm^2	Cyan cells/ cm^2	Total cells/ cm^2	Transfection efficiency (%)
	15	21	66306	22622	31671	71.4
	10	15	52650	18993	28490	66.7
	19	29	85556	22208	33896	65.5
Mean	**15**	**22**	**68171**	**21274**	**31352**	**67.9**
Standard deviation	**5**	**7**	**16532**	**1986**	**2717**	**3.1**

Table 85: Transfection with hexosomes of 10 mol % DOTAP in DOPE and linearised pAmCyan in Opti-MEM reduced serum medium

	Number of cyan cells observed	Total number of cells counted	Area surveyed/ μm^2	Cyan cells/ cm^2	Total cells/ cm^2	Transfection efficiency (%)
	21	28	66306	31671	42228	75.0
	39	54	85556	45584	63117	72.2
	24	32	85556	28052	37402	75.0
	19	26	85556	22208	30389	73.1
Mean	**26**	**35**	**80744**	**31879**	**43284**	**73.8**
Standard deviation	**9**	**13**	**9625**	**9934**	**14087**	**1.4**

Table 86: Transfection with hexosomes of 20 mol % DOTAP in DOPE and linearised pAmCyan in Opti-MEM reduced serum medium

The same experiments were carried out in Opti-MEM reduced serum medium (tables … to …) and DMEM + 5% fetal calf serum (tables … to …).

	Number of cyan cells observed	Total number of cells counted	Area surveyed/ μm^2	Cyan cells/ cm^2	Total cells/ cm^2	Transfection efficiency (%)
	10	70	66306	15082	105571	14.3
	14	108	85556	16364	126233	13.0
Mean	**12**	**89**	**75931**	**15723**	**115902**	**13.6**
Standard deviation	**3**	**27**	**13612**	**906**	**14610**	**0.9**

Table 87: Transfection with hexosomes of DOPE and linearised pAmCyan in DMEM + 5% FCS

	Number of cyan cells observed	Total number of cells counted	Area surveyed/ μm^2	Cyan cells/ cm^2	Total cells/ cm^2	Transfection efficiency (%)
	11	67	66306	16590	101047	16.4
	10	85	85556	11688	99350	11.8
	7	78	85556	8182	91168	9.0
Mean	**9**	**77**	**79139**	**12153**	**97188**	**12.4**
Standard deviation	**2**	**9**	**11114**	**4223**	**5282**	**3.8**

Table 88: Transfection with hexosomes of 5 mol % DOTAP in DOPE and linearised pAmCyan in DMEM + 5% FCS

	Number of cyan cells observed	Total number of cells counted	Area surveyed/ μm^2	Cyan cells/ cm^2	Total cells/ cm^2	Transfection efficiency (%)
	10	55	66306	15082	82949	18.2
	14	62	68445	20454	90584	22.6
Mean	**12**	**59**	**67376**	**17768**	**86766**	**20.4**
Standard deviation	**3**	**5**	**1513**	**3799**	**5399**	**3.1**

Table 89: Transfection with hexosomes of 10 mol % DOTAP in DOPE and linearised pAmCyan in DMEM + 5% FCS

	Number of cyan cells observed	Total number of cells counted	Area surveyed/ μm^2	Cyan cells/ cm^2	Total cells/ cm^2	Transfection efficiency (%)
	25	59	66306	37704	88981	42.4
	32	65	85556	37402	75974	49.2
	31	69	85556	36234	80649	44.9
	33	74	85556	38571	86493	44.6
Mean	**30**	**67**	**80744**	**37478**	**83024**	**45.3**
Standard deviation	**4**	**6**	**9625**	**966**	**5856**	**2.9**

Table 90: Transfection with hexosomes of 20 mol % DOTAP in DOPE and linearised pAmCyan in DMEM + 5% FCS

	Mol % DOTAP in DOPE	Number of cyan cells observed	Total number of cells counted	Area surveyed/ μm^2	Cyan cells/ cm^2	Total cells/ cm^2	Transfection efficiency (%)
Opti-MEM	**0**	23	82	75931	29937	108060	27.7
	5	30	52	78975	36980	64545	57.5
	10	15	22	68171	21274	31352	67.9
	20	26	35	80744	31879	43284	73.8
DMEM + 5% FCS	**0**	12	89	75931	15723	115902	13.6
	5	9	77	79139	12153	97188	12.4
	10	12	59	67376	17768	86766	20.4
	20	30	67	80744	37478	83024	45.3

Table 91: Summary of transfection data from the delivery of hexosomes to HeLa cells.

The following data were used to plot a graph of transfection efficiency against DOTAP concentration for experiments carried out in serum-deficient (Opti-MEM) and serum-containing (DMEM + 5% FCS) medium.

		Transfection Efficiency (%)	
		Opti-MEM	**DMEM + 5% FCS**
Mol % DOTAP in DOPE	**0**	27.7 ± 3.8	13.6 ± 0.9
	5	57.5 ± 6.8	12.4 ± 3.8
	10	67.9 ± 3.1	20.4 ± 3.1
	20	73.8 ± 1.4	45.3 ± 2.9

Table 92: Transfection efficiencies of hexosomes containing varying amounts of DOTAP, in serum-containing and serum-deficient medium.

The cell density was also analysed as a function of DOTAP content in order to determine the relative cytotoxicity of DOTAP-containing hexosomes.

		Cell density/cm^2	
		Opti-MEM	**DMEM + 5% FCS**
Mol % DOTAP in DOPE	**0**	108000 ± 700	116000 ± 15000
	5	64000 ± 11000	97000 ± 5000
	10	31000 ± 10000	87000 ± 5000
	20	43000 ± 14000	83000 ± 6000

Table …: Cell densities after transfection experiments with hexosomes containing varying amounts of DOTAP, in serum-containing and serum-deficient medium.

A measure of transfection efficiency was also obtained from the density of cyan cells, to consider the numbers of cells producing the target protein, irrespective of the number of cells surviving the transfection process.

		Number of cyan cells/cm^2	
		Opti-MEM	**DMEM + 5% FCS**
Mol % DOTAP in DOPE	**0**	30000 ± 4000	16000 ± 1000
	5	37000 ± 7000	12000 ± 4000
	10	21000 ± 10000	18000 ± 4000
	20	32000 ± 10000	37000 ± 1000

Table 93: Density of cyan cells after transfection experiments with hexosomes containing varying amounts of DOTAP, in serum-containing and serum-deficient medium.

Appendix C – Literature Cited

1. Corsi, J.; Dymond, M. K.; Ces, O.; Muck, J.; Zink, D.; Attard, G. S., DNA that is dispersed in the liquid crystalline phases of phospholipids is actively transcribed. *Chemical communications (Cambridge, England)* **2008,** (20), 2307-9.
2. Corsi, J.; Hawtin, R. W.; Ces, O.; Attard, G. S.; Khalid, S., DNA lipoplexes: formation of the inverse hexagonal phase observed by coarse-grained molecular dynamics simulation. *Langmuir* **2010,** *26* (14), 12119-25.
3. Luzzati, V.; Tardieu, A., Lipid Phases: Structure and Structural Transitions. *Annual Review of Physical Chemistry* **1974,** *25* (1), 79-94.
4. Gruner, S. M.; Cullis, P. R.; Hope, M. J.; Tilcock, C. P. S., Lipid Polymorphism:The Molecular Basis of Nonbilayer Phases. *Annual Review of Biophysics and Biophysical Chemistry* **1985,** *14* (1), 211-238.
5. Marsh, D., *Handbook of Lipid Bilayers*. CRC Press: Boca Raton, Florida, 1990.
6. Seddon, J. M., Structure of the inverted hexagonal (HII) phase, and non-lamellar phase transitions of lipids. *Biochimica et biophysica acta* **1990,** *1031* (1), 1-69.
7. Luzzati, V., In *Biological membranes*, Chapman, D., Ed. Academic Press: London, 1973; Vol. 2.
8. Tardieu, A.; Luzzati, V.; Reman, F. C., Structure and polymorphism of the hydrocarbon chains of lipids: a study of lecithin-water phases. *J Mol Biol* **1973,** *75* (4), 711-33.
9. Cullis, P. R.; de Kruijff, B., Lipid polymorphism and the functional roles of lipids in biological membranes. *Biochimica et biophysica acta* **1979,** *559* (4), 399-420.
10. Boni, L. T.; Hui, S. W., Polymorphic phase behaviour of dilinoleoylphosphatidylethanolamine and palmitoyloleoylphosphatidylcholine mixtures. Structural changes between hexagonal, cubic and bilayer phases. *Biochimica et biophysica acta* **1983,** *731* (2), 177-85.
11. Wennerstrom, H.; Lindman, B., Micelles. Physical chemistry of surfactant association. *Physics Reports* **1979,** *52* (1), 1-86.
12. Tate, M. W.; Gruner, S. M., Temperature dependence of the structural dimensions of the inverted hexagonal (HII) phase of phosphatidylethanolamine-containing membranes. *Biochemistry* **1989,** *28* (10), 4245-53.
13. Safinya, C. R., Structures of lipid-DNA complexes: supramolecular assembly and gene delivery. *Curr Opin Struct Biol* **2001,** *11* (4), 440-8.
14. Radler, J. O.; Koltover, I.; Salditt, T.; Safinya, C. R., Structure of DNA-cationic liposome complexes: DNA intercalation in multilamellar membranes in distinct interhelical packing regimes. *Science* **1997,** *275* (5301), 810-4.
15. Koltover, I. S., T; Safinya, C. R., Phase Diagram, Stability, and Overcharging of Lamellar Cationic
Lipid–DNA Self-Assembled Complexes. *Biophysical Journal* **1999,** *77*, 915-924.
16. Koltover, I. e. a., An Inverted Hexagonal Phase of Cationic Liposome-DNA Complexes Related to DNA Release and Delivery. *Science* **1998,** *281*, 78-81.
17. Safinya, C. R.; Ewert, K.; Ahmad, A.; Evans, H. M.; Raviv, U.; Needleman, D. J.; Lin, A. J.; Slack, N. L.; George, C.; Samuel, C. E., Cationic liposome-DNA complexes: from liquid crystal science to gene delivery applications. *Philos Transact A Math Phys Eng Sci* **2006,** *364* (1847), 2573-96.
18. Patil, S. D.; Rhodes, D. G.; Burgess, D. J., DNA-based therapeutics and DNA delivery systems: a comprehensive review. *The AAPS journal* **2005,** *7* (1), E61-77.

19. Podgornik, R.; Harries, D.; Parsegian, V. A.; Strey, H. H., Molecular Interactions in Lipids, DNA, and DNA-Lipid Complexes. In *Gene and Cell Therapy: Therapeutic Mechanisms and Strategies*, Smyth Templeton, N., Ed. CRC Press: Boca Raton, Florida, 2003.
20. Chesnoy, S.; Huang, L., Structure and function of lipid-DNA complexes for gene delivery. *Annual review of biophysics and biomolecular structure* **2000,** *29*, 27-47.
21. Hafez, I. M.; Cullis, P. R., Roles of lipid polymorphism in intracellular delivery. *Adv Drug Deliv Rev* **2001,** *47* (2-3), 139-48.
22. Zabner, J.; Fasbender, A. J.; Moninger, T.; Poellinger, K. A.; Welsh, M. J., Cellular and molecular barriers to gene transfer by a cationic lipid. *J Biol Chem* **1995,** *270* (32), 18997-9007.
23. Lin, A. J.; Slack, N. L.; Ahmad, A.; Koltover, I.; George, C. X.; Samuel, C. E.; Safinya, C. R., Structure and structure-function studies of lipid/plasmid DNA complexes. *Journal of drug targeting* **2000,** *8* (1), 13-27.
24. Yaghmur, A.; Glatter, O., Characterization and potential applications of nanostructured aqueous dispersions. *Adv Colloid Interface Sci* **2009,** *147-148*, 333-42.
25. Boyd, B. J.; Dong, Y. D.; Rades, T., Nonlamellar liquid crystalline nanostructured particles: advances in materials and structure determination. *J Liposome Res* **2009,** *19* (1), 12-28.
26. Farhood, H.; Serbina, N.; Huang, L., The role of dioleoyl phosphatidylethanolamine in cationic liposome mediated gene transfer. *Biochimica et biophysica acta* **1995,** *1235* (2), 289-95.
27. Felgner, J. H.; Kumar, R.; Sridhar, C. N.; Wheeler, C. J.; Tsai, Y. J.; Border, R.; Ramsey, P.; Martin, M.; Felgner, P. L., Enhanced gene delivery and mechanism studies with a novel series of cationic lipid formulations. *J BIol Chem* **1994,** *269* (4), 2550-61.
28. Roche Applied Science DOTAP Liposomal Transfection Reagent. http://www.roche-applied-science.com/pack-insert/1811177a.pdf (accessed November).
29. Francescangeli, O.; Pisani, M.;´, V. S.; Bruni, P.; Weiss, T. M., Evidence of an inverted hexagonal phase in self-assembled phospholipid-DNA-metal complexes. *Europhysics Letters* **2004,** *67* (4), 669-675.
30. Wagner, K.; Harries, D.; May, S.; Kahl, V.; Radler, J. O.; Ben-Shaul, A., Direct Evidence for Counterion Release upon Cationic Lipid-DNA Condensation. *Langmuir* **2000,** *16*, 303-306.
31. Steitz, T. A., Visualizing polynucleotide polymerase machines at work. *The EMBO journal* **2006,** *25* (15), 3458-68.
32. Martin, C. T.; Muller, D. K.; Coleman, J. E., Processivity in early stages of transcription by T7 RNA polymerase. *Biochemistry* **1988,** *27* (11), 3966-74.
33. Cheetham, G. M. T.; Steitz, T. A., Structure of a transcribing T7 RNA polymerase initiation complex. *Science* **1999,** *286* (0036-8075 (Print)), 2305-2309.
34. Tahirov, T. H.; Temiakov, D.; Anikin, M.; Patlan, V.; McAllister, W. T.; Vassylev, D. G.; Yokoyama, S., Structure of a T7 RNA polymerase complex at 2.9A resolution. *Nature* **2002,** *420*, 43-50.
35. Yin, Y. W.; Steitz, T. A., Structural basis for the transition from initiation to elongation transcription in T7 RNA polymerase. *Science* **2002,** *298* (1095-9203 (Electronic)), 1387-1395.
36. Smeekens, S. P.; Romano, L. J., Promoter and nonspecific DNA binding by the T7 RNA polymerase. *Nucleic Acids Res* **1986,** *14* (6), 2811-27.
37. Ma, K.; Temiakov, D.; Anikin, M.; McAllister, W. T., Probing conformational changes in T7 RNA polymerase during initiation and termination by using engineered disulfide linkages. *Proceedings of the National Academy of Sciences of the United States of America* **2005,** *102* (49), 17612-7.

38. Temiakov, D.; Anikin, M.; McAllister, W. T., Characterization of T7 RNA polymerase transcription complexes assembled on nucleic acid scaffolds. *J Biol Chem* **2002,** *277* (49), 47035-43.
39. Guo, Q.; Nayak, D.; Brieba, L. G.; Sousa, R., Major conformational changes during T7 RNAP transcription initiation coincide with, and are required for, promoter release. *J Mol Biol* **2005,** *353*, 256-270.
40. Theis, K.; Gong, P.; Martin, C. T., Topological and conformational analysis of the initiation and elongation complex of t7 RNA polymerase suggests a new twist. *Biochemistry* **2004,** *43* (40), 12709-15.
41. Liu, C.; Martin, C. T., Promoter clearance by T7 RNA polymerase. Initial bubble collapse and transcript dissociation monitored by base analog fluorescence. *J Biol Chem* **2002,** *277* (4), 2725-31.
42. Lyakhov, D. L.; He, B.; Zhang, X.; Studier, F. W.; Dunn, J. J.; McAllister, W. T., Pausing and termination by bacteriophage T7 RNA polymerase. *J Mol Biol* **1998,** *280* (2), 201-13.
43. Macdonald, L. E.; Durbin, R. K.; Dunn, J. J.; McAllister, W. T., Characterization of two types of termination signal for bacteriophage T7 RNA polymerase. *J Mol Biol* **1994,** *238* (2), 145-58.
44. Sousa, R.; Patra, D.; Lafer, E. M., Model for the mechanism of bacteriophage T7 RNAP transcription initiation and termination. *J Mol Biol* **1992,** *224* (2), 319-34.
45. Ambion, Megascript Transcription Kit Protocol. **2005**.
46. Qiagen, RNeasy Lipid Tissue Kit Protocol. 2007.
47. Chattoraj, D. K.; Gosule, L. C.; Schellman, A., DNA condensation with polyamines. II. Electron microscopic studies. *J Mol Biol* **1978,** *121* (3), 327-37.
48. Gosule, L. C.; Schellman, J. A., Compact form of DNA induced by spermidine. *Nature* **1976,** *259* (5541), 333-5.
49. Manning, G. S., The molecular theory of polyelectrolyte solutions with applications to the electrostatic properties of polynucleotides. *Quarterly reviews of biophysics* **1978,** *11* (2), 179-246.
50. Widom, J.; Baldwin, R. L., Cation-induced toroidal condensation of DNA studies with Co3+(NH3)6. *J Mol Biol* **1980,** *144* (4), 431-53.
51. Widom, J.; Baldwin, R. L., Monomolecular condensation of lambda-DNA induced by cobalt hexamine. *Biopolymers* **1983,** *22* (6), 1595-620.
52. Kaiser, D.; Tabor, H.; Tabor, C. W., Spermine protection of coliphage lambda DNA against breakage by hydrodynamic shear. *J Mol Biol* **1963,** *6*, 141-7.
53. Wilson, R. W.; Bloomfield, V., Counterion-intduced condensation of deoxyribonucleic acid. A light-scattering study. *Biochemistry* **1979,** *18*, 2192-2196.
54. Gosule, L. C.; Schellman, J. A., DNA condensation with polyamines I. Spectroscopic studies. *J Mol Biol* **1978,** *121* (3), 311-26.
55. Behe, M.; Felsenfeld, G., Effects of methylation on a synthetic polynucleotide: the B--Z transition in poly(dG-m5dC).poly(dG-m5dC). *Proceedings of the National Academy of Sciences of the United States of America* **1981,** *78* (3), 1619-23.
56. Baeza, I.; Gariglio, P.; Rangel, L. M.; Chavez, P.; Cervantes, L.; Arguello, C.; Wong, C.; Montanez, c., electron microscopy and biochemical properties of polyamine-compacted DNA. *Biochemistry* **1987,** *26*, 6387-6392.
57. Baeza, I.; Ibanez, M.; Wong, C.; Chavez, P.; Gariglio, P.; Oro, J., Possible prebiotic significance of polyamines in the condensation, protection, encapsulation and biological properties of DNA. *Origins of Life and Evolution of Biospheres* **1992,** *21* (4), 225-242.
58. Maslak, M.; Jaworski, M. D.; Martin, C. T., Tests of a model for promoter recognition by T7 RNA polymerase: thymine methyl group contacts. *Biochemistry* **1993,** *32* (16), 4270-4.

59. Maslak, M.; Martin, C. T., Kinetic analysis of T7 RNA polymerase transcription initiation from promoters containing single-stranded regions. *Biochemistry* **1993,** *32* (16), 4281-5.
60. May, S.; Ben-Shaul, A., DNA-lipid complexes: stability of honeycomb-like and spaghetti-like structures. *Biophys J* **1997,** *73* (5), 2427-40.
61. Tarahovsky, Y. S.; Khusainova, R. S.; Gorelov, A. V.; Nicolaeva, T. I.; Deev, A. A.; Dawson, A. K.; Ivanitsky, G. R., DNA initiates polymorphic structural transitions in lecithin. *FEBS Letters* **1996,** *390*, 133-136.
62. Fletcher, S.; Ahmad, A.; Price, W. S.; Jorgensen, M. R.; Miller, A. D., Biophysical properties of CDAN/DOPE-analogue lipoplexes account for enhanced gene delivery. *Chembiochem* **2008,** *9* (3), 455-63.
63. Smisterova, J.; Wagenaar, A.; Stuart, M. C.; Polushkin, E.; ten Brinke, G.; Hulst, R.; Engberts, J. B.; Hoekstra, D., Molecular shape of the cationic lipid controls the structure of cationic lipid/dioleylphosphatidylethanolamine-DNA complexes and the efficiency of gene delivery. *J Biol Chem* **2001,** *276* (50), 47615-22.
64. Zuhorn, I. S.; Oberle, V.; Visser, W. H.; Engberts, J. B.; Bakowsky, U.; Polushkin, E.; Hoekstra, D., Phase behavior of cationic amphiphiles and their mixtures with helper lipid influences lipoplex shape, DNA translocation, and transfection efficiency. *Biophys J* **2002,** *83* (4), 2096-108.
65. Congiu, A.; Pozzi, D.; Esposito, C.; Castellano, C.; Mossa, G., Correlation between structure and transfection efficiency: a study of DC-Chol--DOPE/DNA complexes. *Colloids and surfaces* **2004,** *36* (1), 43-8.
66. Caracciolo, G.; Pozzi, D.; Amenitsch, H.; Caminiti, R., Multicomponent cationic lipid-DNA complex formation: role of lipid mixing. *Langmuir* **2005,** *21* (25), 11582-7.
67. Caracciolo, G.; Ruggero Caminiti, R., Do DC-Chol/DOPE-DNA complexes really form an inverted hexagonal phase? *Chemical Physics Letters* **2005,** *411*, 327-332.
68. Mel'nikov, S. M.; Dias, R.; Mel'nikova, Y. S.; Marques, E. F.; Miguel, M. G.; Lindman, B., DNA conformational dynamics in the presence of catanionic mixtures. *FEBS Lett* **1999,** *453* (1-2), 113-8.
69. Hirsch-Lerner, D.; Barenholz, Y., Hydration of lipoplexes commonly used in gene delivery: follow-up by laurdan fluorescence changes and quantification by differential scanning calorimetry. *Biochimica et biophysica acta* **1999,** *1461* (1), 47-57.
70. Ciani, L.; Casini, A.; Gabbiani, C.; Ristori, S.; Messori, L.; Martini, G., DOTAP/DOPE and DC-Chol/DOPE lipoplexes for gene delivery studied by circular dichroism and other biophysical techniques. *Biophys Chem* **2007,** *127* (3), 213-20.
71. Simberg, D.; Danino, D.; Talmon, Y.; Minsky, A.; Ferrari, M. E.; Wheeler, C. J.; Barenholz, Y., Phase behavior, DNA ordering, and size instability of cationic lipoplexes. Relevance to optimal transfection activity. *J Biol Chem* **2001,** *276* (50), 47453-9.
72. Koynova, R.; Wang, L.; Tarahovsky, Y.; MacDonald, R. C., Lipid phase control of DNA delivery. *Bioconjugate chemistry* **2005,** *16* (6), 1335-9.
73. Meidan, V. M.; Cohen, J. S.; Amariglio, N.; Hirsch-Lerner, D.; Barenholz, Y., Interaction of oligonucleotides with cationic lipids: the relationship between electrostatics, hydration and state of aggregation. *Biochimica et biophysica acta* **2000,** *1464* (2), 251-61.
74. Hofland, H. E.; Shephard, L.; Sullivan, S. M., Formation of stable cationic lipid/DNA complexes for gene transfer. *Proceedings of the National Academy of Sciences of the United States of America* **1996,** *93* (14), 7305-9.
75. Black, C. F.; Wilson, R. J.; Nylander, T.; Dymond, M. K.; Attard, G. S., Linear dsDNA partitions spontaneously into the inverse hexagonal lyotropic liquid crystalline phases of phospholipids. *Journal of the American Chemical Society* **2010,** *132* (28), 9728-32.

76. Wilson, R. J.; Tyas, S. R.; Black, C. F.; Dymond, M. K.; Attard, G. S., Partitioning of ssRNA Molecules between Preformed Monolithic H(II) Liquid Crystalline Phases of Lipids and Supernatant Isotropic Phases. *Biomacromolecules* **2010,** *11*, 3022-3027.
77. Kennedy, M. T.; Pozharski, E. V.; Rakhmanova, V. A.; MacDonald, R. C., Factors governing the assembly of cationic phospholipid-DNA complexes. *Biophys J* **2000,** *78* (3), 1620-33.
78. Evans, R. M.; Fraser, J. B.; Owen, L. N., Dithiols. Part III. Derivatives of Polyhydric Alcohols. *Journal of the Chemical Society* **1949**, 248.
79. Cleland, W. W., Dithiothreitol, a New Protective Reagent for Sh Groups. *Biochemistry* **1964,** *3*, 480-2.
80. Alliegro, M. C., Effects of dithiothreitol on protein activity unrelated to thiol-disulfide exchange: for consideration in the analysis of protein function with Cleland's reagent. *Anal Biochem* **2000,** *282* (1), 102-6.
81. Bewley, T. A.; Li, C. H., The reduction of protein disulfide bonds in the absence of denaturants. *International journal of protein research* **1969,** *1* (2), 117-24.
82. Clayden, J.; Greeves, N.; Warren, S.; Wothers, P., *Organic Chemsitry*. Oxford University Press: Oxford, United Kingdom, 2001.
83. Attard, G. S., Personal Communication: Quantifying the relationship between DNA template concentration and PCR product concentration 2008.
84. Dymond, M. K., Southampton, UK, 2007.
85. Gawrisch, K.; Parsegian, V. A.; Hajduk, D. A.; Tate, M. W.; Graner, S. M.; Fuller, N. L.; Rand, R. P., Energetics of a hexagonal-lamellar-hexagonal-phase transition sequence in dioleoylphosphatidylethanolamine membranes. *Biochemistry* **1992,** *31* (11), 2856-64.
86. Kozlov, M. M.; Leikin, S.; Rand, R. P., Bending, hydration and interstitial energies quantitatively account for the hexagonal-lamellar-hexagonal reentrant phase transition in dioleoylphosphatidylethanolamine. *Biophys J* **1994,** *67* (4), 1603-11.
87. Chirinos, M.; Hernandez, F.; Palacian, E., Transcription of DNA Templates Associated with Histone (H3 [middle dot] H4)2 Tetramers. *Archives of Biochemistry and Biophysics* **1999,** *370* (2), 222-230.
88. Howell, M. L.; Schroth, G. P.; Ho, P. S., Sequence-dependent effects of spermine on the thermodynamics of the B-DNA to Z-DNA transition. *Biochemistry* **1996,** *35* (48), 15373-82.
89. Liu, L. F.; Wang, J. C., Supercoiling of the DNA template during transcription. *Proceedings of the National Academy of Sciences of the United States of America* **1987,** *84* (20), 7024-7.
90. Ewert, K.; Slack, N. L.; Ahmad, A.; Evans, H. M.; Lin, A. J.; Samuel, C. E.; Safinya, C. R., Cationic lipid-DNA complexes for gene therapy: understanding the relationship between complex structure and gene delivery pathways at the molecular level. *Curr Med Chem* **2004,** *11* (2), 133-49.
91. Rosevear, F., The microscopy of the liquid crystalline neat and middle phases of soaps and synthetic detergents. *Journal of the American Oil Chemists' Society* **1954,** *31* (12), 628-639.
92. Rosevear, F., Liquid Crystals: The Mesomorphic Phases of Surfactant Compositions. *J Soc Cosmetic Chemists* **1968,** *19*, 581-594.
93. Seddon, J. M.; Squires, A. M.; Conn, C. E.; Ces, O.; Heron, A. J.; Mulet, X.; Shearman, G. C.; Templer, R. H., Pressure-jump X-ray studies of liquid crystal transitions in lipids. *Philos Transact A Math Phys Eng Sci* **2006,** *364* (1847), 2635-55.
94. Bragg, W. L., *The Development of X-ray Analysis*. Bell: London, 1975.
95. Guinier, A., *X-ray Diffraction: In Crystals, Imperfect Crystals and Amorphous Bodies*. Dover Publications Inc.: 1994.
96. Guinier, A.; Fournet, G., *Small Angle Scattering of X-rays*. Wiley: New York, 1955.

97. de Campo, L.; Yaghmur, A.; Sagalowicz, L.; Leser, M. E.; Watzke, H.; Glatter, O., Reversible phase transitions in emulsified nanostructured lipid systems. *Langmuir* **2004,** *20* (13), 5254-61.
98. Boyd, B. J.; Rizwan, S. B.; Dong, Y. D.; Hook, S.; Rades, T., Self-assembled geometric liquid-crystalline nanoparticles imaged in three dimensions: hexosomes are not necessarily flat hexagonal prisms. *Langmuir* **2007,** *23* (25), 12461-4.
99. Marrink, S. J.; de Vries, A. H.; Tieleman, D. P., Lipids on the move: Simulations of membrane pores, domains, stalks and curves. *Biochimica et biophysica acta* **2009,** *1788* (1), 149-68.
100. Baoukina, S.; Monticelli, L.; Risselada, H. J.; Marrink, S. J.; Tieleman, D. P., The molecular mechanism of lipid monolayer collapse. *Proceedings of the National Academy of Sciences of the United States of America* **2008,** *105* (31), 10803-8.
101. Faller, R.; Marrink, S. J., Simulation of domain formation in DLPC-DSPC mixed bilayers. *Langmuir* **2004,** *20* (18), 7686-93.
102. Pandit, S. A.; Jakobsson, E.; Scott, H. L., Simulation of the early stages of nano-domain formation in mixed bilayers of sphingomyelin, cholesterol, and dioleylphosphatidylcholine. *Biophys J* **2004,** *87* (5), 3312-22.
103. Pandit, S. A.; Vasudevan, S.; Chiu, S. W.; Mashl, R. J.; Jakobsson, E.; Scott, H. L., Sphingomyelin-cholesterol domains in phospholipid membranes: atomistic simulation. *Biophys J* **2004,** *87* (2), 1092-100.
104. Venturoli, M.; Smit, B.; Sperotto, M. M., Simulation studies of protein-induced bilayer deformations, and lipid-induced protein tilting, on a mesoscopic model for lipid bilayers with embedded proteins. *Biophys J* **2005,** *88* (3), 1778-98.
105. Li, D.-W.; Liu, X. Y.; Feng, Y. P., Bond-Angle-Potential-Dependent Dissipative Particle Dynamics Simulation and Lipid Inverted Phase. *The Journal of Physical Chemistry B* **2004,** *108* (30), 11206-11213.
106. Michel, D. J.; Cleaver, D. J., Coarse-grained simulation of amphiphilic self-assembly. *J Chem Phys* **2007,** *126* (3), 034506.
107. Ellison, L. J.; Michel, D. J.; Barmes, F.; Cleaver, D. J., Entropy-driven formation of the gyroid cubic phase. *Phys Rev Lett* **2006,** *97* (23), 237801.
108. Goetz, R.; uuml; diger; Gompper, G.; Lipowsky, R., Mobility and Elasticity of Self-Assembled Membranes. *Physical Review Letters* **1999,** *82* (1), 221.
109. Venturoli, M.; Smit, B., Simulating the self-assembly of model membranes. *PhysChemComm* **1999,** *2* (10), 45-49.
110. Leach, A. R., *Molecular Modelling: Principles and Applications*. 2 ed.; Pearson Education: London, 2001.
111. Allen, M. P.; Tildesley, D. J., *Computer Simulations of Liquids*. Oxford University Press: 1989.
112. Haynie, D. T., *Biological Themodynamics*. 2 ed.; Cambridge University Press: Cambridge, 2008.
113. Bromberg, S.; Dill, K. A., *Molecular Driving Forces: Statistical Thermodynamics in Chemistry and Biology*. 1 ed.; Garland Science: 2002.
114. Marrink, S. J.; Risselada, H. J.; Yefimov, S.; Tieleman, D. P.; de Vries, A. H., The MARTINI force field: coarse grained model for biomolecular simulations. *J Phys Chem B* **2007,** *111* (27), 7812-24.
115. Bond, P. J.; Holyoake, J.; Ivetac, A.; Khalid, S.; Sansom, M. S., Coarse-grained molecular dynamics simulations of membrane proteins and peptides. *J Struct Biol* **2007,** *157* (3), 593-605.
116. Shih, A. Y.; Arkhipov, A.; Freddolino, P. L.; Schulten, K., Coarse grained protein-lipid model with application to lipoprotein particles. *J Phys Chem B* **2006,** *110* (8), 3674-84.

117. Khalid, S.; Bond, P. J.; Holyoake, J.; Hawtin, R. W.; Sansom, M. S., DNA and lipid bilayers: self-assembly and insertion. *Journal of the Royal Society, Interface / the Royal Society* **2008**.
118. Berendsen, H. J. C.; Vanderspoel, D.; Vandrunen, R., Gromacs - a Message-Passing Parallel Molecular-Dynamics Implementation. *Computer Physics Communications* **1995,** *91* (1-3), 43-56.
119. Lindahl, E.; Hess, B.; Van Der Spoel, D., GROMACS 3.0: a package for molecular simulation and trajectory analysis. *Journal of Molecular Modeling* **2001,** *7* (8), 306-317.
120. Marrink, S. J.; de Vries, A. H.; Mark, A. E., Coarse Grained Model for Semiquantitative Lipid Simulations *J. Phys. Chem. B* **2004,** *108*, 750-760.
121. Siegel, D. P.; Green, W. J.; Talmon, Y., The mechanism of lamellar-to-inverted hexagonal phase transitions: a study using temperature-jump cryo-electron microscopy. *Biophys J* **1994,** *66* (2 Pt 1), 402-14.
122. Siegel, D. P., Energetics of intermediates in membrane fusion: comparison of stalk and inverted micellar intermediate mechanisms. *Biophys J* **1993,** *65* (5), 2124-40.
123. Gurtovenko, A. A.; Vattulainen, I., Pore formation coupled to ion transport through lipid membranes as induced by transmembrane ionic charge imbalance: atomistic molecular dynamics study. *Journal of the American Chemical Society* **2005,** *127* (50), 17570-1.
124. Zantl, R.; Baicu, L.; Artzner, F.; Sprenger, I.; Rapp, G.; Radler, J. O., Thermotropic phase behavior of cationic lipid-DNA complexes compared to binary lipid mixtures. *Journal of Physical Chemistry B* **1999,** *103* (46), 10300-10310.
125. Marrink, S. J.; Mark, A. E., Molecular view of hexagonal phase formation in phospholipid membranes. *Biophys J* **2004,** *87* (6), 3894-900.
126. May, E. R.; Kopelevich, D. I.; Narang, A., Coarse-grained molecular dynamics simulations of phase transitions in mixed lipid systems containing LPA, DOPA, and DOPE lipids. *Biophys J* **2008,** *94* (3), 878-90.
127. Farago, O.; Ewert, K.; Ahmad, A.; Evans, H. M.; Gronbech-Jensen, N.; Safinya, C. R., Transitions between distinct compaction regimes in complexes of multivalent cationic lipids and DNA. *Biophys J* **2008,** *95* (2), 836-46.
128. Farago, O.; Gronbech-Jensen, N., Computational and analytical modeling of cationic lipid-DNA complexes. *Biophys J* **2007,** *92* (9), 3228-40.
129. Farago, O.; Gronbech-Jensen, N., Simulation of self-assembly of cationic lipids and DNA into structured complexes. *Journal of the American Chemical Society* **2009,** *131* (8), 2875-81.
130. Farago, O.; Gronbech-Jensen, N.; Pincus, P., Mesoscale computer modeling of lipid-DNA complexes for gene therapy. *Phys Rev Lett* **2006,** *96* (1), 018102.
131. May, S.; Harries, D.; Ben-Shaul, A., The phase behavior of cationic lipid-DNA complexes. *Biophys J* **2000,** *78* (4), 1681-97.
132. Khalid, S.; Hannon, M. J.; Rodger, A.; Rodger, P. M., Shape effects on the activity of synthetic major-groove binding ligands. *J Mol Graph Model* **2007,** *25* (6), 794-800.
133. Felgner, P. L.; Gadek, T. R.; Holm, M.; Roman, R.; Chan, H. W.; Wenz, M.; Northrop, J. P.; Ringold, G. M.; Danielsen, M., Lipofection: a highly efficient, lipid-mediated DNA-transfection procedure. *Proceedings of the National Academy of Sciences of the United States of America* **1987,** *84* (21), 7413-7.
134. Fuerst, T. R.; Earl, P. L.; Moss, B., Use of a hybrid vaccinia virus-T7 RNA polymerase system for expression of target genes. *Mol Cell Biol* **1987,** *7* (7), 2538-44.
135. Elroy-Stein, O.; Moss, B., Cytoplasmic expression system based on constitutive synthesis of bacteriophage T7 RNA polymerase in mammalian cells. *Proceedings of the National Academy of Sciences of the United States of America* **1990,** *87* (17), 6743-7.
136. Fuerst, T. R.; Niles, E. G.; Studier, F. W.; Moss, B., Eukaryotic transient-expression system based on recombinant vaccinia virus that synthesizes bacteriophage T7 RNA

polymerase. *Proceedings of the National Academy of Sciences of the United States of America* **1986,** *83* (21), 8122-6.
137. Wyatt, L. S.; Moss, B.; Rozenblatt, S., Replication-deficient vaccinia virus encoding bacteriophage T7 RNA polymerase for transient gene expression in mammalian cells. *Virology* **1995,** *210* (1), 202-5.
138. Yap, C.-C.; Ishii, K.; Aoki, Y.; Aizaki, H.; Tani, H.; Shimizu, H.; Ueno, Y.; Miyamura, T.; Matsuura, Y., A hybrid baculovirus-T7 RNA polymerase system for recovery of an infectious virus from cDNA. *Virology* **1997,** *231* (2), 192-200.
139. Mounkes, L. C.; Zhong, W.; Cipres-Palacin, G.; Heath, T. D.; Debs, R. J., Proteoglycans mediate cationic liposome-DNA complex-based gene delivery in vitro and in vivo. *J BIol Chem* **1998,** *273* (40), 26164-70.
140. Ross, P. C.; Hui, S. W., Lipoplex size is a major determinant of in vitro lipofection efficiency. *Gene Ther* **1999,** *6* (4), 651-9.
141. Labat-Moleur, F.; Steffan, A. M.; Brisson, C.; Perron, H.; Feugeas, O.; Furstenberger, P.; Oberling, F.; Brambilla, E.; Behr, J. P., An electron microscopy study into the mechanism of gene transfer with lipopolyamines. *Gene Ther* **1996,** *3* (11), 1010-7.
142. Zhou, X.; Huang, L., DNA transfection mediated by cationic liposomes containing lipopolylysine: characterization and mechanism of action. *Biochimica et biophysica acta* **1994,** *1189* (2), 195-203.
143. Hui, S. W.; Langner, M.; Zhao, Y. L.; Ross, P.; Hurley, E.; Chan, K., The role of helper lipids in cationic liposome-mediated gene transfer. *Biophys J* **1996,** *71* (2), 590-9.
144. Friend, D. S.; Papahadjopoulos, D.; Debs, R. J., Endocytosis and intracellular processing accompanying transfection mediated by cationic liposomes. *Biochimica et biophysica acta* **1996,** *1278* (1), 41-50.
145. Wattiaux, R.; Jadot, M.; Warnier-Pirotte, M. T.; Wattiaux-De Coninck, S., Cationic lipids destabilize lysosomal membrane in vitro. *FEBS Lett* **1997,** *417* (2), 199-202.
146. Wrobel, I.; Collins, D., Fusion of cationic liposomes with mammalian cells occurs after endocytosis. *Biochimica et biophysica acta* **1995,** *1235* (2), 296-304.
147. El Ouahabi, A.; Thiry, M.; Pector, V.; Fuks, R.; Ruysschaert, J. M.; Vandenbranden, M., The role of endosome destabilizing activity in the gene transfer process mediated by cationic lipids. *FEBS Lett* **1997,** *414* (2), 187-92.
148. Dowty, M. E.; Williams, P.; Zhang, G.; Hagstrom, J. E.; Wolff, J. A., Plasmid DNA entry into postmitotic nuclei of primary rat myotubes. *Proceedings of the National Academy of Sciences of the United States of America* **1995,** *92* (10), 4572-6.
149. Lechardeur, D.; Sohn, K. J.; Haardt, M.; Joshi, P. B.; Monck, M.; Graham, R. W.; Beatty, B.; Squire, J.; O'Brodovich, H.; Lukacs, G. L., Metabolic instability of plasmid DNA in the cytosol: a potential barrier to gene transfer. *Gene Ther* **1999,** *6* (4), 482-97.
150. Zanta, M. A.; Belguise-Valladier, P.; Behr, J. P., Gene delivery: a single nuclear localization signal peptide is sufficient to carry DNA to the cell nucleus. *Proceedings of the National Academy of Sciences of the United States of America* **1999,** *96* (1), 91-6.
151. Mortimer, I.; Tam, P.; MacLachlan, I.; Graham, R. W.; Saravolac, E. G.; Joshi, P. B., Cationic lipid-mediated transfection of cells in culture requires mitotic activity. *Gene Ther* **1999,** *6* (3), 403-11.
152. Gao, X.; Huang, L., Cytoplasmic expression of a reporter gene by co-delivery of T7 RNA polymerase and T7 promoter sequence with cationic liposomes. *Nucleic Acids Res* **1993,** *21* (12), 2867-72.
153. Lin, A. J.; Slack, N. L.; Ahmad, A.; George, C. X.; Samuel, C. E.; Safinya, C. R., Three-dimensional imaging of lipid gene-carriers: membrane charge density controls universal transfection behavior in lamellar cationic liposome-DNA complexes. *Biophys J* **2003,** *84* (5), 3307-16.

154. Brisson, M.; He, Y.; Li, S.; Yang, J. P.; Huang, L., A novel T7 RNA polymerase autogene for efficient cytoplasmic expression of target genes. *Gene Ther* **1999,** *6* (2), 263-70.
155. Nakano, R.; Nakagawa, T.; Imazu, S.; Katayama, K.; Mizuguchi, H.; Hayakawa, T.; Tsutsumi, Y.; Nakagawa, S.; Mayumi, T., A novel T7 system utilizing mRNA coding for T7 RNA polymerase. *Biochem Biophys Res Commun* **2003,** *301* (4), 974-8.
156. Davanloo, P.; Rosenberg, A. H.; Dunn, J. J.; Studier, F. W., Cloning and expression of the gene for bacteriophage T7 RNA polymerase. *Proceedings of the National Academy of Sciences of the United States of America* **1984,** *81* (7), 2035-9.
157. Spector, D. L.; Goldman, R. D., *Basic Methods in Microscopy*. Cold Spring Harbor Laboratory Press: New York, 2006.
158. Smart, O. S.; Neduvelil, J. G.; Wang, X.; Wallace, B. A.; Sansom, M. S., HOLE: a program for the analysis of the pore dimensions of ion channel structural models. *J Mol Graph* **1996,** *14* (6), 354-60, 376.